Maskless Nanolithography and Imaging with Diffractive Optical Arrays

by

Darío Gil

B.E. Stevens Institute of Technology (1998)
S.M. Massachusetts Institute of Technology (2000)

Submitted to the Department of Electrical Engineering and Computer Science
in partial fulfillment of the requirements for the degree of

Doctor of Philosophy

at the

MASSACHUSETTS INSTITUTE OF TECHNOLOGY

June 2003

© Massachusetts Institute of Technology, 2003. All rights reserved

Author.....
Department of Electrical Engineering and Computer Science
May 2, 2003

Certified by.....
Henry I. Smith
Keithley Professor of Electrical Engineering
Thesis Supervisor

Accepted by.....
Arthur C. Smith
Chairman, Department Committee on Graduate Studies

MASSACHUSETTS INSTITUTE OF TECHNOLOGY
AUG 0 6 2004
LIBRARIES

MASSACHUSETTS INSTITUTE OF TECHNOLOGY
AUG 0 6 2004
LIBRARIES

BARKER

MITLibraries
Document Services

Room 14-0551
77 Massachusetts Avenue
Cambridge, MA 02139
Ph: 617.253.2800
Email: docs@mit.edu
http://libraries.mit.edu/docs

DISCLAIMER OF QUALITY

Due to the condition of the original material, there are unavoidable flaws in this reproduction. We have made every effort possible to provide you with the best copy available. If you are dissatisfied with this product and find it unusable, please contact Document Services as soon as possible.

Thank you.

Due to the quality of the original material there is some bleed through.

Maskless Nanolithography and Imaging with Diffractive Optical Arrays

By

Darío Gil

Submitted to the Department of Electrical Engineering and Computer Science
on May 2, 2003 in partial fulfillment
of the requirements for the degree of
Doctor of Philosophy

Abstract

Semiconductor lithography is at a crossroads. With mask set costs in excess of one million dollars, long mask turn-around times, and tools that are characterized by their inflexibility and skyrocketing costs, there is a need for a new paradigm in lithography. The work presented in this thesis, Zone-Plate-Array Lithography (ZPAL), bypasses some of the most pressing problems of current lithography equipment by developing a maskless lithography tool that will be scalable, flexible and cost-effective. It is the departure from a century-old tradition of refractive optics, in combination with the use of advanced micromechanics and fast computing, that enables ZPAL to open up a new application space in lithography.

This thesis addresses in detail all levels of the ZPAL system, from the micromechanics, to the diffractive optics, to the control system. Special emphasis is placed on the design, fabrication and characterization of high-numerical-aperture diffractive optical elements for lithography and imaging. The results achieved provide conclusive evidence that diffractive optics in general, and zone plates in particular, are capable of state-of-the-art lithography.

Thesis Supervisor: Professor Henry I. Smith
Title: Keithley Professor of Electrical Engineering

Acknowledgements

To Professor Henry Smith, for his enthusiasm, guidance and generosity in allowing me to pursue my own ideas and research directions. I will forever be grateful to him for giving me increasing levels of responsibility as my graduate experience progressed. His leadership style, believing in people and providing an environment where they can succeed, is at the core of the great achievements that his laboratory has obtained. I will take this with me as one of the most valuable lessons I have learned during my MIT years.

To Rajesh Menon for sharing our entire MIT experience together. I remain impressed by his intelligence and good nature.

To Dr.David Carter, for his mentorship and for the too-numerous-to-count contributions to the research presented in this thesis.

To Professor George Barbastathis, for all his advice, support, and good nature. For having become both an advisor and a friend.

To Todd Hastings and Mike Walsh, my great office-mates. Beyond all our technical discussions, our conversations about politics, society, and the MIT-trucks (or how to avoid them), made some of our 16-hour days seem like 12-hour days.

To Mark Mondol, because I am always happy to see him. Love of science, avid reader, great sense of humor, well-traveled, progressive politics: all traits I admire and make him special.

To Jim Daley, for always going the extra mile when I needed it.

To Tim Savas, for his ability to keep people honest.

To Dr. Juan Ferrera, Dr. Tom Murphy, Dr. Mike Lim, Dr. Fernando Castaño, Amil Patel, Euclid Moon, Feng Zhang, Dr. James Goodberlet, Tom O'Reilly, Minghao Qi, Tymon Barwicz, Jimmy Carter, Cindy Lewis, and all the other inspiring members of the NanoStructures Laboratory.

To Paul Herz for his contagious joy of life.

To Tinker, for his willingness to share experiences, and his unique perspective on life. The trip to Spain remains one of my fondest memories, *profesor.*

To Dave Grewal, for being the best friend one could hope for. From our high-school years, through college, through graduate seminars at Harvard, we keep sharing our experiences and life together. Few know me better, and few would I like to know better. I am both honored and proud to be your friend.

To Travis Godsoe, for all the movies. The club will remain active through the years.

To Hillary Zipper for her passions

To the Godsoes and Rathbuns, for making me feel at home away from home. I am a proud member of your family.

To my family in Spain, because they are always there for me. The generosity of Jesús, his career advice, and his example of creating your opportunities, have enabled Amanda and me to be where we are. To Román for going through it all first. I will always be learning from you. To Marco, for his inspiration, and for showing us how to bring art into our daily experience to live better. To Carola and Julie, for making our family whole. To the children, Román, Pedro, Nicolás and Francesca. Our daughter will be joining you soon. To my parents, for their unrelenting love and for believing I can achieve anything. My success is their success.

But above all, to my wife Amanda, the love of my life. We go through it all together, and nothing makes me more excited than our future. Our coming daughter makes me feel so full of hope and joy, that I can barely believe one can be so happy. When choices arise in the future, I know which way to go: more of you.

Contents

List of Figures

List of Tables

Chapter 1

Introduction – Maskless Lithography

Lithography is clearly a cornerstone of the semiconductor industry and the information revolution. High-resolution lithography is crucial to a wide variety of devices, from integrated circuits (IC) for computers, to filters for optical communication, to high-density magnetic-information storage. Since the invention of the transistor and the fabrication of the first IC, lithography's goal has been to print reliably smaller and smaller features, leading not only to a high-degree of integration, but also to a dramatic increase in performance, as illustrated in Fig.1-1.

Lithography development has traditionally been dominated by the needs of the semiconductor industry. As a result of the ever-increasing demand for finer features, improved alignment, and higher throughputs within the industry, a rapid acceleration in the complexity and the cost of lithography tools has taken place, causing a bifurcation in the lithography world. Fewer and fewer customers can afford lithographic tools that, although capable of high-resolution and high-throughput, are inherently inflexible and based on a manufacturing model involving millions of chips with fixed designs. As a consequence, customers requiring production alternatives capable of quick-turn-around customized chips have been left out of a market that is increasingly consolidated by a

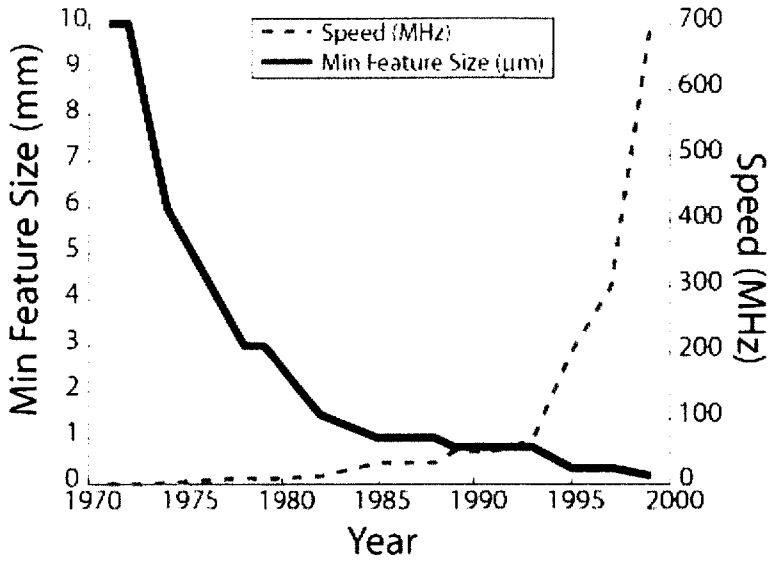

Figure 1 - 1. Keeping up with Moore's Law. The graph shows a correlation between the ability to print smaller and smaller features through lithography and the increase in performance (with speed as a metric) of microprocessors (in this case Intel's). Note that being able to get into the sub-1 µm regime has provided a fantastic increase in performance.

handful of semiconductor multinationals. It is in this context of international consolidation and narrow production alternatives that the work presented in this thesis acquires its relevance. With the development of a flexible, high-resolution affordable maskless lithography technique, a solution is finally offered to the currently disenfranchised sectors that require advanced nanofabrication processes.

1.1 Lithography – The Machine Shop of the XXI Century

The goal of lithography is to create a relief pattern in a radiation sensitive "resist film" coated on a substrate's surface by exposing the resist to some pattern of incident radiation. Because lithography is the step that transfers geometric information onto the substrate's surface, it is indispensable in the fabrication of semiconductor-electronic and optoelectronic devices and circuits. Also, because the lithography process is often applied to substrates many separate times in the process of manufacturing, it is, very

often, the technology whose cost and efficacy has the greatest impact on the final circuit cost. In fact, it is estimated that the lithography steps account for about 1/3 of the total cost of the manufactured *chip*.

The future of lithography still looks bright. Beyond its immediate practical application in semiconductor production, it is important to see this technology as key in the development of nanoscale science and nanotechnology. The nanoworld, a source of fascination for scientist, engineers, and even writers, has recently risen to new heights of awareness in the academic community, the political arena, and with the public at large. This, incidentally, has the potential of being both a blessing and a curse. A blessing due to the increased availability of funding, new ideas, and the commitment of a whole new generation of scientists to the nanotech field. And a curse because too much hype too soon can cause irreparable damage to a nascent discipline. Given the market hysteria experienced with the dot-com boom and the telecom sector of the late 90s, it is somewhat disturbing to experience the tidal wave of market attention shifting to nanotechnology as the *New New Thing* [Ref 1-1]. While demonstrations of novel devices in laboratories around the world abound, the commercial viability of many of these novel devices remains to be proven, especially in the absence of suitable manufacturing techniques.

As a consequence of ignoring the finer details of nanomanufacturing, economies of scale, and the deep interrelation of multiple micro/nanofabrication processes, the typical reporting coming out of laboratories around the world often tends to be rather disingenuous, with researchers employing a logic that can be summarized as follows:

(1) It typically starts with a news brief from a journalist after interviewing the scientist with a claim of the kind: "The Future of Computing Redefined", or "New nanodevices that will change the world", etc, etc, etc

(2) Then depending on whether they belong to the "top-down" approach to nanotech, or to the "bottom-up", the claims that follow have two different but recognizable bents:

a. From the "top-down" camp:

   Logical statement #1: We have made a new device in our laboratory employing the planar process.

   Logical statement #2: The planar process is also employed by the semiconductor industry.

   Logical conclusion: It will be possible to manufacture our device with the same tools that are employed by the semiconductor industry, and therefore our device will be readily available for consumers shortly.

b. From the "bottom-up" camp:

   Logical statement #1: We have been able to move some atoms and arrange them in precise order.

   Logical statement #2: All matter is formed by the precise arrangement of atoms.

   Logical conclusion: Our new process has the potential of revolutionizing how ALL things are made.

The attempt of the above caricature of the current state of reporting on nanotech research is to frame scientific and technological progress in a wider context, one that takes into account current manufacturing processes, coordination problems, and economies of scale. While the *logical statements* presented from both camps (i.e. the "top-down" and the "bottom-up") are genuinely exciting and worthy of support on their own right, the *logical conclusions* leave much to be desired. Let's look at them.

The logical conclusion of the "top-down" approach suffers from the common misconception that the tools used to mass-produce silicon microchips are readily suitable to manufacture the proposed new devices. It is often not realized that these machines and techniques are inflexible and hyper-specialized to the kinds of materials that can be used (i.e. only Si), the size of the substrates (currently 12" wafers), the size of the devices (all structures must be smaller than the size of a die, currently 25mmX12.5mm), and a number of other placement tolerance limitations. And these are just the technical

limitations. Added to these shortcomings, the absence of economies of scale and the skyrocketing costs of the manufacturing tools currently employed in the semiconductor industry (see Section 1.2.2) do not allow for new players to come into the market given the enormous start-up costs required. The alternative of working through and with the quasi-monopolies of the semiconductor industry faces the additional problem of the "not-invented-here" syndrome, and, more importantly, the inability of large established companies to support the emergence of so-called "disruptive technologies". This term, coined by Clayton M. Christensen [Ref 1-2] of the Harvard Business School, refers to technological breakthroughs (such as those often reported in nanotechnology) that while initially offer worse performance than existing products (e.g. molecular transistor's much lower mobility when compared with conventional silicon transistors), they typically offer other features that a fringe (and generally new) customers values (e.g. low power consumption in the case of molecular transistors). As Prof. Christensen indicates, such products are typically "cheaper, simpler, smaller, and, frequently, more convenient to use" [Ref 1-2]. The problem arises from the dilemma facing the managers of the large established companies that have products in the market place and are exploring novel developments that the field of, say, nanotechnology, has to offer. The managers of such companies will listen to their customers and adjust their product portfolio accordingly, by investing aggressively in new technologies that would provide their customers more and better products of the sort they *currently* need. This is typically referred to as "good management". However, through careful research Prof. Christensen presents many examples of companies, most of them leaders in their fields (such as IBM, Apple, Xerox and Digital), that through "good management" failed to incorporate disruptive technologies into their companies early enough with devastating consequences in some cases.

The above digression is relevant because it is important to contextualize the impact that innovation can have in the world at large, in the absence of interrelated manufacturing processes that are suitable. While lithography and the planar process are almost certainly the right technique for "top-down" approaches to nanotechnology, the semiconductor industry model of manufacturing might not be, at least in its current form. By enabling the possibility of fabricating high-resolution devices with moderate

throughputs, capable of low-and-medium-volume production (all without the need for masks and fixed designs), the research presented in this thesis is an attempt to relieve the bottleneck caused by the $20M lithography tools and $1M mask sets currently limiting the potential of novel devices and processes.

The "bottom-up" approach suffers from a different kind of problem, that of counting too quickly. Let me explain. This is a phenomenon that allows people to make progressions like this: one, two, three, four, infinity. This kind of thinking, typically born out of excitement and an unfettered belief in our capacity for technological progress, attracts an enormous amount of media attention and name recognition by providing grandiose scenarios that claim to have the potential of altering life on earth as we know it (see for example Eric Drexler from the Foresight Institute). We have all heard stories of the "gray goo" scenario, in which self-replicating nanobots destroy life on earth, or milder alternatives that "simply" alter the entire manufacturing model of the world by being able to create all objects (from chips, to chairs, to cars) by means of molecular manufacturing. Atoms have indeed been moved [Ref 1-3] in a controlled manner in some very beautiful experiments, but to go from the fact that ultra-cold inert atoms were painstakingly arranged by means of very small nanoprobes to claims of a new manufacturing model that will change the world economy is indeed *counting too quickly*, to say the least, and hyperbolic logic at worst.

A more likely scenario is that of a gradual integration of novel "bottom-up" inventions (like nanotubes) into state-of-the-art "top-down" approaches based on lithography and the planar process. If more flexible and cost-effective alternatives to such "top-down" processes are developed, new and exciting devices will find their way to the market and achieve their full potential. It is in this context that lithography has the potential to be the "machine shop of the XXI century".

1.2 Maskless Lithography – A Technology whose Time has Come

Semiconductor lithography is at a crossroads. With mask-set costs in excess of one million dollars, long mask-turn-around times, and tools that are characterized by their inflexibility and skyrocketing costs, there is a need for a new paradigm in

lithography. The ever-increasing demand for finer features, improved alignment, and high throughput is causing a rapid acceleration in the complexity and the cost of lithography tools. Optical projection steppers, although capable of deep submicron and sub-100nm resolution, suffer from an inherent lack of flexibility that renders them inappropriate for the requirements of a number of disciplines and applications outside of Si semiconductor manufacturing. Furthermore, even within the realm of the Si semiconductor industry, there is a growing awareness that quick-turn-around in lithography is becoming extremely important both for designers and for special low-volume products. In addition, the cost of low-volume commercial lithography has been growing at an alarming rate, since the high cost of masks can't be amortized over a large-volume chip production.

The quick creation and delivery to customers of customized chips is becoming important as microprocessors reach performance levels that often exceed the needs of all but a few customers. In the coming years customers will likely be willing to pay extra for a product that is extraordinarily reliable, or one that has been customized to meet their specific needs [Ref 1-4]. If flexibility and quick turn-around time do indeed become a new element in the Si semiconductor industry, then maskless lithography would appear to be the preferred choice. Because of the cost of modern-day photomasks, and the sometimes long turn-around time, maskless lithography would also be preferred in research and in a large variety of applications, from microphotonics to microelectromechanical systems.

1.2.1 Historical Trends and Analogies

The evolution of the semiconductor lithography industry and its current state of affairs leads itself to a number of relevant comparisons with the development of other industries. The trend of going from hand manufacturing, to mass manufacturing with fixed processes, to the commoditization of the manufactured product, to the customer desire to have a personalized and customized product (but still at the low prices accustomed to by mass manufacturing) is a recurring story that a number of industries have experienced and that the semiconductor sector is likely to enter in the near future.

Maskless Lithography Systems are like Laser Printers

The first comparison worth presenting is that of the printing industry. From the first recording of printing in China during the Han Dinasty (25-220 AD), to the invention of the movable type in the 1040s by Bi Sheng in China, to the development of typography and Gutenberg press in Europe, we see a 1,400 year journey that literally changed the world [Ref 1-5]. The Gutenberg press allowed for mass printing of books, and evolutionary progress took care of the rest until the advent of the personal computer in the XX century, in which a new form of printing was enabled: custom desktop publishing. The explosion of desktop publishing for business and personal applications can be traced to development of a printing process capable of high-resolution and low to medium throughput: the laser printer. The ability to print dozens of pages per minute, even in color, provides a sufficient level of performance for the vast majority of the printing needs of private consumers (printing family albums and photographs, high-school and college papers, invitations to family events, etc) and many business applications (interim reports, white papers, proofs of catalogues, etc). While it still does not make sense to print the NY Times with such techniques, for low to medium-volume runs the versatility and efficiency of "maskless" printing has proven to be a market winner. The characteristics of this successful model are based on compatibility and flexibility (i.e. they print on regular paper, photographic paper, etc), low cost, high-resolution (very important for photography applications) and sufficient throughput (if laser printers took one hour to print one page, as opposed to a few seconds, their utility and market penetration would be dramatically reduced).

An appropriate comparison could then go as follows: *maskless lithography will produce a revolution in semiconductor manufacturing akin to that observed in the printing industry with the advent of the laser printer* (see Fig.1-2). For this comparison to hold, the maskless lithography system, like the laser printer, would have to provide a *high-resolution* (i.e. be capable of achieving the minimum feature size at each technology node), *sufficient throughput* (a few wafers per hour), *compatibility* with current processes

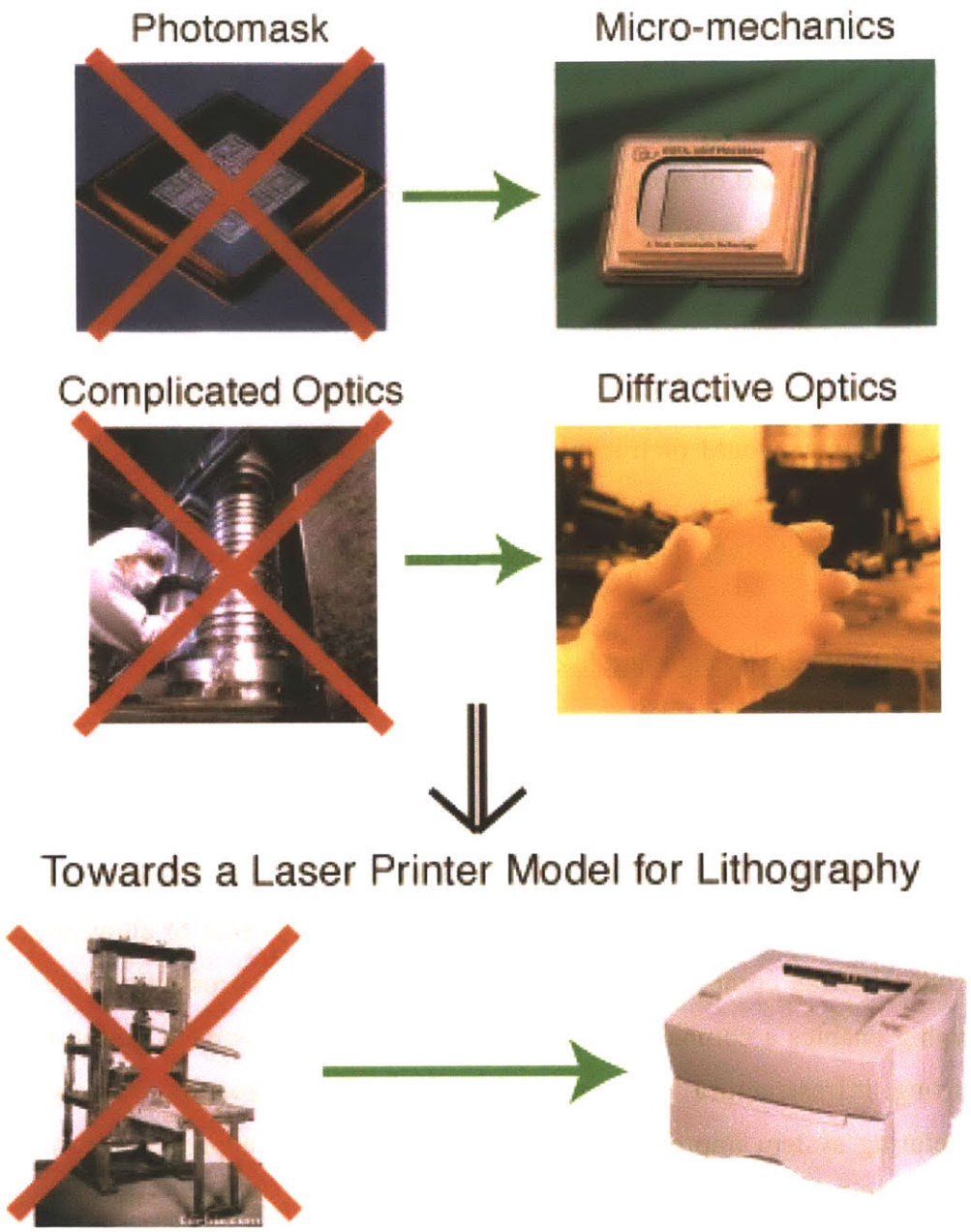

Figure 1 - 2. Towards a laser printer model for lithography. The utilization of micromechanics, in combination with cost reducing solutions like diffractive optics (that can be fabricated with the planar process) could lead to revolution in semiconductor lithography akin that experienced in the printing world with the advent of the laser printer.

(silicon wafers, standard resists, etc) and a *moderate cost.* At the same time, it is fair to acknowledge the limits of this comparison, by noting that laser printers are consumer products accessible to millions of consumers, while maskless lithography systems, even

if their costs are dramatically reduced compared to present $20M lithography systems, will always remain a part of the micro and nanofabrication process that requires other expensive processing equipment and clean-room environments for their realization. However, in the context of small and medium companies, research labs, and universities that have an interest in micro and nanofabrication, maskless lithography would indeed open up a much needed space, since, as was mentioned before, the lithography process is very often the technology whose cost and efficacy has the greatest impact on the final device cost. By enabling low and medium volume production, the lithography equivalent to the laser printer would permit talented small teams of researchers, with moderate budgets and novel designs, to offer alternatives to entrenched products that sometimes remain unchallenged solely due to high-cost-of-entry reasons.

Maskless Lithography Systems are like Rapid Prototyping Tools

The second analogy that is worth exploring in our effort to understand the likely potential impact of maskless lithography, is the comparison of maskless systems to *rapid prototyping tools*. Rapid prototyping offers the capability of combining computer-assisted design and manufacturing with rapid fabrication methods in order to allow inexpensive part production (as compared to the cost of a conventional production line). Rapid prototyping enables a company to test several different inexpensive prototypes before committing infrastructure investments to a specific approach. Combined with manufacturing system improvements to allow flexibility of approach and machinery, rapid prototyping can lead to an *agile manufacturing* capability. In an alternative approach, the company can use its virtual capability to design and then outsource product manufacturing, thus offloading capital investment and risk. This capability is in synergy with IT revolution in the sense that it is a further factor in globalizing manufacturing capability and enabling organizations with less capital to have a significant technological effect [Ref 1-6].

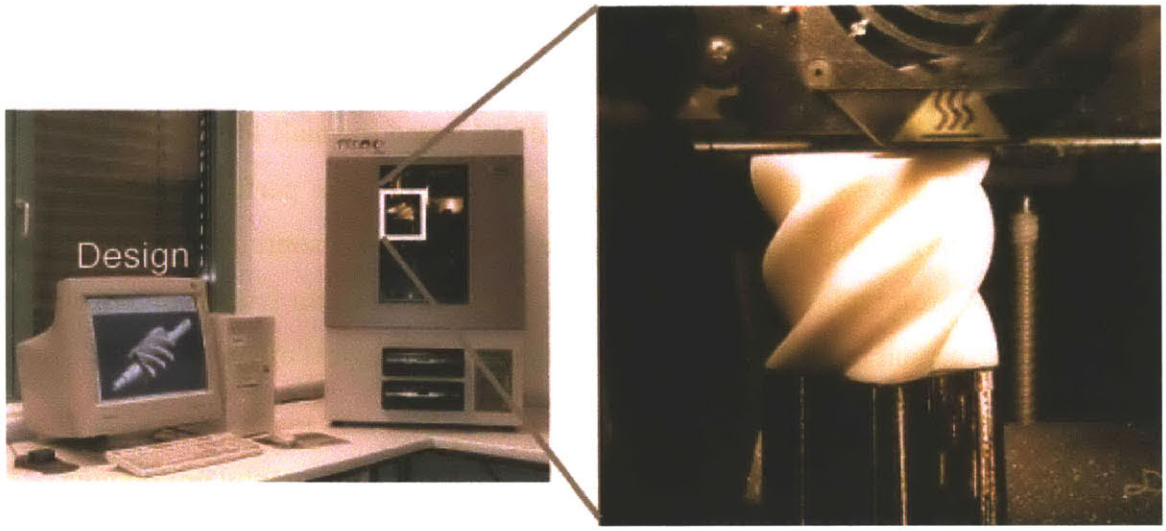

Figure 1 - 3. Rapid prototyping system. Test structures and prototypes can be quickly created in order to verify and test alternative designs.

Rapid prototyping systems (see Figure 1-3), create plastic prototypes that closely resemble the intended production material in order to verify the appearance of the design before committing to large-volume production. Functional parts can be tested, changes in the design can be made, and more sets of parts can be quickly created as needed. With rapid prototyping, projects can move more quickly, and products can enter the market sooner.

The typical sequence of a rapid prototyping process is as follows:

1. A computer generated design file (typically a 3-D CAD drawing) is generated.
2. The material in which to fabricate the part is chosen.
3. A precision roller mechanism automatically spreads a thin layer of the appropriate powdered material across the build platform.
4. Using data from the design file, a laser draws a cross section of the object on the layer of powder. As the laser draws the cross section, it selectively "sinters" (heats and fuses) the powder, creating a solid mass that represents one cross section of the part.
5. The system repeats these steps, forming layer upon layer, growing the object until complete.

Maskless lithography tools have the potential to offer the same kind of advantages for micro and nanofabrication as the ones provided by rapid prototyping systems in manufacturing. Chip designs can be fabricated and tested in small lots, designs can be altered as needed, new chips created, and once the devices perform according to specifications, large volume production can be arranged by outsourcing it to foundries. As with rapid prototyping systems, maskless lithography would enable organizations with moderate capital resources to have a significant technological effect.

For comparison purposes, the typical sequence of a maskless lithography prototyping process would be as follows:

1. A computer generated design file is generated (in kic, or other industry standard formats).
2. The substrate in which to fabricate the device is chosen (Si, GaAs, etc).
3. The substrate is coated with a photosensitive material (a resist) that is compatible with standard semiconductor fabrication procedures.
4. Using data from the design file, an array of radiation beams (could be photons, electrons, ions) "draws" on the resist the desired pattern. The substrate is then processed to achieve the printed pattern.
5. The substrate is processed as needed (evaporations, etching, implantation, etc)
6. The system repeats these steps, forming layer upon layer, "growing" the device until complete.

As can be seen from comparing the typical fabrication sequences from the rapid prototyping and the maskless lithography processes, the similarity is rather remarkable. It is hence reasonable to conclude that maskless lithography systems, if available, would offer advantages of the kind we find in manufacturing with rapid prototyping processes. The existence of these new sets of advantages would then, in turn, alter the current semiconductor design sequence, in favor of more experimental approaches that can be tested prior to ramping up manufacturing. Unleashing the creativity of designers that currently operate with overly conservative designs would be one of the positive consequences of introducing maskless lithography into the market place.

We have seen then, that maskless lithography systems have the potential to offer benefits akin those seen in the printing market with the introduction of the laser printer, and those obtained in the manufacturing world obtained due to rapid prototyping processes. Maskless lithography is like a laser printer in the sense that the throughput is sufficient for low to medium volume production (this is not the case for rapid prototyping tools), but is like a rapid prototyping system in the sense that these systems are not consumer products and fit as a part of a larger manufacturing process.

As a final note regarding possible analogies and comparisons with other industries that could shed some light on what we are likely to see within the realms of the semiconductor industry in the near future, a possible scenario is that the industry will become a manufacturer of commodities (just as cars are in the automotive industry). Product differentiation will then not arise from new innovations, but rather from *customization* (as is the case in the automotive industry, where car manufacturers differentiate their products through customized stereo systems and leather interiors, rather than through radical new engine designs). Were this scenario to be the case, maskless lithography tools would be capable of adapting to the commoditization of the industry by allowing custom chips to be produced in a cost-effective manner.

1.2.2. Cost of Masks and CoO Models

There are many "Moore's Laws" in the semiconductor industry. The original law, and by far the best known, states that on average, the number of transistors in a state-of-the-art integrated circuit doubles every 18 months [Ref 1-7]. The other "Moore Laws" do not necessarily originate from Gordon Moore, co-founder of Intel, but appear due to exponential growth of many aspects of the semiconductor manufacturing process, ranging from the complexity of designs, to the exponential growth in the cost of fabs, tools, masks and processes, to name just a few. The relevant question is not determining whether Moore's Law will continue to go on forever (it obviously can't), but rather to figure out what wall will be hit first. Is it a technical wall (i.e. we can not print smaller features, or grow oxide that is thin enough)? Is it a design wall? Is it a cost wall?

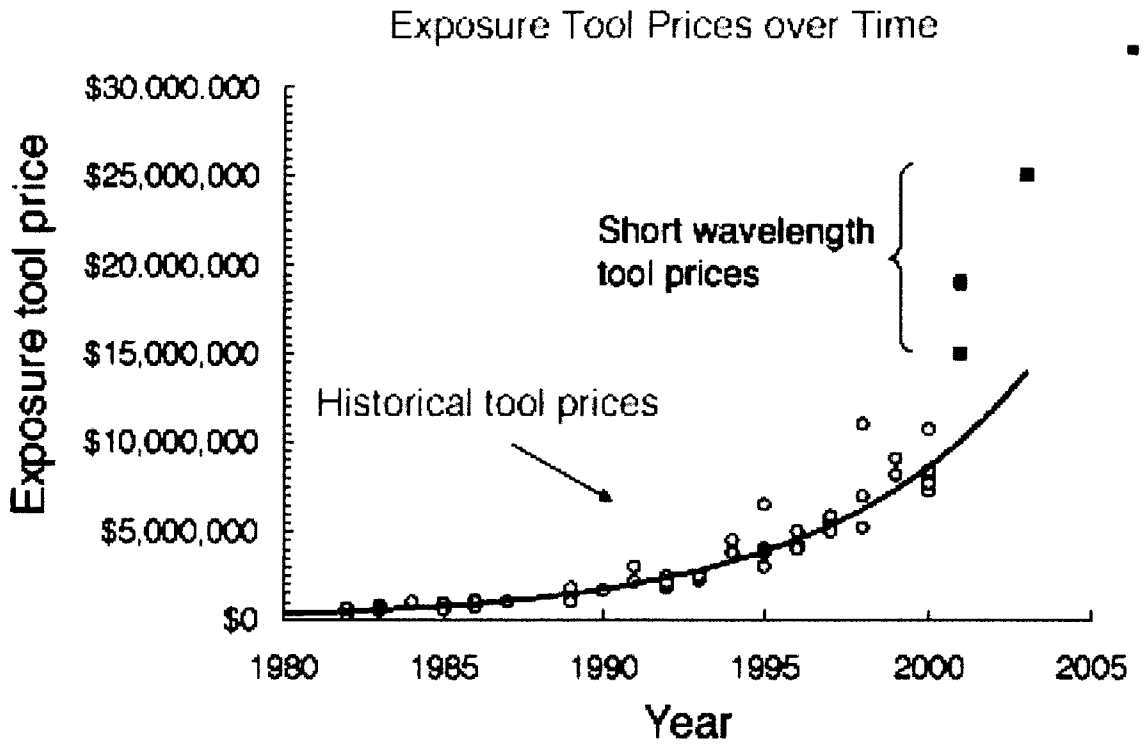

Figure 1 - 4. Plot of exposure tool prices over time. The cost of semiconductor lithography tools has been growing exponentially. Source: The Semiconductor Research Corporation

Not being the keeper of the magic crystal ball, it is hard to anticipate the future of the $200B semiconductor industry, but it is clear that cost concerns are currently running pretty high on the list of the most likely contender to spoil the amazing run of the industry over the last 40 years. To keep the discussion confined to lithography, let's analyze some trends to see the unsustainable nature of the current cost structure. The cost of semiconductor lithography tools is growing exponentially, as depicted in Fig.1-4. The continuation of this trend indicates, as illustrated in Fig.1-5, that the $100M lithography tool will be here in the next three technology generations. Compounded to the skyrocketing prices of lithography tools are the rapidly growing costs of photomasks. Million-dollar mask-sets are already a reality, and under the most optimistic model, the

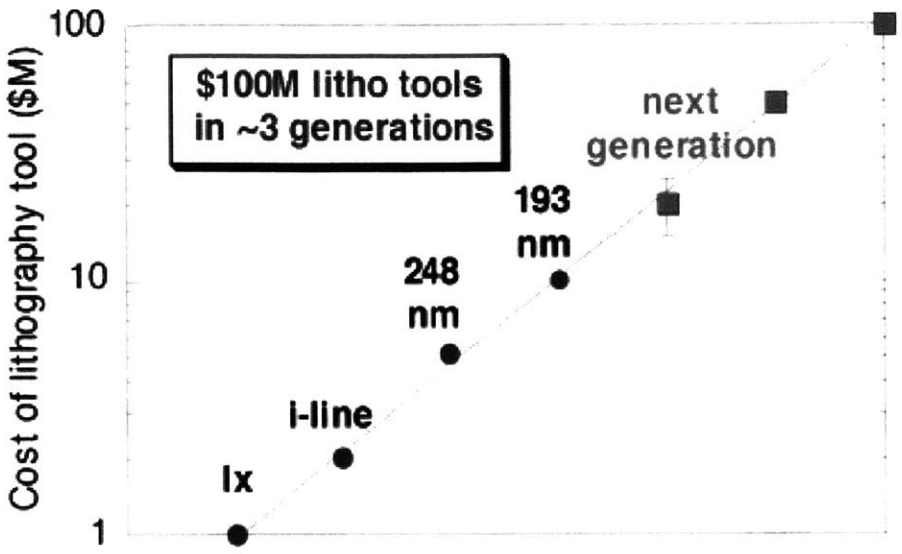

Figure 1 - 5. Cost of lithography tools. In three generations, the $100M tool will be a reality. Source: The Semiconductor Research Corporation

cost will be in excess of $2.5M if the EUV tools are introduced at the 50 nm node[1], as indicated in Fig.1-6. The complexity of the masks is increasing to such an extent, and the costs are so high, that we can expect mask costs to dominate future Cost-of-Ownership (CoO) structures in semiconductor manufacturing. According to the calculations of Bill Arnold, ASML Lithography's executive scientist, if we assume that a typical mask is able to print ~2,200 wafers before having to replace it, the CoO impact of masks on the total fabrication process will rise from 30% with 193nm systems to 60-70% if EUV systems are utilized (see Fig.1-7).

One of the reasons the cost of masks is coming to dominate the CoO of semiconductor lithography processes arises from the fact that the task of masks now goes beyond just making a larger version (say 4x) of the intended pattern. The mask has become an integral part of the imaging system, contributing significantly to optimizing image delivery of the optical system. As a consequence, the mask no longer looks like the final pattern that is to printed, but rather contains all sorts of serifs, phase shifting features and other tricks in order to enhance the quality and process latitude of the final

[1] The $2.5M EUV mask set assumes 8 critical EUV layers, at $250K/layer, and sixteen noncritical layers, at $30K/layer.

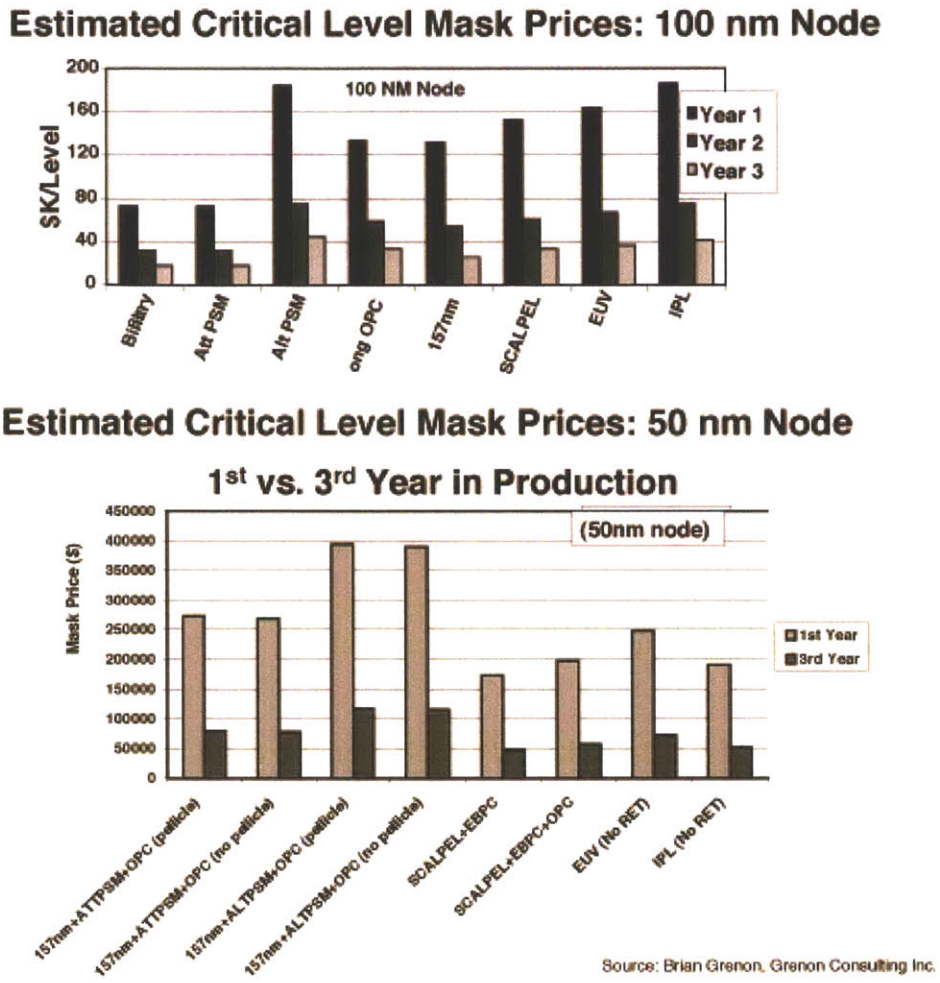

Figure 1 - 6. Estimated critical level mask prices for the 100nm node (TOP) and the 50nm node(bottom). At the 50 nm node, if EUV technology is used, a mask set will cost in excess of $2.5M

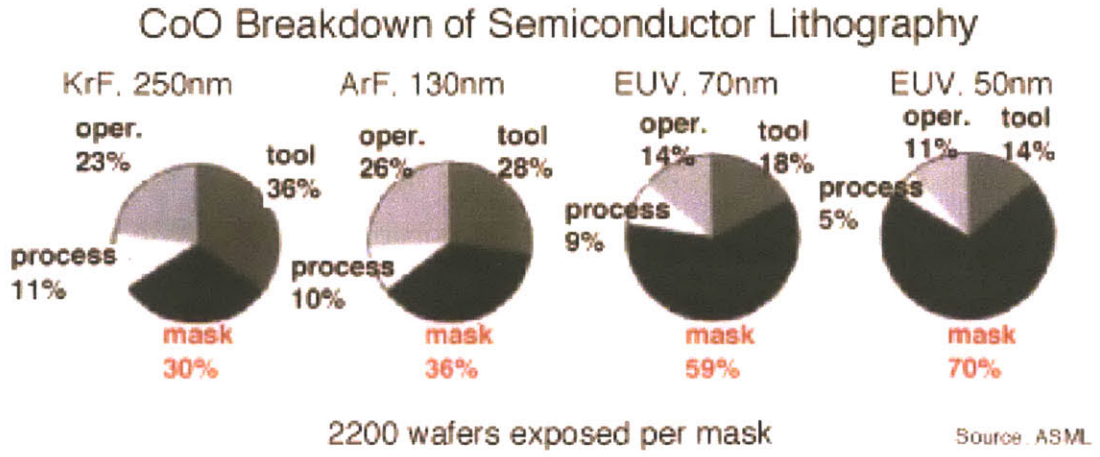

Figure 1 - 7. Mask Costs may dominate future CoO structure for semiconductor lithography. The CoO impact of masks on the total fabrication process will rise from 30% with 193nm systems to 60-70% if EUV systems are utilized.

image. Inspection, metrology and repair technology are also significant contributors to the cost of masks. The repair technology area has been identified as critical to reducing mask cost and cycle time. Since defects are the primary yield-loss mechanism in mask making, and the repair process occurs relatively late in the mask fabrication sequence, the impact of loss of the mask from lack of sufficient repair capability is quite high for both cost and cycle time.

The industry is also exploring ways to make the use of masks more efficient, especially for relatively low wafers-per-mask business where mask costs are a significant issue. Combining multiple customers on a single mask has been proposed as a remedy to the rising cost of mask for customers requiring low volume production. However, this "sharing" approach to chip production introduces other market coordination problems between customers who might need different products at different times. Sharing masks implies sharing production times, and this is a second-best solution.

An alternative economic (and not technological) strategy has been proposed by DuPont Photomask, one of the largest providers of photomasks for the semiconductor industry. The strategy relies on breaking into different domains the needs and requirement of different customers within the industry. Since device designs vary by customer, by end-use application, by process, and by mask layer, the strategy realizes that the "one process fits all" approach to photomask product offerings is inefficient and outdated. The strategy aims to lower costs to different users by offering different mask technologies, at different price points for different types of chips. The market is divided into three distinct segments: high performance, high volume devices, such as DRAMs and microprocessors; medium wafer runs of devices, such as system-on-chip (SoC) and field-programmable gate arrays (FPGA); and low-volume, high-performance devices, such as application-specific integrated circuits (ASICs). Depending upon the technology node, typical masks will cost $750,000 for the high-volume ICs, $550,000 for medium wafer runs, and $450,000 for ASICs [Ref 1-8]. As can be seen, the strategy might offer some temporary economic pain relief to certain customers, but it is clear that the costs remain high for low-and-medium-volume users, and that in the long run, better solutions will have to be found.

As a consequence of the limited technological alternatives to the high-cost high-volume model currently operating within the industry, it is becoming increasingly difficult to bring new designs to market via conventional methods. Instead, potential new designs are being abandoned in favor of other alternatives, such as software implementations using fast processors, DSPs, gate arrays or programmable ASICs—all options that seek to reduce or eliminate the need for new reticles. In the end, raising the barrier to new designs could have devastating consequences for the industry. Lithography, which has for so long been the technology enabler, is becoming an obstacle. [Ref 1-9]

1.2.3. Market Potential

Based on *current* market conditions, it would be cost-effective to produce approximately 25% of today's integrated circuit (IC) chips with a maskless lithography tool if one existed.[2] Maskless tools would also enable design verification and rapid prototyping of chips, something that *cannot* be done with the present cost structure of IC fabrication facilities. The flexibility afforded by a maskless tool will generate additional market demand for maskless lithography.

A number of major manufacturers of lithography equipment have identified the existence of this market, and have expressed the intent of developing *some* form of maskless lithography. Micronic of Sweden is already developing and selling a maskless system for the semiconductor industry (ASML is associated with this venture). KLA-Tencor, although not currently a manufacturer of lithography equipment, has expressed interest in developing a tool in the future. Applied Materials, the largest equipment manufacturer of the semiconductor industry, also has active plans to explore the opportunities offered by maskless lithography. Micronic is likely to be first to the market. They will not be there alone for long.

---

[2] Private communication, Kevin Cummings, PhD, Director, Advanced Reticle Technology, ASML. The maskless lithography tool assumes a throughput of at least one 300mm wafer per hour.

$M	CAGR	2002	2003	2004	2005	2006	2007	2008
Lithography Tool Market[3]	15%	4,945.00	5,686.75	6,539.76	7,520.73	8,648.84	9,946.16	11,438.09
%Maskless[4]		0.0%	1.0%	1.7%	2.9%	5.0%	12.0%	20.0%
Maskless Market		0.00	56.87	111.83	219.91	432.44	1,193.54	2,287.62

Table 1 - 1. Lithography and maskless tool market estimates.

In 2001 the market for lithography tools was $4.3B.[5] Historical growth rates for semiconductor capital equipment sales over the last 20 years have been 10-15%.[6] *Using* 12.5% CAGR, the lithography tool market will be ~$10B by 2007. By that time, the maskless lithography market will be in excess of $1B.

1.3 Review of Maskless Lithography Techniques

A number of research groups around the world, from academia as well as industry, have proposed over the years a large variety of maskless lithography techniques. While it is not the purpose of this section to provide a comprehensive account of all the proposed techniques (they are far too numerous), it is worthwhile to provide a flavor of some of the leading candidate techniques and a brief assessment of their main virtues and deficiencies. In this context, it will be easier to appreciate the relative position of the technique that was developed in this thesis, ZPAL. For clarity the relevant techniques have been divided into photon-based systems and charged-particle systems.

---

[3] 2000-1 data from Standard & Poors Industry Surveys, "Semiconductor Equipment," August 15, 2002. Semiconductor Capital Equipment CAGR 10-15% over 20 years from Lehman Brothers, "Semiconductor Capital Equipment: Estimate Leapfrog Continues," 9/12/2002. However, lithography costs historically "have risen faster than overall [semiconductor equipment] costs," (R. Castellano, *The lithography equipment marketplace*, Solid State Technology 1/1/2001). The model assumes a CAGR of15% for lithography tools.

[4] Assume first maskless wafer tool 2003 (Micronic), grow to 25% of market (based on current wafers/lot.

[5] Standard & Poors Industry Surveys, "Semiconductor Equipment," August 15, 2002.

[6] Lehman Brothers, "Semiconductor Capital Equipment: Estimate Leapfrog Continues," 9/12/2002

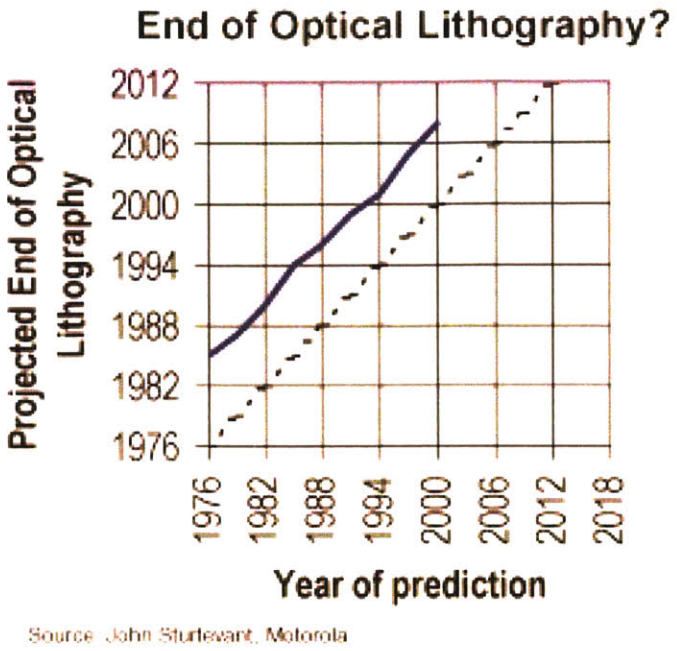

Figure 1 - 8. Expert opinions on the death of optical lithography. As can be seen, optical lithography has been a survivor over decades, despite experts predicting its demise 7-8 years down the road of any given year.

1.3.1. Optical Systems

Optical lithography has been the technology of choice for the semiconductor industry for more than 30 years, taking the feature sizes from 10 microns in the late 1960's to present production feature sizes of 0.13 microns and below (90 nm node). Currently, the most advanced lithographic tools used in high-volume manufacturing employ deep-ultraviolet (DUV) radiation with a wavelength of193nm, with plans to move to 157nm in the near future. An interesting piece of trivia, that nonetheless sheds some light onto the remarkable run that optical lithography has had in the industry, is shown in Fig.1-8. The figure plots expert opinions on the death of optical lithography with respect to any given year of production. Interestingly enough we observe an almost constant belief that the demise of optical lithography will come 6-7 years down the road. While I am not sure my credentials warrant the title of expert, it is rather amusing to think that, if asked today, I too would say that in terms of resolution, the end of optical

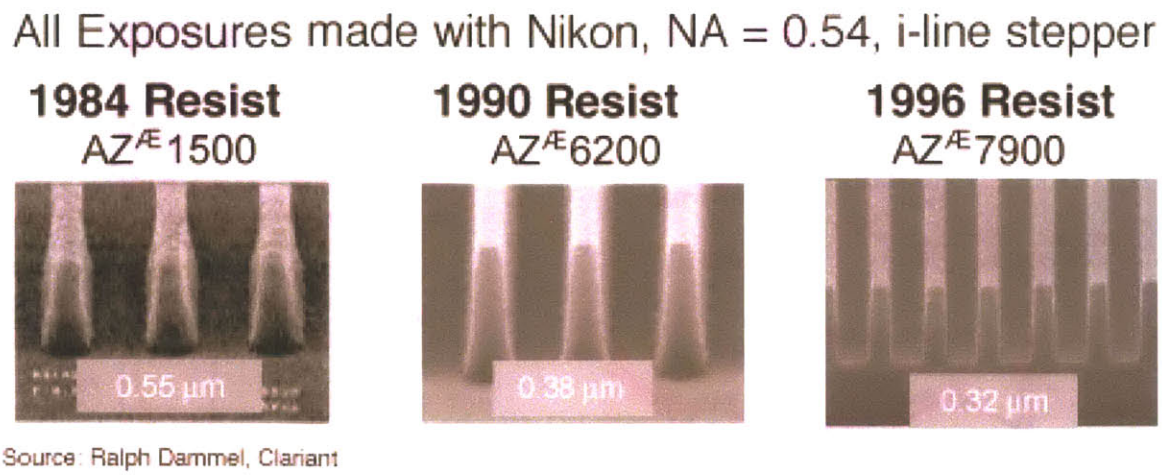

Figure 1 - 9. Contribution of resist advancements to high-resolution lithography. Using the same I-line lithography stepper, improved resist chemistry enables finer resolution and better profiles. All three resists used were considered state-of-the-art at the time. The experiment was performed by Ralph A Dammel from Clariant.

lithography will come 6-7 years down the road. At the same time, considering the alternatives, it is perfectly possible that optical lithography will remain the only *economically viable* technology even far into the future. Time will tell whether I become one more data point of an updated graph in the near future

The 30-year run success story of optical lithography has brought with it numerous improvements in related technologies. Laser systems have been developed that operate at ever decreasing wavelengths. These lasers are more reliable, stable, and powerful than ever before. UV optics have also improved dramatically. It is now possible to obtain deep-UV lenses with NA's of ~0.8 and over 10^{10} pixels per field. Resist technology has also improved tremendously, as illustrated in Fig.1-9. It is probably not unfair to claim that historically, the contribution from resist and resist processing has outweighed stepper improvements [Ref 1-10].

The interrelated set of technological improvements that we have just mentioned (better lasers, better optics, mature resists, etc) in combination with the power of fast computers, form the basis for, and provide the rationale, developing all-optical maskless lithography systems. Let's look at two of the leading optical maskless systems currently present in the market.

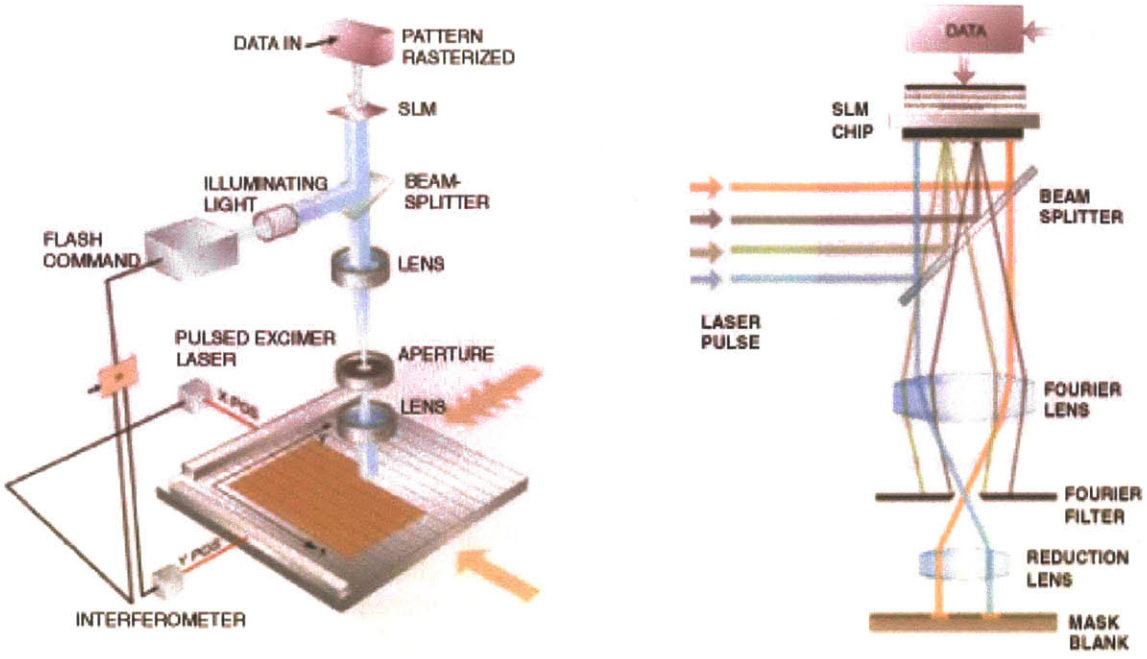

Source: Micronic Laser Systems

Figure 1 - 10. Schematic of Micronic's maskless lithography system (Sigma7000 series).

1.3.1.1 The Micronic System

Micronic Laser Systems of Sweden [Ref 1-11], a leading manufacturer of high-end laser pattern generators for the production of photomasks and flat panel displays, has been developing maskless optical lithography systems since the 1980s. Until recently the systems the company developed were aimed at the fabrication of photomasks, since the limited throughput and lack of massively parallel architectures prevented the use of such tools for direct wafer patterning.

With the introduction of the Sigma7000 Series, Micronic is, for the first time, attempting to develop an optical maskless lithography system capable of printing on wafers. The system, depicted schematically in Fig.1-10, utilizes a pulsed laser, a spatial light modulator, and conventional refractive optics (akin to those used in steppers but with much higher demagnification) to print directly onto wafers. In order to maximize process compatibility with existing techniques, the system is designed to resemble as much as possible a stepper.

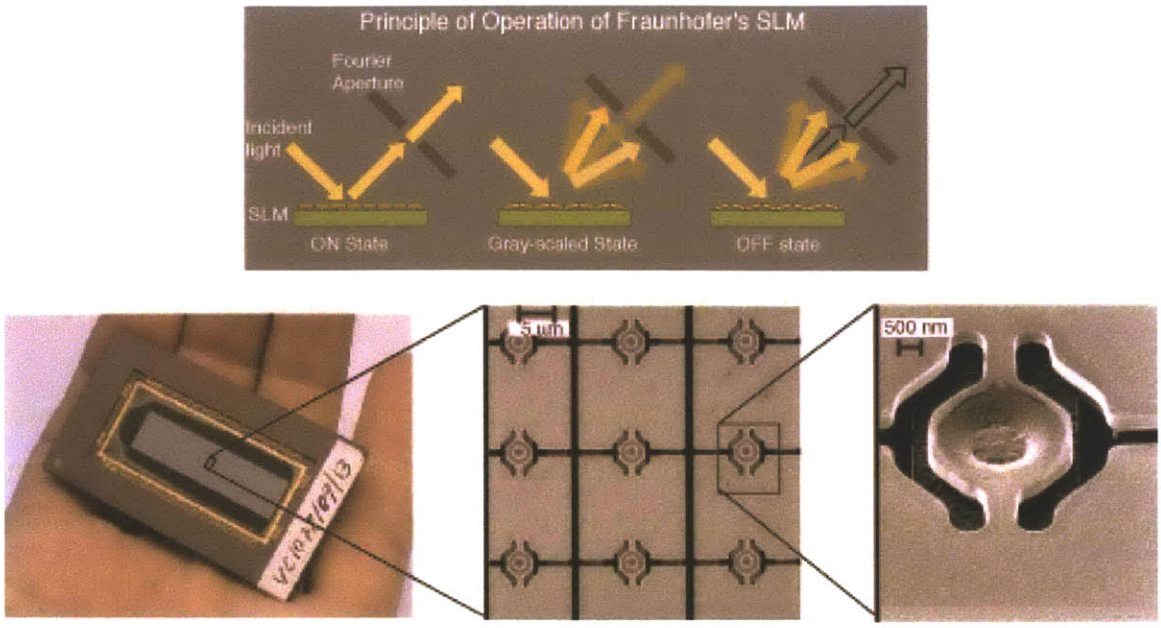

Figure 1 - 11. The Fraunhofer Spatial Light Modulator (SLM). TOP: Principle of operation of the SLM. The SLM is an integrated circuit with a flat, mirror-like surface. Individual mirrors are either flexed or remain flat. The ON-State maintains the mirrors in the flat position, allowing the reflected light to pass through the Fourier aperture. By controlling the deflection of the mirrors, light is scattered from the mirrors, allowing either partial transmission (gray-scaling), or no transmission (OFF-State) through the aperture. BOTTOM: Pictures of the SLM. The mirrors are 16µm x 16µm in size and are electrostatically actuated. The mirrors can torque about a pair of hinges located at the top and bottom of each element.

The architecture of the Micronic system is as follows. Pattern modulation is created by programming a spatial light modulator (SLM). The SLM has a flat surface composed of a million mechanical micro-mirrors, which can be deflected at will by means of electrostatic forces (see Fig.1-11). Areas of the SLM with deflected mirrors scatter light outside of a Fourier aperture (see Fig.1-10), and can be totally blocked by the aperture (and hence prevented from reaching the substrate), or can be attenuated, providing a grayscale exposure. The stage with the substrate is scanned continuously with precision by means of a laser interferometer that also commands the laser to flash when it reaches the position of the next field. The short flash time, about 20ns, ensures that the moving stage is virtually "frozen" at each exposure. After each flash, the SLM is reloaded with a new pattern in time for the next flash. Large area patterns are stitched together by overlapping fields.

The current implementation of the system utilizes 248nm wavelength, and numerical aperture of 0.75. As previously mentioned, one of the rationales behind Micronic's maskless solution was to provide an architecture that is virtually identical to a stepper. By doing this, standard techniques such as annular, dipole and quadrupole illumination can be used. These techniques are aimed at expanding the process latitude and the resolution of optical lithography systems. They also add to the complexity and the cost.

Micronic's current "maskless stepper" is one to two orders of magnitude slower than a stepper, capable of printing 1Gpixels/sec. With a projected pixel size of 50nm, and given that a 300mm wafer contains $2.8x10^{13}$ pixels, assuming a single pass exposure (in reality two passes will be needed for their system), it would take close to 8 hours to expose one 12" wafer. For this reason, the tool is currently marketed as a mask writer. However, plans are in place to build a system that will be capable of printing two 300mm wafers/hour, with a NA = 0.7, operating λ = 248nm and with a resolution of 130nm. The necessary data delivery rate for such a system is 30 Gpixels/sec.

1.3.1.2. The ALTA System

Since first introduced in the mid-1980's, raster-scanned laser pattern generators have become the workhorse volume production systems for mask-making in the semiconductor industry. The best known of these systems are the ALTA-based tools, manufactured by Etec Systems, an Applied Material's company [Ref 1-12]. Although all ALTA tools are aimed exclusively at mask-making, and not at direct write applications, it is worth describing such systems because: (1) they are maskless lithography tools, (2) they provide some level of parallelism (e.g. multiple beams write simultaneously), and (3) proposal have been made to increase their throughput significantly. By analyzing in some detail their architecture, valuable lessons can be extracted concerning the achievements and limitations of these raster-scanned laser pattern generators.

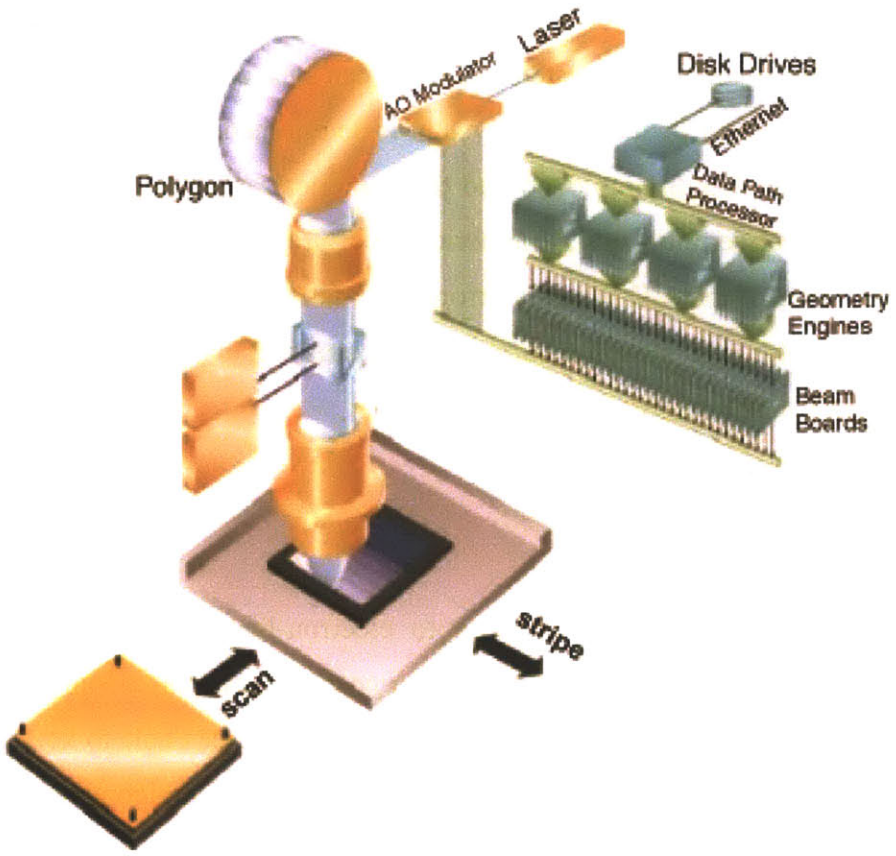

Figure 1 - 12. The ALTA system architecture. Source: ETEC Systems.

The ALTA raster-scanned reticle writer is depicted schematically in Fig.1-12. A CW laser beam (the latest tools operate using a λ=257nm frequency-doubled Ar-ion laser) is split into 32 individually addressable beams, called a brush. An Acousto-Optic Modulator (AOM) controls and modulates the intensity of the beams. The brush is scanned across the mask by means of a rotating 24-facet polygonal mirror. A single polygon facet scanning the brush "paints" an area that is 4096 pixels wide by 32 pixels high. As the brush is scanned across the mask by the polygon, the laser-interferometer-controlled air-bearing stage moves at constant velocity in a direction perpendicular to the scan, called the stripe direction. By stitching successive "brush-strokes", large area patterns can be written.

At the mask, the pixels lie on a rectangular grid, with a spacing that is typically one-half the size of the focused beams (measured at full-width-at-half-max (FWHM)). Beam intensity at each grid position is varied by means of the AOMs to enable the

necessary gray-scaling to achieve accurate edge placement. In addition, by printing each pattern as many as four times, systematic errors can be averaged out.

The resolution of the ALTA system is determined, as is all optical lithography tools, by the wavelength employed and the numerical aperture of the imaging system. The latest models employ a 0.8 numerical aperture, 33x reduction lens operating at λ=257nm. At tolerable CD linearity errors (e.g. % deviation of exposed feature from its intended width/length), 200nm features can be patterned. This resolution is sufficient to meet the mask making needs of the 130nm node.

The Limits of the ALTA Architecture

Laser mask writing, compared to electron-beam mask writing, offers the advantage of high-writing speeds and a lower cost-of-ownership. Since the mid 1980s, through evolutionary forces, laser pattern generators have been able to keep pace with the mask-making industry, and currently represent 40% of the semiconductor mask-writers sold [Ref 1-13]. However, laser pattern generators based on the ALTA architecture are currently at their resolution limit, and are often not capable of writing the most critical masks necessary for 100nm production. They have become complements to e-beam lithography systems, relegated to the manufacturing of all the non-critical layers.

The leading problem facing the ALTA architecture is its insufficient level of parallelism. With only 32 beams, the system is limited to CW sources (in order to maintain some decent throughput, since short-wavelength pulsed laser tend to have low repetition rates). Increasing the number of beams in the ALTA systems is not an easy task, since each parallel beam requires its own macroscopic AOM and an independent data path. While it is conceivable that the number of beams could be doubled by some painstaking engineering integration, the number of beams would sill fall short by over four orders of magnitude to those required for pulsed lasers. Constrained to CW sources, the ALTA architecture can not scale the wavelength below the current 257nm, hence limiting the only solution available to keep pace with the resolution requirements of the industry.

1.3.2 Short Wavelength Systems

There is a simple and plausible reason for drastically reducing the wavelength of an imaging system that is to be used for high-resolution lithography. The reason comes from two of the most fundamental equations that describe the characteristics of an imaging system. These equations are usually expressed as

$$\text{Min.Linewidth} = k_1 \cdot \frac{\lambda}{NA} \qquad 1\text{-}1$$

$$DOF = k_2 \cdot \frac{\lambda}{NA^2} \qquad 1\text{-}2$$

where λ is the wavelength of the radiation used and NA is the numerical aperture of the imaging system. What's apparent from these equations is that we can improve the resolution of an optical system by decreasing the wavelength and increasing the NA. But we can also see that if we do so we have to pay a price for it, that is, the reduction of the depth-of-focus. The case $k_1=1/2=k_2$ corresponds to the usual definition of diffraction limited imaging.

The question of how much one should reduce the radiation's wavelength is the source of much controversy. The first thing to consider is what optics can be used as we move to shorter wavelengths. Every material becomes absorbing for wavelengths shorter than 110 nm [Ref 1-14]. This absorption decreases gradually toward shorter wavelengths, while at the same time the refractive index approaches a value close to 1. These facts eliminate the possibility of using refractive optical elements, such as lenses and transmission masks at EUV wavelengths, making it necessary to have the imaging system entirely reflective and carried out in vacuum. Alternatively, diffractive optical systems can also be utilized.

But even reflective surfaces are a tremendous challenge at wavelengths below 110nm, and to achieve a reasonable reflectivity, multilayer structures have to be used. These structures consist of a large number of alternating layers of materials having dissimilar optical constants at the wavelength of interest, and they provide a resonant reflectivity when the period of the layers is approximately $\lambda/2$.

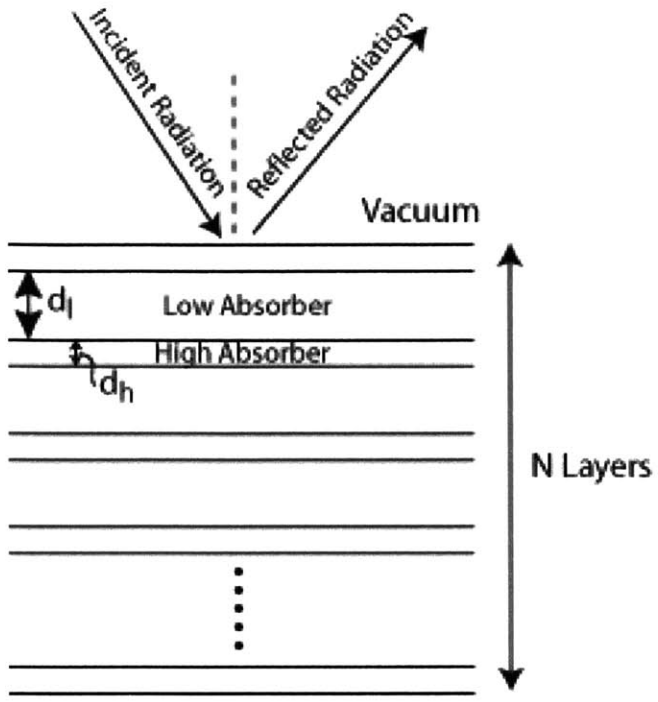

Figure 1 - 13. Principle of operation of multilayer mirrors

High reflectivity multilayer mirrors are obtained when all boundaries, or at least all periods, add in phase with the reflected wave. Multilayer mirrors consists of alternate layers of materials with high and low absorption (Fig.1- 13). The periodicity of the structure is $d = d_h + d_l$, but the thicknesses d_h and d_l need not be constant as functions of z, the depth of the multilayer, so long as d remains constant. As previously mentioned, the purpose of using multilayers is to get around the strong absorption that all materials exhibit at short wavelengths. To minimize the detrimental effect of absorption, the standing wave field that gets produced within each multilayer can be utilized advantageously. The basic idea is to position the highly absorbing material in very thin layers into the nodes of the standing wave field, and fill the remaining space with a material with very low absorption. The standing wave field is produced due to superposition of the incident and reflected waves. By placing thin absorbers at the nodes of the standing-wave (see Fig.1-14), the small contributions from all the thin films will

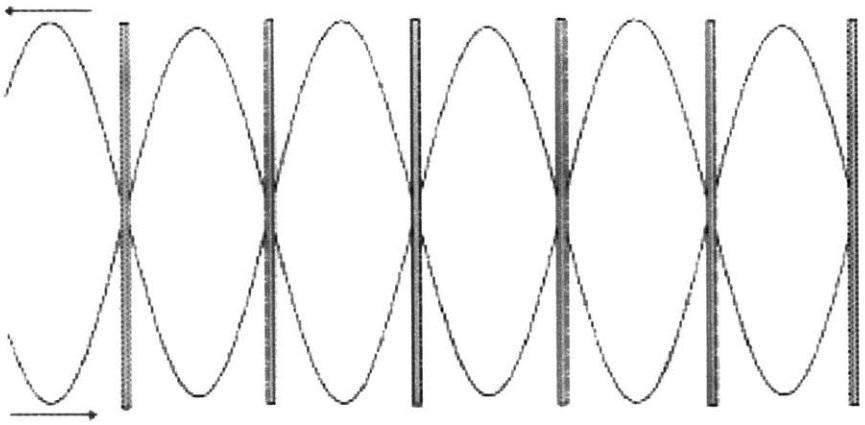

Figure 1 - 14. Standing wave field

add in phase with the reflected wave. In the limit of very thin films, and very large number of periods, the absorption losses approach zero and the reflectivity 100% [Ref 1-14]. Even though in theory reflectivities of 100% are possible, the measured performance of a multilayer is much lower than this value due to errors in layer thickness, contamination, uncertainties in the optical constants and quality of the boundary, just to name a few parameters. As a consequence, EUV researchers are required to fabricate multilayer mirrors with unprecedented perfection.

Surface figure errors on the mirrors must be within 0.25 nm rms [Ref 1-15] and the roughness of the substrate must be better than 1/10th of the period (Period = $\lambda/2$=6.75 nm) [Ref 1-16].

1.3.2.1 Maskless EUVL

Identifying the resolution advantages of short-wavelength systems, as well as the importance of maskless lithography, researchers at the University of California at Berkeley are currently investigating maskless EUV approaches [Ref 1-17]. In the proposed maskless EUV approach, the EUV mask is replaced by a digitally configurable mirror array whose reflectance properties can be varied by modulating the mirror's tilt or translational positions. Although the system is maskless, it nevertheless requires EUV projection optics to image the micromirror array onto the wafer, with the added complication that the 20 to 40X demagnification required for the mirror array far exceeds

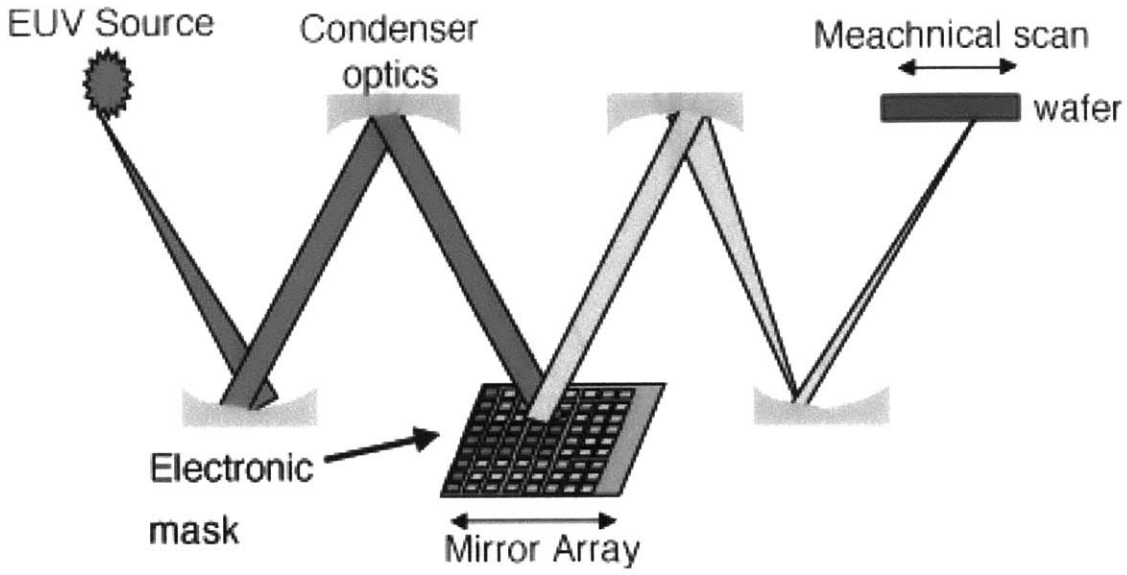

Figure 1 - 15. Schematic diagram of the maskless EUV system proposed by researchers at UC Berkeley. The system employs an EUV source, conventional EUV reflective optics and substitutes a digitally configurable mirror array for the mask. The wafer is mechanically scanned with respect to the fixed array of mirrors in order to transfer the desired pattern

the 4X EUV optical systems currently under development. A schematic diagram of the proposed EUV maskless system is depicted in Fig.1-15.

The EUV light modulator mirror array designed to replace the mask is depicted in Fig.1-16. Instead of using absorbers to create dark and bright areas in the image, selected mirrors can be modulated using on-chip electronics. The pattern is demagnified and focused to expose the photoresist. The wafer is mechanically scanned while the pattern is electronically scrolled across the stationary mirror array. As the image is electronically scanned over the array, every feature on the wafer receives multiple exposures, each one coming from different mirrors in the array. This built-in redundancy enables defects on the mirror array to be averaged, and hence avoids printing defects on the wafer.

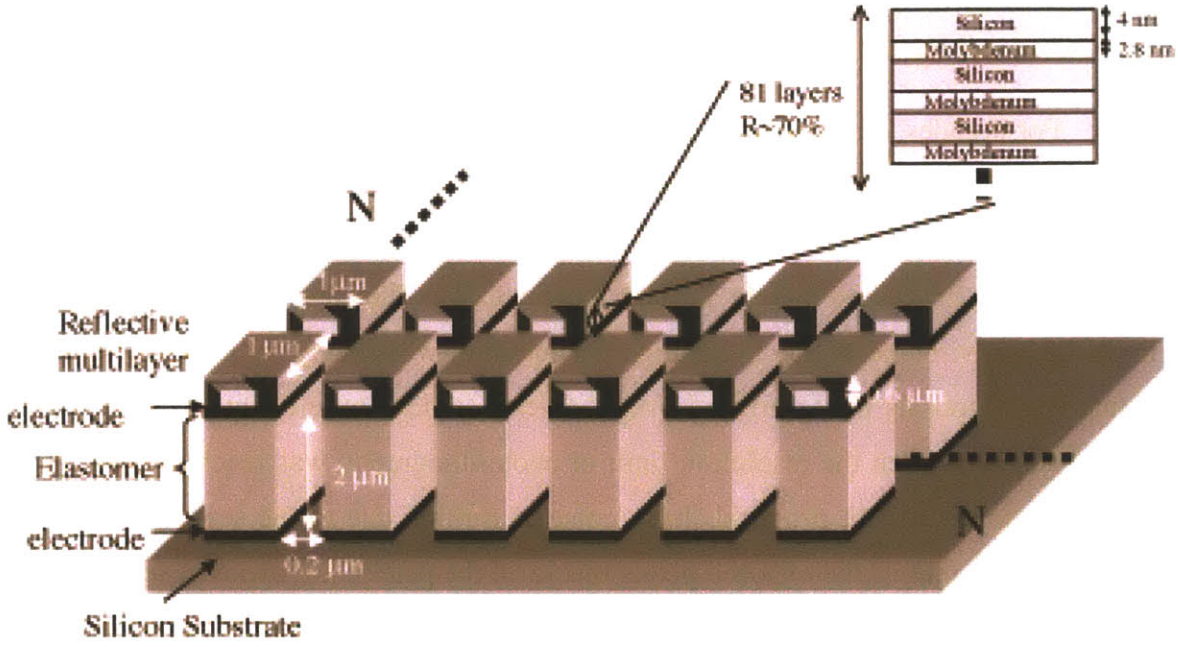

Figure 1 - 16. Pixels of elastometer pillar spatial light modulator. Each pixel is composed of a elastic layer capable of deflection (enabling light modulation) as well as a Mo-Si multilayer coating (in order to achieve high reflectivity)

The maskless-EUV system has the appeal of providing a solution that is compatible with the industry momentum towards the introduction of EUV lithography. In this manner, the technology is linked to the success of this initiative, which still faces enormous hurdles, even after many hundreds of millions of dollars spent. The introduction of EUV keeps getting pushed back (Intel recently announced that EUV is not ready for the 65nm node in 2005, so it will be pushed back to 2009), and with it the viability of this technology. While it remains a worthwhile effort for the very long run, the complexity of a multimillion-micron-sized mirror array sitting on a standard EUV tool (but requiring an even higher degree of demagnification) is likely to achieve a level of unprecedented cost and complexity.

1.3.3. Charged Particle Systems

For decades, electron-beam lithography (EBL) has provided a maskless approach to lithography. First demonstrated in 1958 [Ref 1-18] electron-beam lithography systems have evolved over time to become an integral part of semiconductor manufacturing processes, mainly as mask making tools. They are also widely employed in research environments due to the high-resolution of which they are capable (~20nm). Numerous proposals have surfaced over the years to develop e-beam tools to replace optical steppers when the resolution limit of photolithography was reached [Ref 1-19]. However, none of these proposals have come to fruition due to the serial nature of e-beam systems; that is, the exposed pixels that form the pattern are exposed sequentially, one after the other. Increasing the exposure rate of e-beam lithography has been one of the major priorities in the development of the technology. The following three sections provide brief summaries of some of the most recent proposals on how to circumvent the problem of throughput in electron-beam lithography.

1.3.3.1. Parallel Electron-Beam Lithography Systems

Throughput in electron-beam lithography is fundamentally limited by a combination of beam current and resist sensitivity [Ref 1-20]. In order to increase throughput in electron-beam lithography it is necessary to vastly increase the beam current from that of current state-of-the-art systems (currently ~1nA). To give an idea of what kind of current would be required, we can consider that in order to write one 300mm wafer in one minute (a 60 wafer/hour system), the writing speed required is 11.8 cm^2/s (including overhead). This is over one order of magnitude faster than any combination of e-beam and processes demonstrated to date. E-beam currents far short of the required current of 100μA [Ref 1-21]. In practice, however, the usable current is limited by stochastic Coulomb interaction in the beam path, since it causes loss of resolution at high current. This is due to the need to pass all the writing current through an aperture.

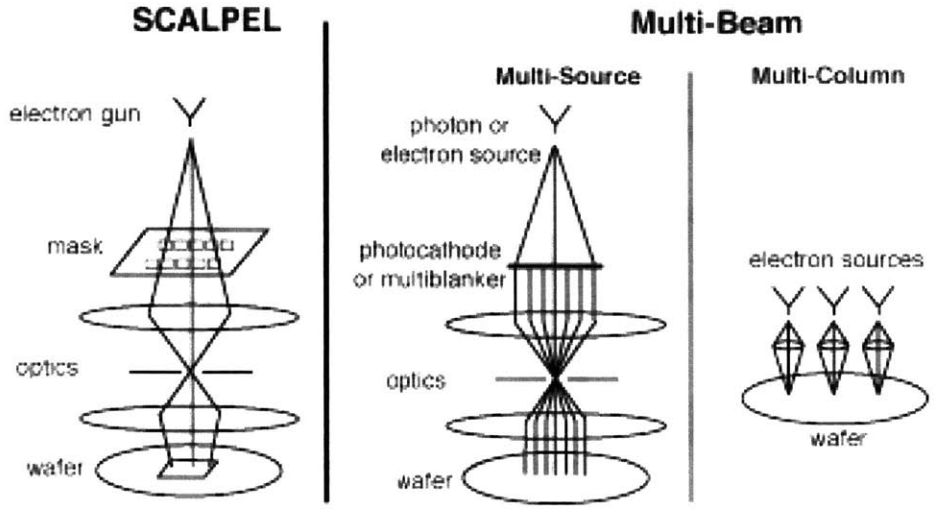

Source: Mark A. McCord, Stanford Univ

Figure 1 - 17. Schematic representation of three approaches to high-throughput electron-beam lithography. For the SCALPEL and multisource approaches, all the electrons share the same set of optics (all electrons passing through at least one crossover). The multicolumn approach minimizes space charge effects by completely separating the beams, but requires a complete set of optics for each individual beam.

A solution to the high-current limitation is provided by distributed systems that are capable of spreading the current over a large volume, minimizing space charge effects. Some of the best known proposals are SCALPEL (**SC**attering with **A**ngular **L**imitation **P**rojection **E**lectron-beam **L**ithography, originally developed by Lucent Technologies), and a variety of multiple beams techniques. The multiple beam approaches can be further subdivided into two categories: multisource [Ref 1-22] where multiple beams are generated in a single optical column, and multicolumn [Ref 1-23] where each beams has its own individual micro-column.

In this section, a multi-beam proposal is briefly analyzed as an example of a distributed electron-beam lithography systems aimed at direct write applications.

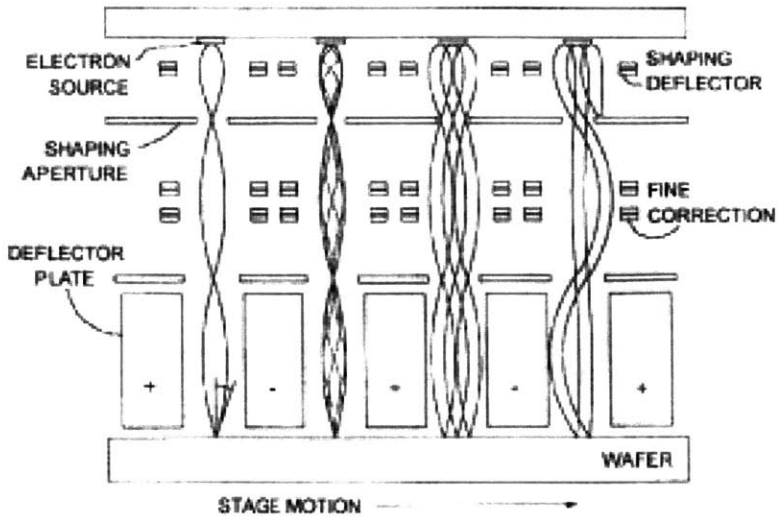

Source: T.H.Groves and R.A.Kendall

Figure 1 - 18. Schematic of multiple-beam DiVa system. Multiple electron sources are imaged onto a square-shaping aperture. Imaging is accomplished by means of a uniform magnetic field, oriented along the focusing axis, permeating through the entire apparatus. A shaping deflector translates the image of the source on the shaping aperture. This produces a rectangular shaped spot of variable size (between 0 and 0.5μm). The spot is imaged onto the wafer, and can be deflected in the direction orthogonal to the stage scanning direction.

1.3.3.2 Distributed Multiple Variable Shaped Electron Beam Lithography (DiVa)

First proposed in 1998 by Tim Goves and R.A.Kendal [Ref 1-24] a maskless DIstributed axis VAriable shaped system (DiVa), in which a uniform magnetic field focuses many beamlets simultaneously. The principle of operation is depicted in Fig.1-18. The system utilizes a planar cathode patterned with a rectilinear array of square emitters. Focusing is accomplished by a uniform, axial magnetic field, oriented along the focusing axis. By a superposition of the magnetic field with a uniform axial electro-static field, a one-to-one image of the emitters onto the writing surface is produced. Deflection plates between adjacent rows of electron beams control the motion in one Cartesian axis, while mechanical translation of the stage achieves patterning in the orthogonal axis.

Multiple beamlets can be positioned next to each other, as shown in Fig.1-18. Each electron source can be controlled independently, allowing for parallelism and increased throughput. Typical spacing between adjacent sources is ~1mm. The appeal of

this system, especially when compared with the multicolumn approaches originally proposed by Chang [Ref 1-25] relies on it relative simplicity. Only one cathode, one lens, and one major deflector are employed. Resolution is limited by diffraction to a few nanometers. The fundamental limitation of the system in terms of throughput is the cathode technology, requiring uniformity and stability to better that 1% during exposure.

A number of the other photocathode based multiple electron beam column approaches have appeared in the last couple of years that are worth mentioning. They are described in the following two sections.

1.3.3.3 The ALTA-MEBES System

Advocated by ETEC Systems, this maskless technique relies on the "marrying" of the two core technologies of the company, the ALTA laser pattern generator (previously described in section 1.3.1.2), and the MEBES electron-beam lithography tools [Ref 1-26]. The idea is schematically depicted in Fig.1-19. Leveraging their existing ALTA technology, an array of 32 individually modulated lasers beams is focused onto a photocathode, creating an array of electron beams. The e-beams are accelerated to 50keV, demagnified 10-20 times, and subsequently imaged onto the substrate. Most of the e-beam column is taken from the MEBES product line.

The technology is a classic example of a multi-source system (see Fig.1-17). It is also a classic example of evolutionary tendencies run amok. What a coincidence that the"right" maskless lithography approach proposed by ETEC happens to be the combination of their two aged lithography solutions! The ALTA-MEBES system could benevolently be seen as a natural extension, a means to combine the parallelism of ALTA with the resolution of MEBES. Not so benevolently, it can be seen as a maskless tool having the problems of both. The means of illuminating the photocathode still relies on a macroscopic AOM for each independent beam, limiting the parallelism of the system, and ignoring simpler and more elegant solutions that employ advances in micromechanical light modulators.

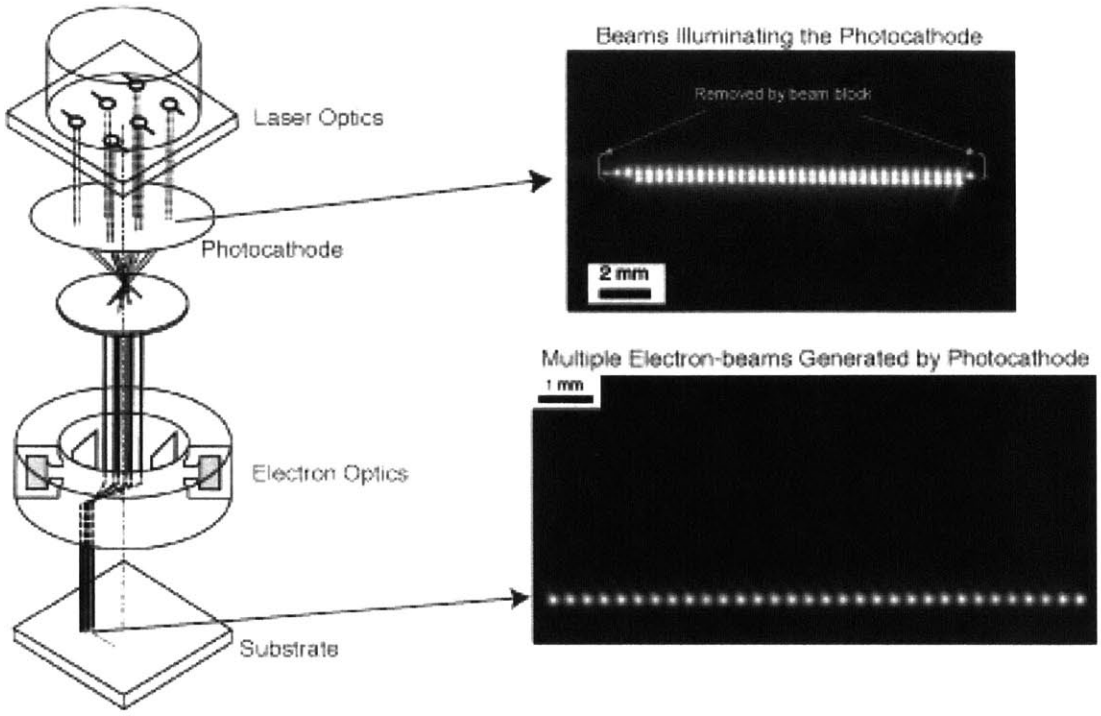

Source: ETEC Systems (an Applied Materials Company)

Figure 1 - 19. The proposed ALTA-MEBES system for raster multi-beam lithography. Multiple independently modulated laser beams are focused onto a photocathode, generating and array of electron beams. These beams are imaged and scanned across the substrate by means of electron optics.

The reliance on the same electron-beam optics employed for the MEBES systems, requiring a common crossover for all the parallel beams, fundamentally limits the current that can be passed through the system due to stochastic Coulomb interaction of the electrons. This limitation will restrict the system to mask making applications alone, provided all the technical hurdles can be bypassed. As a final problem, one shared with the previously described DiVa approach, concerns the sensitivity of photocathodes to surface contamination. Such effects can have very deleterious effects on the ability to dimensionally control each independent beam to a high-degree of repeatability.

The combination of a very expensive and complicated ALTA architecture with a very expensive and complicated MEBES architecture, will no doubt result in a VERY expensive and VERY complicated system. It is doubtful that the exacerbation of cost and complexity of future systems is the right approach for either mask-making and/or maskless lithography.

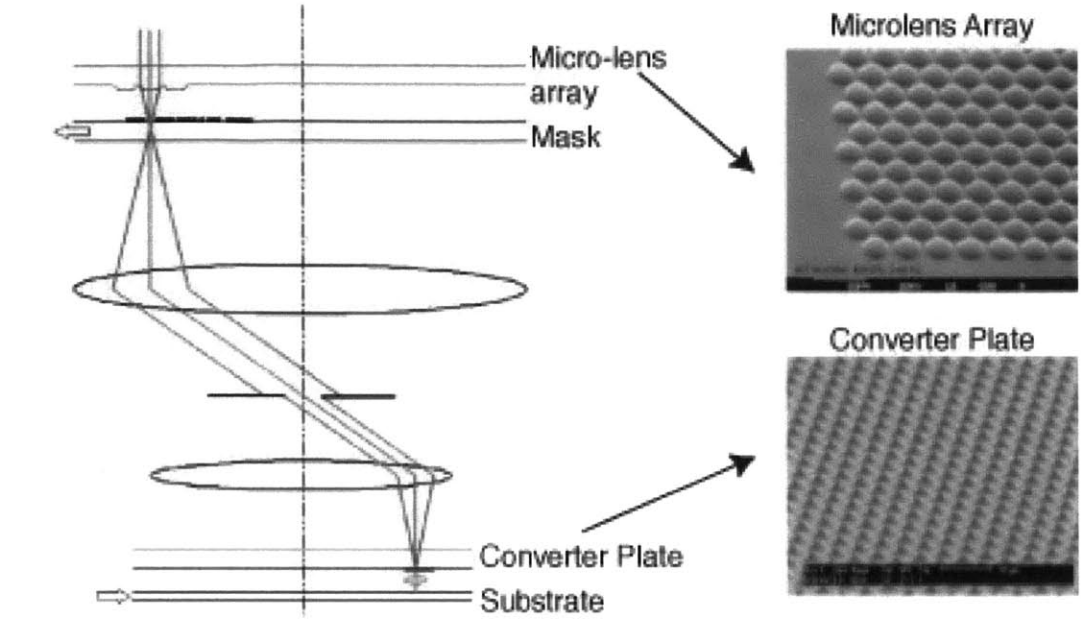

Figure 1 - 20. MAPPER schematic. For the mask-based version of MAPPER, a microlens array focuses an array of diffraction-limited spots onto a mask. The mask is then scanned in synchrony with the wafer. An optical system is designed to allow for the spots that get transmitted through open areas of the mask to reach a converter plate (could be a photocathode). By having an external uniform axial magnetic field, the emitted electrons are imaged onto the wafer.

1.3.3.4 MAPPER Lithography

MAPPER lithography, which stands for "**M**ultiple **A**perture **P**ixel by **P**ixel **E**nhancement of **R**esolution", was first proposed in 1998 by Pieter Kruit, from Delft University [Ref 1-27]. Currently being developed by a small startup in the Netherlands [Ref 1-28], this approach is partially backed by KLA-Tencor, the well-known semiconductor inspection and metrology company. MAPPER is developing two types of lithography systems, both based on an electron-beam microlens arrays controlled by means of an optical illuminator that can have up to one million light sources. For the maskless approach, the idea can be seen as a hybrid between the DiVa approach and the ALTA-MEBES system. It is partly DiVa on its conception because the use of electron

beams remains distributed, with no single cross-over for all beams, allowing for potentially large currents and high throughput. It is partly like the ALTA-MEBES because it relies on an optical imaging system of diffraction-limited spots as the cathode control mechanism to switch the e-beams ON and OFF. However, by relying on massively parallel microlens arrays, a much higher degree of parallelism can be achieved compared to the ALTA-MEBES system, making it a much more powerful architecture.

The principle of operation is the following. In the mask-based version of MAPPER technology, a conventional chromium on glass mask is illuminated by a lerge number of diffraction limited spots. These spots are obtained by means on an array of microlenses, with 10^6 to 10^8 elements potentially. By scanning the mask under the light beams, the clear and opaque parts of the mask act as optical switchers, allowing light to propagate or not. A demagnifying optical system images the array of light spots onto a "converter plate" (could be a photocathode). The converter plate is responsible for generating electrons upon the arrival of the imaged photons. The resolution of the system is enhanced because the electron source is made smaller than the light spot. This can be achieved either by using electron field emitters that are triggered by light, or by using a photocathode with apertures smaller than the size of the focused spots. In order to transfer the mask pattern onto the wafer, the wafer is scanned in synchrony with the mask. Finally, the maskless MAPPER concept is conceptually very similar, except for the fact that instead of relying on a fixed mask to turn ON and OFF individual light spots, the beamlets are controlled by a massive array of electronically controlled light sources.

While the MAPPER system is appealing in terms of its large parallelism, mix-and-match optical-ebeam systems will undoubtedly remain very complex and expensive systems no matter what. Electron-beam based systems, because they are easily disturbed by all sorts of stray fields, need to be extraordinarily well isolated. Unless active feedback techniques are incorporated [Ref 1-29] the fixed cost for this system will remain high. Furthermore, even with a high degree of isolation, pattern placement requirements will likely remain outside the acceptable margins of the sub-70nm regime unless feedback can somehow be introduced. Systems such as MAPPER, aimed at nanofabrication, will suffer from all these well-known e-beam limitations in addition to new ones arising from the reliance on photocathodes and field emitters. If the later are

used, local variations of electron emission efficiency (a sure thing for field emitters), will require a high degree of redundancy on the writing strategy, severely affecting the throughput. If photocathodes are used, contamination problems will have to be mitigated. Even the illumination optics responsible for activating the converter plate are a significant challenge, since the system has to operated at ultra-high vacuum, under large potentials and magnetic fields that provide a challenging environment.

1.4 Conclusions

Given the current industry interest in maskless lithography, it is crucial that the community investigates all the proposed maskless alternatives with an open mind. The techniques outlined in this chapter are only a representative sample of some of the most visible proposals, with many other approaches no doubt in development. The maskless techniques reviewed range significantly on resolution capabilities, complexity, throughput potential and cost.

This thesis presents yet another maskless alternative, offering a dramatically simpler architecture that is capable of chip-production and is scalable to the limits of the lithographic process. It is an all-optical approach, adaptable to all wavelengths with massive parallelism, and a simple optical train. All these characteristics are crucial for a successful maskless system capable of chip production.

Optical lithography still remains king in manufacturing today, and will be extendible until the end of this decade at a minimum. Taking advantage of existing infrastructure in terms of available light sources, resists, etc is crucial if new maskless systems are to be introduced in the near future. Furthermore, dealing with non-charged particles allows for simpler isolation control and better pattern placement and dimensional control.

Massive parallelism is key, since at least a few wafers per hour are needed in order to introduce maskless lithography into industrial fabrication facilities. Systems with 32 beams are no longer enough. A million beams is more like it.

A simple optical train is important in order to reduce cost. Some of the proposed maskless lithography systems have enormously complex optics, building on already mammoth systems that are only affordable to a few multinational corporations. It is not

at all clear that a low-throughput system can cost the same as a high-throughput system, even if it affords a maskless advantage. The author remains convinced that a different cost structure will be needed for the successful introduction of maskless lithography into the semiconductor manufacturing world, let alone smaller operations that will pop-up along the nanotech bonanza.

And finally, a maskless system would ideally be extendible to many future generations. The history of the semiconductor industry has taught us that not all problems have to be solved at once, but that there has to a path to solve them. This applies to maskless lithography as well. There is tendency to want to start at the end of the road, proposing systems with throughputs of 100 wafers per hour and sub-50 nm resolution, whatever the cost. The community must make a decision whether the introduction a commercially viable maskless systems should be *leading, lagging,* or *at* the production lithography node. Careful economic studies have to be undertaken to understand the market for each of these alternatives, and resources can then be allocated appropriately. It is quite possible that the answer might surprise us, and that the pursuit of stratospherically expensive maskless systems with 100 wafers per hour and sub-50 nm resolution might not make sense, either technically, or economically.

Chapter 2

The ZPAL Concept

The work presented in this thesis, Zone-Plate-Array Lithography (ZPAL), bypasses some of the most pressing problems of current lithography equipment by developing a maskless lithography tool that will be scalable, flexible and cost-effective. It is the departure from a century-old tradition of refractive optics, in combination with the use of advanced micromechanics and fast computing, that enables ZPAL to open up a new space in the lithography world.

2.1 From Refractive to Diffractive Optics

The advantages of diffractive optics in maskless lithography include: uniformity, high quality, reliability, and cost-effectiveness. *Diff*ractive optics are manufactured using highly reliable, mass-production-compatible lithography-based planar-fabrication technology. In contrast, *ref*ractive optics, even to this day, require both technological sophistication and craftsmanship (including hand grinding and polishing, and macroscopic assembly). *Ref*ractive optics have the added disadvantage that materials

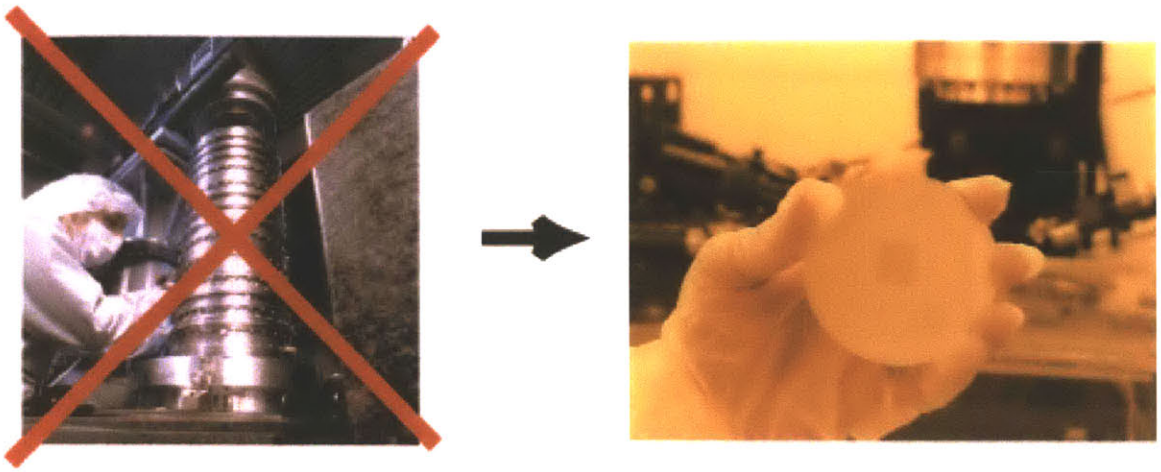

Figure 2 - 1. Vision of the power of employing diffractive optics for lithography. Diffractive optics are manufactured using nanofabrication, with techniques similar to those used in chip production

become opaque as wavelength is decreased. In contrast, *diff*ractive optics, such as zone plates, can operate at any wavelength; even neutral atoms have been focused [Ref 2-1]. Furthermore, by employing large arrays of diffractive optics, the tradeoff between image resolution and field size can be bypassed. This tradeoff is at the core of much of the complexity and cost of current lithography and microscopy systems. An image of the vision underlying our push for diffractive optics is illustrated in Figure 2-1.

2.2 ZPAL System Overview

In conventional semiconductor lithography, glass masks are illuminated with laser light and their image is reduced through a lens onto the substrate to define circuitry. As feature sizes are pushed toward 100 nm and below, lithography is becoming increasingly costly and difficult. Zone-plate-array lithography (ZPAL) is a considerably simpler approach. ZPAL would not have been possible even a few years ago. It is made possible by inexpensive, high-speed computation, advances in nanofabrication, and micromechanics. ZPAL replaces the "printing press" of traditional lithography with a technology more akin to that of a laser printer.

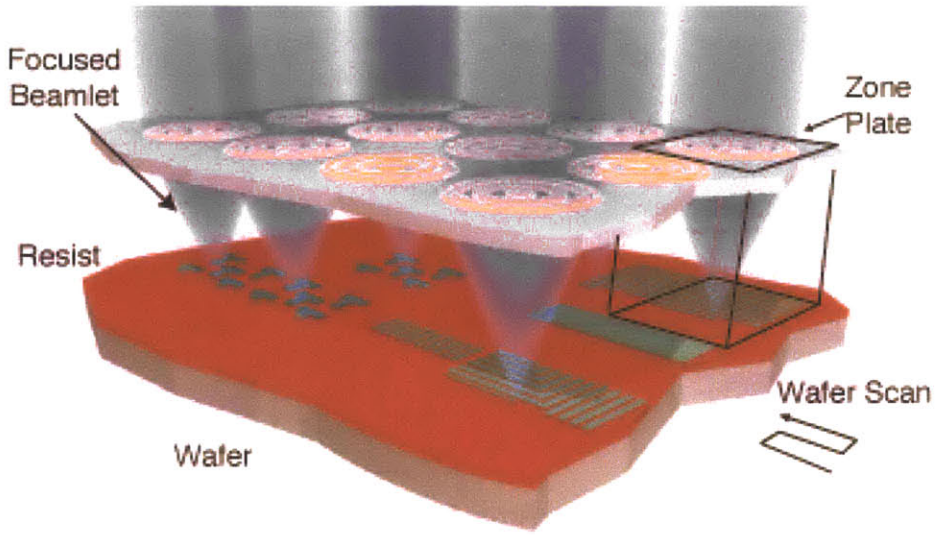

Figure 2 - 2. Schematic of zone-plate-array lithography (ZPAL). An array of Fresnel zone plates focuses radiation beamlets onto a substrate. The individual beamlets are turned on and off by upstream micromechanics as the substrate is scanned under the array. In this way, patterns of arbitrary geometry can be created. The resolution of the system is determined by the numerical aperture of the zone plates and the wavelength of light.

Instead of a single, massive lens, an array of one million microfabricated Fresnel-zone-plate lenses is used, each focusing a beam of light onto the substrate. A computer-controlled array of micromechanical mirrors turns the light to each lens on or off as the stage is scanned under the array, thereby printing the desired pattern in a dot-matrix fashion. No mask is required, enabling designers to rapidly change circuit designs.

Zone Plate Array Lithography (ZPAL) is depicted schematically in Figure 2-2. An array of diffractive optical elements (Fresnel zone plates in this case) focuses incident radiation into an array of spots on a substrate. The spot size is approximately equal to the minimum feature size of a zone plate (i.e. the outer zone width). By using micromechanics to independently turn on or off the radiation to each zone plate, and simultaneously scanning the substrate underneath, arbitrary patterns can be generated. ZPAL combines the advantages of maskless lithography with the high throughput of parallel writing provided by an array of zone plates.

ZPAL was first proposed by Henry I. Smith in 1996 [Ref 2-2] in a paper which detailed a basic writing strategy and presented a design for a ZPAL system utilizing 4.5 nm radiation from an undulator on a compact synchrotron. Subsequent work presented

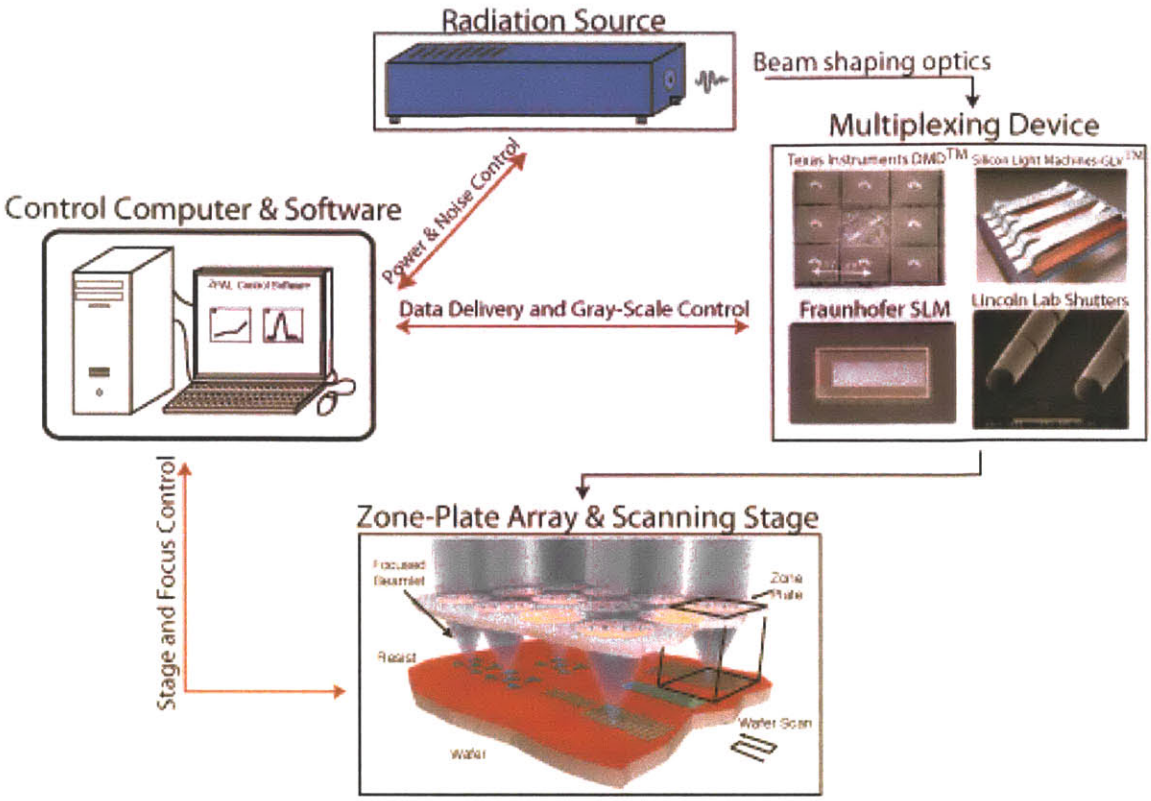

Figure 2 - 3. Core elements of a ZPAL system.

resist exposures using phase zone plates in the deep UV (λ =193 nm) and demonstrated rudimentary parallel patterning with a zone-plate array [Ref 2-3,Ref 2-4]. A ZPAL system was then developed at the NanoStructures Lab at MIT that provided the first demonstration of multiplexed lithography with ZPAL [Ref 2-5].

2.3 Key Technical Challenges

The area of research covered in this thesis is multidisciplinary in scope, ranging from nanofabrication, to optical and mechanical design (including extensive use of MEMS), to circuit and software design. This section will discuss some of the key technical challenges.

The core elements of a ZPAL system are depicted in Figure 2-3. The system is comprised of four major components: a radiation source, an array of micromechanical elements, a zone plate array and a scanning stage. A control computer with custom

designed hardware and software will provide the necessary control and feedback for the successful integration of the four core ZPAL components.

2.3.1 The Radiation Source

Because zone plates can focus any type of radiation of interest in lithography, from blue, to deep UV, to x-rays, and even neutral atoms [Ref 2-1], the zone plate design and the multiplexing can be scaled with the wavelength to meet future needs (as is the case with many other forms of lithography, by using light of shorter wavelengths, higher resolution can be achieved). While very short wavelengths are appealing in terms of the resolution that can be achieved with them, their use can be costly and flexibility is often sacrificed. A much better solution at the present stage of development of ZPAL technology is to employ tabletop laser sources at UV that don't require the system to operate in vacuum (with the added advantage that glass and fused silica optical elements can still be employed). For these reasons, we have developed ZPAL technology at near UV with lasers operating at 442nm (He-Cd gas laser) and at 400nm (a solid-state laser). The system is capable of achieving sub-wavelength resolution and therefore deep sub-micron lithographic structures.

2.3.2 The Micromechanics

It is apparent from Figure 2-2 that if we want each optical element to write independently we have to be able to independently control the illumination of each zone plate. This control is provided by upstream micromechanics. The reason we need micromechanics is because the area of a unit cell, which is the area over which we want to control the illumination, ranges from 10 to 100 μm^2. There are a variety of options available, ranging from the use of micromirrors (such as the DMD manufactured by Texas Instruments [Ref 2-6]), to diffraction based MEMS (such as the Grating Light Valve (GLV) manufactured by Silicon Light Machines [Ref 2-7]) to micro-shutters (prototyped by MIT-Lincoln Laboratory).

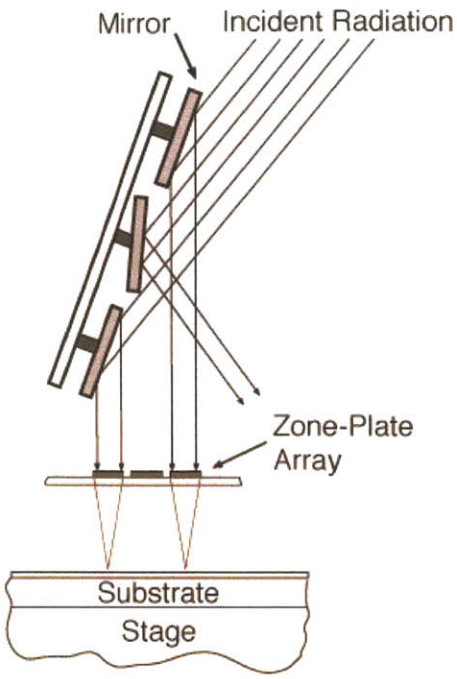

Figure 2 - 4. Schematic of a micromirror array for ZPAL. Radiation is modulated by means of micromirrors, which can tilt to two angles by means of electrostatic deflection.

The use of micromirrors for ZPAL is depicted schematically in Figure 2-4. The idea is to place a micromirror array in the path of the radiation beam, so that each mirror, with proper alignment and use of optics, will be responsible for the illumination of an individual zone plate. This is possible because the mirrors can tilt to two positions responding to the control of a computer, and hence, when they are latched in one position the light will be reflected to the appropriate zone plate, and when in the other the radiation will be deflected out of the imaging system.

An alternative micromechanical solution explored in this thesis is the Silicon Light Machines Grating Light Valve™ (GLV™) linear array. Although the GLV™ has a smaller number of pixels (1,088) compared to the DMD™ micromirror array (~1 million or more), the higher speed of operation of the GLV™ (20ns rise time as opposed to 20 μs for the DMD™), the fact that gray-scaling is built in, and its diffractive mode of operation (making it compatible with shorter wavelengths, possibly even down to 157nm) have the potential of making the GLV™ a superior choice for ZPAL.

The GLV™ is a micromechanical phase grating consisting of parallel rows of reflective Al ribbons. Alternate rows of ribbons can be pulled down electrostatically in a

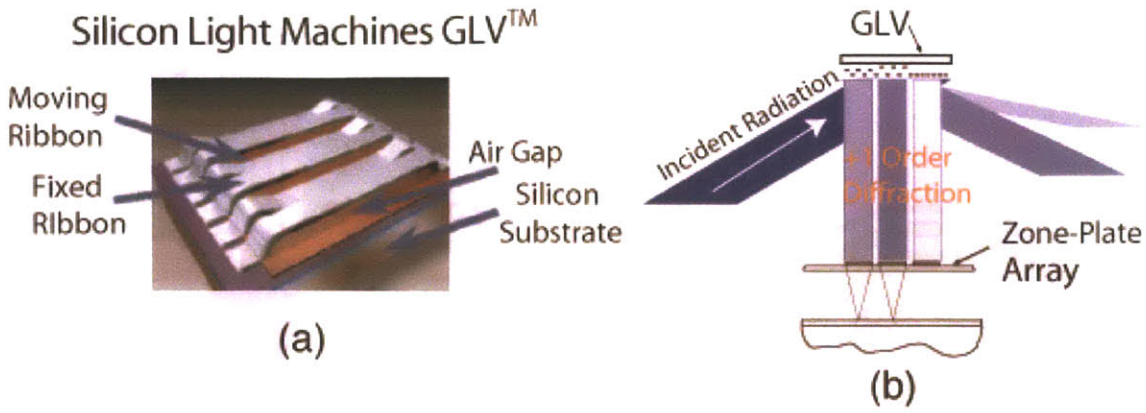

Figure 2 - 5. The Silicon Light Machines Grating Light Valve™ (GLV™) (a) one pixel of the GLV™ (each pixel can be thought of as a "mini-grating"), (b) intended implementation of the GLV™ with our linear array of zone plates indicating gray scaling.

controlled manner to create diffraction effects on incident light. When no force is applied, all the ribbons lie in the same plane. If illuminated, incident light will be reflected from their surfaces at the same angle at which it is incident. When alternate ribbons are pulled down, a grating structure is created. In this state, diffraction will produce light at an angle different from that of the incident light.

By alternating between these two states (i.e. from flat ribbons to a grating structure) the GLV™ can switch light ON and OFF. Furthermore, by tuning the applied electrostatic force, the depth to which the ribbons are pulled down can be controlled, impacting the amount of light diffracted into the first order. Grayscaling of the incident light can be achieved in this manner. Each of the 1088 pixels present in the linear array can accept 8-bits of grayscaling (256 levels). Since the motion involved in switching the pixels of the GLV™ is small (one-quarter wavelength), the GLV™ is capable of very high switching speeds, with a rise time from the ON to the OFF position of only 20ns [Ref 2-7]. One pixel of the linear array is depicted schematically in Figure 2-5(a), along with the intended implementation in ZPAL, Fig. 2-5(b).

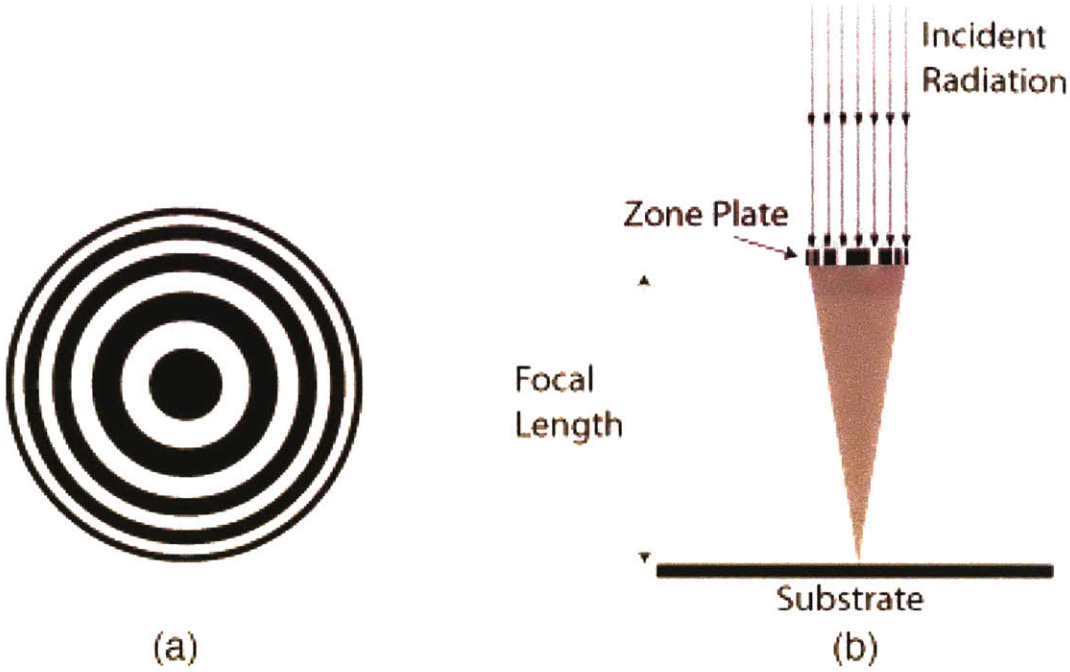

Figure 2 - 6. Zone Plates. (a) Top view (b) Cross section

2.3.3 The Zone Plate Array

A zone plate is a diffractive optical element of circular symmetry in which the local spatial period depends on the radius in such a way, that the first-order diffracted radiation from any radius value crosses the axis at the same point, the focal length. This concept is illustrated in Figure 2-6. It goes without mention that the zone plates are the core of ZPAL, and that they are the innovative idea of a completely new paradigm in lithography. Chapters 4, 5 and 6 will deal extensively with the theory, design, fabrication, and characterization of these elements.

2.3.4 The Scanning Stage

The last of the four major components of ZPAL is a precision movable stage. Its function is to raster scan the substrate over a zone plate unit cell in order to produce the desired patterns. Alternative scanning strategies are also feasible, perhaps desirable, as described, for example, by Feldman [Ref 2-8].

This thesis presents the first lithographic results obtained by continuous scan ZPAL. The scanning system utilizes a piezo-actuated stage from Physik Instrumente (model P-770). This model offers a scan range of 200x200 μm^2 with a positioning accuracy of less than 10nm. Capacitive sensors are used for position sensing, with custom-built velocity-feedback circuits implemented to enable continuous-velocity scanning.

The stage scans the substrate in a raster fashion. In terms of writing strategy, it is important to differentiate the concepts of spot size, determined by $w_{\min} = k_1 \lambda / NA$, and that of pixel size, which refers to the address grid (i.e. the locations on the substrate where spots are flashed at appropriately controlled doses). Based on simulations and previous work [Ref 2-9], 5-bits of grayscaling in combination with an address grid of one half the spot size is sufficient to control linewidths to better than 10%. Furthermore, this writing strategy allows all edges of the exposed features to be controlled independently and accurately to a fraction of the spot size.

Chapter 3

Zone Plate Design and Fabrication

3.1 History of Zone Plates

The invention of zone plates originates from the work of Fresnel (1788-1827) on diffraction. In 1808 the Paris Academy proposed the theme of diffraction for a prize, and Fresnel presented a paper [Ref 3-1] synthesizing Huygens's (1629-1695) principle and Young's (1773-1829) Principle of Interference. The resulting theory is now known as the Huygens-Fresnel Principle. Despite strong opposition from Poisson, a member of the jury and an ardent critic of the wave theory of light, Fresnel won the prize from a jury also composed of Pierre Laplace, Jean B. Biot, Dominique F. Arago, and Joseph L. Gay-Lussac [Ref 3-2].

The paper is worth examining, for it presents the foundations necessary for zone plates to be invented. The most important concept that concerns us in Fresnel's paper is the idea of what later would be called Fresnel Zones. Let's examine where they come from.

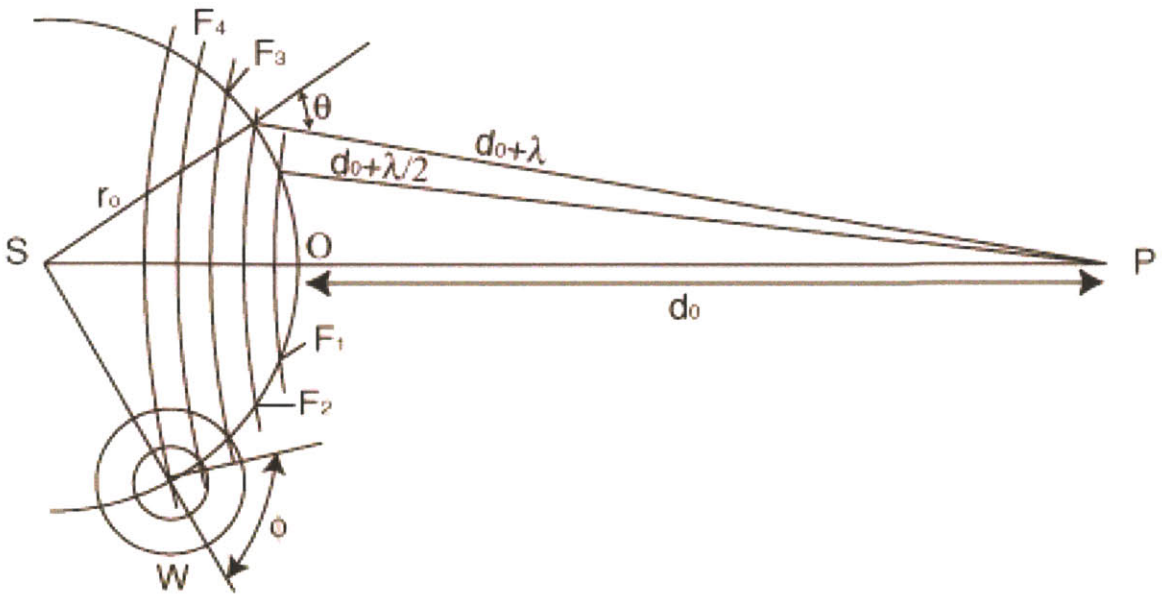

Figure 3- 1. The Fresnel Zones

Fresnel's treatment of diffraction was based on the idea of Huygens principle, which states that each point of a wavefront may be regarded as the center of a system of secondary disturbances that gives rise to spherical wavelets. The position of the wavefront at any later time is defined by the common tangent of these waves. The breakthrough came from the realization that by taking into account the mutual interference that takes place between these secondary waves, diffraction effects could be explained. It is in the theoretical development of this explanation of diffraction that the Fresnel zones arise, and as an extension, the Fresnel zone plate.

Fig. 3-1 shows a wavefront arising from a point source at S. Fresnel maintained that the effect of the point source at a point where the light disturbance is to be determined, P, could be found either by allowing this wavefront to proceed until it reaches P, or by dividing the wavefront into small areas so that each one can be assumed to generate one wavelet (see W in the graph). Each of these wavelets then produces an effect at P, which can be summed according to the principle of superposition to give the total effect at P of the point source. Obviously, these two methods should yield identical results, but the second allows the calculation of the effect at P if edges or apertures obscure parts of the wavefront.

Going back to Fig. 3-1 we can see that the shortest distance between the wavefront and P is d_0 (=OP). Other parts of the wavefront will cause disturbances at P that are out of phase with that produced by the nearest part (at O) due the difference in length that the light has to travel. This can be analyzed by constructing a set of concentric spheres centered at P with radius $d_o+n\,\lambda/2$, with n = 1,2,3,... These spheres cut the wavefront at F_1, F_2, F_3, etc. Let's focus on the first of these circles, F_1. Within this circle the phase of the disturbances arriving at P varies between 0 an π. If we now look at circle F_2 we see that the disturbances arriving at P from the area between these two circles (F_1 and F_2) will have a phase that will vary between π and 2π.

Further annuli or zones can be constructed, each having an effect at P varying by 180° of phase. These hypothetical zones are known as **Fresnel zones**. The size of these zones is dependant upon the wavelength of the light used as well as the distance to the point P. It's easy to prove that when we have a spherical wavefront, and the wavelength of the light used is small compared to d_0, the areas of the zones are all very nearly equal to $\pi d_0 \lambda$, and the radii of their boundaries are proportional to the square roots of natural numbers.

As the areas of these zones are equal, we can assume that they produce the same number of secondary wavelets from equal element areas. However, Fresnel had to introduce a correction here. If each wavelet radiated uniformly in all directions, in addition to generating a forward traveling wave, there would also be a reverse wave traveling back towards the source. No such wave is found experimentally, so the radiation pattern of the secondary waves had to be modified. Fresnel introduced an *obliquity* or *inclination factor*, which is a function of θ (see Fig. 3-1), in order to describe the directionality of the secondary emissions. To be historically correct, Fresnel postulated the need for it, but it was Kirchoff who provided an expression for it [Ref 3-2].

We are now at a position to deduce what happens at P. We had assumed that each zone produces the same number of secondary wavelets since they all have equal areas, but, taking into account the obliquity factor, which increases as we go out from the central zone, we can see that the amplitude at P due to the zones will gradually diminish from the central zone outwards. From the way in which the zones have been constructed,

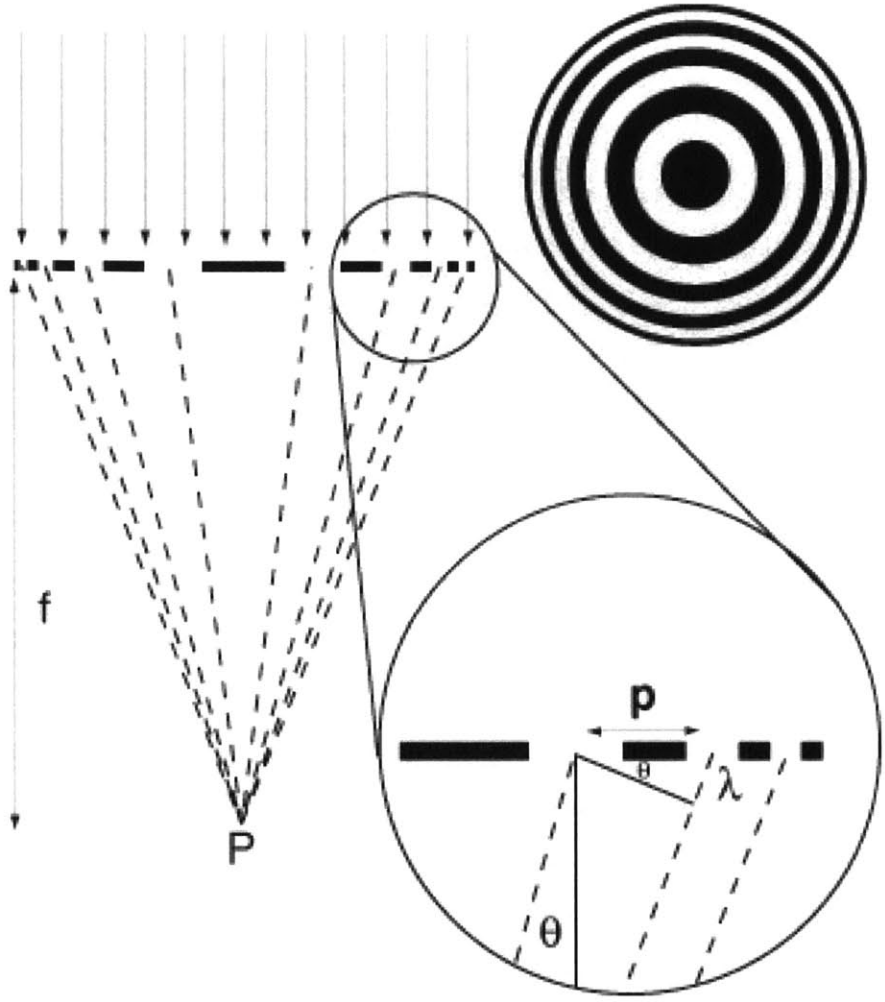

Figure 3- 2. Zone plate schematic. Zone plates, like gratings, work by diffraction.

it follows that the effect at P from any one zone is exactly opposite in phase from that of an adjacent zone.

With these concepts in mind, and avoiding the analytical work in favor of doing it just for zone plates in the following section, we are ready to make the jump to the concept of a zone plate. In the previous considerations it was noted that successive Fresnel zones nullify each other due to variations in phase. If we prevent the light propagation from alternate zones from reaching P, that from the remaining zones, since they will all arrive with the same phase, will add up constructively and produce a greatly increased illumination at this point. This concept is illustrated in Fig. 3-2.

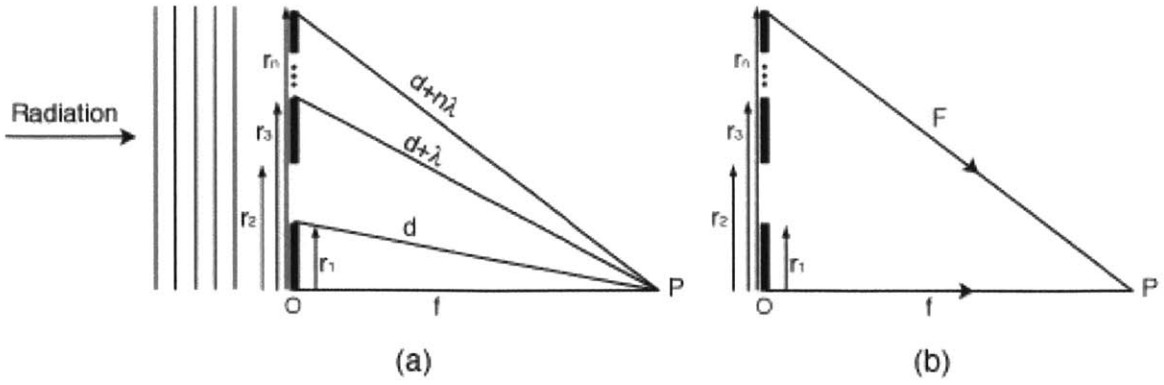

Figure 3- 3. Zone plate geometry

An even higher increase in light concentration would be obtained if, instead of blocking alternate zones (amplitude zone plate), the phases of the wavelets from these zones were changed by π. The disturbances from all zones would then arrive at P with the same phase. This is called a phase zone plate.

Let's now take a look in a more quantitative manner at how a zone plate works.

3.2 Zone Plate Theory

3.2.1 Geometry of Zone Plates

Fig. 3-3 presents a schematic cross section along a zone plate radius, with a ray diagram indicating the lengths of possible light paths from an incoming plane wave to P. The objective is to derive the necessary expressions for the radii of the zone boundaries. Since we are trying to model a zone plate, we will assume that the total optical path to P via the nth zone differs by $\pm\lambda/2$ from the path through the corresponding point on a neighboring zone. To avoid confusions, it should be noted that zones are constituted both by open and closed annuli. If the zone plate is to work efficiently, the difference in path length between any point in an open zone and the corresponding point in the next open zone should be equal to the wavelength of the light used, λ[1].

[1] There are two basic types of zone plates: amplitude and phase. If alternate zones are blocked, an amplitude zone plate is created. If alternate zones are appropriately phase-shifted, the diffraction emanating from all zones will constructively interfere at the focal spot. These are phase zone plates.

We determine the values of r_n by demanding that the optical paths F and f (see Fig. 3-3) differ by $\frac{n\lambda}{2}$, so

$$F = f + \frac{n \cdot \lambda}{2} \qquad \textbf{3 - 1}$$

Since $r_n^2 = F^2 - f^2$, we find that

$$r_n = \sqrt{n \cdot \lambda \cdot f + n^2 \cdot \frac{\lambda^2}{4}} \qquad \textbf{3 - 2}$$

The term $n^2\lambda^2/4$, which represents the spherical aberration of zone plates, can be ignored for short-wavelength low numerical aperture designs, in which $f >> n\lambda/2$. The numerical aperture of a zone plate, defined as the sine of the maximum angle that gets diffracted by the optic, is given by

$$NA = \sin\theta = \frac{R}{\sqrt{R^2 + f^2}} \qquad \textbf{3 - 3}$$

where R is the radius of the zone plate and f is the focal length. Solving for f in equation 3 – 3, an expression for the focal length of a zone plate in terms of the numerical aperture and the radius can be obtained.

$$f = \frac{R}{NA}\sqrt{1 - NA^2} \qquad \textbf{3 - 4}$$

The above equations are all that are needed to design basic zone plates. The following sequence was used for all the zone plates designed for this thesis. First, a *numerical aperture - focal length* combination is chosen. Then, using equation 3-4 and solving for R, the outer radius of the zone plate is calculated. The next step consists in finding the total number of zones that the resulting optic will have. This can be obtained by rearranging equation 3-2 to obtain:

$$N = \frac{-f + \sqrt{f^2 + R^2}}{\lambda/2} \qquad \textbf{3 - 5}$$

Having N, the total number of zones, the radii of each of the zones can be calculated by iteratively solving equation 3 - 2 until $n = N$.

An Intuitive way to Think about Zone Plates

A useful and intuitive way to think about how a zone plate works is provided by analyzing its behavior in terms of spatial frequencies. The idea behind this approach is to think of a zone plate as an optical element that is created by a combination of a large number of small-area gratings of many different periods. Each one of these gratings generates a plane wave, and each one of them can be described with a characteristic spatial frequency. At the focal plane of the optic, all plane waves interfere, forming a spot. Let's see how such a spot is formed.

Interference of two plane waves

Let's begin by analyzing what happens when two monochromatic plane waves interfere on a surface, as depicted in Figure 3-4 (a-b). The electric field for both waves is oriented along the $\hat{z}$ direction (Fig. 3-4(b)), with magnitude E_0. The phase offset of each wavefront (π_1, π_2) is specified with respect to the origin. To total field at the point of interference is obtained by the superposition of the incoming fields:

$$\begin{aligned}\vec{E} &= E_0\hat{z}\left[e^{-jk_{x1}x}e^{-jk_{y1}y}e^{+jk_{z1}z}e^{j\pi_1} + e^{jk_{x2}x}e^{-jk_{y2}y}e^{+jk_{z2}z}e^{j\pi_2}\right] \\ &= E_0\hat{z}\cdot e^{-j\frac{1}{2}(k_{x1}x+k_{y1}y-k_{z1}z-\pi_1-k_{x2}x+k_{y2}y-k_{z2}z-\pi_2)} \\ &\cdot 2\cos\left[\frac{1}{2}(k_{x1}x+k_{y1}y-k_{z1}z+k_{x2}x-k_{y2}y+k_{z2}z-\pi_1+\pi_2)\right]\end{aligned} \qquad \textbf{3 - 6}$$

The intensity of the aerial image is proportional to $\left|\vec{E}\right|^2$, and is given by:

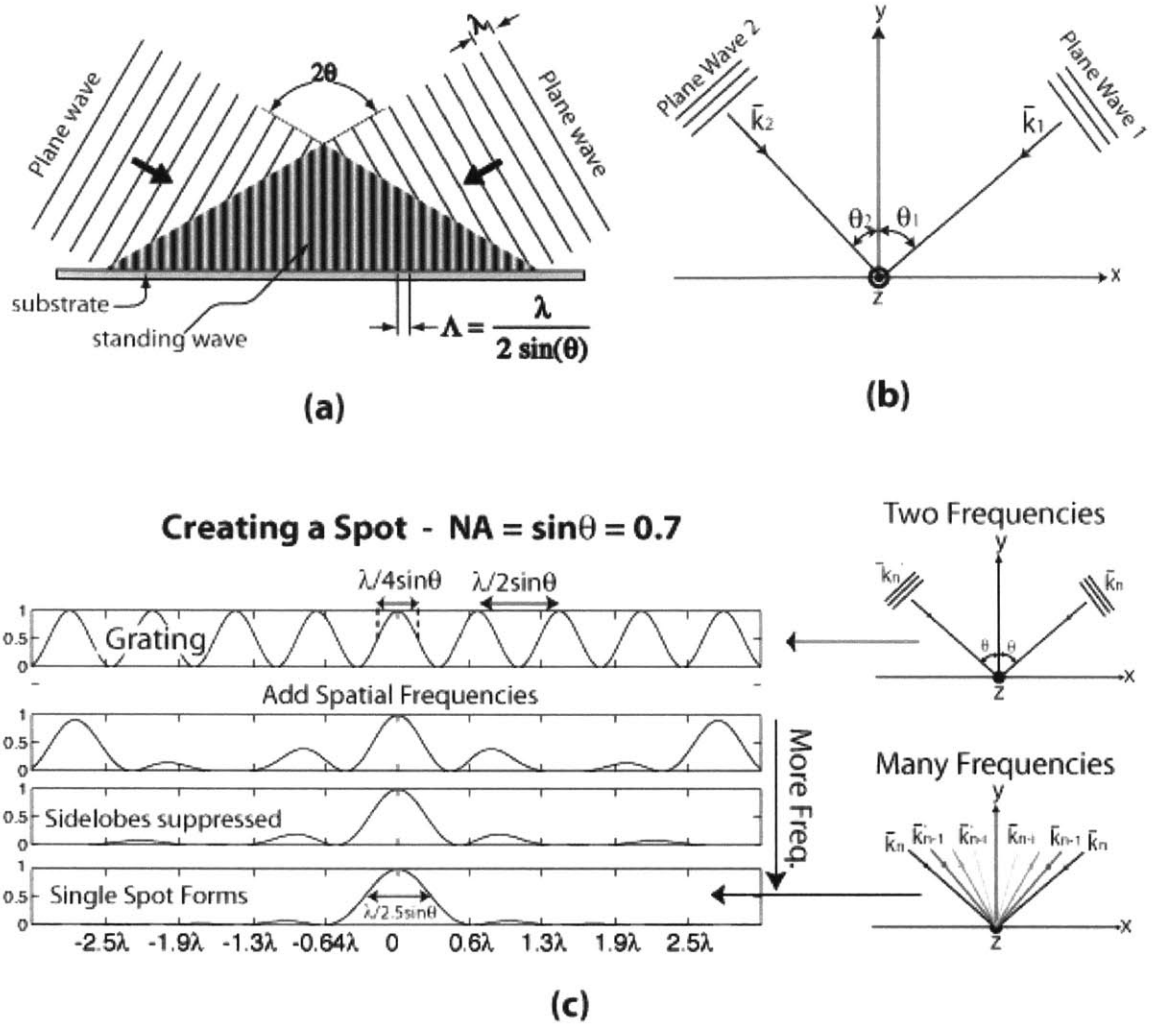

Figure 3- 4. When two plane waves interfere standing wave is formed. The period of the resulting periodic pattern is related to the illuminating wavelength and the angle of intersection. By adding plane waves coming from different angles (each angle can be associated with a distinct spatial frequency), a single spot can be formed.

$$\begin{aligned}\left|\vec{E}\right|^2 &= 4E_0{}^2\cos^2\left(\frac{1}{2}(k_{x1}x + k_{y1}y - k_{z1}z + k_{x2}x - k_{y2}y + k_{z2}z - \pi_1 + \pi_2)\right) \\ &= 2E_0{}^2\left[1 + \cos\left((k_{x1} + k_{x2})x + (k_{y1} - k_{y2})y + (k_{z2} - k_{z1})z - \pi_1 + \pi_2\right)\right]\end{aligned} \qquad \textbf{3 - 7}$$

For the purpose of this analysis, let's ignore the magnitude of the intensity (this is of little importance if the intensity of this field is to be used for lithography, since the amount of energy that is deposited in the resist can be varied at will simply by changing

the exposure time). The important quantity that is to be extracted from equation 3-7 is the periodicity of the resulting standing wave, since this will determine the maximum resolution achievable. In principle, the standing wave should form a perfectly *spatially coherent* periodic pattern. By spatial coherence we mean that by knowing the position of one local minima in the standing wave, one could predict the positions of all the other minima. The spatial coherence of the standing wave is of course related to the spatial and temporal coherence of the interference beams, which is in turn related to the bandwidth and spatial character of the illuminating source.

Equation 3-7 can be rewritten as

$$\begin{aligned} \left|\vec{E}\right|^2 &= 2E_0{}^2\left[1+\cos\left(\kappa_x x+\kappa_y y+\kappa_z z-\varphi\right)\right] \\ &= 2E_0{}^2\left[1+\cos\left(\vec{\kappa}\cdot\vec{r}-\varphi\right)\right] \end{aligned} \qquad \textbf{3 - 8}$$

where $\varphi=\pi_1-\pi_2, \kappa_x=k_{x1}+k_{x2}, \kappa_y=k_{y1}-k_{y2}$, and $\kappa_z=k_{z2}-k_{z1}$.

The grating period is hence given by

$$p=\frac{2\pi}{|\kappa|} \qquad \textbf{3 - 9}$$

In the simple case illustrated in Fig. 3-4(a-b), both incoming waves propagate in the x-y plane, hence $k_{z1}=k_{z2}=0$. Both π_1 and π_2 are set to zero. From the figure $k_{x1}=k\sin\theta_1$ and $k_{x2}=k\sin\theta_2$, where $k=2\pi/\lambda$. The aerial image at y = 0 is the given by

$$\left|\vec{E}\right|^2=2E_0{}^2\left[1+\cos\left(k(\sin\theta_1+\sin\theta_2)x\right)\right] \qquad \textbf{3 - 10}$$

Therefore the period of the grating is

$$p = \frac{2\pi}{k(\sin\theta_1 + \sin\theta_2)} = \frac{\lambda}{\sin\theta_1 + \sin\theta_2} \qquad \textbf{3 - 11}$$

If $\theta_1 = \theta_2 = \theta$ Eq. 3-11 reduces to the following expression

$$p = \frac{\lambda}{2\sin\theta} \qquad \textbf{3 - 12}$$

Since angles of $\theta \approx 90°$ are possible geometrically with plane waves, the limiting period that can be created is λ/2 (this correspond to a numerical aperture of 1). A grating, with a periodicity determined by equation 3-12, created with a NA = sin θ = 0.7 is depicted at the top of Fig.3-4(c).

The effect of adding more spatial frequencies is illustrated in Fig.3-4(c). Different plane waves arriving at the origin with different angles interfere in such a way that only the central peak gets reinforced, while all the other periodic peaks (let's call them sidelobes) get progressively smaller and smaller. Note that the width of the central peak, defined at full-width-at-half maximum (FWHM) gets wider as more spatial frequencies are added, growing from a FWHM = λ/4 to a FWHM ~ λ/2.5 (for a NA=0.7). A zone plates recreates the above analysis in a circular symmetric manner, with different spatial frequencies arriving at the focal spot from a cone of different angles to create a circularly symmetric spot[2]. The spatial frequency description of zone plates also allows us to understand how inner and outer zones contribute differently to the overall shape of the final spot. The outer zones, those having the smallest periods, contribute the high spatial frequencies, and are hence the leading contributors to how small a spot is achievable. The inner zones contribute low spatial frequency components, and are responsible for suppressing the sidelobes surrounding the central spot. Blocking certain areas of the zone plate can hence enable the creation of a finer spot size, but at the prize

[2] This simple description does not take into account the vector nature of light. Polarization effects, especially in combination with high-numerical aperture zone plates, can cause spots that lack circular symmetry.

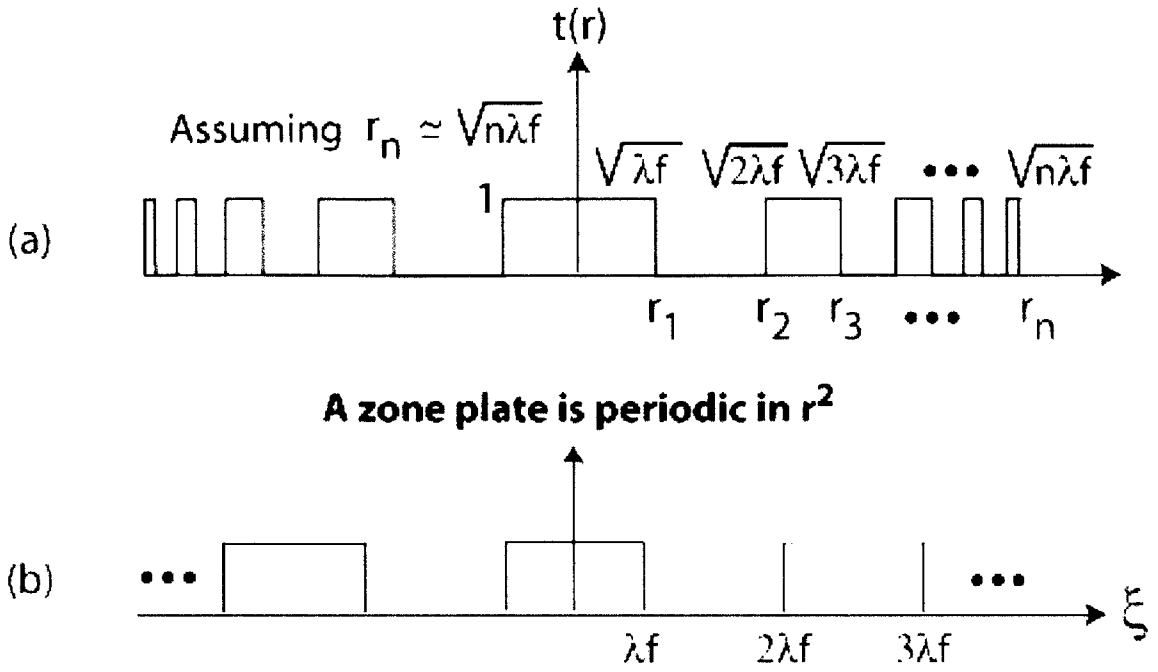

Figure 3- 5. (a) Cross section of zone plate. The radius is described using the small angle approximation. (b) A zone plate is periodic in r^2, and can therefore be analyzed using Fourier analysis.

of higher sidelobes. Well-understood concepts such as apodization can be readily applied to zone plates, with the result of further suppression of the sidelobes. In this manner, one of the virtues of utilizing zone plates for lithography becomes readily apparent: diffractive optics provide many "knobs" that can be tuned in order to maximize or minimize a particular focusing effect. That is, is some cases a smaller spot size might be preferred *even if* the sidelobes increase. By simply controlling what areas of the zone plate are illuminated, such effects can be realized.

Fourier analysis can further provide insight into the focusing behavior of zone plates, especially as it refers to the presence of multiple diffraction orders. Consider the cross section plot of a zone plate illustrated in Fig.3-5. If, for the purpose of simplifying the analysis, we ignore the spherical aberration component of equation 3-2, the expression of the radius of a zone plate can be simplified to the following expression:

$$r_n \approx \sqrt{n\lambda f} \qquad \textbf{3 - 13}$$

where n is the zone number, λ is the wavelength of light, and f the focal length.

We can now proceed with the analysis by realizing that zone plates are periodic elements in r^2, and hence they can be described by a Fourier series decomposition. The transmission function for a zone plate of unity absorption in the opaque zones can be describes as:

$$t(\xi) = \frac{1}{2} + \frac{1}{\pi}\left[\cos 2\pi\frac{\xi}{\Lambda} + \frac{1}{3}\cos 2\pi\frac{3\xi}{\Lambda} + \frac{1}{5}\cos 2\pi\frac{5\xi}{\Lambda} + \ldots\right] \qquad \textbf{3 - 14}$$

where $\Lambda = 2\lambda f$. Substituting for Λ and given that $\xi = r^2$, we get

$$t(\xi) = \frac{1}{2} + \frac{1}{\pi}\left[\cos\frac{\pi r^2}{\lambda f} + \frac{1}{3}\cos\frac{\pi r^2}{\lambda f/3} + \frac{1}{5}\cos\frac{\pi r^2}{\lambda f/5} + \ldots\right] \qquad \textbf{3 - 15}$$

Given the circular symmetry of zone plates, $r^2 = \sqrt{x^2 + y^2}$. The above equation can then be expressed as:

$$t(\xi) = \frac{1}{2} + \frac{1}{2\pi}\left[e^{i\pi\frac{x^2+y^2}{\lambda f}} + e^{-i\pi\frac{x^2+y^2}{\lambda f}} + \frac{1}{3}e^{i\pi\frac{x^2+y^2}{\lambda f/3}} + \frac{1}{3}e^{-i\pi\frac{x^2+y^2}{\lambda f/3}} + \frac{1}{5}e^{i\pi\frac{x^2+y^2}{\lambda f/5}} + \frac{1}{5}e^{-i\pi\frac{x^2+y^2}{\lambda f/5}} + \ldots\right] \qquad \textbf{3 - 16}$$

Looking at the terms of equation 3-16, we can deduce the following:

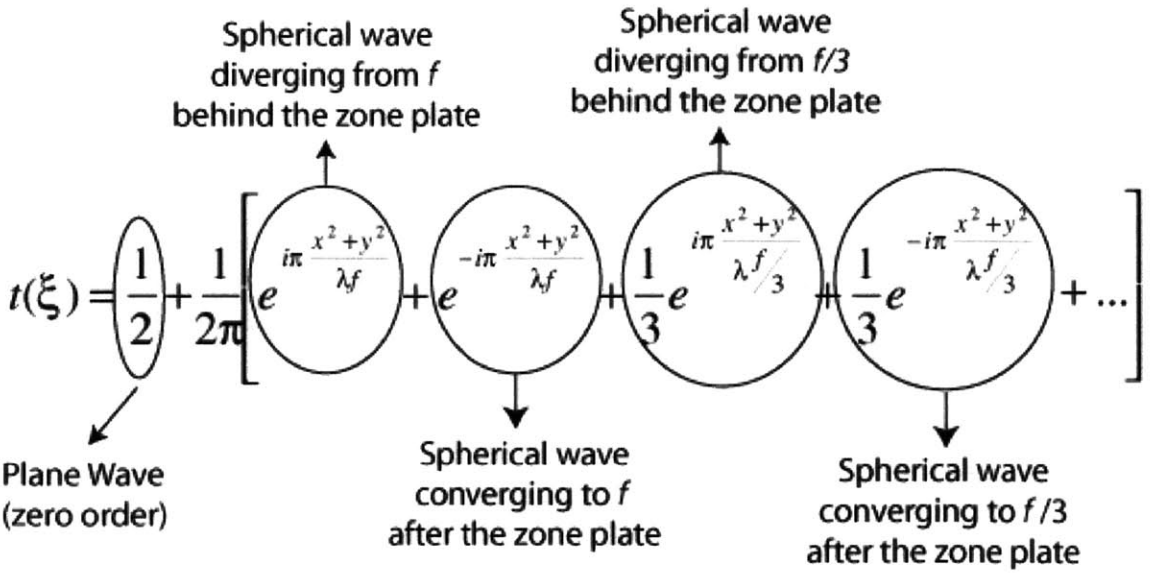

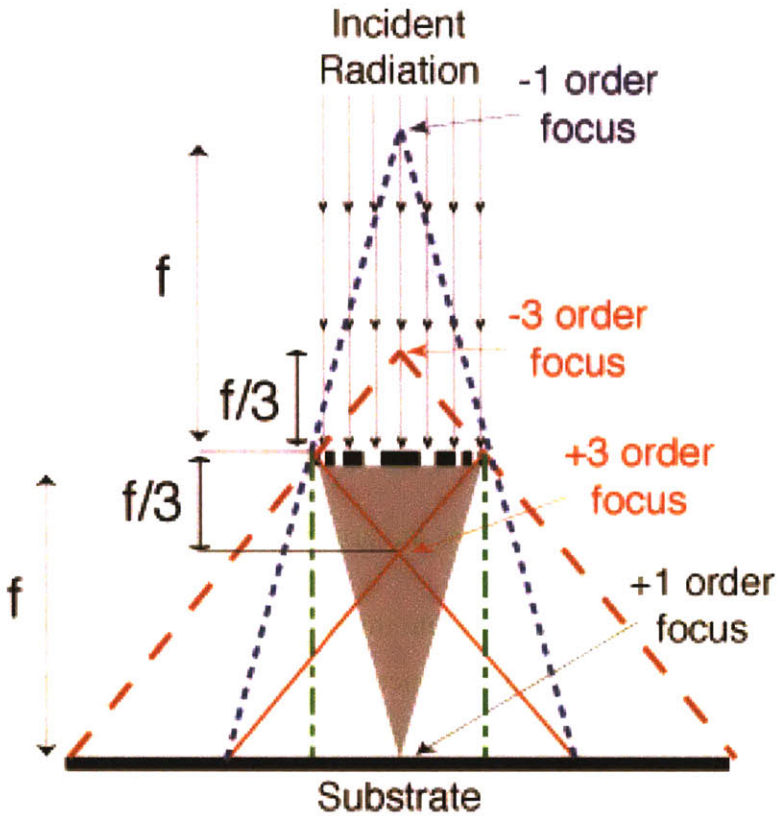

Figure 3- 6. Zone plate, being diffracted optical elements, focus light into a number of orders. For a zone plate with a 50-50 duty cycle, only odd orders are present. The zero order can be cancelled in the case of phase zone plates.

Figure 3-6 illustrates the multiple orders that a zone plate generates, as described by equation 3-16.

The analysis presented so far has provided a description of the origin of zone plates, their basic geometrical configuration, as well as how the different focusing orders appear. A spatial frequency analysis has also provided insight on how the main focusing spot is formed. While it is not the objective of this thesis to expand significantly from the kind of zone plate theory that has been presented so far, it is worth mentioning that in order to fully understand the detailed behavior of these elements, a more rigorous electromagnetic model is needed. A scalar approximation of Maxwell's equations provides a valuable staring point. Below, we briefly outline how such an analysis might proceed.

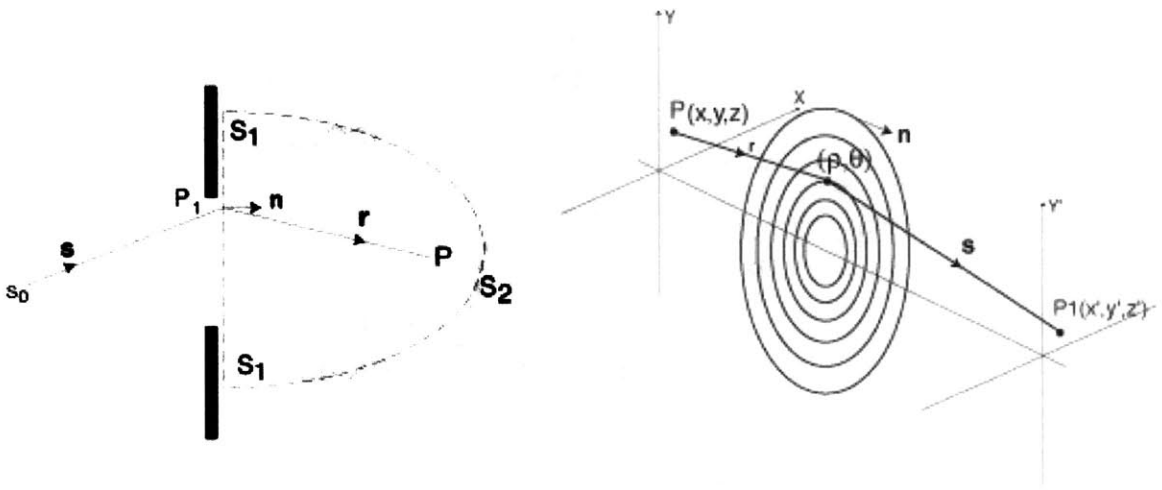

Figure 3- 7. Left: Diffraction by an arbitrary aperture. Right: Fresnel-Kirchhoff diffraction for a zone plate.

Fresnel-Kirchhoff diffraction theory provides a rigorous starting point to understand the behavior of light as it encounters a zone plate. We can begin by obtaining an expression of the electric field that results after an electromagnetic wave originating from an arbitrary point encounters an aperture. If we then deconstruct a zone plate as a combination of numerous apertures, an expression for the total field created by the zone plate can be obtained at any arbitrary distance after the zone plate by appropriately adding the diffraction effects of all the apertures. Following the coordinate system defined in Fig. 3-7, the field at P resulting from an electromagnetic field Uo that originates from So, taking into account the effect of the aperture placed in between these two points, is given by [Ref 3-3].

$$U(P) = \frac{iU_o}{\lambda}\iint_{\Sigma}\frac{\exp(-ik(r+s)}{rs}\frac{\cos(\mathbf{n},\mathbf{s})-\cos(\mathbf{n},\mathbf{r})}{2}dS \qquad \textbf{3 - 17}$$

For the case of an amplitude zone plate, the above expression can be modified in order to accommodate to the geometrical aperture configuration of these elements to obtain:

$$U(P_1,P) = \sum_{n=1}^{N-1}\frac{iU_o}{\lambda}\int_{\rho=R_n}^{\rho=R_{n+1}}\int_{\theta=0}^{\theta=2\pi}\frac{\exp(-ik(r+s)}{rs}\frac{\cos(\mathbf{n},\mathbf{s})-\cos(\mathbf{n},\mathbf{r})}{2}\rho d\rho d\theta \qquad \textbf{3 - 18}$$

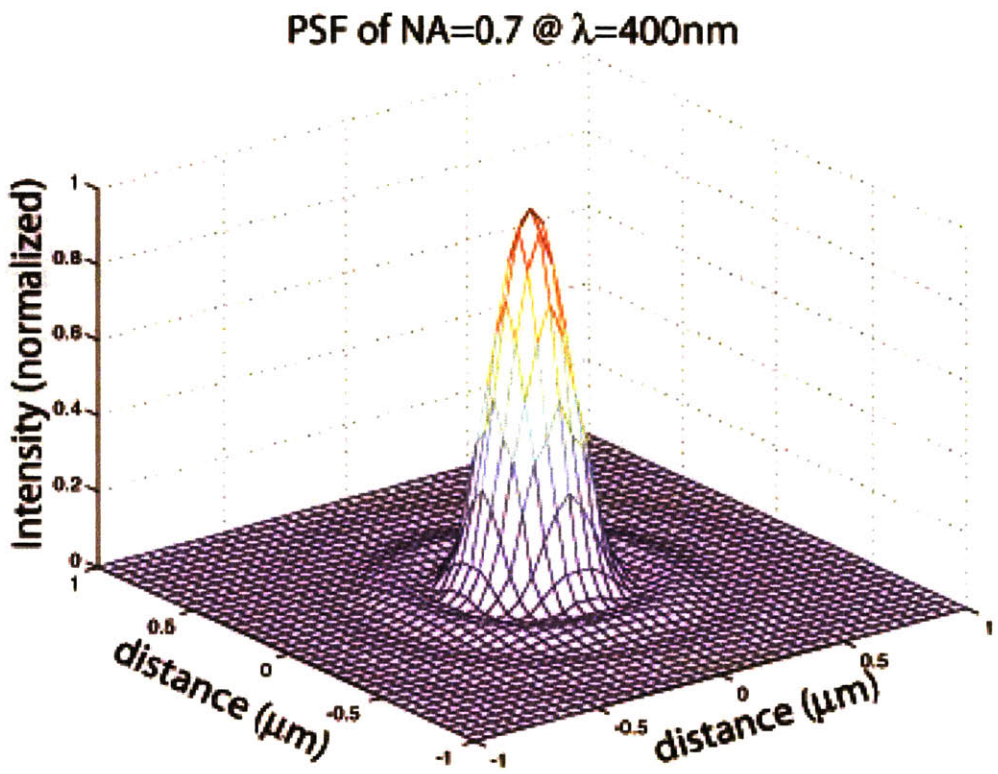

Figure 3- 8. Plot of the point-spread-function (PSF) of a NA=0.7 zone plate simulated using a finite-difference time-domain method. Simulation performed by Rajesh Menon.

where (ρ,θ) is a point on the zone plate in cylindrical coordinates. The sum on the above expression is only performed over the open zones, that is, it represents the field that would be obtained at P_1 for the case of an amplitude zone plate. In the case of a phase zone plate, all zones contribute to that total field, and equation 3-18 can be modified to obtain:

$$U(P_1,P) = \sum_{n=1}^{N-1}(-1)^{n+\mu}\frac{iU_o}{\lambda}\int_{\rho=R_n}^{\rho=R_{n+1}}\int_{\theta=0}^{\theta=2\pi}\frac{\exp(-ik(r+s)}{rs}\frac{\cos(\mathbf{n},\mathbf{s})-\cos(\mathbf{n},\mathbf{r})}{2}\rho d\rho d\theta \quad \mathbf{3-19}$$

where $\mu = 0$, if the first zone has a π phase shift or else $\mu = 1$. Without taking into account the effect of the illuminating source bandwidth, the total intensity distribution at P_1 is given by:

$$I(P_1) = \iint_S |U(P_1,P)|^2 \, dS \qquad \textbf{3 - 20}$$

where S is the cross-sectional area of the source illuminating the zone plate, and $U(P_1,P)$ is given by equation 3-19.

Scalar diffraction theory, however, fails to account for all the electromagnetic interactions (e.g. polarization), especially for zone plates of very high numerical aperture. In order to take all the effects into account, one needs to solve the vector form of Maxwell's equations. One of the most efficient methods of solving this problem for diffractive optics is the finite-difference time-domain method. This is used to analyze the performance of zone plates in the thesis of Rajesh Menon [Ref 3-4].

3.3. Fabrication Techniques

The first zone plates for visible light were made in the 19th century by Lord Rayleigh, Soret, and Wood by photographically demagnifying drawings of zone plates [Ref 3-5]. Through decades of research and improvements in fabrication techniques, zone plates capable of focusing light at almost all ranges of the electromagnetic spectrum, including soft x-rays, were fabricated. It was Baez in 1961 [Ref 3-6] who first constructed zone plates capable of working with extreme ultra-violet and soft x-ray radiation. Because at these wavelengths radiation is absorbed by photographic plates, it was necessary for Baez to either fabricate unsupported zone plates, or support them on very thin transmitting membranes. He was able to fabricate unsupported zone plates for imaging for 253.7 nm radiation. The zone plates consisted of 19 rings of gold with a diameter of 2.6 mm, an outer zone width of 17 μm, and a focal length of 15 cm.

However, it soon became apparent that other techniques besides photo-reduction and mechanical ruling were necessary to fabricate high-resolution zone plates capable of operating at such short wavelengths. The challenges for the fabrication were twofold: the smallest linewidth desired was (and still is) beyond the resolution of optical projection systems, and the number of zones could sometimes be very large. Another important aspect is the placement of the features. For diffraction-limited performance, the errors in the positioning of the each section of each ring has to be a small fraction of the zone

period. Baez proposed holography in 1961 to produce zone plates with large number of zones [Ref 3-7]. However, lasers were not yet available at this time, and the requirements for spatial and temporal coherence reduced the intensity of conventional sources too much to be of practical use for the production of high quality zone plates. Holography became an easy method only after high-quality laser sources became available, and interference patterns with huge number of fringes could be produced routinely.

Electron beam systems for the fabrication of fine microcircuit patterns were first developed in the 1960s, and zone plates were often used as test patterns to demonstrate the resolution. Ever since, with holography still being the choice for certain applications, electron-beam lithography has been the main tool for the fabrication of zone plates. The strength of holography is the large field; the strength of e-beam systems, the high resolution and the flexibility [Ref 3-8].

3.3.1. Critical Parameters

The fabrication of efficient diffractive optical elements requires the precise patterning of a large number of sub-wavelength binary surface-relief structures. For close to ideal performance, three critical parameters are required: (1) the local duty-cycle of each pair of zones must remain close to 50-50, (2) the period of each pair of zones must be accurately controlled, and (3) the phase-shift between alternate zones must be as close to π as possible. The following three sections detail the need for these three requirements and the impact of errors in each of these critical requirements on the performance of the zone plates.

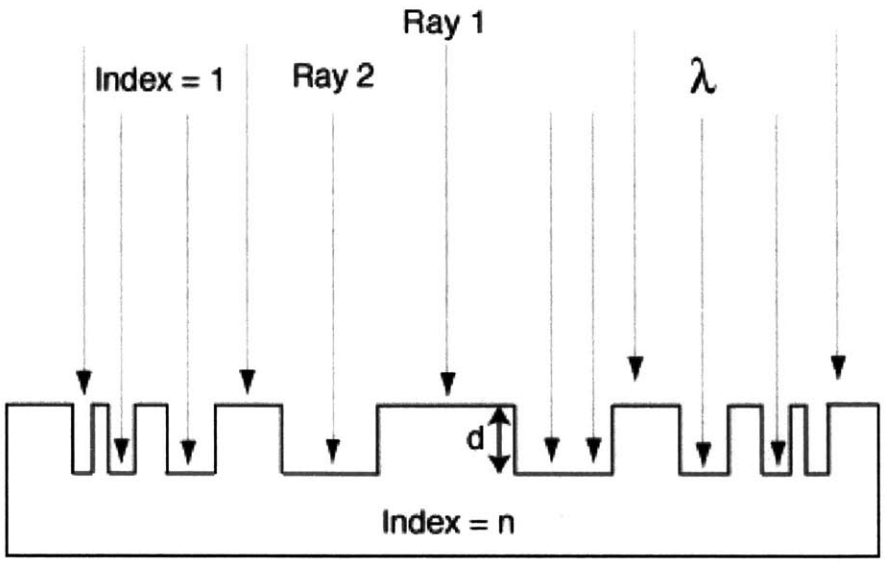

Figure 3- 9. Cross-section of a phase zone plate. Alternate zones are phase-shifted to maximize the efficiency into the first order as well as to cancel the zero order.

3.3.1.1 Phase-Shift Errors

Let's begin by calculating an expression for the depth of the groove necessary to obtain a π phase shift between adjacent zones (assuming the zone plates operate in air). If we refer to Fig,3 - 9, we can model the radiation illuminating the zone plate as a plane wave, with a wavefunction Ψ. Therefore, we can write

$$\Psi = A \cdot e^{i \cdot \vec{k} \cdot \vec{r}} \qquad \textbf{3 - 3}$$

$$\text{where } k = \frac{2\pi}{\lambda} \cdot n$$

and n is now the index of refraction of the material

As the radiation goes through paths 1 & 2 in Fig, 3–9, for path 1, light goes through the material a distance d, and the wavefunction for light can be written as:

$$\Psi_1 = A \cdot e^{i \cdot \vec{k} \cdot d} = A_1 \cdot e^{i \cdot \frac{2\pi}{\lambda} \cdot n_r \cdot d} \qquad \textbf{3 - 4}$$

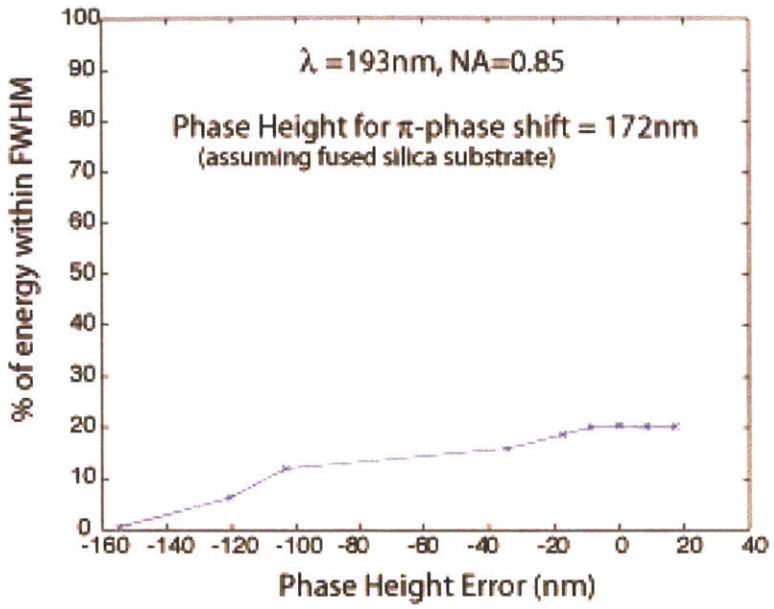

Figure 3- 10. Simulation of the first order diffraction efficiency versus phase-height error (phase-shift error). The simulation was performed with a NA = 0.85 at λ = 193nm. Simulation by Rajesh Menon.

Light going through path 2 will only travel in air, so n = 1.

$$\Psi_2 = A \cdot e^{i \cdot \vec{k} \cdot d} = A \cdot e^{i \cdot \frac{2\pi}{\lambda} \cdot d} \qquad \textbf{3 - 5}$$

At depth d, we want a π shift between the radiation that traveled path 1 and the one that traveled path 2, therefore:

$$\Delta\Theta = \pi = \frac{2\pi}{\lambda} \cdot n_r \cdot d - \frac{2\pi}{\lambda} \cdot d = \frac{2\pi}{\lambda} \cdot d \cdot (n_r - 1) \qquad \textbf{3 - 6}$$

Solving for d:

$$d = \frac{\lambda}{2} \cdot \frac{1}{n_r - 1} \qquad \textbf{3 - 7}$$

Even though fabrication techniques have been developed that can achieve depth control to ~1%, it is important to understand how phase fabrication errors affect the performance of zone plates. Phase errors can result in a degradation of the focused spot in terms of efficiency, since all zero-order radiation will no longer be cancelled. Fig.3-10 provides a plot illustrating the effect of phase-error on the efficiency of the zone plate.

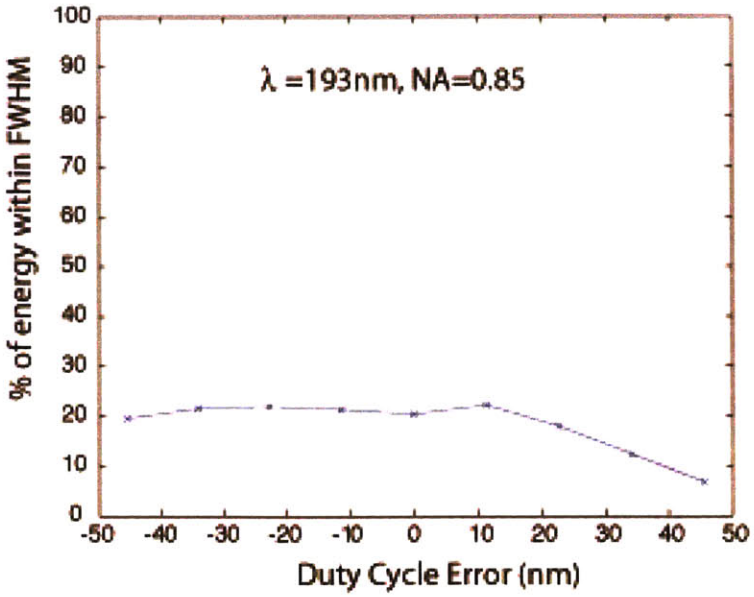

Figure 3- 11. First order diffraction efficiency versus duty cycle errors. The simulation was performed with a NA = 0.85 at λ = 193nm. Simulation by Rajesh Menon.

3.3.1.2 Duty-Cycle Errors

Duty-cycle errors are defined as the percent deviation of each pair of zones in a zone plate from their intended linewidths. This concept is easier to explain for the case of a regular grating. A grating with period *P* is said to have a 50-50 duty cycle if all the lines and spaces constituting the grating have a width of *P/2*. If the lines are wider than the spaces, or vice-versa, the grating's duty cycle is no longer 50-50, and a percent error can be associated with this deviation. As was mentioned earlier, a zone plate can be described as a diffractive element containing a large number of small-area gratings, and locally, they should have duty cycle that are as close to 50-50 as possible. Deviations from such a situation will result in the appearance of even orders in the diffracted radiation, in addition to the always-present odd orders, resulting in a degradation of the focused spot in terms of efficiency. Fig.3-11 provides a plot illustrating the effect of duty-cycle errors on the efficiency of the zone plate.

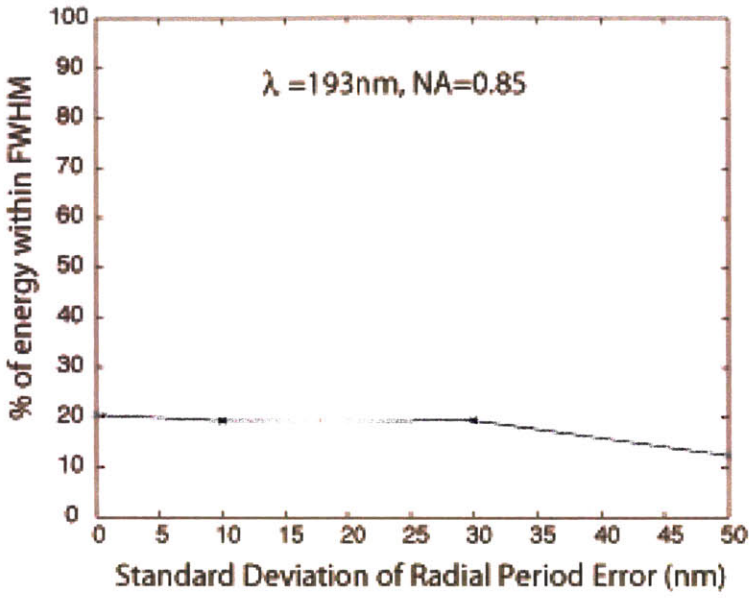

Figure 3- 12. Simulation of radial period errors versus zone-plate efficiency at a fixed focal plane. The simulation was performed with a NA = 0.85 at λ = 193nm. Simulation by Rajesh Menon.

3.3.1.3 Radial Period Errors

Radial period control is the determining factor in optimizing how well-tuned zone plates are to the wavelength of choice, in turn determining our ability to control the focal length of the zone plates. This last parameter, the focal length, is critically important, since for large zone-plate arrays that can span many square centimeters in area. Focal length uniformity is paramount if we want all zone plates to create a diffraction-limited spot at the same focal plane. Deviations from a single focal plane will result in different zone plates in the array writing features with different dimensional control, something unacceptable in state-of-the-art lithography. An appropriate metric to analyze this type of error consists in measuring how the PSF degrades in terms of efficiency, for a fixed focal plane, as radial period errors are introduced. Fig.3-12 provides a plot illustrating the effect of radial period errors on the efficiency of the zone plate.

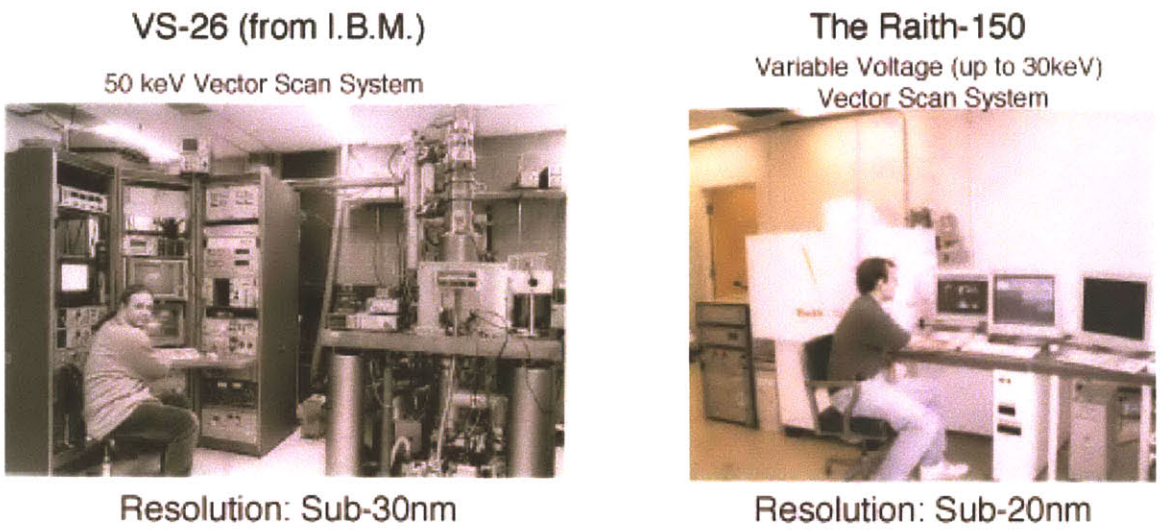

Figure 3- 13. Electron beam lithography systems available at the NanoStructures Laboratory at M.I.T.

3.3.2 Fabrication of Zone Plates by Means of Electron-Beam Lithography

The fabrication of zone plates requires the definition of large number of circular structures requiring precise width and pitch control. Electron-beam lithography systems are particularly well tailored for this application. The following three sections provide a description of some of the key challenges that have to be solved in order to fabricate high-resolution phase zone plates with good fidelity by means of electron-beam lithography.

Two different electron-beam lithography systems were utilized for the fabrication of zone plates and zone-plate arrays. A picture of the two systems along with some of their key specifications can be seen in Fig.3-13. Both e-beams are vector scan systems capable of high-resolution, but have very different electron-beam optics and acceleration voltages. These considerations can be important, depending on the application requirements.

3.2.2.1 Writing Strategies for Zone Plates

There are a number of important considerations that have to be well understood prior to fabricating circular diffractive elements by means of electron beam lithography.

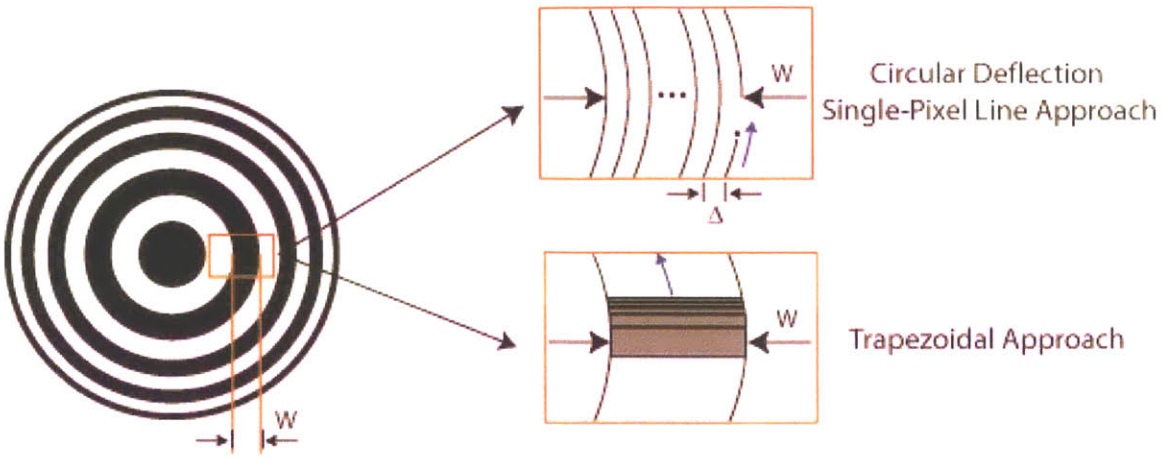

Figure 3- 14. Electron beam lithography writing strategies for curved-shaped structures.

They can be summarized as: (1) the challenge of writing circular features for systems that are typically optimized for Manhattan geometries, (2) pattern placement considerations, (3) the presence of proximity effects. This section addresses these three key concerns.

Writing Circular Features with E-Beam Lithography

The use of vector-scan electron-beam lithography is most practical when the pattern to be exposed can be efficiently broken down into a set of primitive shapes that the system knows how to fill in. Traditionally, systems are optimized for the generation of trapezoidal structures, which form the basic structures of Manhattan geometries. However, since this writing strategy involves the creation of the desired pattern by adding trapezoids of different sizes, it is very inefficient for circular geometries. For these geometries, with a large number of curved shapes, the trapezoidal process implies an unacceptable tradeoff between storage, writing time and pattern fidelity requirements [Ref 3-9].

We have implemented a solution in the two available e-beam systems at the NanoStructures Laboratory (shown in Fig. 3-13) that is capable of writing structures with curved shapes efficiently, bypassing the trapezoidal approach altogether.

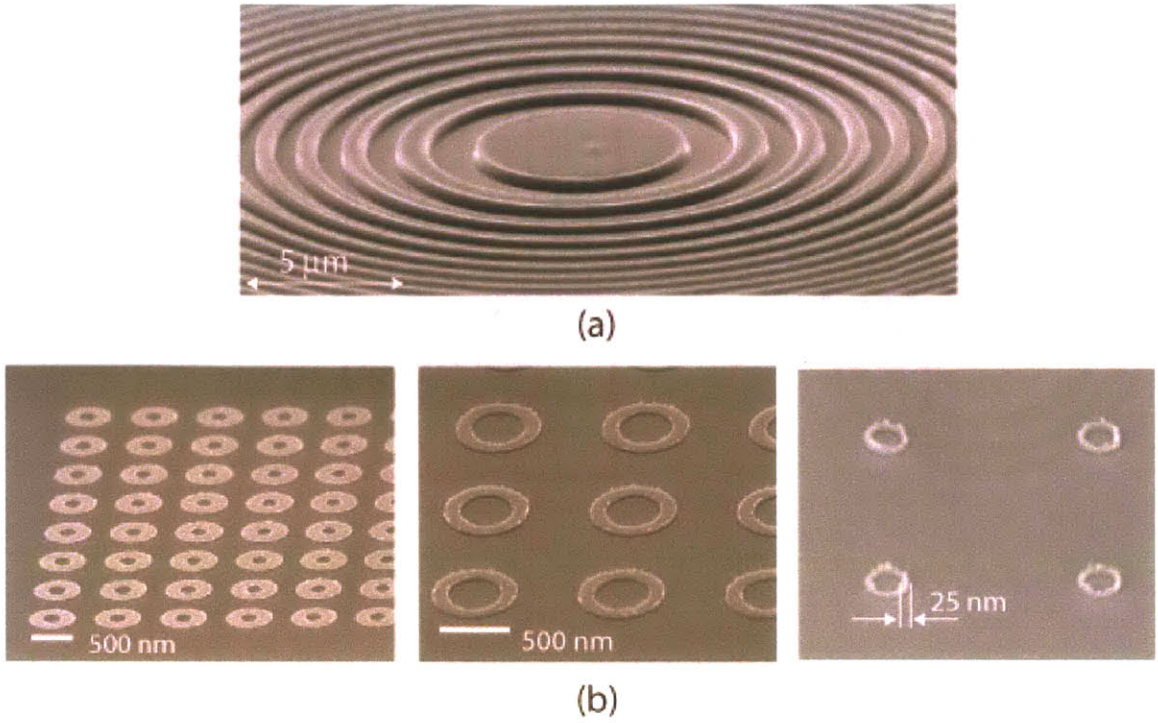

Figure 3- 15. Circular structures created with the RAITH-150 electron-beam lithography system. These circular elements were written with the single-pixel-line circular deflection writing strategy. (a) central zones of a zone plate (note the absence of pixilation of the curved elements thanks to the circular deflection of the beam), (b) arrays of magnetic nanorings (as small as 25nm) to be used for magnetic memory applications.

The writing strategy relies on the ability to deflect the beam in a circular manner, and hence create large area circular patterns by the addition of many circular single-pixel scans. A schematic of the *trapezoidal approach* and the *circular deflection technique* applied to the fabrication of circular structures is depicted in Fig. 3 – 14. In the circular deflection technique each zone of the zone plate is broken into an integer number of single-pixel line polygons with more that one thousand points each (therefore creating an excellent approximation to a circle). By exposing sequentially each of these single-pixel circles of increasing radius (the circles are typically spaced 18nm apart, but this spacing can vary at will), zones with precise dimensional control and excellent uniformity can be created. This writing strategy allows for the fast creation on zone plates, with relatively small files that don't require millions of trapezoids to approximate the circular structures of zone plates. Electron beam settling times are also much reduced with this method, since no settling is required during the exposure of each single pixel circle, as opposed to

the case requiring large number of trapezoids (for each trapezoid, some beam settling time is involved). The *circular deflection* technique has the added advantage that the dose can be controlled within each zone. This control becomes relevant for diffractive optics applications that require sloped zone profiles and zones with different phase heights (see section 4.1.3 for an analysis on why this turns out to be very useful). Fig. 3-15 contains four scanning electron micrographs showing a variety of circular structures that can be written employing the circular deflection technique. Fig.3-15(a) provides a view of the central zones of a zone plate, and one can note the excellent patterning fidelity that can be achieved with this technique in terms of concentricity and absence of pixelization effects (resulting in low edge roughness). Circular structures of very small dimensions (with features as small as 25nm) can be readily achieved, as shown in Fig.3-15(b). The figure contains nanoring magnetic elements intended for magnetic memory applications.

Another important consideration concerning the fabrication of diffractive optical arrays by means of electron-beam lithography concerns the ability of e-beam systems to accurately place features on the substrate. Since for the Zone-Plate-Array Lithography application large area patterns must be stitched by means of multiple zone plates, pattern-placement errors introduced by the e-beam lithography tool will be a significant contributor to how well a ZPAL system performs in terms of stitching. There are other key contributors to this overall stitching error budget, namely *angular illumination errors* (i.e. if zone plates are illuminated at an angle, the spot will swivel accordingly, introducing a placement error), and *stage scanning errors* (in ZPAL, pattern control is ultimately limited by how accurately the stage can be scanned). This section considers the pattern placement requirements for e-beam generation of diffraction optical arrays to be utilized in ZPAL systems.

In order to allocate appropriate budget errors, we will assume a ZPAL-tool that will meet the demands of the 100nm node. According to the International Technology Roadmap for Semiconductors 2001, the 100nm node must have 3-sigma Critical Dimension (CD) control values that range from 12.2 nm for DRAM devices to 5.3nm for ASIC devices. Assuming a ZPAL tool employing 1 million diffractive elements, the zone-plates would cover a 10x10cm area (at λ = 193nm typical zone plate diameters are

~100 μm). This area, similar to that of a conventional mask, would have to meet the above-mentioned specs.

In terms of pattern placement, state-of-the-art pattern generators such as Etec's MEBES-eXara electron-beam-lithography system can achieve placement accuracies of ~20nm (3 sigma) over the area of a mask. Given this fact, the placement accuracy of the writing tool eats up our entire CD error budget for a ZPAL tool (and more). However, it is important to realize that, (1) *local* placement errors are likely to be much smaller (something that can be of use depending on writing strategy), (2) the placement errors can be mapped and later corrected via software in the ZPAL tool, and (3) a solution to improve the pattern placement of e-beam lithography systems exists and can be used to achieve 1 nm pattern placement over large areas (this technique is called Spatial-Phase-Locked Electron-Beam Lithography, SPLEBL).

Spatial-phase-locked e-beam lithography (SPLEBL) is a technique under development at MIT for about 10 years, designed to achieve nanometer-level placement accuracy in e-beam lithography. The technique is unique to MIT. The basic idea is to use fiducial grids, fabricated using interference lithography (or a derivative thereof) to determine the placement of features written with the e-beam by continuously tracking the position of the e-beam. Any deviation of the beam from its intended location on the substrate is sensed, and corrections are fed back to the beam-control electronics to cancel errors in the beam's position. The virtue of interference lithography (IL) is that the gratings and grids produced have the property of long-range spatial-phase coherence and hence can be used as metrological standards or fiducial grids.

There are several modes of SPLEBL (see Fig.3-16), including the "segmented-grid mode" and the "global-fiducial-grid mode." For fabricating a regular array of zone plates, the segmented-grid mode (SGM) is preferred. In the SGM, a vector-scan e-beam system is used. A grid, produced by IL, is transferred to the substrate upon which the zone plates are to be written, but only in the corners of the e-beam writing field. These grid-based alignment marks might be, for example, about 1 or 2 microns square, and the grid period might by 200 nm. Gold is an ideal material for the grid-based alignment marks; this is the only material that has been used to date. Gold produces a strong secondary-electron or backscattered-electron signal. Alignment of the e-beam scan field

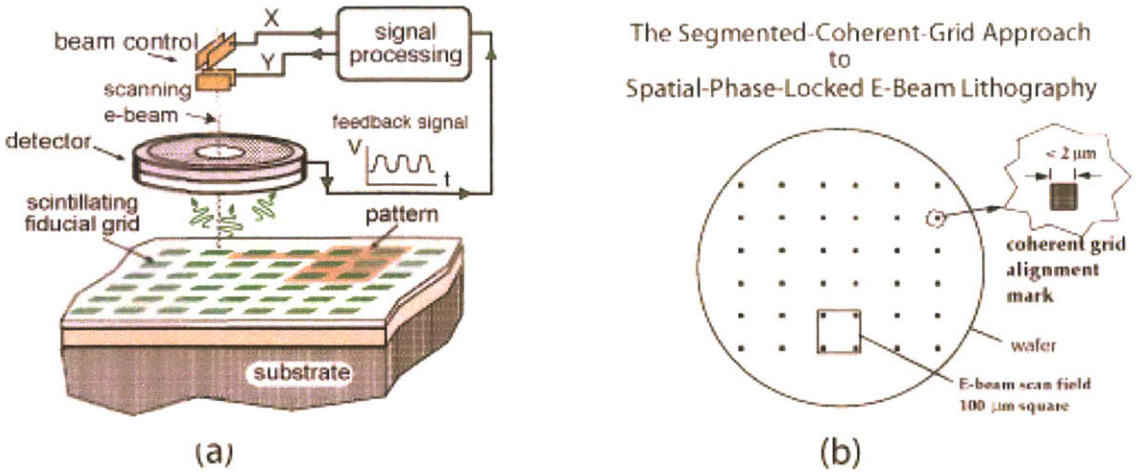

Figure 3- 16. Illustration of two modes of spatial-phase-locked e-beam lithography (SPLEBL), (a) the global-fiducial-grid mode, and (b) the segmented-fiducial-grid mode. In (a) a periodic signal is emitted from a grid placed on the substrate as the beam is scanned, enabling a feedback loop to ensure sub-1 nm accuracy of beam placement. In (b) an array of marks, consisting of segments of an interferometrically produced coherent grid, ensure sub-1nm placement via phase detection on the signal from the marks. Such marks could be placed in the spaces between zone plates of a ZPAL array.

relative to the grid-based alignment marks is done using Fourier-domain techniques, as these, in principal, allow alignment to within about 1/2000 of the grating period, or about 0.1 nm.

Experimental results to date have shown an absolute pattern-placement-accuracy, mean plus 3-sigma, of 6 nm. This number is limited by two factors, the least-count of the laser interferometer, and the fact that the SGM is a "look then write" scheme, i.e., drift can occur in the time between the locking and the writing. The real time version of SPLEBL, in which a fiducial grid is patterned over the entire area of the substrate as opposed to only in the corners of the field, has been shown to achieve a pattern-placement accuracy of 1nm [Ref 3-10].

And additional important benefit of employing a technique such as spatial-phase locking is that it would enable one to match the outer periods of zone plates to better than 1 nm, and hence ensure that all zone plates in the array focus at the same focal plane (to within the depth of focus, which in the case of high-NA zone plates operating at 193nm is about 400nm). This requirement is critical in order to maintain CD control. As was described in Section 3.3.1.3, the focal length of a zone plate is fundamentally determined

by the pitch of the zones. The ability to control to sufficient accuracy this pitch will hence determine how repeatable zone plate arrays can be manufactured in terms of focal length.

According to the SIA Roadmap, electron-beam lithography systems must have placement accuracies of 21nm for the 100nm node over the entire area of the mask. This implies that no feature of the mask can be misplaced by more than 20nm from its intended location over a 10x10cm area. This requirement does not contain enough information to assess the quality of the zone plates that can be manufactured by means of commercial high-throughput electron-beam lithography systems. In a way, it provides a worst-case scenario, indicating that any given zone within a zone plate can have a misplacement of ±20nm with respect to its intended position. That is, according to this placement accuracy, the local pitch of the zone plates can be controlled to no better than 40nm (i.e. since the pitch of our outer-most zones will be 200nm for the 100nm node, all that can be guaranteed is that the pitch will be between 180-220nm, since the previous to last zone could be misplaced –20nm from its intended position and the last zone could be misplaced +20nm in a worst-case scenario situation). Were this to be the case, it would be impossible to fabricate 1 million zone plates with matched focal lengths by means of electron-beam lithography that adhered to the letter of the SIA specification.

However, this is certainly not what the 20nm placement accuracy metric is indicating. It must be the case that the local pitch control of a state-of-the-art e-beam system is much better than this, closer to the nanometer mark that will be required for the fabrication of large zone-plate arrays. For one, the ability to control the pitch in electron beam lithography is chiefly determined by the accuracy to which the e-beam writing fields can be calibrated. This calibration can be controlled to 1 part in 100,000 if necessary. That is, if 200nm period outer zones are to written (to achieve 100nm resolution with a ZPAL system), the error in the pitch due to field calibration is in the order of a few picometers. At the same time, it is true that a characteristic of all e-beam systems not operating with SPLEBL is that they are open loop, and that the beam's position with respect to the substrate can drift due to stray fields, vibration, etc. It is indeed quite possible that significant placement errors are present within any given field, but it is more likely that long term drifts due to thermal expansion, sample height variations and stage errors are the key contributors to the 20nm placement

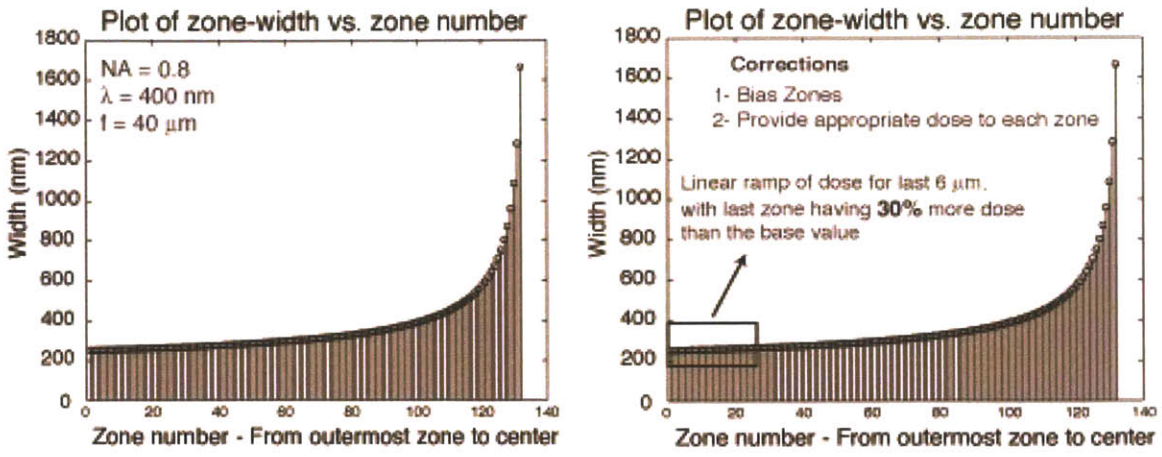

Figure 3- 17. Zone plates contain a large number of features requiring precise dimensional control, requiring careful optimization of the e-beam writing strategy to compensate for proximity effects. Left: Plot of the widths of the zones of a zone plate versus zone number. Note that for the 0.8 NA zone plate designed for $\lambda = 400$nm, widths vary continuously from ~200nm all the way up to 1.6 μm. Right: Extensive experimental tests as performed and corrections are applied to compensate for proximity effects. Among the corrections performed, the last zones of the zone plate receive a larger dose than the inner zone's dose.

accuracy, and that locally, for any given zone plate, the pitch of the zone plates can be controlled to a fraction of this value. As a final point, it is worth noting that the chief concern in terms of zone-plate-array fabrication is repeatability from zone plate to zone plate, and that pitch errors can be tolerated so long as they are consistent across the array.

3.2.2.2 Proximity Effect Correction for Zone Plates

Although zone plates can be fabricated with the planar process utilizing standard lithographic equipment, careful optimizing has to be performed in order to create diffractive elements with optical performance close to ideal. Zone plates are challenging structures to write with electron-beam lithography systems. So much so that they have long been used as resolution structures to test the performance of e-beam systems. The chief reason for the challenge lies on the circular nature of the pattern (which we have just addressed), and the large number of precisely controlled linewidths that must be achieved in a dense grating like structure. Fig.3-17 illustrates this last point with a plot of

the zone width versus the zone number for a λ = 400nm, 0.8 numerical aperture with a 40μm focal length. As can be seen, zone widths ranging from ~200nm all the way up to 1.6 μm have to be addressed in a continuous manner. The problem is very similar to writing a chirped grating, except that it is done in a radially symmetric fashion.

The radially-symmetric chirped grating present three key challenges for an electron-beam lithography system. *The first* one has to do with astigmatism of the beam. It is very important to properly adjust the beam prior to and during exposure to create round spot with minimized stigmatism, in order to prevent different parts of the circular zones from having different widths. This problem is somewhat mitigated in that the size of the beam is much smaller than the size of the features being exposed, as is the case when writing zone plates for the UV, where the minimum feature size in well over 100nm and e-beam diameters are less than 20nm.

The second challenge has to do with the digital-to-analog converter (DAC), responsible for allowing a discretized digital pattern to be converted into an analog signal (a current) capable of deflecting the beam to the right position on the substrate. Digital-to-analog converters for electron-beam-lithography systems can have different capabilities, ranging from 14 to 16 bits. The VS-26 lithography system available at the NSL has a 14-bit DAC, whereas the RAITH-150 has a 16-bit DAC. A brief calculation will illustrate why this is important. Let's assume that a zone plate has a diameter of ~200 μm, and therefore we utilize a 200 μm electron-beam field size. A 14-bit DAC will result in a 12.2nm address grid, where a 16-bit DAC would enable a user to have a 3 nm grid. This can have important consequences for zone plate writing, since the outer zones of high-numerical-aperture zone plates can vary in pitch by figures closer to the nanometer mark than to the tens of nanometer figure.

The third challenge concerns the presence of proximity effects in electron-beam lithography. Proximity effects arise because of electron back-scattering from the substrate, with the result that the exposure dose at a given location depends not only on the local incident dose, but also on the dose incident at all points within the electron range [Ref 3-11]. This effect, in combination with the forward spreading of the electron beam, causes the pattern obtained in resist to differ from the geometric pattern addressed by the beam. While this effect has been known for decades, and serious

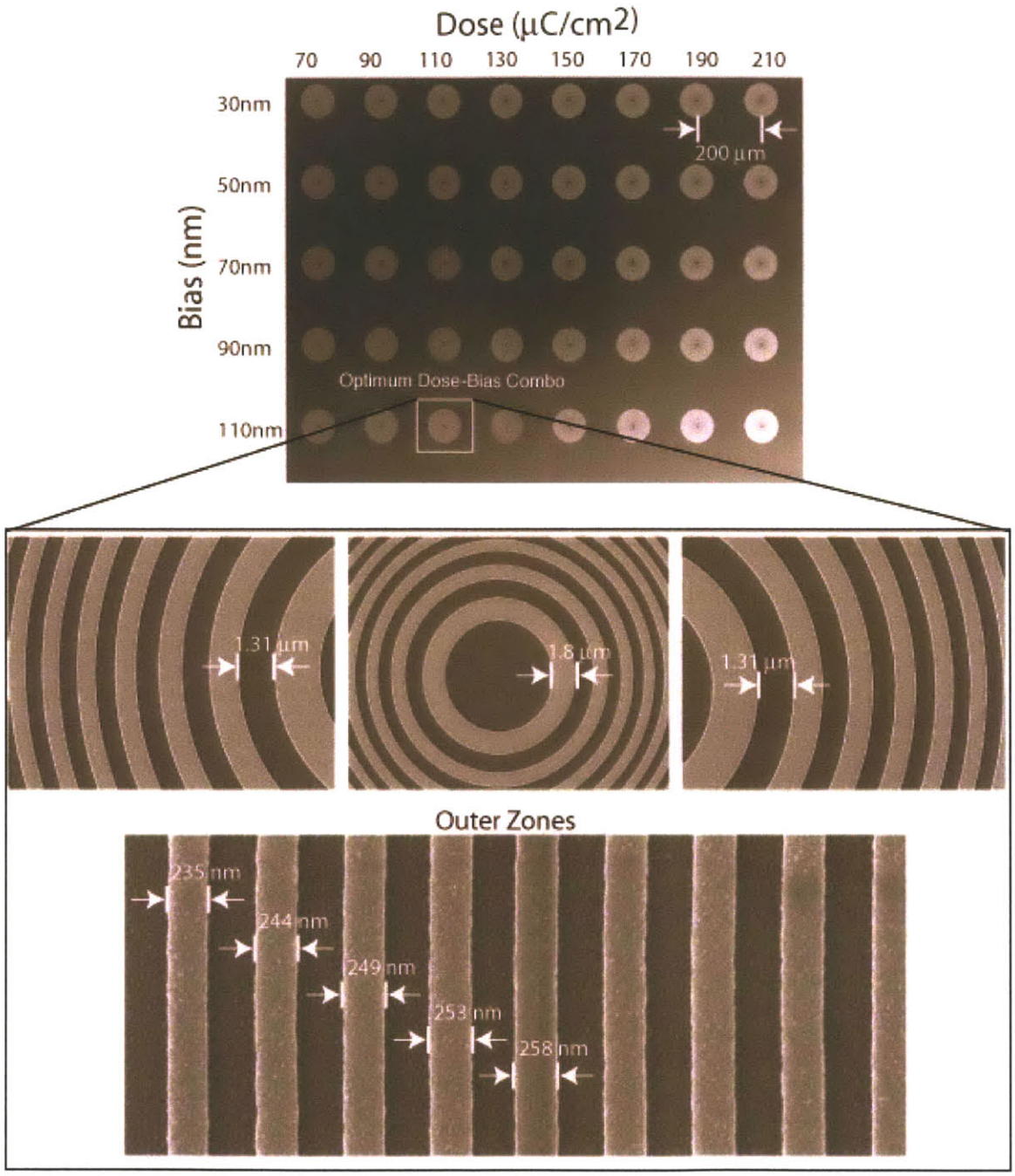

Figure 3- 18. Scanning electron micrographs of an array of zone plates exposed with the RAITH-150 at different doses and different biasing aimed at optimizing dimensional control. Each zone plate of the array is inspected and measured in order to tabulate the effect of various dose-bias combinations.

modeling efforts have been undertaken by both industry and academia, there is no standard solution available to the e-beam user community. Because proximity-effect correction depends on the substrate, pattern, acceleration voltage and resist used, no general technique is likely to work for all users. Hence, one must address and solve this problem on a case-by-case basis. To correct for this effect we can: (1) vary the dose applied to each feature, and (2) change the shape and/or width of features to compensate for these effects (changing the width of features is typically known as *biasing).*

Extensive and detailed efforts were undertaken in order to minimize proximity effects for the exposure of zone plates. The process is laborious, but good results can be achieved. It starts by exposing an array of a given zone plate at a large number of doses, as well as with different zone-width biasing combinations, as illustrated in Fig.3-18. Each zone plate of the array is then inspected and measured in order to tabulate the effect of various dose-bias combinations. After selecting the optimal dose-bias combo, some proximity effects will still remain present if a single and uniform bias was provided to all zones of the zone plate. In particular, it is unlikely that the central zones and the outer-most zones will have close to 50-50 duty cycle for the same dose-bias combo. As indicated in Fig. 3-18 (right), this limitation can be tackled by providing a dose correction that can vary according to a specified dose progression for the last X-μm of the zone plate. This again involves an experimental confirmation, with the results depending on the acceleration voltage of the e-beam, the substrate used and the pattern exposed. It was experimentally determined, that for 30kev acceleration voltage, with fused silica substrates, a linear correction for the last 6μm (this roughly corresponds to the backscattered range at this voltage), in which the dose is increased linearly from the base value up to a 30% higher dose for the last zone, can achieve nearly optimal dimensional control across all the zones of the zone plate. In order to also optimize for sidewall profiles, linear zone plates were fabricated with all the previously mentioned proximity effect correction techniques, with the goal of being able to cleave these samples and look at them edge-on with a scanning electron microscope. A sample of some of the results obtained from these experiments, are shown in Fig.3-19. The linear zone plates were designed to have the exact same dimensions as the ones intended for the final circular zone plates. It is worth noting, that despite the laborious

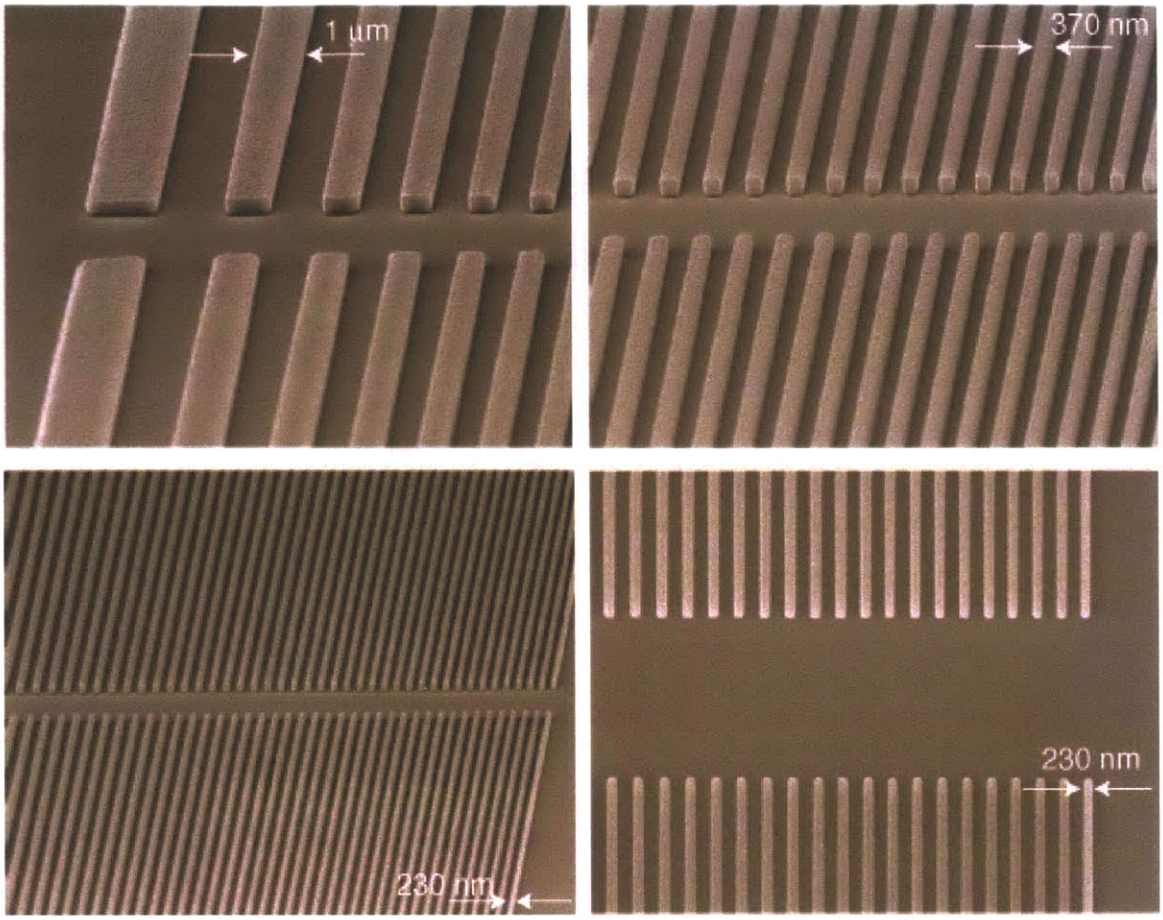

Figure 3- 19. Scanning electron micrographs of linear zone plates aimed at testing proximity effect correction schemes and optimizing sidewall profiles. The zone plates were exposed with the RAITH-150, at 30 keV acceleration voltage. The resist utilized was HSQ, a negative spin-on-glass resist from Dow Corning.

nature of the optimization process, the final result was excellent. Zone profiles were smooth and vertical, and duty-cycle control was achieved throughout all zones.

3.2.2.3 Choices of Resist

The choice of resist is an important consideration for the fabrication of zone plates and other diffractive elements. While the choice of resist is dependent on a number of other factors having to do with the post-processing of the zone plate substrate, at a minimum it is worth considering what options are enabled by choosing a positive or a negative resist.

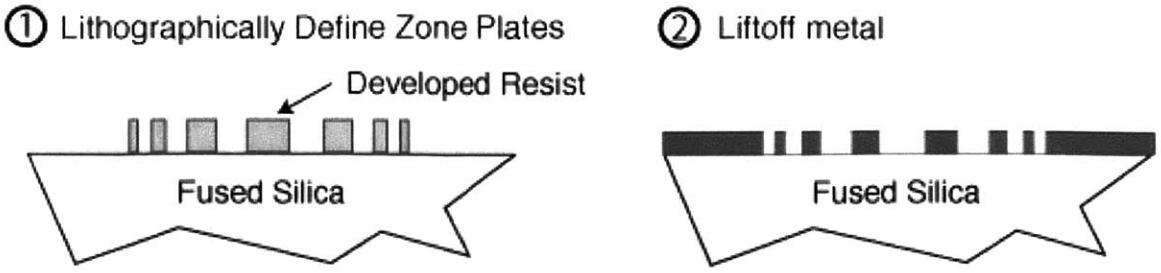

Figure 3- 20. A negative resist exposure in combination with a lift-off process provides the simplest fabrication procedure for an amplitude zone plate

As a reminder, in a positive resist the areas that are exposed to radiation will later be removed by mean of a developer, whereas in a negative resist the opposite will occur, that is, only the exposed areas will remain after development.

A negative resist exposure in combination with a lift-off process provides the simplest fabrication procedure for an amplitude zone plate (see Fig.3-20). Amplitude zone plates are clearly not as useful their phase counterpart if they are to be used for lithography applications (ZPAL).

In order to fabricate phase zone plates, processes can be developed with both positive and negative resists. Section 3.2.4 will describe in detail three fabrication procedures aimed at this goal, with the final one, utilizing a negative tone resist, being the preferred and simplest method of all.

3.3.3 Fabrication of Zone Plates by means of X-Ray Lithography

X-ray lithography was first suggested by Spears and Smith in 1972 [Ref 3-12, Ref 3-13].The principle of operation is relatively simple. The technique is a shadow-printing scheme, in which a source of radiation (x-rays in this case, with wavelengths between 6 and 14 Å) is shaped by a mask to produce the desired pattern in a resist that is sensitive to the radiation utilized (Fig.3-21). Unlike the situation for electrons and optical photons, it is very difficult to construct any type of optics for x-rays (zone plates are the only exception), and as a consequence, the x-ray exposure setup employs a 1X mask.

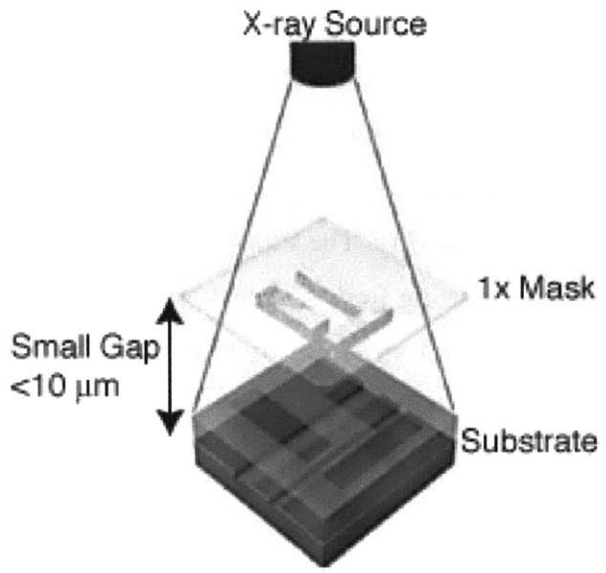

Figure 3- 21. X-ray lithography schematic.

The mask and the wafer are maintained in close proximity, typically a distance of the order of a few microns. The resolution, or more precisely, the minimum printable line width W, is dominated, to first order, by diffractive blurring at the finite wavelength λ and gap G [Ref 3-14].The relationship between mask-substrate gap G and the minimum feature size W is given by

$$G = \alpha \frac{W^2}{\lambda} \qquad \textbf{3 - 21}$$

where α is typically in the range 1-1.5 [Ref 3-15, Ref 3-16].

The 1X mask is the heart of the x-ray lithography process, and it consists of an absorber pattern on a thin membrane. The mask structure is dictated by the optical properties of the x-rays. The membrane must be transparent enough to allow for fast exposures, and yet be able to withstand handling and radiation damage. In general, the membrane will be on the order of 1 to 2 μm thick, and be made of low-Z materials for high transmission. Currently used mask membranes are fabricated with silicon, silicon nitride, or silicon carbide, while high Z materials such as gold, tantalum, and tungsten, are used as absorbers [Ref 3-17].

Since exposure is a 1X process, the placement accuracy of the pattern must be within the bounds dictated by the error allocation budget. This implies that the membrane must be rigid enough so that no distortion of the pattern is induced by the handling and exposure process. The membrane is not self-supporting, so it must be fastened to some support to provide the necessary rigidity. The support structure is usually a Pyrex ring. In general, the mask is fabricated starting from a 75 or 100mm silicon wafer, using a variety of techniques, but the fundamental structure of a mask is the same: a thin, uniform membrane is mounted on a structurally rigid holding frame. The pattern is applied on the membrane, typically by means of electron-beam lithography[3].

3.3.3.1 Zone Plates for UV-Radiation

The availability of x-ray lithography systems at the NSL provides an appealing incentive to use them for the fabrication of zone plate arrays. This section briefly describes some of the x-ray lithography masks containing zone plate arrays designed to operate at the UV. An added incentive to develop a mask-based process was provided by the desire to "cast in stone" a zone plate design that had been carefully optimized through e-beam lithography to have nearly perfect dimensional control for all the zones in the zone plates.

Although the precise details of the process are included in Appendix A, the key steps are briefly highlighted here. The objective of the process is to create a structure such as the one depicted in Fig 3-22. Starting with a standard x-ray mask, consisting of a 30mm-diameter SiN_x membrane supported on a Si ring bonded anodically to a pyrex frame, a thin layer of plating base (10 nm of Ti and 1.8 nm of Au) is evaporated onto the

[3] Pattern distortion is a serious problem in x-ray masks. The distortions are present not only from the writing of the mask via e-beam, but also due to the built-in stress in the absorber. At the NanoStructures Laboratory at MIT, an effort is underway in correcting for such distortions by means of localized heat correction techniques [Ref 3-18].

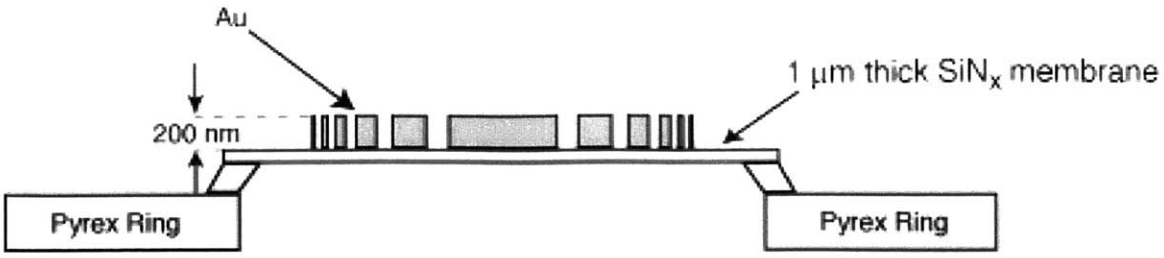

Figure 3- 22. Schematic of an X-ray mask.

mask. After spin coating the mask with the desired e-beam resist (PMMA in this case), patterning by means of e-beam lithography can take place. The mask is then developed and gold plated.

After removing the remaining resist, an absorber relief structure is left on the mask. The process must be optimized by carefully controlling and testing a large number of doses and biases during the e-beam patterning in order to achieve the right duty cycle and dimensional control in the final mask.

Figure 3-23 shows the final result of an x-ray mask with 5 sets of zone plates with numerical apertures ranging from 0.7 to 0.95. Each set of numerical apertures consists of a linear array of 4 zone plates (designed to operate at blue wavelengths) surrounded by 3 zone plates with matched focal lengths but designed to operate at λ = 633 nm (these *satellite* zone plates will be used to set the zone plate array at the right focal distance with respect to the substrate to be exposed in a ZPAL system). The top of the figure shows a number of scanning-electron-micrographs illustrating the ability to achieve a duty cycle and outer-zone-width (OZW) dimensional control on the mask, after all the processing is done, that is very close to specificatin. The bottom of Fig. 3-23 shows an optical micrograph of the central zones of one of the *satellite* zone plates after plating. Following an identical process, x-ray masks with zone plates designed to operate at λ = 400 nm containing sets of different numerical apertures, as well as larger linear arrays of zone plates, were also fabricated. All masks were also daughtered (i.e. a copy of the mask resulting in the negative of the *mother,* the original) to safeguard the originals, as well as to enhance the processing capabilities by having masks with different polarities. Different mask polarities enables the possibility the utilization of both positive and negative resists.

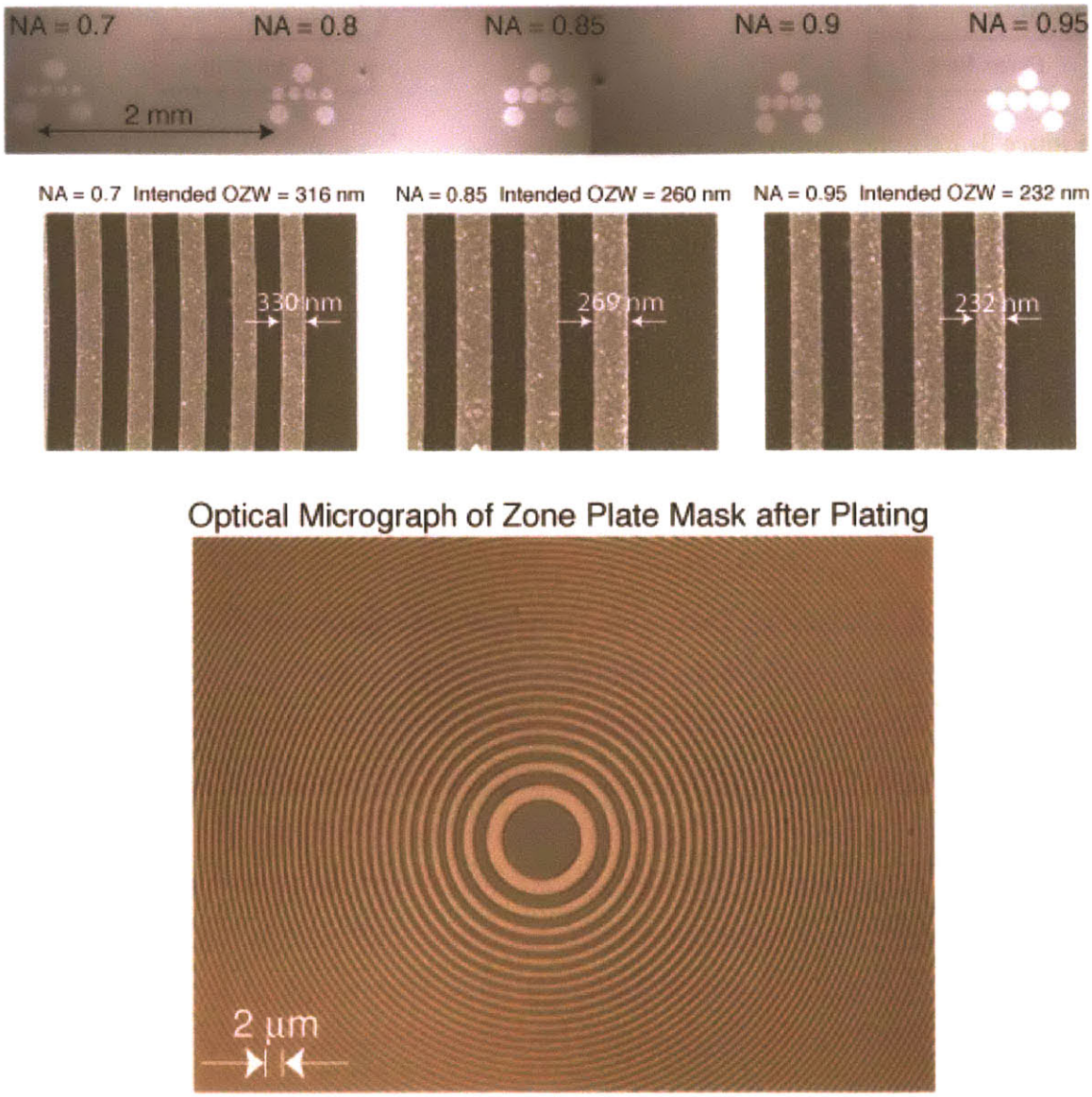

Figure 3- 23. Top: Scanning electron micrographs of x-ray mask with 5 sets of zone plates with numerical apertures ranging from 0.7 to 0.95. By careful processing, close to ideal dimensional control can be achieved. Bottom: Optical micrograph of the central zones of a 0.9 numerical aperture zone plate designed to operate at $\lambda = 633$nm.

3.3.3.2 Zone Plates for Short-Wavelength Radiation

One of the key strengths of zone-plate-array lithography comes from its extendibility to be very short wavelengths, making it potentially capable of reaching the limits of the lithographic process. For the wavelength scaling to occur, it is crucial that fabrication techniques are developed to create zone-plate arrays capable of operating in these regimes (from EUV to soft and hard x-rays). Short wavelength zone plates are also crucial for x-ray microscopy applications, and there is a rich body of work that has been devoted to fabricating and testing x-ray zone plates that can have resolution as small as 30nm [Ref 3-19, Ref 3-20].

For hard x-ray microscopy applications (this technique allows one to nondestructively investigate microproperties in the bulk of thick samples), high-aspect-ratio zone plates are required in order to obtain sufficient efficiency into the first order[4]. The high-aspect-ratio (can be several microns high) must be combined with very high resolution, with outer zone widths that can be as small as 25nm. This would imply aspect ratios in excess of 40:1 in photoresist. This is simply not achievable with standard processing, since surface tension during wet photoresist development, the drying process, and the mechanical rigidity of photoresists lead to pattern collapse [Ref 3-21].

X-ray lithography provides a technique that can accommodate the need for high-resolution and high aspect ratios. The process relies on the utilization of self-aligned multiple exposures, as illustrated in Fig.3-24[5]. Starting with a conventional x-ray mask, using a high-resolution negative resist (such as HSQ from Dow Corning), the zone plates are patterned by means of electron-beam lithography. After development, the mask is plated to the maximum thickness that can be achieved (determined by the resist height).

---

[4] The optimal thickness of the zone plate, determined by a π-phase shift requirement, depends on the wavelength, λ, and the absorber/phase shifter material properties. The exact relationship is determined by the following relation:

$$t(\pi) = \lambda/2\delta$$

where δ is determined from the complex refractive index, $n = 1-\delta-i\beta$

[5] The idea was first proposed by Azalia A. Krasnoperova, et al [Ref 3-22] and developed independently (i.e. reinvented) by the author and by Todd Hastings (also graduate student in the NSL)

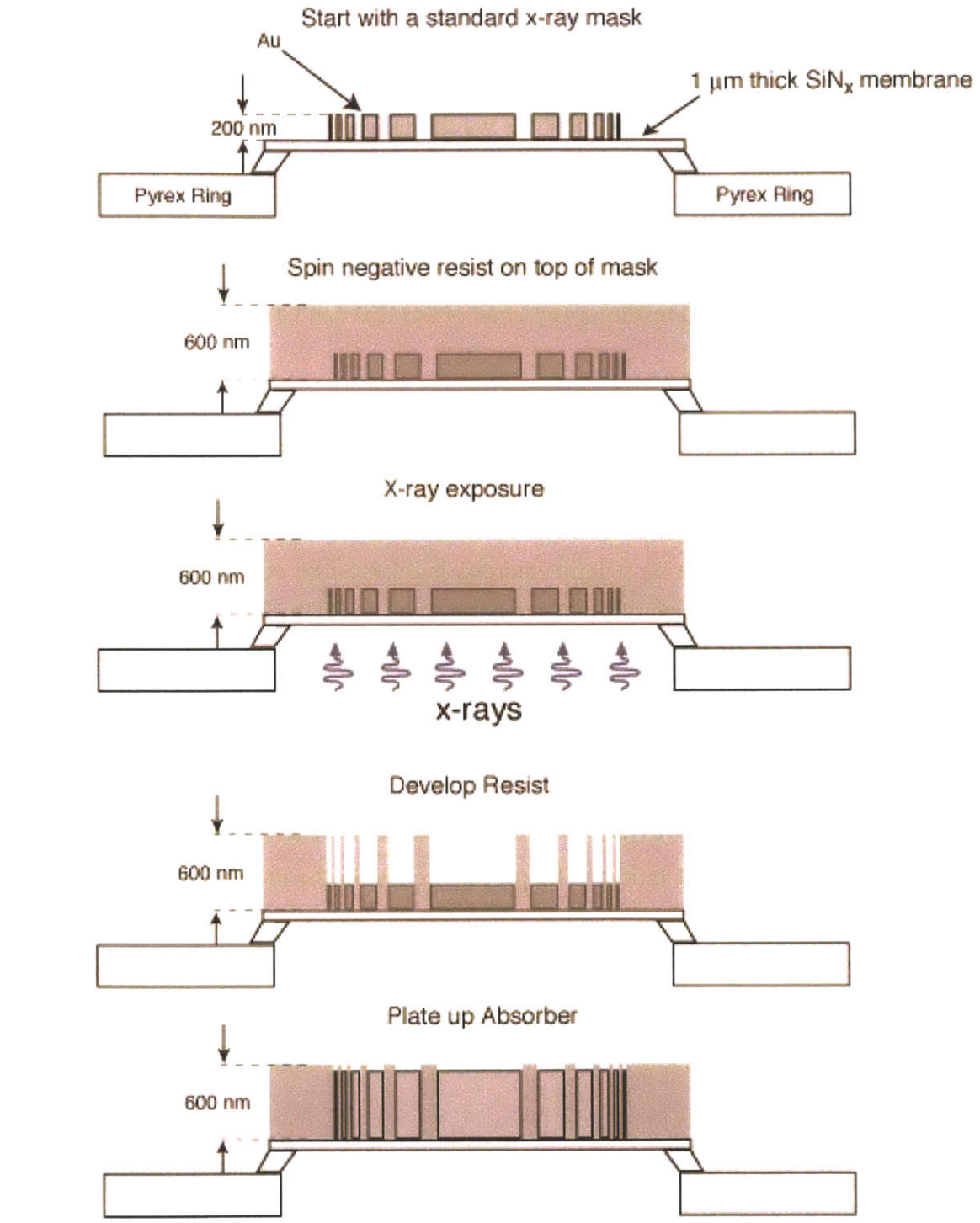

Figure 3- 24. Self-aligned x-ray lithography process flow for the fabrication of x-ray microscopy zone plates.

For high-resolution patterning, this height will typically be at most ~200nm. After plating, another layer of negative resist sensitive to x-ray wavelengths is spun on the mask (HSQ is a good solution, since it is also sensitive to x-rays). The mask is then mounted in the x-ray lithography exposure apparatus and is simply exposed from the back. The existing absorber will prevent the x-rays from reaching the negative resist that sits on top of the absorber, while all other areas will be exposed. After development, all unexposed areas will be dissolved away (this is why it is important that the resist has a negative tone). The mask can then be plated again, resulting in a higher aspect ratio zone plate with perfect alignment. This process can be repeated until the necessary aspect ratio is obtained.

The details of the process are now described in more detail. The zone plates on the x-ray mask were created by means of x-ray lithography, through a daughtering process of a mask patterned with a RAITH-150 electron-beam lithography system. The resist utilized for the daughtering process was 250nm of PMMA, baked at 180°C for 1h. The x-ray exposure time was 24 hours. A separate exposure with an optical aligner was done in order to remove all the areas surrounding the membrane that were covered with PMMA (this is important to allow an adequate contact area for electroplating). Development was done in a solution of 1:3 methyl isobutyl ketone: isopropanol (MIBK:IPA) for ~90sec (the development was monitored with an AFM). After a 20s O_2 clean, the mask was plated in a gold bath having the following parameters: conductivity = 76.5 mS/cm, temperature = 39°C, current = 14.1mA, resulting in a rate of ~20nm/min. The resulting mask, after the PMMA was removed in an acetone bath, consisted of 220nm-thick gold zone plates.

The mask was then spun-coated with a spin-on-glass negative resist (FoX-16, by Dow Corning, also known as HSQ) at 3000 RPM for 60sec, resulting in a layer 500nm thick. The resist was oven baked at 150°C for 30min, followed by a 220°C bake for another 30min. At this point, the mask was ready for the self-aligned x-ray exposure. A 14h exposure was performed. The mask was then developed in CD-26 (a TMAH based developer) for 20 min. It was then introduced in the plating bath with similar conditions to the ones previously described, except for the fact that the current was 12.9mA, as

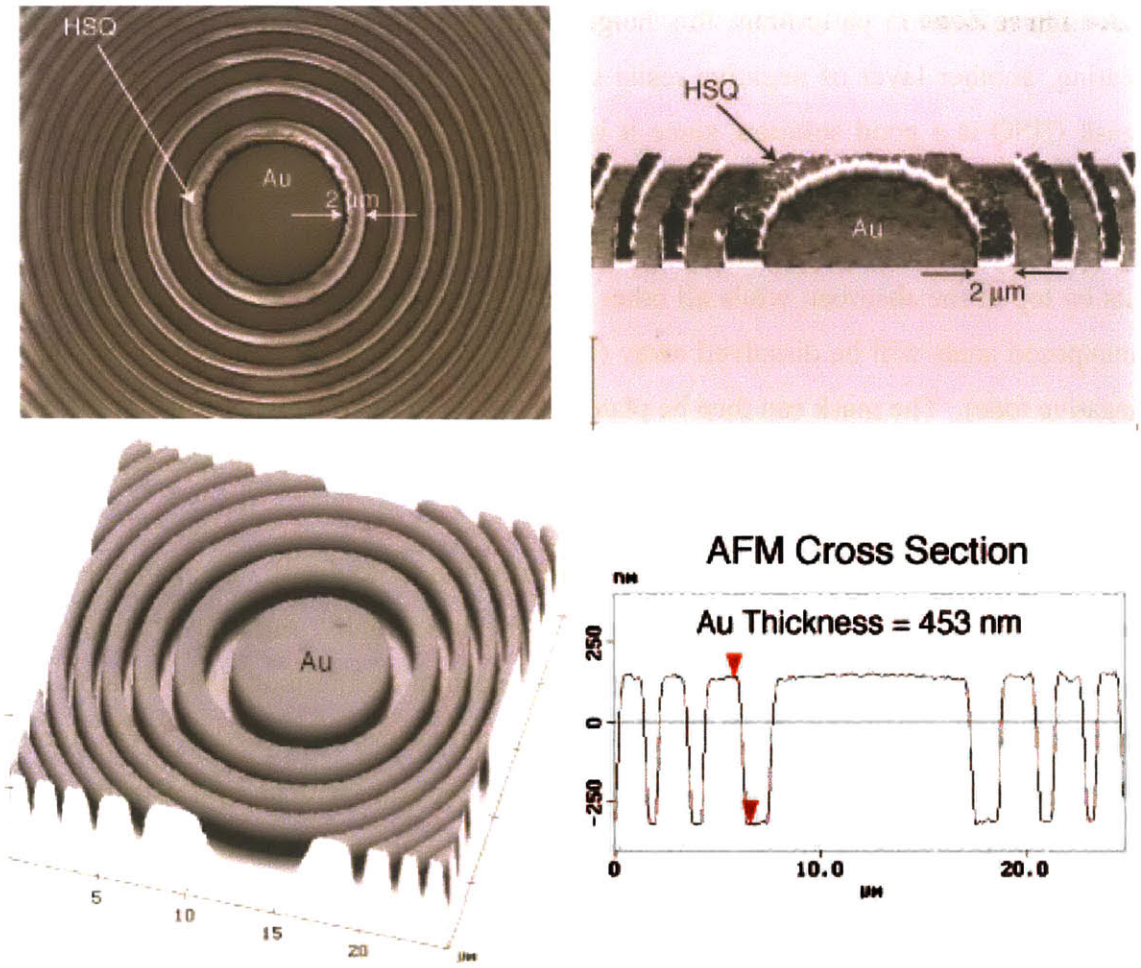

Figure 3- 25. Results of self-aligned high-aspect ratio zone plate mask with applications for x-ray microscopy. Top-Left: Scanning electron micrograph of the central zones after the self-aligned electroplating. Top-Right: AFM scan of central zones after electroplating. Bottom: After the resist (HSQ) was removed a high-aspect ratio structure remains, with an absorber thickness that could not be achieved with a single layer exposure.

opposed to 14.1mA, to compensate for the smaller plating area. The plating was monitored by means of an atomic force microscope until the gold reached the top of the resist. Fig.3-25 shows the results of this process, where zone plates were created with an absorber thickness that was 453nm, twice the height achievable with standard single-layer mask-making techniques. Higher absorber thicknesses can be readily achieved by repeating this process a number of times, since it is a self-aligned, self-planarizing technique.

3.3.4 Three Zone Plate Fabrication Processes for Lithography Applications

The following sections describe three techniques aimed at the fabrication of zone-plate arrays designed to be used for a ZPAL system operating at the UV. The processes are described chronologically, showing how the eventual final fabrication technique evolved in time from the partial successes of the original processing ideas.

The requirements for fabricating phase zone plates at UV for lithography applications can be clearly defined. *First*, as previously described, it is crucial that the dimensional control of the zones of the zone plates be as close to perfect as possible. Duty-cycle and radial-period errors should be kept to a minimum to enhance the lithographic performance of the elements. *Second*, on the substrate containing the zone plates, as illustrated in Figure 3-26, it is necessary to place an absorbing layer on the areas surrounding the elements. This absorbing layer prevents unwanted radiation from reaching the substrate when the zone plates are used for lithography. Alignment between the absorber layer and the zone plates is critical. The *third* and last key challenge, requires achieving a phase shift of π between alternate zones.

Before embarking on a description of the individual processes, let's analyze in general how these three challenges can be tackled with standard fabrication techniques. The first challenge, of dimensional control, was addressed in detail in previous sections in relation to electron-beam-lithography patterning. It is important to understand, however, that what matters is that the *final* processed zone plate achieves the dimensional control (right duty cycle and so on), and that it is of little use to start with a nearly perfect e-beam patterned zone plate if, after subsequent steps (be it reactive ion etching, be it baking, etc), the painstakingly optimized e-beam defined features are altered. The second challenge, that of placing an absorber in the areas surrounding the zone plates, can be achieved by means of two aligned lithography steps. For example, one lithography step would define the circles that would contain the zone plates (as well as a set of alignment marks), and a second step (after registering to the alignment marks) would write the actual zone plates. How well these two exposures can be aligned will have an impact on the lithographic performance of the optics, since unwanted radiation will leak through the misaligned edges of the absorber.

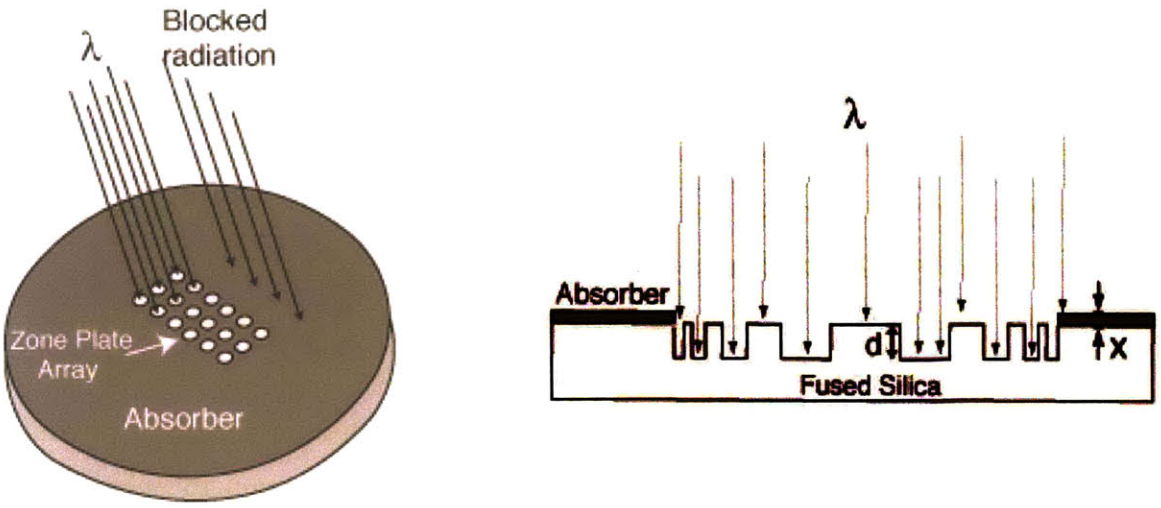

Figure 3- 26. Need for an Absorber. (a) Three dimensional view of the diffractive optical array and the substrate underneath. A layer of an absorbing material surrounding the optics is needed in order to prevent undesired radiation from reaching the substrate. (b) Side view of the fused-silica substrate with a phase zone plate etched into it.

Given the fact that zone plates will typically be patterned by means of electron-beam lithography, it is important to realize that aligned exposures with e-beam systems are always complicated and time consuming, since fields have to be aligned one at a time. The final process presented here will bypass the need for this alignment, greatly simplifying the entire procedure. The third challenge, that of creating the right phase-shift between alternate zones, is a relatively less challenging problem than the previous two. Reactive-ion etching in combination with atomic force microscopy provides a process that is both powerful and reliable. The main challenge arises from the large number of features of different dimensions that are present in zone plates, which can result in different etching rates for different areas of the zone plate. Obtaining good sidewall profiles can also be of importance in order to maximize efficiency.

3.3.4.1 The Chromium Process

The first fabrication approach undertaken is schematically illustrated in Fig.3-27. The objective was to define by means of two aligned lithographic exposures: (1) the circular area that will later contain the zone plates, and (2) the actual zones that define the optic.

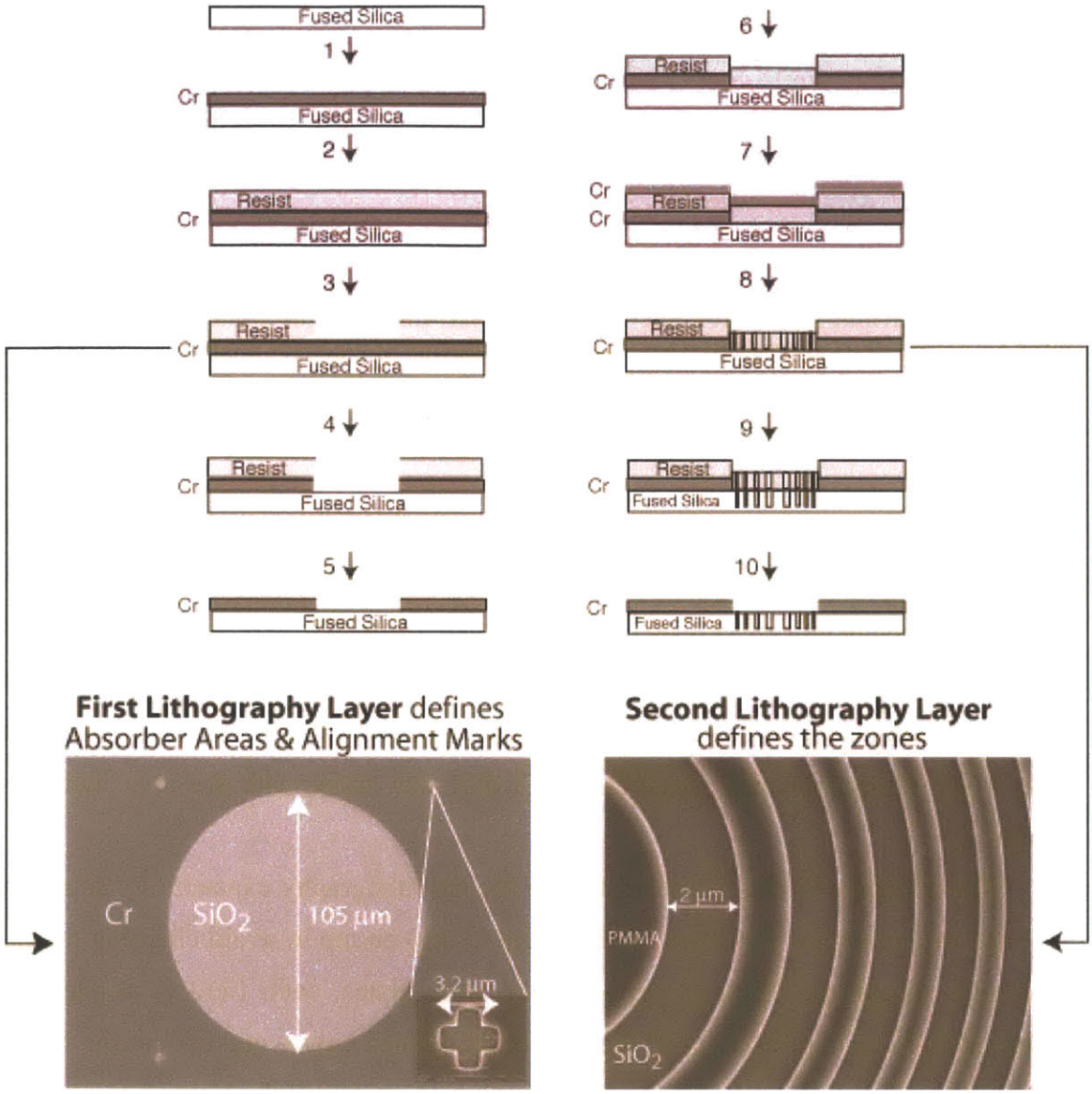

Figure 3- 27. *Chromium Fabrication Process* for UV and DUV Zone Plates. Steps 1-5 define the area where the diffractive optics will be placed in subsequent steps. Chromium (Cr) is used as the absorber material in this process, but a number of other materials could also be employed. Steps 6-8 define the diffractive optics. Steps 9-10 transfer the resist patterns into the fused silica substrate by means of reactive-ion-etching.

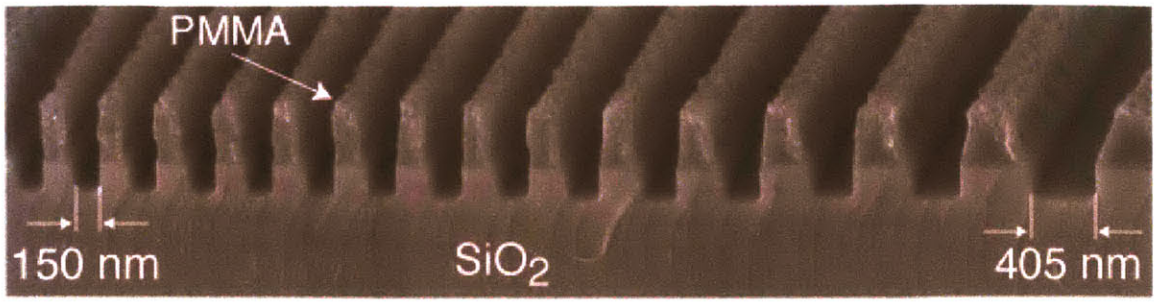

Figure 3- 28. Scanning electron micrograph of fused silica sample etched in CHF_3 with PMMA as a mask. The PMMA was patterned by means of electron beam lithography. The chamber conditions inside the RIE were the following: Pressure = 20 mT, DC Bias = 200V, Gas = 20 sccm of CHF_3.

Starting with a fused-silica substrate, a layer of chromium is evaporated. The thickness of this layer is chosen such that it will absorb close to 100% of the incident light at the wavelength of choice. After spinning resist (PMMA was used for this process), the circular apertures are defined, along with a set of alignment marks placed at the edges of each electron-beam lithography field. Once developed, with the resist as a mask, a wet chromium etch removes the Cr that was underneath the area that was exposed.

The substrate is then prepared for the second lithography exposure by spinning resist and evaporating a thin layer of chromium (5 nm) on top to avoid charging during the e-beam exposure. Prior to exposing the zone plates, each field is aligned by appropriately scanning the edges of the previously defined circles and registering to the existing alignment marks. The system then proceeds to expose all the zone plate zones in the manner described in Section 3.2.2.1. Development of the resist defines a relief structure containing the zones. The resist is then used as a mask in a reactive-ion-etching (RIE) step used to create a π-phase shift between alternate zones, as illustrated in Fig.3-28. Process monitoring zone-plates are placed in particular locations on the substrate, allowing one to check etch depths by means of atomic-force-microscopy after locally removing the resist mask through a controlled oxygen ashing step. Great accuracy can be achieved in terms of phase-etch control by such careful processing. The remaining resist is removed through an oxygen etch. The final processing steps consist in covering up the

alignment marks that surround each zone plate of the array. This can be done by spinning a positive resist and by opening up the areas over the alignment marks by means of an optical lithography exposure[6]. After development, chromium is evaporated and a lift-off is performed. The zone plates are now ready.

While this process provides a viable method for zone plate fabrication, it suffers from some serious deficiencies. Let's briefly analyze them. The first and most serious limitation is created by the chromium wet-etching step. The complications are twofold: (1) the etch is isotropic, making it difficult to control the final dimension of the circle, (which can cause a deleterious misalignment between the outer zones and the absorber), and, (2) chrome on oxide is a problematic combination to etch, with the Cr having a tendency to leave small nanometer-sized islands that can not be removed. This problem is severe, and becomes critical because the small islands of un-etchable Cr serve as a mask in the SiO_2 RIE step (step 9 in Fig.3-27), causing "grass" in the etched zones. The author could not find a systematic way to solve this problem, despite valiant and desperate efforts that spaned many months. The author still regrets such long, and ultimately wasted, days.

The process suffers form other limitations that are less serious, but that nevertheless hinder the applicability of the technique for large-array manufacturing. The double lithography step requires aligning each zone plate one at time. This process takes a few seconds per field, if electron-beam lithography is used. If a million zone plates are required, even ignoring the actual zone plate writing time, the process would take millions of seconds (spent just doing alignment), a clearly unacceptable figure.

---

[6] This exposure was done with an optical microscope. The process is as follows: With a filter preventing the illuminating light from exposing the resist, each alignment mark is located. An iris is closed to illuminate only an area only slightly larger that the mark. The filter is removed for a brief time allowing the white light to reach the substrate and hence locally expose the resist. The process is repeated for each mark, four per zone plate.

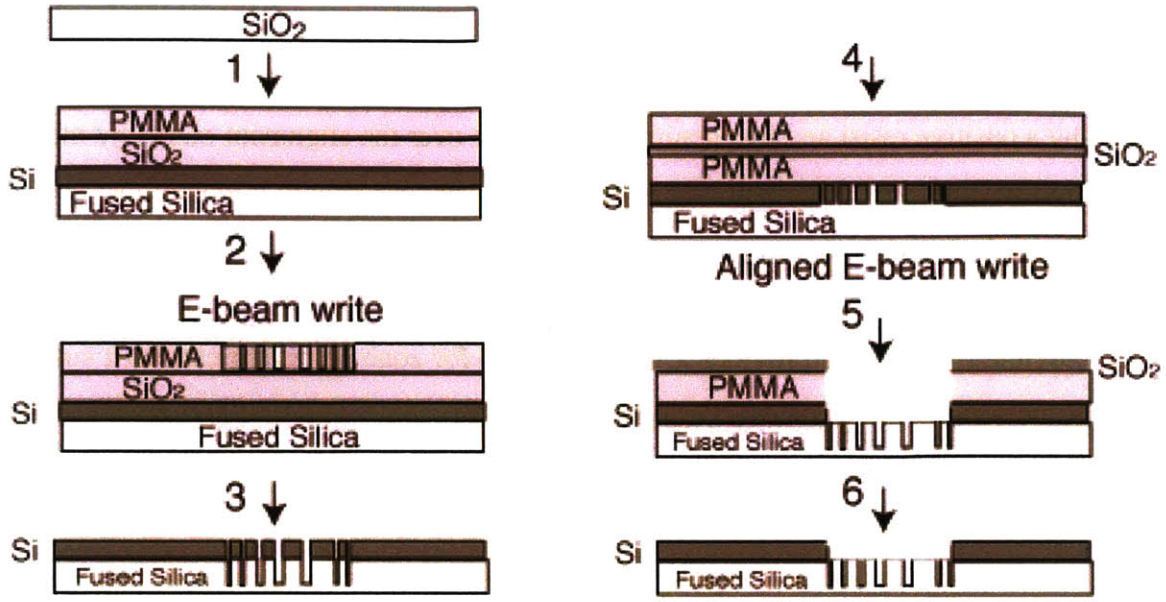

Figure 3- 29. *Silicon Fabrication Process* for UV and DUV Zone Plates. Steps 1-3 define the zone plate zones and alignment marks, which get transferred first into silicon, and then into the fused silica. Steps 4-6 remove the silicon mask the remains over the zones.

3.3.4.2 The Silicon Process

The desire to remove all wet-etch-based steps became a priority in order to develop a robust zone plate fabrication process. Given the difficulty of etching metals with the RIE capabilities available at the NSL, it was decided to utilize silicon as the absorber layer, instead of chromium. The process is depicted in Fig.3-29. The chief advantage of using Si as an absorber relies on the fact that a dry-etch technique is available to remove it (there are a number of reactive-ion etching recipes, with Cl_2 being the most widely used).

Starting with a fused silica optical flat, silicon is sputtered. The height of the Si is chosen in order to provide over 99% attenuation at the wavelength of choice (λ = 442nm). Silicon dioxide is then evaporated (this oxide layer will serve as a mask to etch the Si). The zone plates are then patterned by means of e-beam lithography. An atomic-force-microscope image of the PMMA after development is shown in Fig.3-30.

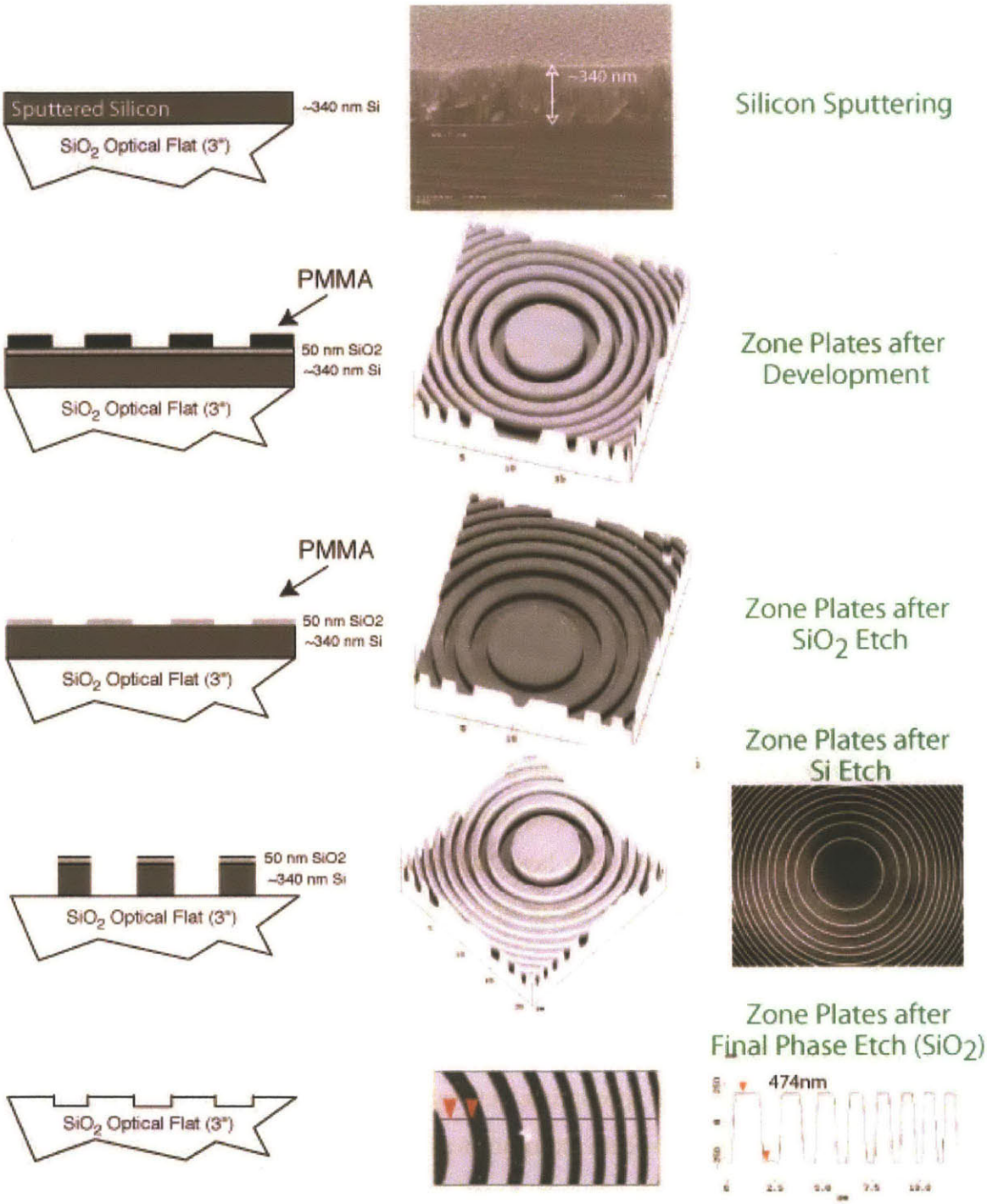

Figure 3- 30. Atomic Force Microscope images of fabricated zone plates using the *Silicon Process*. Note that careful processing allows one to obtain almost perfect phase control (see bottom AFM cross-sectional image; the etch goal was actually 474nm)

With the PMMA as mask, the zones get transferred in to the oxide layer, which in turn serves as the mask to etch the silicon layer. This later step is achieved by means of a chlorine etch inside a reactive ion etcher (RIE). At this point, we have a fused-silica substrate that contains zone plates with zones defined in silicon. The final fused-silica etch can now take place. This etch will define a π-phase shift between alternate zones, so careful control is necessary. The fused silica is etched with CHF_3 inside a RIE in a series of steps. After each step, the total etched height is measured by means of atomic-force microscopy. Nearly perfect π-phase shifts can be achieved with this technique, as illustrated at the bottom of Fig.3-30, where the goal to create a 474nm etch depth was accomplished with nanometer precision. The remaining steps of the process involve removing the Si that remains on top of the unetched zones. This is done, as is depicted in Fig.3-29 (4-6), through a second aligned exposure and subsequent RIE steps.

The above description provides a big-picture overview of the required process. Although zone plates can indeed be fabricated with this method, it is very complicated, with lots of subtle processing tricks and optimizations that were sometimes hard to reproduce. Fabricating new sets of zone plates with the process took weeks, even once all the parameters were more or less optimized. As is well known to anybody with processing experience, for every new layer that is added to a fabrication procedure, the total processing time goes up by a factor of n, where n is a number between 2 and 100, depending on the size of the moon.

Jokes aside, the process does suffer from an excess of complexity. Too many RIE steps made it hard to maintain appropriate duty-cycle control of the zones. In addition, a second aligned lithography e-beam exposure was still required, resulting in all sorts of problems due to the fact that the alignment marks were buried into the fused silica by the time all the zone etching was finished. Being able to image those marks through all the spun-on layers later added was a big challenge. And the fact remains (as was mentioned in the chromium process description) that having to go through a second aligned exposure prevents large array manufacturing.

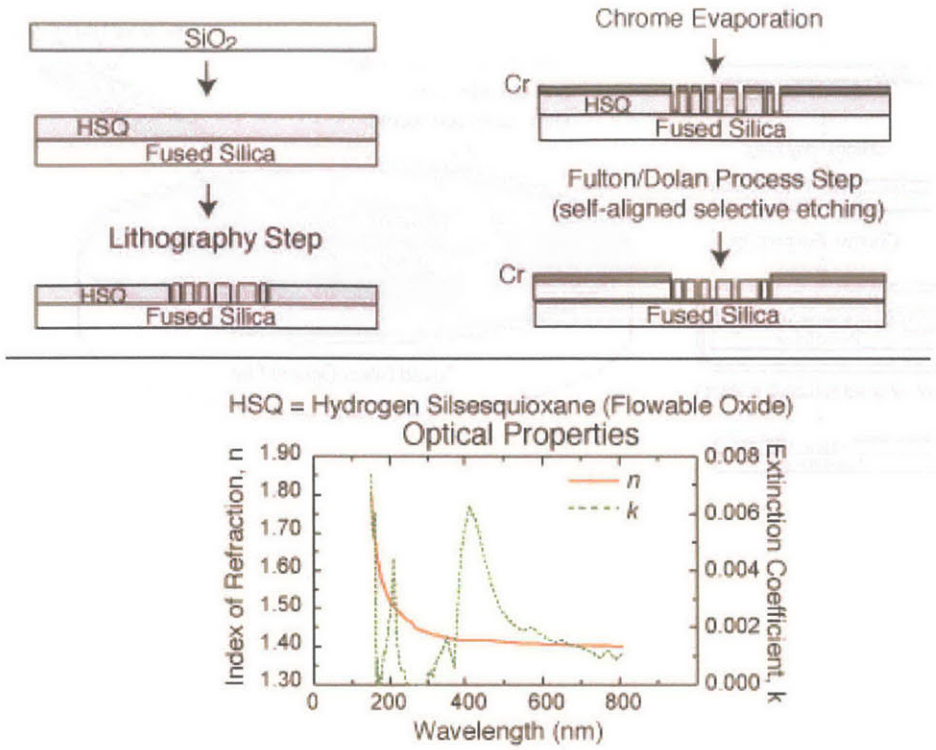

Figure 3- 31. Top: Typical sequence of the self-aligned process requiring a single-lithography step. Starting with a transparent blank material, HSQ is spun on it. The thickness of the HSQ is chosen to provide the appropriate phase step for the diffractive optical element. After patterning the elements in HSQ, the absorber material is evaporated. Note that the absorber (chrome in this case) inside the diffractive element and outside is not electrically connected. The absence of electrical connectivity will allow for the absorber within the diffractive elements to be removed by means of a wet-etch Fulton/Dolan technique. Bottom: The optical properties of HSQ are almost identical to those of fused silica.

3.3.4.3 The Self-Aligned Process

A solution to all the problems encountered in the two previously described processes has been devised and implemented through the work of this thesis. This novel fabrication process for zone-plate arrays is capable of high resolution, requires a single lithography step, and no etching (even for the case of phase zone plates). For this process the negative resist HSQ (hydrogen silsesquioxane, by Dow Corning) is used, which is sensitive at both e-beam and x-ray wavelengths. HSQ's extraordinarily high resolution (~10nm) and its glass-like properties make it an optimal choice for fabricating diffractive-optical elements that operate in the UV and DUV regimes. HSQ has an index of refraction very close to that of fused silica, and a negligible absorption down to

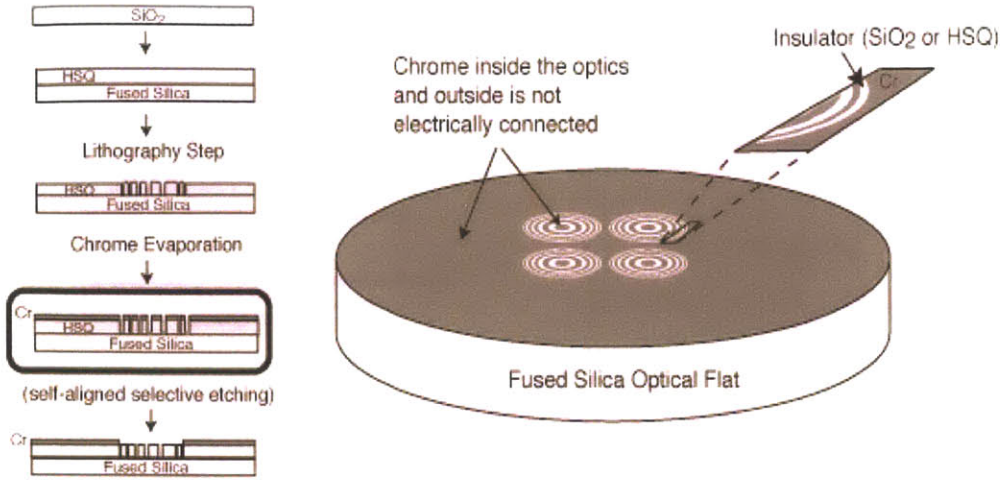

Figure 3- 32. Detail of the process after the absorber has been evaporated. Note that the absorber (chrome in this case) inside the diffractive element and outside is not electrically connected. The lack of electrical connectivity will allow for the absorber within the diffractive elements to be removed by means of a wet-etch Fulton/Dolan technique (see Figure 3-34).

157nm. As a result, if the resist is spun to the thickness corresponding to the desired phase step for the optic, patterning and development are the only required steps. The process is schematically illustrated in Fig. 3-32.

The process bypasses the need for a second lithography step while achieving perfect alignment between the absorber and the zones of the zone plates. The solution arises from the realization that if one patterns the zone plate and then evaporates the absorber material onto the substrate, the absorber material (typically a metal) that lands in the trenches and on top of the zones is not electrically connected to the metal area surrounding the zone plates. This situation is depicted in Figure 3-33 (right). Rather that having to perform a second lithography step requiring nanometer level alignment so as to remove the absorber that is on the zones, the lack of electrical connectivity between the metal inside and outside the zone plates allows for the removal of either the inside metal, or the outside metal, with one single high-resolution wet etch step.

The self-aligned wet etch technique was first proposed by T.A. Fulton and G.J.Dolan in 1982 [Ref 3-33, Ref 3-34]. The process, initially named "Brushfire Lithography" and later "Canyon Lithography", was proposed as a means to speed-up electron-beam lithography writing of chrome-on-glass masks.

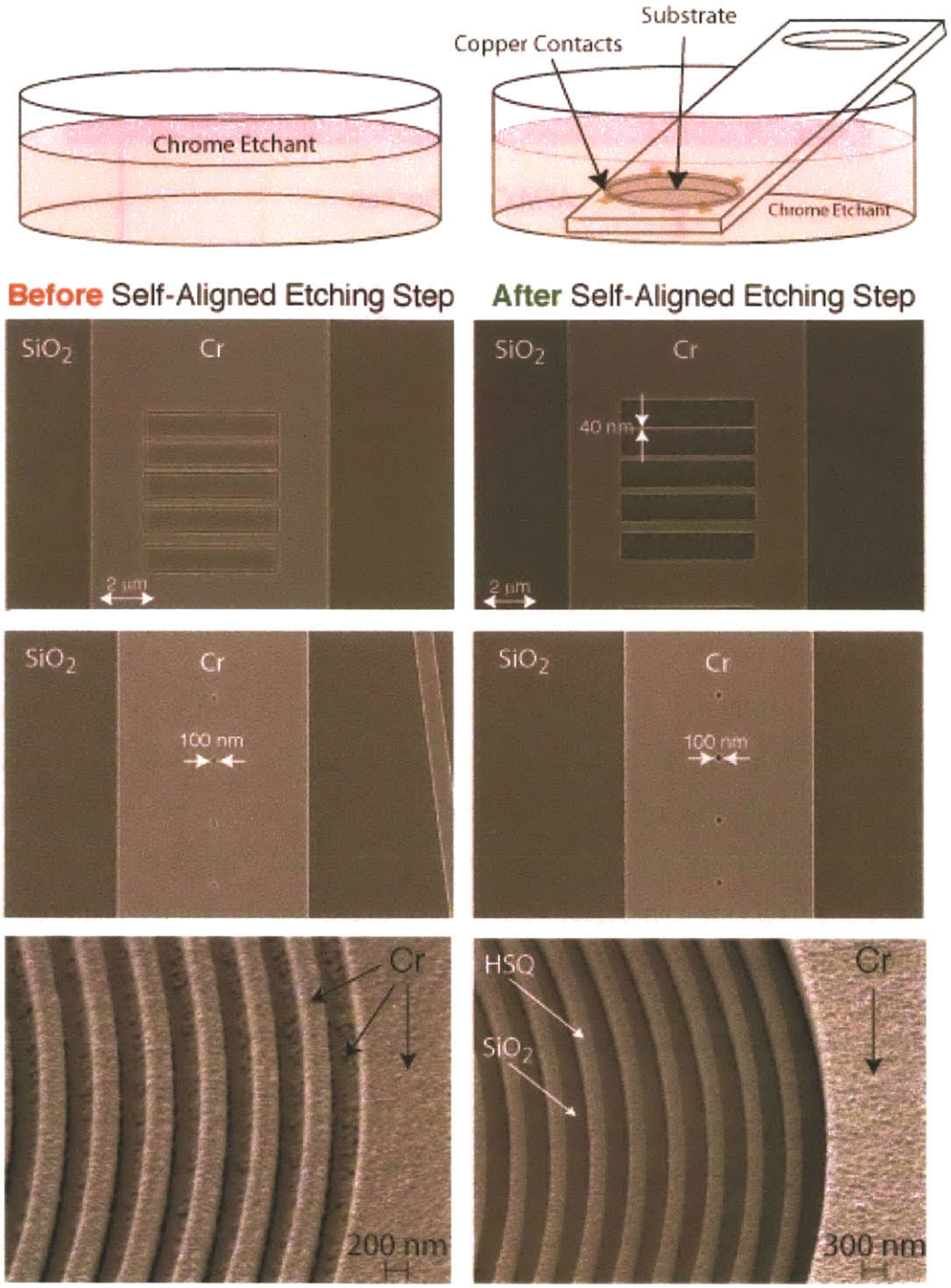

Figure 3- 33. Self-aligned etching process results. Top: Schematic illustrating the experimental implementation. Bottom: Scanning electron micrograph of a variety of patterns illustrating the high-resolution capabilities of the process, as well as its applicability to zone plate fabrication. Bottom Right: The Cr from the top of the zones and in the trenches is removed after the self-aligned etching process was applied. Note the perfect alignment between the surrounding absorber and the last zone of the zone plate.

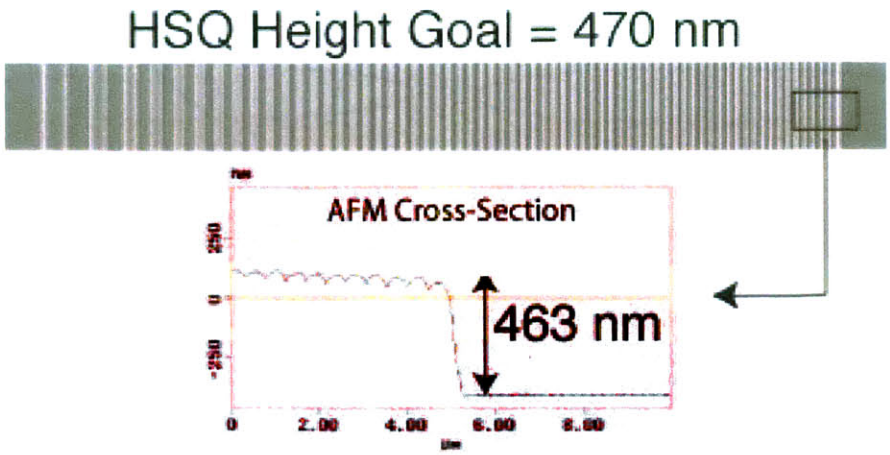

Figure 3- 34. By spin-coating the HSQ, the phase shift of the zone plates can be controlled to ~1%. Top: Scanning electron micrograph of a section of a high-numerical aperture zone plate. Bottom: Atomic force microscope scan of the outer zones of the zone plate. While the trenches in the outer zones can not be resolved due to their small size, the overall height-step can be accurately measured.

Instead of fully exposing a pattern with the e-beam system, only the outlines of the individual features in the pattern are exposed, leaving the completion of the pattern ("the filling in") to the electrochemical wet etch step. The principle behind the technique arises due to the fact that by biasing electrically connected regions of a metal film at different potentials one can selectively etch, electroplate, or anodize appropriately patterned substrates.

The technique was implemented for the fabrication of zone plates, with chromium as the etching material. Cr is a particularly suitable metal, since the active-passive transition provides a strong inhibition or enhancement of etching rates for suitable bias and etchants [Ref 3-34]. The Fulton-Dolan process is capable of both positive and negative tone etching. In the positive-tone case, the one of interest for zone plate fabrication, all metal that is biased will stay after the substrate is introduced in the etchant, and all parts not electrically connected will be etched away. Figure 3-33 illustrates the experimental implementation of the technique as well as some of the patterning capabilities that can be achieved. The technique is as simple as contacting the Cr metal with copper contacts spaced symmetrically around the edges of the substrate, and then immersing the substrate and the contacts inside chrome etchant (ceric

ammonium nitrate). The copper passivates the contacted regions while isolated features etch. In this process copper is consumed and a significant current flows through the chrome film. The resulting voltage variations in the thin film limit the distance over which passivation is effective, so that for large-area patterns the contacts must be sufficiently closely spaced (or the etchant sufficiently diluted) to passivate the desired region. The process latitude of the technique is simply fantastic. The chrome film can be "over-etched" (i.e. left inside etch bath after apparent completion) for as long as one wants without apparent degradation in the final pattern. As can be seen in Fig.3-33, the technique is capable of very high resolution. When applied to zone plate fabrication, perfect alignment between the outer-most zone and the absorber (the Cr) can be achieved.

By spin-coating the HSQ, the phase shift of the zone plates can be controlled to ~1%, as shown in Figure 3-34. The figure presents an atomic-force-microscope scan of the outer zones of a zone plate. While the trenches in the outer zones can not be resolved due to their small size, the overall height-step can be accurately measured, showing that a 463nm height difference is present (the goal was ~470nm). Furthermore, since the height was achieved by spin-coating, all zones of the zone plate have the same phase-step, something that is more difficult to achieve with a reactive-ion-etch based procedure.

The self-aligned process has enabled the capability of fabricating large arrays of zone plates in reasonable times. Figure 3-35 shows the largest high-numerical-aperture array fabricated in this thesis, with over 1,000 zone plates designed to operate at λ=400nm. Local duty-cycle was maintained throughout the array, and no errors were detected across the array. The Fulton-Dolan process achieved perfect alignment for all the elements in the array. Local random checks across the array confirmed that the phase height across the zone plates was uniform[7].

[7] More details of the process are provided in Appendix B.

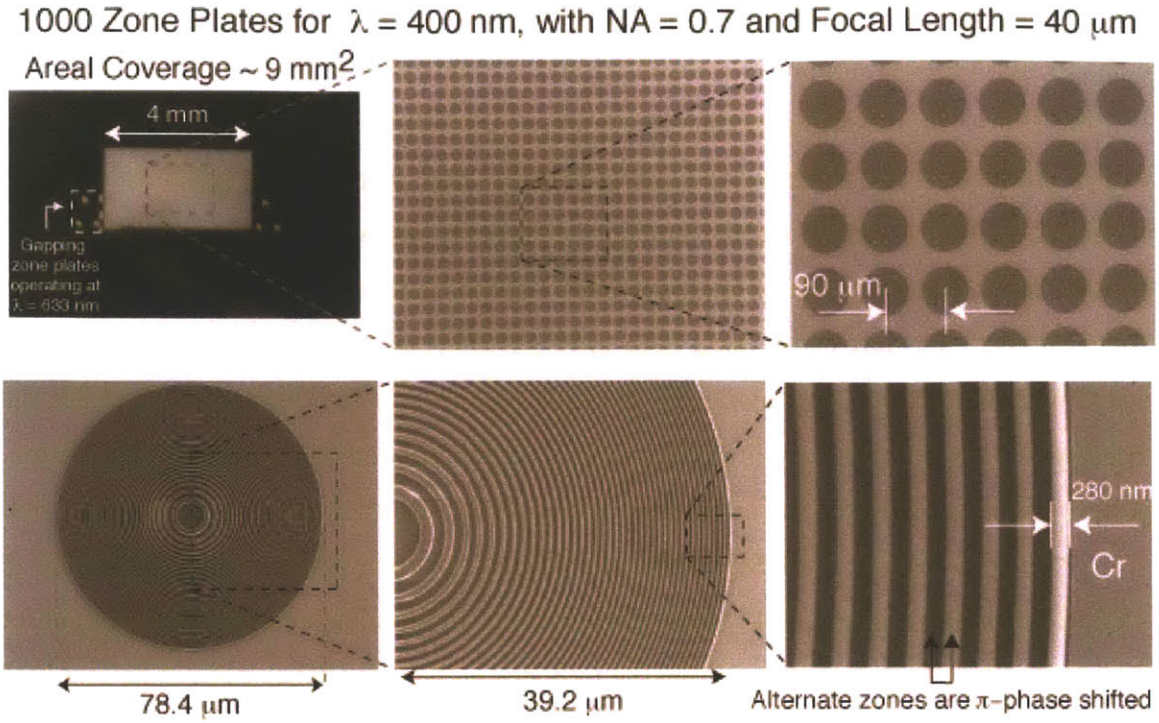

Figure 3- 35. Large zone plate arrays can be readily fabricated with our novel process that requires a single lithography exposure and no etching, even for the case of phase zone plates. Top-left: Optical micrograph indicating showing an array containing over 1,000 zone plates with an aerial coverage of 9 mm^2. Bottom-right: Detail of the outer-most zones. The duty-cycle is very close to 50%, and the phase shift between alternate zones was controlled to about 1%.

3.3.4.4 Order Sorting Apertures

The existence of multiple diffracted orders reduces the available contrast of zone plates in lithography applications. It would therefore be advantageous to include some form of order-sorting aperture in the space between the zone plate and the substrate to be exposed, in order to block all unwanted orders while allowing for first-order to go through. The idea is illustrated in Fig.3-36. Contrast can be dramatically improved in this configuration.

This section briefly presents a possible self-aligned fabrication procedure for the creation of order-sorting apertures. The process is outlined at the top of Figure 3-38. Starting with a phase-zone plate fabricated in fused silica (or HSQ), a thin piece of fused silica is bonded by means of a high-temperature bake. Since for ZPAL the order-sorting

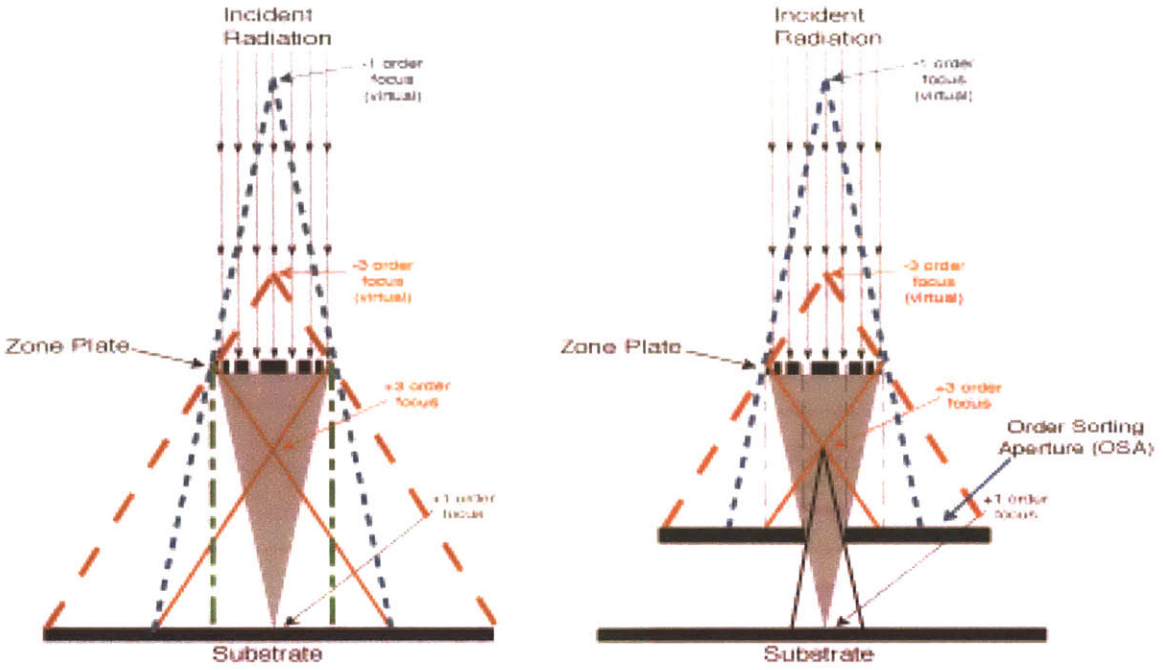

Figure 3- 36. Left: The existence of multiple diffracted orders reduces the available contrast of zone plates in lithography applications. Right: Order-sorting apertures can block unwanted orders while allowing first-order diffraction to go through.

aperture will have to be placed between the zone plate substrate and the wafer to be exposed, the bonded piece must be very thin (tens of microns). If need be, a thicker piece might be bonded and then thinned down with a carefully controlled polishing step. The scanning electron micrographs of Figure 3-37 show the first results that were obtained in our efforts[8] to bond two fused silica wafers (one of them containing a large-area phase grating). The results are very encouraging, indicating that the high-temperature bake (~1000°C) still maintains the grating profiles.

Once bonded, the remaining steps of the process consist of spinning negative resist onto the bonded piece and exposing through the back of the zone plate, as illustrated in Fig.3-37. The converging beam of light will expose the negative resist, which after development, will leave a self-aligned island that can be used in a lift-off process to produce the desire order-sorting aperture.

[8] This work was done in collaboration with Dr. David J. Carter.

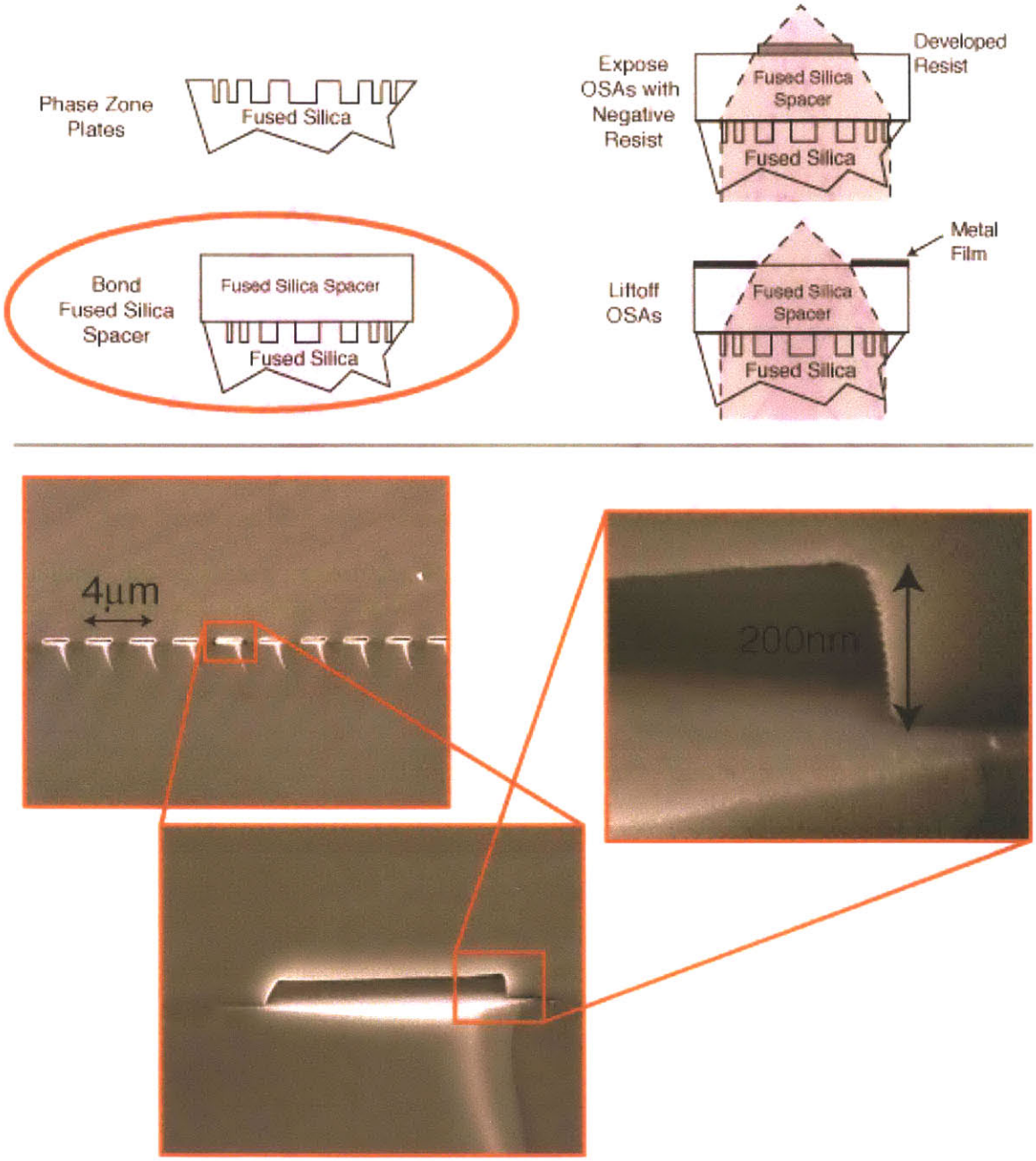

Figure 3- 37. Top: Process flow for fabricating self-aligned order-sorting apertures. Bottom: Scanning electron micrographs showing the results of bonding two fused silica wafers (one if them containing a large-area phase grating). Note that the visible spikes coming down from the edges of the bonded grooves are an artifact of the cleave. The results are very encouraging, indicating that the high-temperature bake still maintained the grating profiles.

3.4 Replication Techniques

If ZPAL is ever to be commercially introduced in the marketplace, it is crucial that viable zone plate manufacturing techniques are developed. By viable, we mean expanding beyond small-array manufacturing in a laboratory setting, to arrays containing one million zone plates. It must also be done in a cost-effective manner. The following sections address a number of proposals that have large-array fabrication as a goal.

3.4.1 Throughput in Electron-Beam Lithography: How many zone plates can one make?

If we were to use either of the e-beam systems we have at MIT's NSL, given that each zone plate requires a few minutes to write, a million zone plates would take a couple of years to be completed! This is clearly not an option. With both the RAITH system and the VS-26 (both vector-scan systems), the writing of zone plates is limited to arrays containing thousands of elements, but certainly not hundreds of thousands, let alone one million.

All hope is not lost with the prospect of utilizing e-beam systems for large array manufacturing. It is possible that such arrays could be fabricated utilizing a mask-making electron-beam-lithography tool such as the MEBES system from ETEC [Ref 3-35], since writing time for this tool is pattern-independent. Fabricating an array of 1000x1000, assuming each zone plate is ~100 microns in diameter, would require an area coverage of 10x10cm. This area is similar to a conventional mask, which can be written in 6.5 hours using a 120nm beam size, or 20 hours if a 60nm beam size is utilized [Ref 3-36]. Assuming that a MEBES systems can meet all the tolerances for zone plates, the issue of absolute placement of the centers of the zone plates still remains. With a 21nm (3-sigma) pattern placement, and given the fact that in ZPAL this error does not get reduced as is the case of the masks written for steppers (ZPAL is a one-to-one lithography system), it would probably be required to map out these errors once the master plate has been

fabricated and then correct via software the writing of the ZPAL tool. The details of how this is to be done remain to be worked out, but this issue of placement is of paramount importance and needs to be carefully addressed. Once again, it is possible that an implementation of the SPLEBL principle in a high-throughput e-beam system such as the MEBES® eXara™ will make absolute pattern placement budgets of only a few nanometers.

3.4.2 Proposals for Large-Array Fabrication

Although in section 3.2.4.3 a fabrication procedure for relatively large zone plate arrays (~1,000) utilizing e-beam lithography in combination with the Fulton-Dolan process was described, it is the opinion of the author that it will be necessary to decouple the effort of fabricating a master zone-plate array, from that of manufacturing (in a cost effective manner) a relative large number of identical zone-plate arrays. A possibility is to employ a mix-match technique that would make use of e-beam lithography for fabricating the master (or part of it) and either *x-ray, holographic, ZPAL or imprint* lithography to replicate it (or fully create it). The main advantage of this methodology, as opposed to relying on electron-beam lithography for the manufacture of identical arrays, lies in the fact that great pains can be taken in the fabrication of one (or a few) zone plate masters that contain very few and well characterized errors. Rather than having a different set of possible errors each time the e-beam writes a new zone plate array, by replicating the well characterized original master, the optics of all ZPAL systems will all behave in the same way.

The following sections address four possible routes that could be undertaken in order to replicate large arrays with high fidelity and in a cost effective manner.

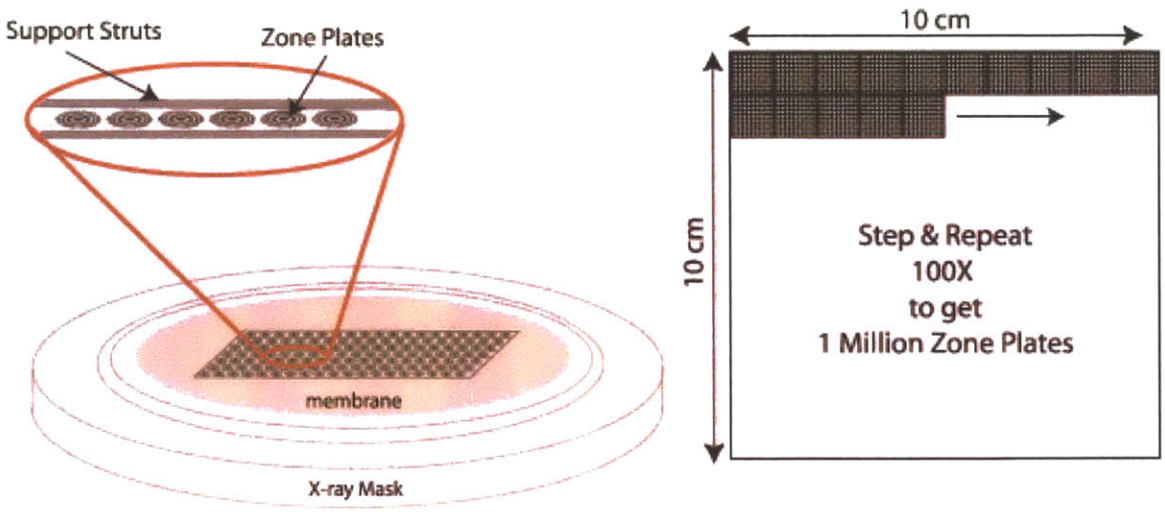

Figure 3- 38. Replication of zone plates by means of x-ray lithography. Left: Schematic of an x-ray mask containing an array of zone plates. The zone plates are surrounded by support struts in order to avoid membrane distortions. Right: With an x-ray lithography exposure system, the mask is exposed multiple times (step and repeat) in order to obtain a one-million-zone-plate array.

3.4.2.1 Replication by Means of X-ray Lithography

X-ray lithography provides a viable technique for large array fabrication. The idea is illustrated in Figure 3-38. On an x-ray mask, the maximum tolerable array size that can be e-beam written is plated. The zone plates are placed in between support struts in order to avoid membrane distortions. It is conceivable that 10,000 zone plates, spanning an area of 1cm X 1cm, could be written with an e-beam, even with the two systems available at the NSL. Then, provided an x-ray exposure apparatus with a sufficiently powerful x-ray source is used[9], 100 exposures would suffice to pattern one million zone plates. The only requirement would be to ensure alignment of the exposed sub-arrays of zone plates by means of a laser-interferometer-controlled stage.

One of the advantages of utilizing an x-ray based process is the fact that HSQ is sensitive at these wavelengths, and hence phase UV-zone plates can be patterned in one shot, as previously described. Experiments were performed in order to optimize this process, with some of the results obtained shown in Fig.3-39.

---

[9] Perhaps the x-ray lithography exposure tool available at University of Wisconsin, Madison, which uses a synchrotron as its x-ray source.

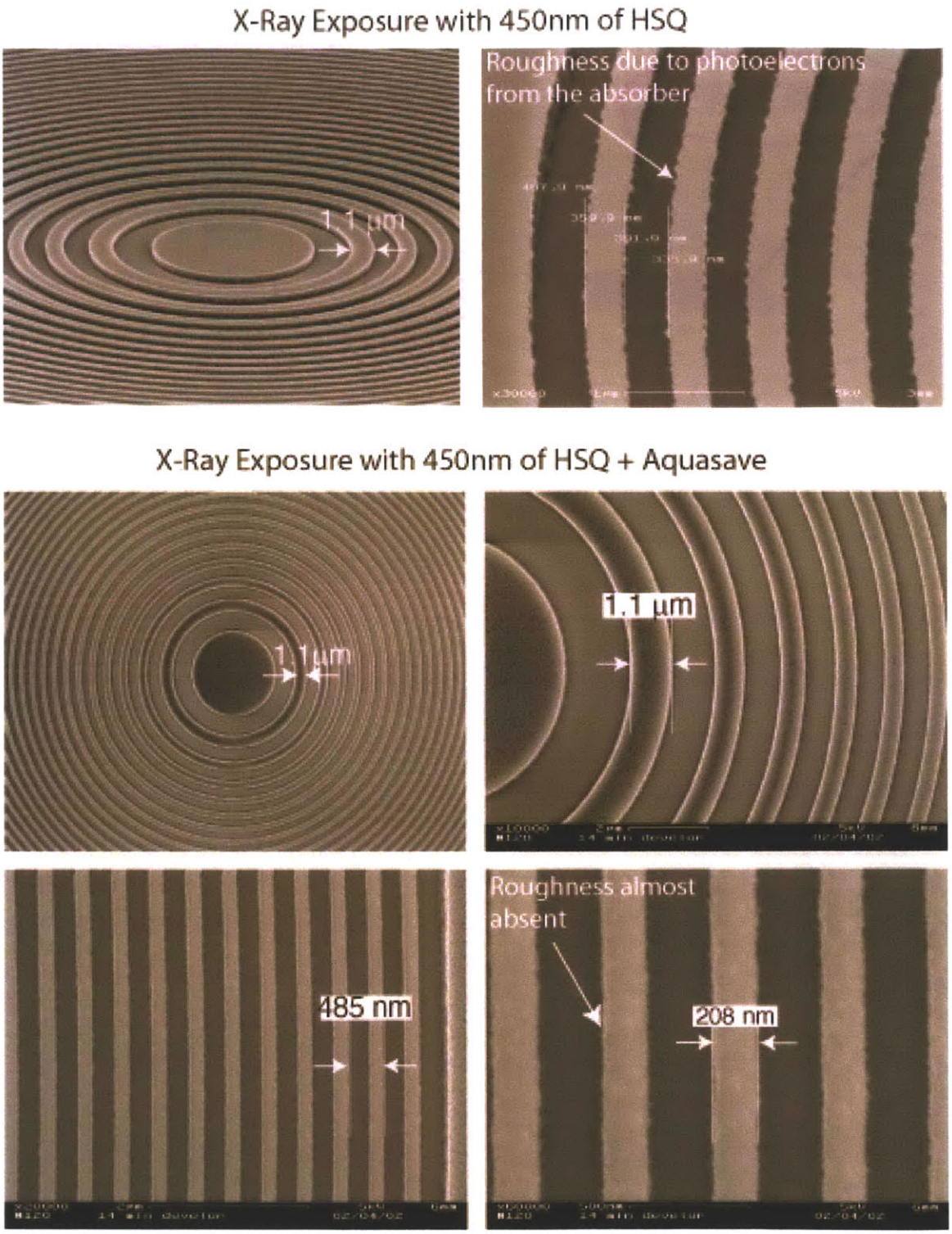

Figure 3- 39. The negative resist HSQ can be patterned by means of x-ray lithography. Top: Photoelectrons emitted from the absorber during the exposure causes roughness in the final HSQ pattern. Bottom Four: By adding a layer of Aquasave (a conductive aqueous solution) on top the HSQ, the roughness problem can be almost entirely mitigated.

The results presented in the figure indicate that good patterning can be achieved with this process. The only problem that had to be resolved was the presence of roughness in the zones of the zone plate due to photoelectrons emitted from the absorber during the exposure. The problem was solved by adding a layer of Aquasave (a conductive aqueous solution) on top the HSQ[10], as shown in the bottom four scanning electron micrographs of Figure 3-39.

3.4.2.2 Replication by Means of Holography

The scheme for reproducing zone plates by means of holography consists of interfering two wavefronts in such a way that the desired Fresnel-zone pattern is obtained. The scheme can work as follows: light is incident on a lens or an array of lenses (these can be a phase or amplitude zone plates, microlens, spatial light modulator pixels ,or other phase/amplitude modulating elements which creates the right modulation of the incident wavefront); after being modulated by the lens, the light interferes with another wavefront (which itself might have been modulated by a similar configuration) to create a hologram, which can be recorded to create the pattern for a diffractive element. This interference can be on-axis or off-axis. A few of the possible specific cases are described below. Figure 3-40 illustrates the fact that a zone plate is a hologram.

A uniform plane wave incident on a zone plate (phase or amplitude or a lens) is focused to a first order spot and diverges from there as a spherical wave. Interfering this diverging spherical wave with a plane wave traveling in the opposite direction, and then recording the interference fringes, results in the creation of a zone plate pattern. The geometry of this zone plate would depend on the distance at which the fringes are recorded. If this distance is twice the focal length of the original zone plate, the daughter zone plate is a clone of the original one. The plane waves can be illuminated from the

[10] Polyvinylalcohol (PVA) was also tried as a solution, with very mixed results.

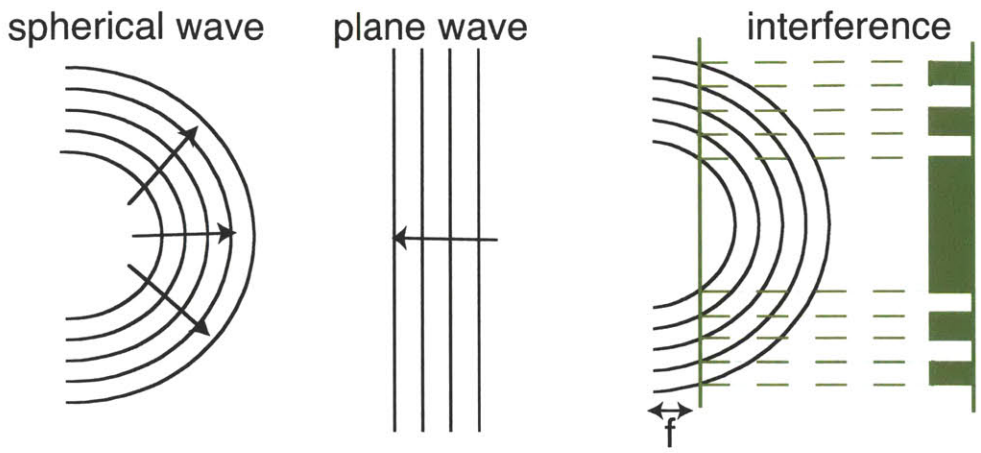

Figure 3- 40. A zone plate is a hologram, resulting from the interference of two spherical waves or one spherical wave and one plane wave.

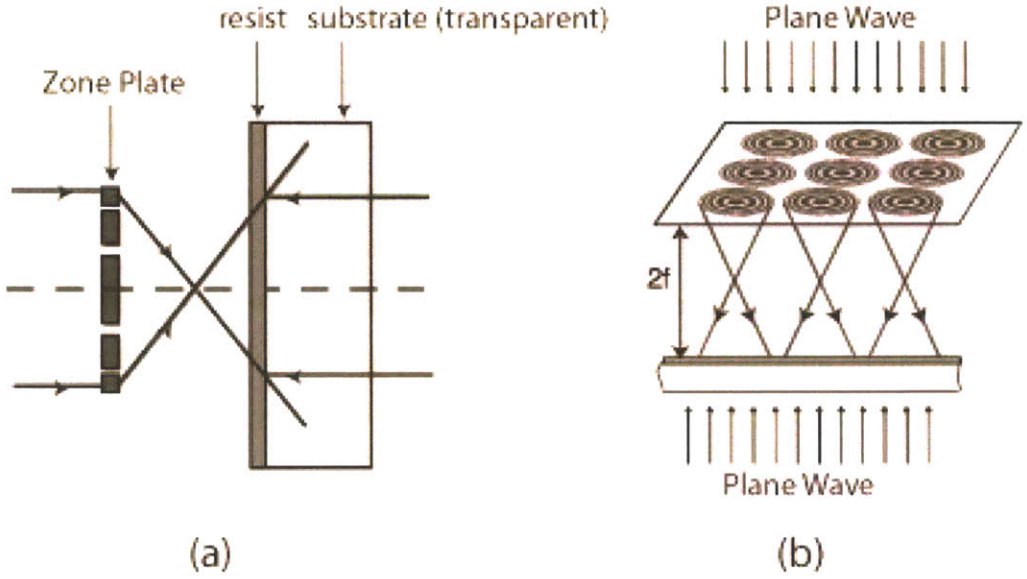

Figure 3- 41. Holographic reproduction of zone plates. (a) A uniform plane wave incident on a zone plate) is focused to a first order spot and diverges off as a spherical wave beyond the focal plane of the zone plate. The interference of this diverging spherical wave with a plane wave traveling in the opposite direction, gets recorded in the resist, obtaining the pattern of a zone plate, (b) generalization of this concept to arrays of zone plates.

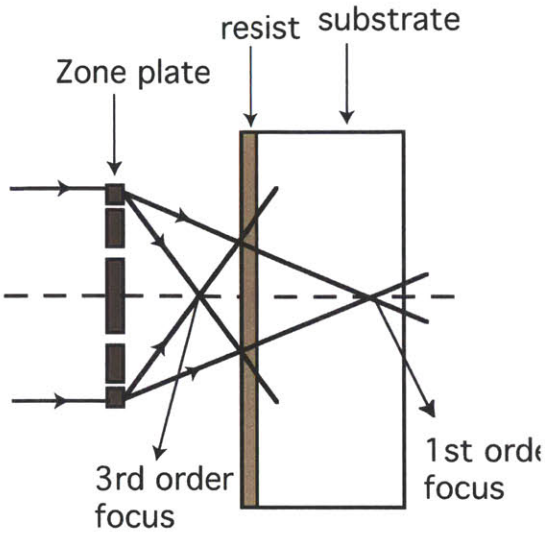

Figure 3- 42. The interference of the first and third orders of the same parent zone plate can be recorded in resist to create a daughter zone plate with smaller features.

backside of a glass substrate and the fringes can be recorded in photoresist on the front surface. This scheme is depicted in Figure 3-41.

Another related idea is to use the interference of the first and third orders of the same parent zone plate to create fringes, which could be recorded as a daughter zone plate with smaller features. In this case, plane waves are incident on the zone plate (phase or amplitude), and after diffracting, several orders will be produced, with the first and the third being the strongest. Now, if a recording medium is placed at a position between the zone plate and its focal plane, a daughter zone plate with higher spatial frequencies is obtained. Figure 3-42 illustrates this scheme.

3.4.2.3 Replication by Means of Zone-Plate-Array Lithography

Zone-plate-array lithography also offers the possibility of large array fabrication. One can envision a system, initially operating with a few thousand zone plates, that can write larger and larger arrays of zone plates in parallel. As in a regular ZPAL system, the substrate is scanned underneath the master zone-plate array and the radiation illuminating the elements is flashed at appropriate times to create the desired pattern. No micromechanics would be needed for this application, since all zone plates would be

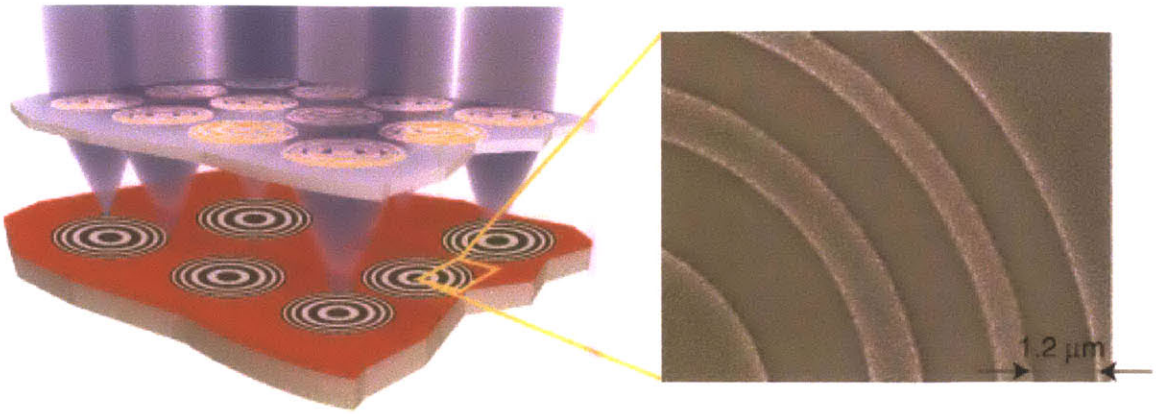

Figure 3- 43. Zone plate arrays can be used as means to replicate zone plate arrays. The substrate is scanned underneath the master zone plate array and the radiation illuminating the elements is flashed at appropriate times to create the desired pattern. Right: Scanning electron micrograph illustrating the viability of the technique. The zone plate was patterned by means of a 0.7 numerical aperture master zone plate operating at λ=400nm.

writing the same pattern (i.e. a zone plate). Figure 3-43 shows a scanning electron micrograph illustrating the viability of the technique. The zone plate was patterned by means of a 0.7 numerical aperture master zone plate operating at λ = 400nm.

3.4.2.4 Replication by Means of Imprint Lithography

Imprint lithography techniques have seen a surge of popularity in recent years due to their extraordinary resolution, ease of use, and potentially low cost. It is not the objective of this section to give a comprehensive review of the numerous imprint techniques, but rather to simply raise the possibility of replicating the e-beam fabricated diffractive optical arrays by means of one of such techniques.

Some imprint techniques have shown sub-25nm resolution [Ref 3-37], and active research and development has taken place over the last five years in all areas concerning nano-imprint lithography (NIL), from masks, to resists, to processes. NIL patterns a resist by deforming the resist shape through embossing (with a mold), rather than by altering resist chemical structures through radiation . After imprinting the resist, an anisotropic etching is typically used to remove the residue resist

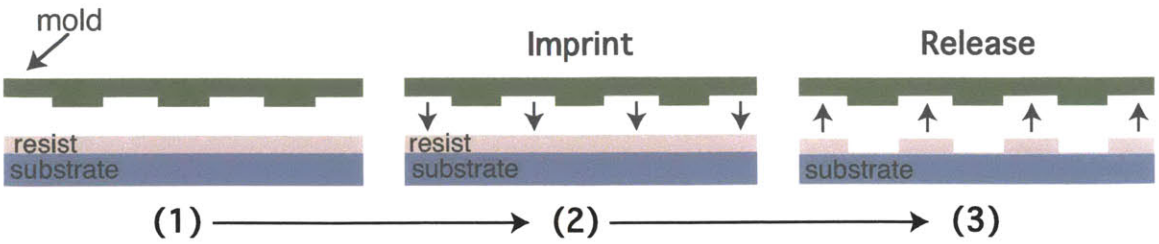

Figure 3- 44. Schematic of imprint lithography process

in the compressed area. The nano-imprint lithography process is depicted schematically in Figure 3-44.

While the inability of almost all imprint processes to achieve state-of-the-art multilevel alignment prevents using this process to build large arrays starting with smaller arrays, the technique could prove very cost-effective if used to replicate large number of substrates once a master plate has been fabricated.

Chapter 4

Zone Plate Characterization

This chapter presents an extensive experimental characterization of zone plates for both lithography and microscopy applications. The elements are characterized in terms of resolution, depth of focus, and efficiency. The results presented provide the first experimental evidence that UV zone plates are capable of diffraction-limited focusing even at very high numerical apertures.

4.1 Focusing Performance

4.1.1. Spot Characterization

In Chapter 3, a description of how zone plates focus radiation was provided. A useful rule-of-thumb that can be extracted from the analysis is the following: zone plates can create spots with a resolution (measured at full-width-at-half-maximum -FWHM) that is roughly the size of the outer-most zone. That is, for a given wavelength λ, the spot size that can be created with a zone plate with an outer-zone-width w, will also be w (so long as $\sim w \geq \lambda/2$).

We now present a method for characterizing the resolution capabilities of zone plates for a variety of numerical apertures. All zone plates were fabricated with the

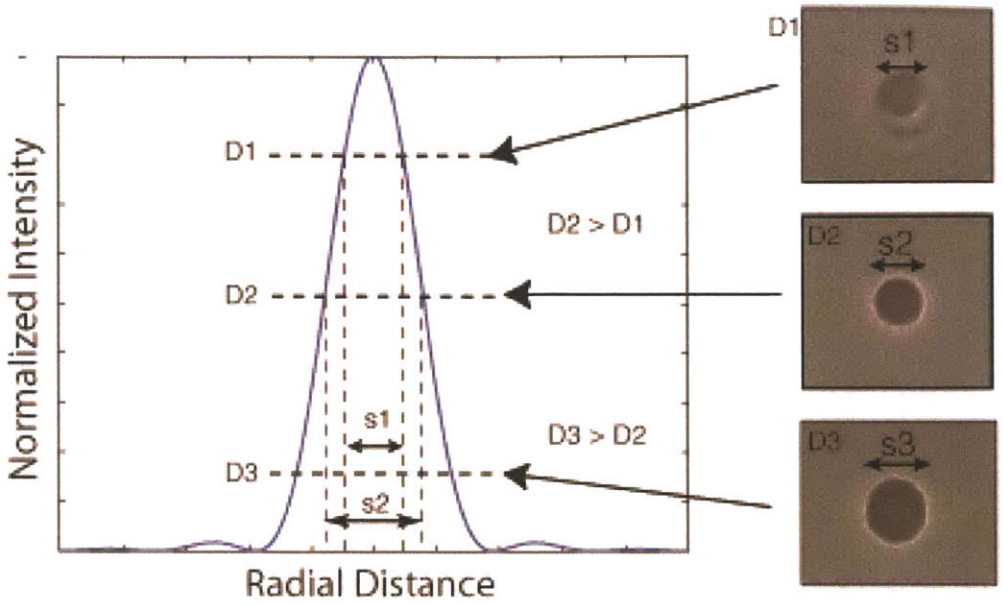

Figure 4 - 1. Methodology for extracting the PSF of a zone plate by means of lithographic exposures on resist. The PSF can be sampled by exposing a resist-coated substrate with different illumination intensities. Different exposure dwell times will produce different diameter spots, which can be measured by means of scanning electron microscopy. The information can then be used to reconstruct the PSF, as shown in Figure 4-2.

self-aligned HSQ process described at the end of Chapter 3.

A plot illustrating the methodology used to extract the PSF of a zone plate by means of lithographic exposures on resist is illustrated in Figure 4-1. The idea is to expose spots in different locations of a resist coated substrate, at a large variety of doses. The exposed resist effectively clips (i.e. samples) the point-spread function (PSF) at different levels. By carefully measuring the radii of the exposed spots with a scanning-electron microscope, the full PSF can be reconstructed. From Figure 4-1, it is clear that as the exposure dose increases, the exposed spot gets wider, effectively sampling the PSF at *D1, D2, D3*, etc. Further increases in dose will create in the resist patterns that will indicate the position of the side-lobes. The procedure can then be repeated for zone plates of different numerical apertures and the results compared with the full-vector simulation of the PSF.

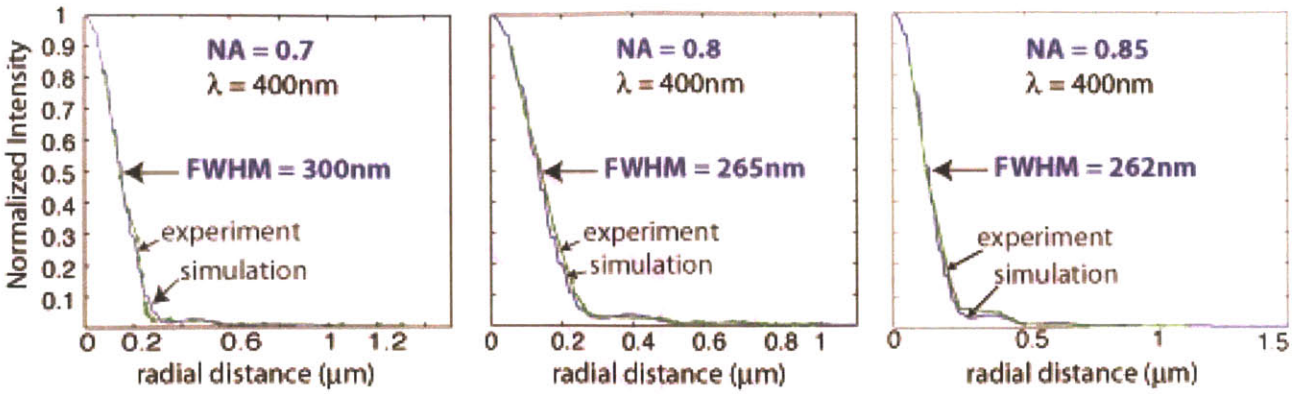

Figure 4 - 2. Comparison of the experimentally determined and the simulated PSF of three zone plates with numerical apertures 0.7, 0.8, 0.85 operating at λ=400nm. Note the excellent agreement between experiment and simulation, from which we can conclude: (1) careful processing allows the fabrication of zone plates with close to ideal performance, and (2) the full-vector simulation procedure is in excellent agreement with experiment.

The results of this process are illustrated in Figure 4 – 2. The figure provides a comparison of the experimentally determined and the simulated PSF of three zone plates with numerical apertures 0.7, 0.8, 0.85 (operating at λ=400nm). Note the excellent agreement between experiment and simulation, from which we can conclude: (1) careful processing allows the fabrication of zone plates with close to ideal performance, and (2) the full-vector simulation procedure is in excellent agreement with experiment. And more importantly, the results provide, for the first time, experimental confirmation that high-numerical-aperture zone plates are capable of diffraction-limited performance at the UV.

4.1.2 Depth of Focus

The depth of focus (DOF) of a lens or imaging system is the maximum permitted displacement, away from the focal or image plane, for which the on axis intensity is diminished by some permissible small amount (i.e. the image resolution is only slightly degraded). The quality of the focused spot varies with focus because the relative phase among the rays responsible for forming the PSF change with focus. It is to be expected that the DOF will scale with the wavelength and the numerical aperture.

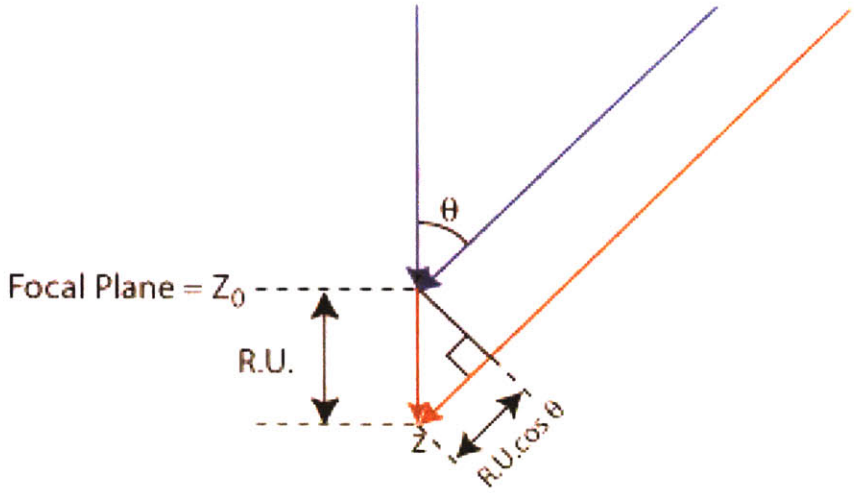

Figure 4 - 3. Two rays (spatial frequencies) contributing to spot formation. The depth of focus is proportional to the wavelength and inversely proportional to the square of the numerical aperture.

Consider Figure 4-3, which shows two rays contributing to the spot (PSF) formation, one from the center of the optic (central zone) and one from the edge (the outer-most zone). At focus, the rays interfere at z_0, at an angle θ (the numerical aperture will hence be $NA=\sin\theta$). Let's now consider the defocus case, in which the rays interfere at distance z away from z_0. The relative phase change between the two rays will then be:

$$\frac{2\pi}{\lambda}(z - z\cos\theta) \qquad \textbf{4 - 1}$$

It is common practice in the literature [Ref 4-1] to define a depth of focus unit, *R.U.* (which stands for Rayleigh Unit), defined as the distance that results in an optical path difference between the two rays of 1/4λ. The expression for the *R.U.* is then:

$$R.U. = \frac{\lambda}{4}\frac{1}{1-\cos\theta} = \frac{\lambda}{4}\frac{1}{2\sin^2(\theta/2)} \cong \frac{\lambda}{4}\frac{1}{2\left(NA/2\right)^2} \qquad \textbf{4 - 2}$$

$$R.U. = \frac{\lambda}{2NA^2} \qquad \textbf{4 - 3}$$

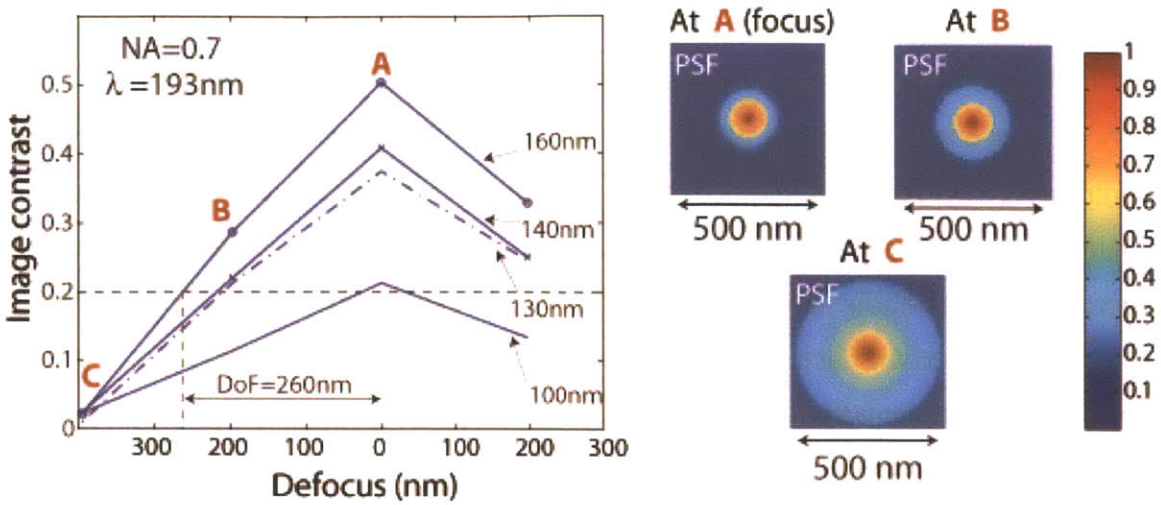

Figure 4 - 4. Plot of the impact of defocus on image contrast for ZPAL (operating at λ=193nm). Zone plates have a depth-of-focus similar to that of conventional refractive lenses. The dept-of-focus is dependent on the wavelength of the light and the numerical aperture. Defocus is an important consideration in ZPAL, as can be seen in the figure. Left: Simulated plot of image contrast as a function of defocus for dense 1:1 gratings exposed with ZPAL at different resolutions (from 160 nm to 100 nm). Right: Top view of simulated PSF of a 0.7NA zone plate operating at λ=193nm at different Raylegih Units (R.U.) of defocus (marked A, B, C in the left graph). Note how the background in creases as the defocus increases (i.e. less energy is going into the diffraction-limited spot).

The quantity $R.U. = \frac{\lambda}{2NA^2}$ is the Rayleigh unit of defocus. It is proportional to the wavelength and inversely proportional to the square of the numerical aperture. For the case of a perfect circular lens, with plane wave illumination, it can be shown [Ref 4-2] that one R.U. of defocus corresponds to an on-axis intensity decrease of 20%.

Depth-of-focus is a very important parameter affecting the optical performance of zone plates for lithography applications. Finite resist thickness, focus fluctuations due to wafer topography, zone-plate-substrate non-flatness, and wafer and chuck non-flatness can all cause a decrease in the quality of the final printed patterns. Figure 4 –4 illustrates the impact of defocus on image contrast for a ZPAL system operating at λ = 193nm (the wavelength required to achieve sub-100nm patterning). Plots of image contrast for simulated dense gratings of different minimum feature sizes are shown as a function of defocus. Mature resist will be able to resolve image contrasts in excess of 0.2. As can be observed, the image contrast is significantly degraded as the defocus increases. One and

one-half R.U.of defocus away from perfect focus, results in an image contrast below 0.2 for a 100nm linewidth. We can then conclude, that at λ=193nm, a zone plate with a 0.7 numerical aperture exhibits a depth-of-focus of ~± 200nm, in terms of tolerable image contrast. However, it is important to consider that a number of other factor also contribute to the image contrast that can be achieved with ZPAL (e.g. duty-cycle control, appropriate phase-shifts between alternate zones, and radial period errors, as described in Chapter 3). Given this fact, the tolerance for defocus decreases to a number that has to be quantified experimentally for each ZPAL system, with an upper bound given by a factor of one to two times the expression obtained in Equation 4-3.

4.1.3 Dealing with Multiple Diffraction Orders

This section addressed what is perhaps the most commonly expressed concern regarding the use of zone plates for lithography, namely, whether the presence of multiple diffracted orders in zone plates presents a critical problem for high-resolution lithography. As we will see, while it is true that the existence of multiple orders limits the performance of the zone plates, even with such orders present, zone plates are adequate for state-of-the-art lithography. Alternative diffractive optical designs that can mitigate the presence of multiple orders are also discussed.

4.1.3.1 The Issue of Background in Lithography

Lithography is based on the ability to produce sufficient image contrast in a resist sensitive to some form of radiation. In lithography, pattern formation involves two distinct but interrelated contrasts. The first relates to the image quality at the image plane of the lithographic system. The second contrast relates to the interaction of the aerial image with the resist material. The latter interaction is responsible for the final pattern formation, that is, the *writing in stone (*the literal meaning of lithography). Two contrast metrics are hence present. One relating to the aerial image formed, and the other to the ability of the resist film to take this aerial intensity distribution and convert it into a binary pattern. Understanding this is crucial in order to analyze all forms of lithography,

including ZPAL. A fundamental point that is worth remembering through the ensuing discussion is the following:

A low-contrast aerial image can result in a high-quality lithographic pattern *provided* the resist has enough contrast and conversely.

Contrast is defined as

$$contrast = \frac{\max - \min}{\max + \min} \qquad \textbf{4 - 4}$$

where *max* and *min* are, respectively, the maximum and minimum intensity values in the final image to be resolved by the resist.

Photoresist Interaction with the Aerial Image

Photoresist is typically an organic polymeric compound that changes its solubility in another chemical (known as developer) as a result of radiation exposure. The performance of any photoresist can be characterized by its contrast curve. Figure 4-5 depicts the contrast curve for a fictitious positive resist. The thickness of resist remaining after development is plotted against exposure dose (plotted in log scale for clarity).

Near E_0, we can represent the contrast curve by the following equation

$$T = T_0 \gamma \ln\left(\frac{E_0}{E}\right) \qquad \textbf{4 - 5}$$

where T is the thickness of resist remaining, T_0 is the initial resist thickness, γ is the resist contrast, E_0 is the dose at which no resist remains (clearing dose) and E is the exposure dose. This equation is illustrated by the dotted linear portion of the curve in Figure 4-5. We want to relate the image contrast to the resist contrast. We need only consider the

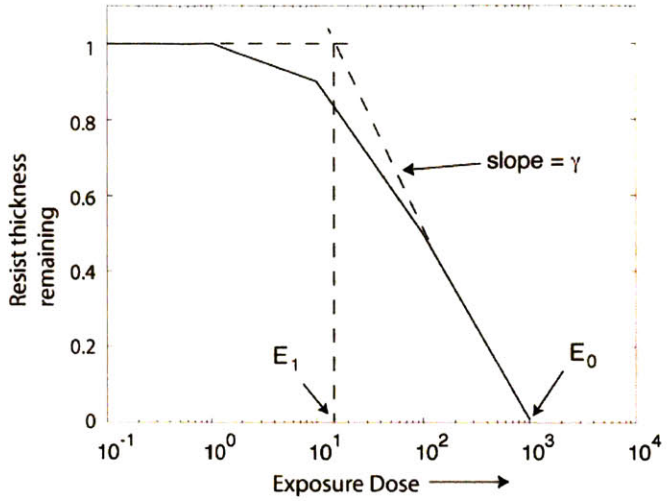

Figure 4 - 5. Typical contrast curve of a positive photoresist. Thickness of photoresist remaining is plotted as a function of the exposure dose.

minimum of image intensity I_{min} and the maximum of image intensity I_{max}. It is clear that for $I_{min} < E_1$ and $I_{max} > E_0$, the resist will produce the desired "binary" image with vertical sidewalls. These conditions imply

$$\begin{aligned} I_{\min} &< E_1 \\ I_{\max} &> E_0 \end{aligned} \qquad \textbf{4 - 6}$$

This further means

$$C = \frac{I_{\max} - I_{\min}}{I_{\max} + I_{\min}} > \frac{E_0 - E_1}{E_0 + E_1} \qquad \textbf{4 - 7}$$

$$C_{\min} = \frac{e^{-\frac{1}{\gamma}} - 1}{e^{-\frac{1}{\gamma}} + 1} \qquad \textbf{4 - 8}$$

In Figure 4-6, the minimum resolvable image contrast (C_{min}) is plotted against the resist contrast (γ). From this plot, we can see that to resolve an image that has a contrast of about 0.2, a resist contrast, γ, better than 2.5 is needed. As was described in Chapter 1,

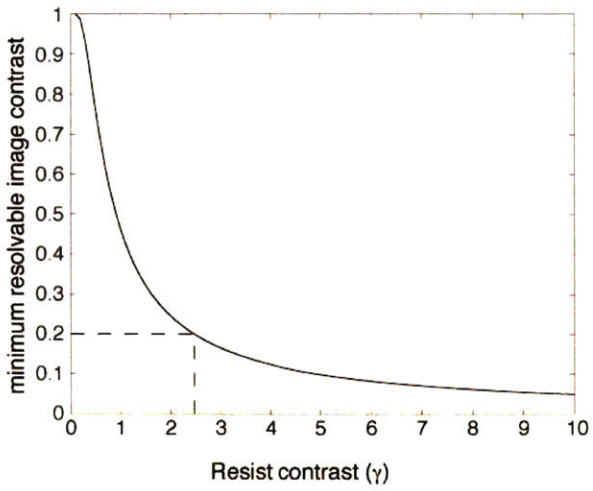

Figure 4 - 6. The minimum resolvable image contrast is plotted against the resist contrast. Note that in order to resolve an image of contrast about 0.2, the resist contrast must be better than 2.5. Mature resists are able to resolve image contrasts as low as 0.2.

resist technology has improved tremendously (recall Fig.1-9), with dramatic effects on the quality of the patterning that can be achieved with any given lithographic system. Mature resists are able to resolve image contrasts as low as 0.2.

The Effect of Zone-Plate Background Radiation in Lithography

The first point that is important to get across regarding the effect of multiple orders on lithography applications, is that the background power in zone plates, although of the same order-of-magnitude as the first-order power, is **spread over a very large area**. An important metric to understand in lithography is that the power-density (i.e. power per unit area) of the radiation incident on the photoresist defines the quality of the printed pattern. On a first pass, it is tempting to provide the following analysis for the case of zone plates (let's call it the *Simple Analysis*). It goes as follows:

"Simple Analysis":

> "If, at best, only 40% of the light goes into the first order, the remaining 60% will go into unwanted areas on the substrate; the 40-60 split seems intuitively an insufficient number for state-of-the-art lithography. After all, *most of the light* is going to areas where we don't want it to go, isn't it?"
>
> Anonymous ZPAL Critic

In order to answer the concerns expressed by the "simple analysis", one must begin by realizing that patterning in ZPAL is achieved by the incoherent addition of spots. When a single spot is exposed, it is true that 40% of the radiation goes into the spot, and 60% is spread over a much larger area. However, this spreading results in a *power density* for the unexposed pixels that is drastically lower than that of exposed pixels. It is simply wrong to reach the conclusion that the *overall* pattern will receive only 40% of the radiation into the desired areas, and that 60% will go into areas intended to remain unexposed. The error lies in not realizing that part of the background radiation also goes into areas that *are* intended to be exposed. In this manner, an exposed pixel will *always* receive a *higher* exposure dose than all unexposed pixels in its vicinity.

An example will help: Consider the case of exposing a dense 1:1 line/space grating. The "simple analysis" would predict that 40% of the radiation would go into the lines (the exposed areas), and that 60% would go to the spaces (the intended unexposed areas). The grating would not be resolved. However, given that for a grating one half of the total number of pixels are exposed, 1/2 of the 60% background will end up in the exposed pixel areas, with the result that the lines will receive 70% of the radiation (40% from direct exposure + 30% from indirect exposure), and the spaces only 30%. The grating will be readily resolved. This example showcases a general fact that is true for all patterns. If the point-spread function (this function determines how energy is distributed each time a spot is exposed) is well known, it is always possible to account for the background so as to include its contribution to the exposed areas (this is part of the science of proximity effect correction). The image contrast is hence much better than it at first appears. The caveats are that (1) the PSF has to be sufficiently well characterized[1], (2) dose control for each pixel is necessary, and (3) a pattern dependent dose correction needs to be applied[2]

Let's proceed with an experimental confirmation of the ability of phase-zone plates to provide sufficient contrast for state-of-the-art lithographic patterning. In

---

[1] As shown in Figure 4-2, our simulations provide excellent agreement with experiment (i.e. we know the PSF of zone plates very well).

[2] This is not necessarily a problem, since it is a calculation that can be done offline prior to exposure. For some results showing the implementation of this technique see section 5.2.1.3 in Chapter 5.

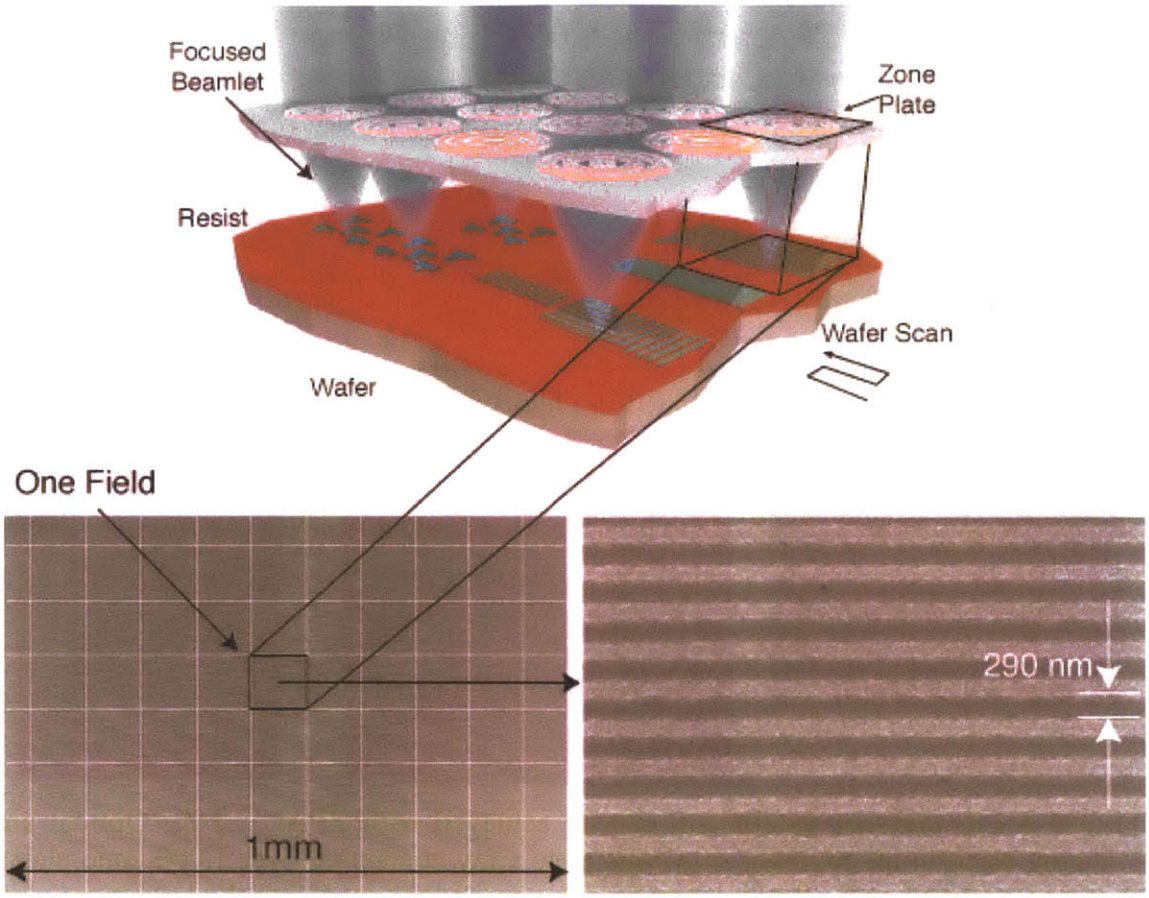

Figure 4 - 7. Top: Schematic of the ZPAL system without the micromechanics. Large area patterns are created by stitching adjacent fields, with a field defined as the square area located underneath any given zone plate (a field, depicted with black lines, is shown in the figure). Bottom-left: Proof that full-field patterning is possible with ZPAL despite the existence of multiple orders. A dense pattern with 300nm lines and spaces was exposed (with 400nm light). The total patterned area contained 1,000 fields, spanning a $10mm^2$ area. Bottom-right: Zoomed in SEM of the center of the full field grating.

ZPAL, large areas are written by stitching together multiple fields, as is done in scanning-electron-beam lithography. While what defines a field in ZPAL depends on the writing strategy, for simplicity a field can be defined as the square area enclosing the projection onto the substrate of an individual zone plate (i.e. for a zone plate with 100 μm diameter, the field size will be a 100μm x 100μm square located directly underneath the zone plate). Each zone plate is "responsible" for patterning the field that lies directly underneath it, and stitching at the edges of the fields allows features to be connected with patterns written in adjacent fields.

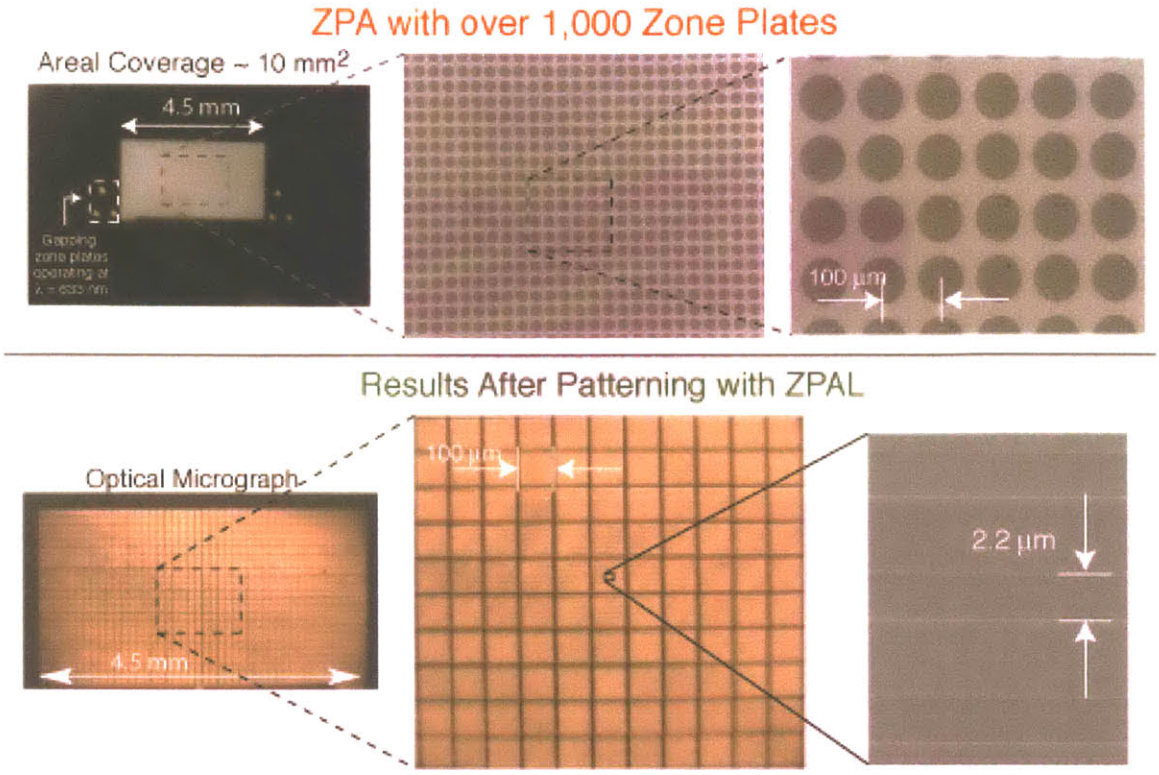

Figure 4 - 8. Massive parallelism can be achieved with ZPAL. Top: Optical and scanning electron micrographs of a zone plate array containing over 1,000 zone plates, spanning a $10mm^2$ area. Bottom: Lithographic results obtained with the large zone plate array. The exposed pattern is a $6\mu m$ period grating with a total area of $10mm^2$. Bottom Right: Scanning electron micrograph of a small section of the $10mm^2$ grating.

For the purpose of experimentally evaluating contrast, it is sufficient to pattern full fields at the maximum resolution. If this test is passed, it is clear that entire wafers could be patterned by combining large numbers of fields written in parallel. Figure 4-7 demonstrates that full fields, with dense lines and spaces patterned at the minimum feature size of the zone plate, can be written with high-NA ZPAL. The top of the figure is a schematic of ZPAL (without the micromechanics) illustrating the previously described concept of parallel writing by stitching multiple fields. The bottom of the figure contains an experimental result in which $100\mu m$ x $100\mu m$ fields were exposed with a 0.7 NA zone plate operating at λ=400nm and a focal length of 40 μm. The exposed pattern consists of 1:1 dense lines and spaces with 300nm features (the exposure wavelength is 400nm). The zoomed in SEM at the bottom-right of Figure 4-7 provides a clear view of what the pattern looks like, namely a 600nm-period, dense 1:1 grating. For contrast purposes, only next-neighbor fields will affect patterning, due to the highly localized structure of the

point-spread function. The results presented in Fig.4-7 and Fig.4-8, present full-field ZPAL patterns that were exposed in the presence of a very large number of neighboring fields. The results confirm that ZPAL will be able to pattern dense full fields at the diffraction limit even with arrays of one million elements or more[3]. In conclusion, high-numerical-aperture zone plates are capable of providing sufficient contrast for state-of-the-art lithography. Although multiple diffracted orders exist, the background exposure that they produce is not decisively deleterious. It should be pointed out that orders-sorting apertures, as described in Chapter 3, would further increase the patterning capabilities of zone plates by blocking most of the undesired radiation from reaching the substrate to be exposed.

Alternative Diffractive Optic Designs for Background Reduction

Diffractive optical elements more efficient than phase zone plates exist that are capable of focusing light into a single diffraction-limited spot with a very high efficiency (and hence with very little background). It is based on a principle of blazed diffraction gratings. The term blazing implies the creation of a sloped profile for alternate zones, folding the phase of the propagating wavefront by 2π as it goes through the optical element. In this way, it mimics the effect created by conventional refractive lenses, with the added advantage that it can be fabricated with microfabrication processes.

A "blazed Fresnel phase plate" is depicted in Figure 4-9. Such a diffractive-optical element can focus 100% of the incident radiation into the first-order focus, assuming there in negligible attenuation through the material, which is the case for UV and deep UV radiation in glasses such as fused silica, and single crystals such as calcium fluoride. However, despite the fact that micro-fabrication procedures can be employed for the creation of these elements, high-resolution blazed-elements remain very challenging structures to fabricate. The bottom of Figure 4-9 (c-d) illustrates two of the traditional fabrication procedure for these elements.

[3] As a matter of fact, a zone plate located at the center of an array containing 7 hexagonal close-packed zone plates will pattern identically to a zone plate located in the center of an array containing 1 million or more zone plates.

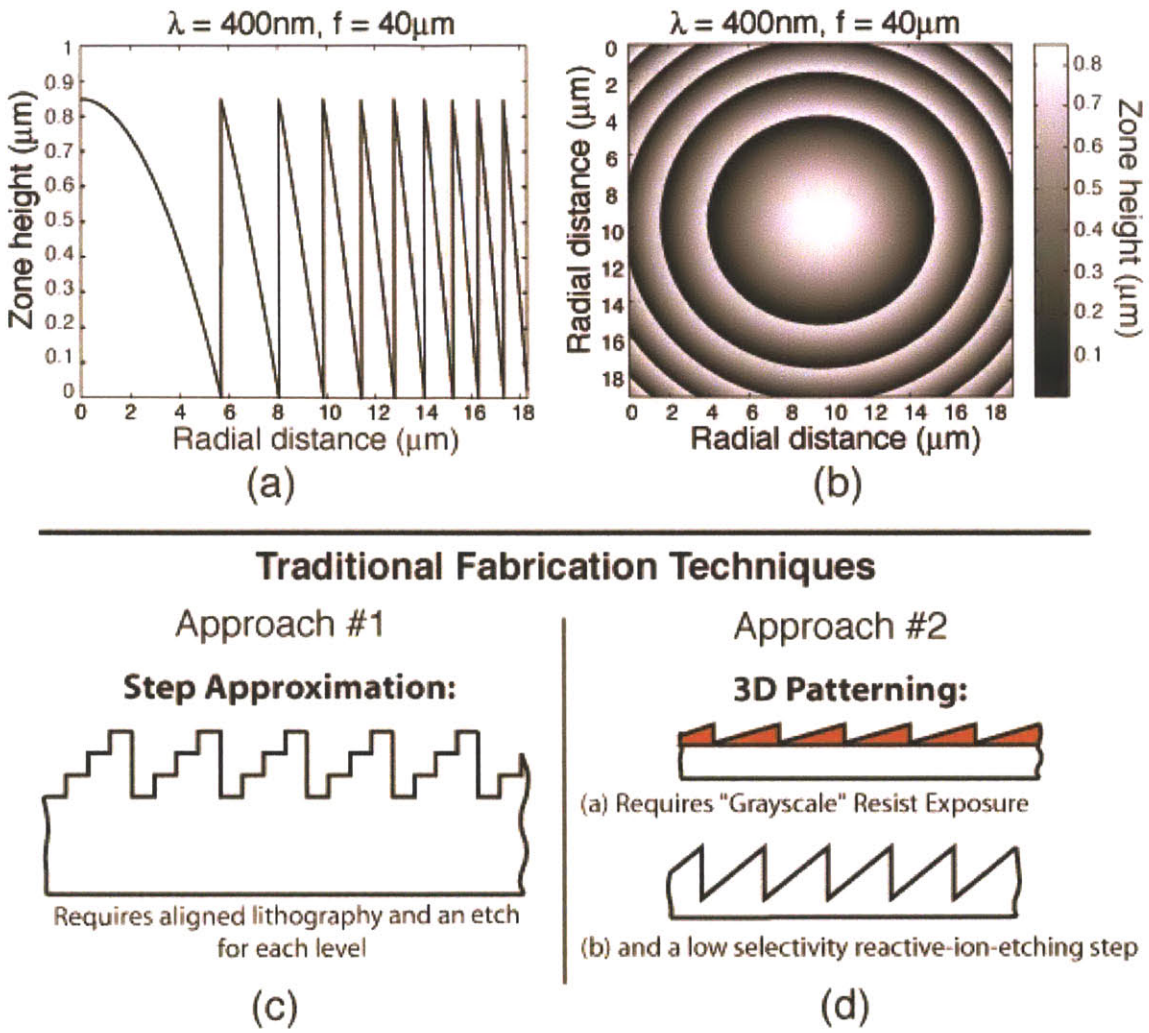

Figure 4 - 9. Blazed zone plates can provide close to 100% efficiency into a diffraction-limited spot. Top of figure: (a) Cross-section of a blazed zone plate designed for λ=400nm. (b) Top-view of the central zones of a blazed zone plate. Bottom of figure: Traditional fabrication techniques for blazed diffractive elements. (c) the blazed profile can be approximated by a series of aligned steps, (d) a "grayscale" resist exposure enables the transfer of a blazed profile into the substrate by means of a low-selectivity reactive-ion-etching step.

Figure 4-9(c) depicts a technique for blazing based on approximating the sloped profile by a series of steps. While four steps can achieve efficiencies into the first order in excess of 80%, each step requires an aligned lithographic exposure, something that can be very challenging for high-resolution zone plates that have outer-zone-widths as small as 100nm (and potentially even smaller). An alternative method is illustrated in Figure 4-9(d). It relies on the use of a "grayscale" resist exposure, which then enables the transfer

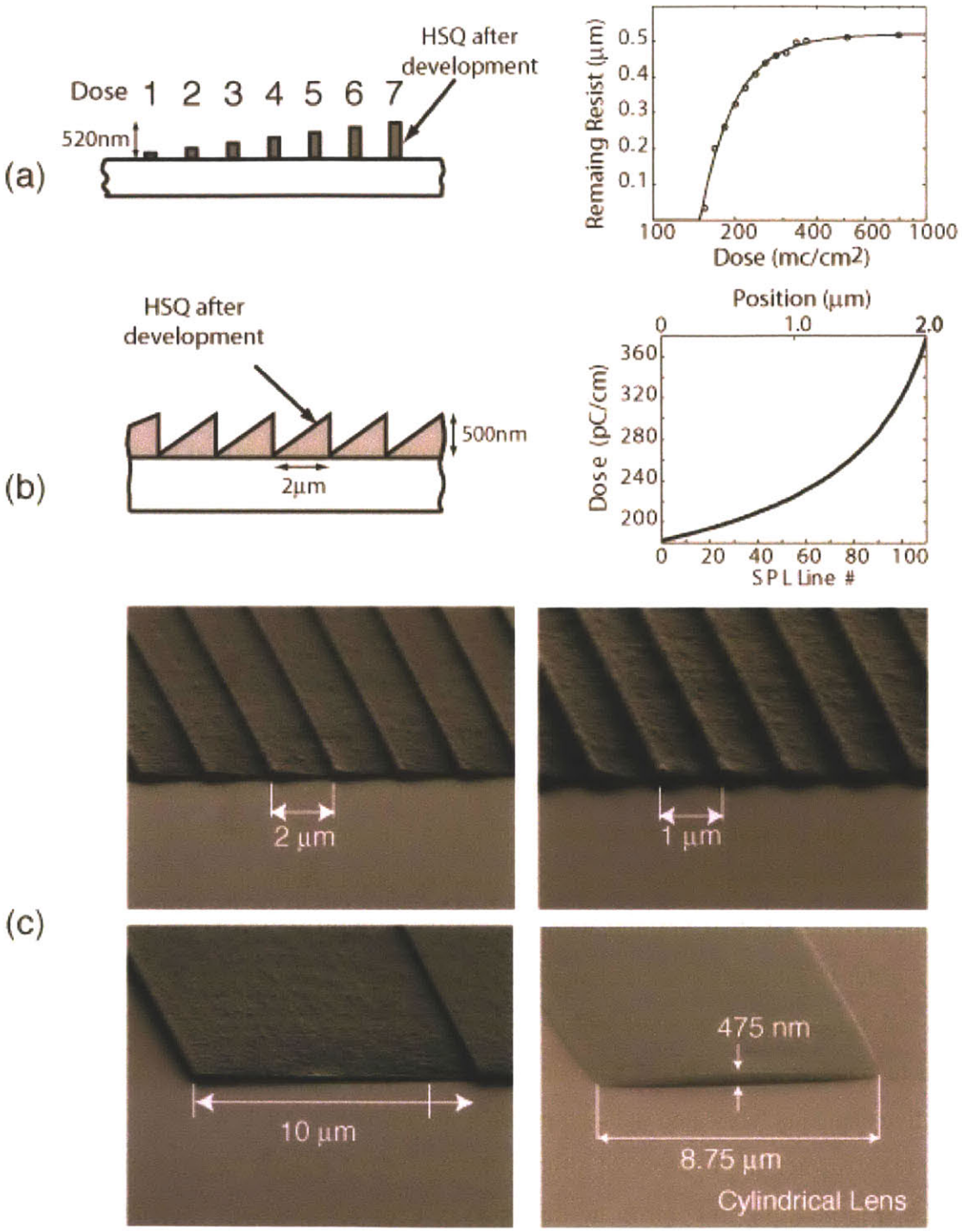

Figure 4 - 10. Direct 3D Patterning with HSQ. (a) Left: Schematic illustrating the fact that the thickness remaining of HSQ after development can be controlled, Right: plot of the thickness of remaining resist after development versus dose delivered, (b) Left: Schematic of characteristic blazed structure, Right: Dose required across each tooth of the blazed grating in order to achieve a linear slope (note that the dose required is not a linear function). (c) Scanning electron micrographs of blazed structures fabricated with HSQ

of a blazed profile into the substrate by means of a low-selectivity reactive-ion etching step. Although only one lithography step is required with this process, the reactive-ion etching can be quite tricky, requiring careful control of the etching selectivity of both the resist and the substrate.

An alternative fabrication method for blazed structures requiring a single lithography exposure and no etching was developed through the work of this thesis[4]. The technique borrows heavily from the self-aligned zone plate fabrication procedure described at the end of Chapter 3, in that it makes use of HSQ (hydrogen silsesquioxane) as the final layer responsible for creating the appropriate phase-shift at each zone. For very thin layers, HSQ, being glass like, will introduce negligible attenuation at UV and deep UV wavelengths. The trick that will allow the creation of sloped profiles with this resist comes from the fact that for a given initial thickness of HSQ, the thickness remaining depends on the electron beam dose, as indicated in Figure 4-10(a). Accordingly, by varying the dose in scanning-electron-beam lithography one can vary the thickness of the zones. Note that, as illustrated in Figure 4-10(b) the dose required in order to achieve a linear slope across each tooth of the blazed grating is not a linear function. Figure 4-10(c) shows a first attempt at creating 3D structures in one step. Among the patterns created were entirely curved structures (mimicking the central zone of a zone plate), as well as gratings with a linear blaze. While much works remains to be done in order to fabricate blazed zone plates, these results provide early indications that such a task might indeed be achievable. As mentioned earlier, this would enable a ZPAL system to obtain nearly 100% efficiency into the first order focus while still utilizing diffractive elements fabricated with the planar process.

One further application of this technique is the apodization of zone plates. Because it is possible to control the thickness of each of the zones by controlling the amount of e-beam dose delivered into the HSQ, we can effectively "attenuate" certain zones. This attenuation, if properly designed, can reduce the size of the sidelobes of the zone-plate PSF, which can have beneficial effects in terms of contrast in ZPAL.

---

[4] The work on blazed structures was done in collaboration with Todd Hastings

4.2. Numerical Aperture Studies

One of the key contributions of the work presented in this thesis has been the design, fabrication and testing of the highest-numerical aperture UV zone plates ever reported. The results presented in the following sections are compelling. Zone plates with numerical apertures as high as 0.95 were fabricated and tested. The zone plates were capable of diffraction-limited performance. It is well known that high-numerical-aperture refractive lenses pose enormous design and fabrication challenges, especially for large fields-of-view. With diffractive optics, fabricating high-numerical-aperture optics is not significantly more challenging that low-numerical-aperture elements. Furthermore, the distributed nature of ZPAL bypasses the tradeoff between resolution and wide field-of-view, which is at the core of much of the complexity (and the cost!) of the high-numerical aperture lenses used in many optical systems, including optical-projection lithography.

4.2.1 Characterization of Numerical Aperture by means of Zone-Plate-Array Microscopy (ZPAM)

With a minor modification, the ZPAL system can be made to operate as a high-resolution microscope. As will be described in Chapter 5, the microcopy mode of ZPAL (we call it Zone-Plate-Array Microscopy, ZPAM) enables one to set the substrate to be exposed at the right gap (i.e. at the focal plane of the zone plate array), as well as offering the potential for level-to-level alignment.

4.2.1.1 The ZPAM Principle

Zone plates have been used for many decades as imaging elements, primarily for x-ray microscopy. In many respects one can think of a zone plate as a lens, and as such, one should, in principle, be able to image with it. With this concept in mind, if the zone plate is used as the focusing lens of a traditional confocal microscope [Ref 4-3] one

would obtain a signal that varies with the gap and that achieves its maximum value exactly at the focal length of the zone plate. The concept is illustrated in Figure 4-11(b).

Any confocal scheme is at a minimum comprised of two lenses (an objective lens and a detector lens), a light source, a pinhole and a detector. The mode of operation is very straightforward. Light (typically from a laser) is passed through a beam splitter cube and is then focused by a lens onto a sample. If the sample is exactly at the focal plane of the lens, the light will be focused to a diffraction-limited spot at precisely the surface of the sample. Assuming for now a specular reflection at the substrate, the light will travel back through the same lens, come out of it collimated, and then travel to the beam splitter to be reflected and go through a second lens (the detector lens). At the focal plane of this last lens a pinhole is placed, followed by a detector. This path is illustrated with a solid line in Figure 4-11(a).

If the sample is not at the focal plane of the objective lens the detector lens will no longer see collimated light, and it will focus the light at a different distance than before. The pinhole's role is now apparent. Its purpose is to improve contrast by allowing only light that comes from the focal plane of the objective lens to go through and reach the detector. The signal obtained as the gap is varied is shown in Figure 4-11(c). The signal allows for the precise determination of the focal length of a zone plate. A peak detection algorithm can be used to find the maximum intensity of the signal. The focal length determination can be further improved by taking the center of gravity of the axial response (Figure 4-11(c)-right). [Ref 4-4].

Since each zone plate provides a signal from the substrate, by processing these signals while scanning the substrate, high-resolution images of the sample can be obtained, as show in Figure 4-11(d).

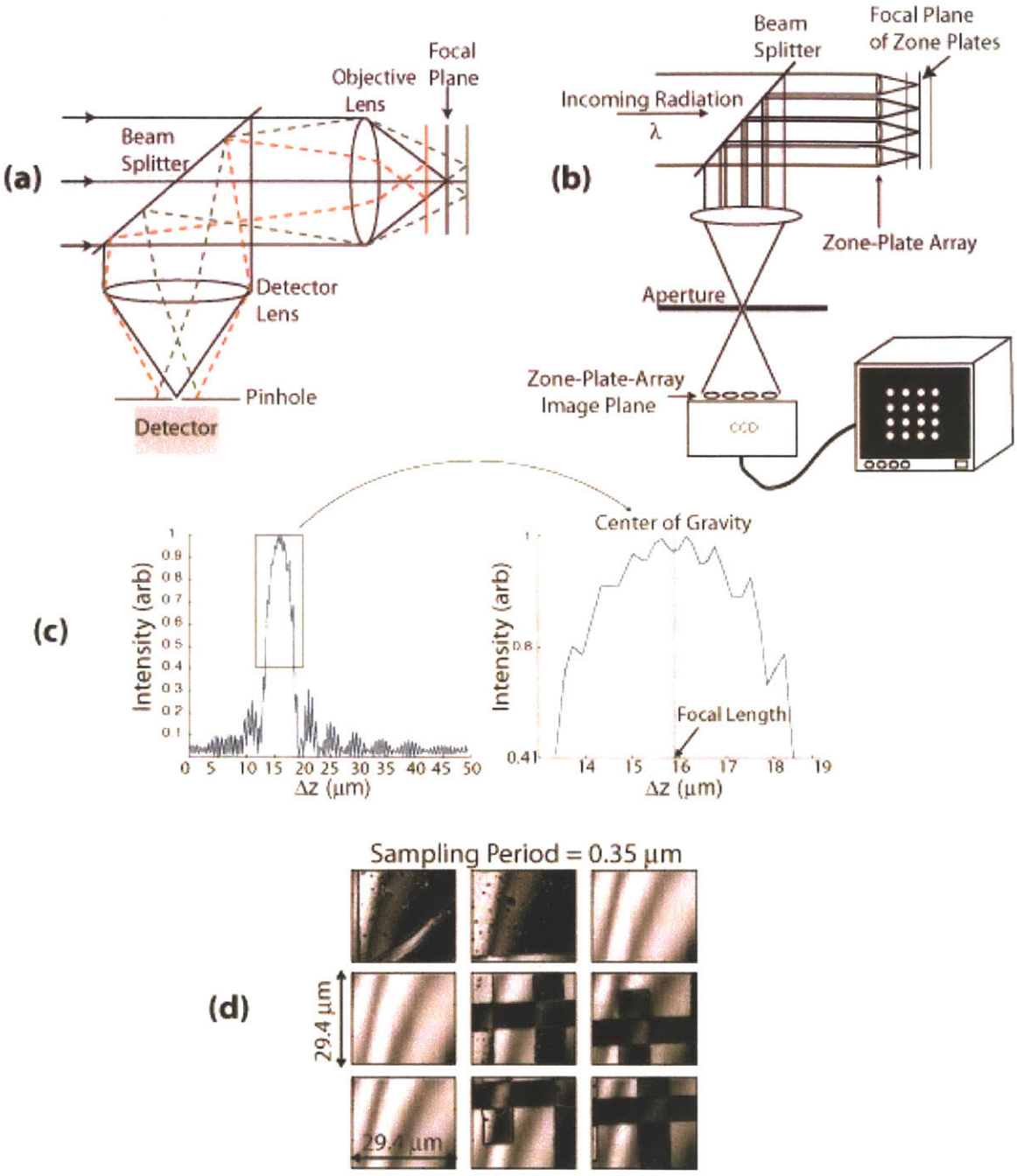

Figure 4 - 11. Confocal microscopy. (a) Conventional implementation of confocal microscopy (a single objective lens is used). (b) Schematic of ZPAM. The zone plates are used as an array of objective lenses. The CCD detector is placed at the image plane of the zone-plate array, after the confocal aperture, allowing the light from each zone plate to be analyzed independently. (c) Typical axial confocal signal obtained with ZPAM. The peak of the signal (which gives the exact location of the focal length of the zone plate) is obtained by calculating the Center of Gravity (CoG) of the signal. (d) Nine ZPAM images obtained in parallel (with nine zone plates). The sampling period was 350nm.

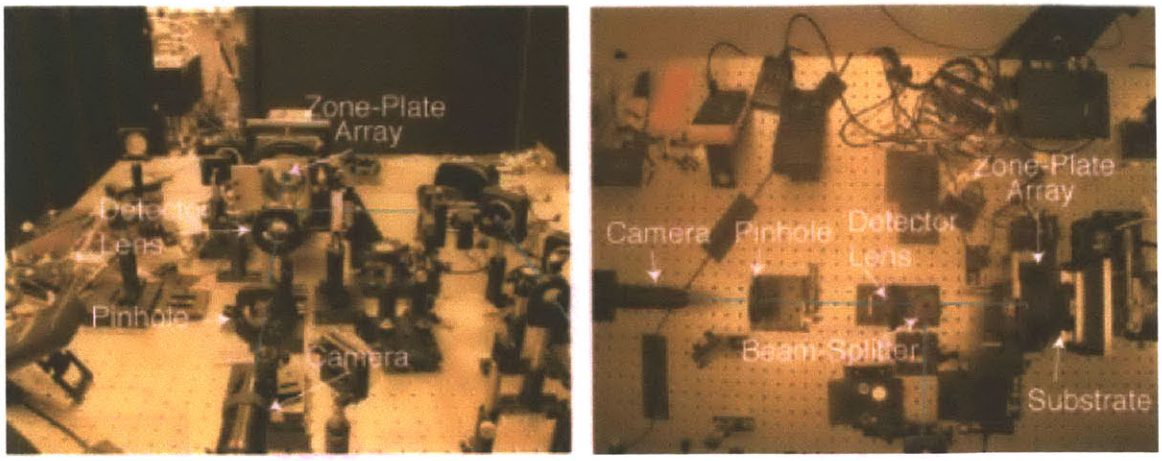

Figure 4 - 12. Experimental implementation of Zone-Plate-Array Mircoscopy.

4.2.1.2 Experimental Setup

The principle of operation of the massively parallel confocal microscope, ZPAM, is schematically depicted in Figure 4-11(b), and its experimental implementation is shown in Figure 4-12. Collimated light coming from a laser goes through a beam splitter and is focused by the zone-plate array, forming a 2-D array of diffraction-limited spots at the focal plane of the zone plates. The 2-D array of points get reflected back and pass through the zone plates one more time, coming out collimated if the substrate is at the focal plane. The array of collimated rays (one for each zone plate) gets reflected off the beam splitter, and is then focused by a lens. After passing through an aperture, the array of light beams reaches the CCD-chip of the camera. One signal per zone plate is obtained. The image of the camera is processed by a computer with a frame-grabber. The image is digitized and stored in memory for subsequent processing.

As in traditional confocal microscopy, if the object that is to be imaged is moved out of the focal plane, the array of spots generated by the zone plates will not form collimated rays when they pass through the zone plates for the second time, causing the detector lens to focus the light from the array into a focal plane that is different than when the substrate was at the focal plane of the zone-plate array. The pinhole will hence block most of the radiation. Again, the objective of the pinhole/aperture is to improve contrast by allowing only light from the focal plane of the zone-plates to reach the detector/CCD.

The CCD is placed in the conjugate plane of the zone-plate array, and therefore, the zone plates themselves are imaged with the camera. As a consequence the pinhole cannot be arbitrarily small in order to maximize contrast as in traditional confocal microscopy. It must be sufficiently large as to enable the image of each zone-plate to reach the CCD.

4.2.1.3 Imaging Results

In an effort to understand the focusing performance of high-numerical-aperture zone plates, a set of five linear arrays of phase zone plates, with NAs ranging from 0.7 to 0.95, were fabricated. The zone plates were then tested, with the ZPAL system operating in microscopy mode, by having the different numerical-aperture zone plates image a chirped circular-grating resolution standard, with linewidths varying from 1 μm to 150 nm (the resolution standard was custom fabricated for this application by means of electron-beam lithography). A schematic of the resolution standard along with two scanning-electron micrographs of the first and last zones of the standard can be seen at the top of Figure 4-13. The figure also includes five ZPAM images of the resolution standard acquired with the various NA zone plates. Note that as the NA increases, even the finest period gratings can be resolved, demonstrating that very high-NA zone plates (all the way up to 0.95) maintain good focusing properties and can hence be utilized for high-resolution imaging. These results represent the first report of such high-NA optical imaging with zone plates.

4.2.1.4 Knife-Edge Results

With the objective of obtaining a more precise characterization of the PSF of the high-numerical aperture zone plates, knife-edge measurements were performed. This technique, which consists of scanning a sharply defined edge through the focused spot that is intended to be measured, is a well-known procedure routinely used to measure

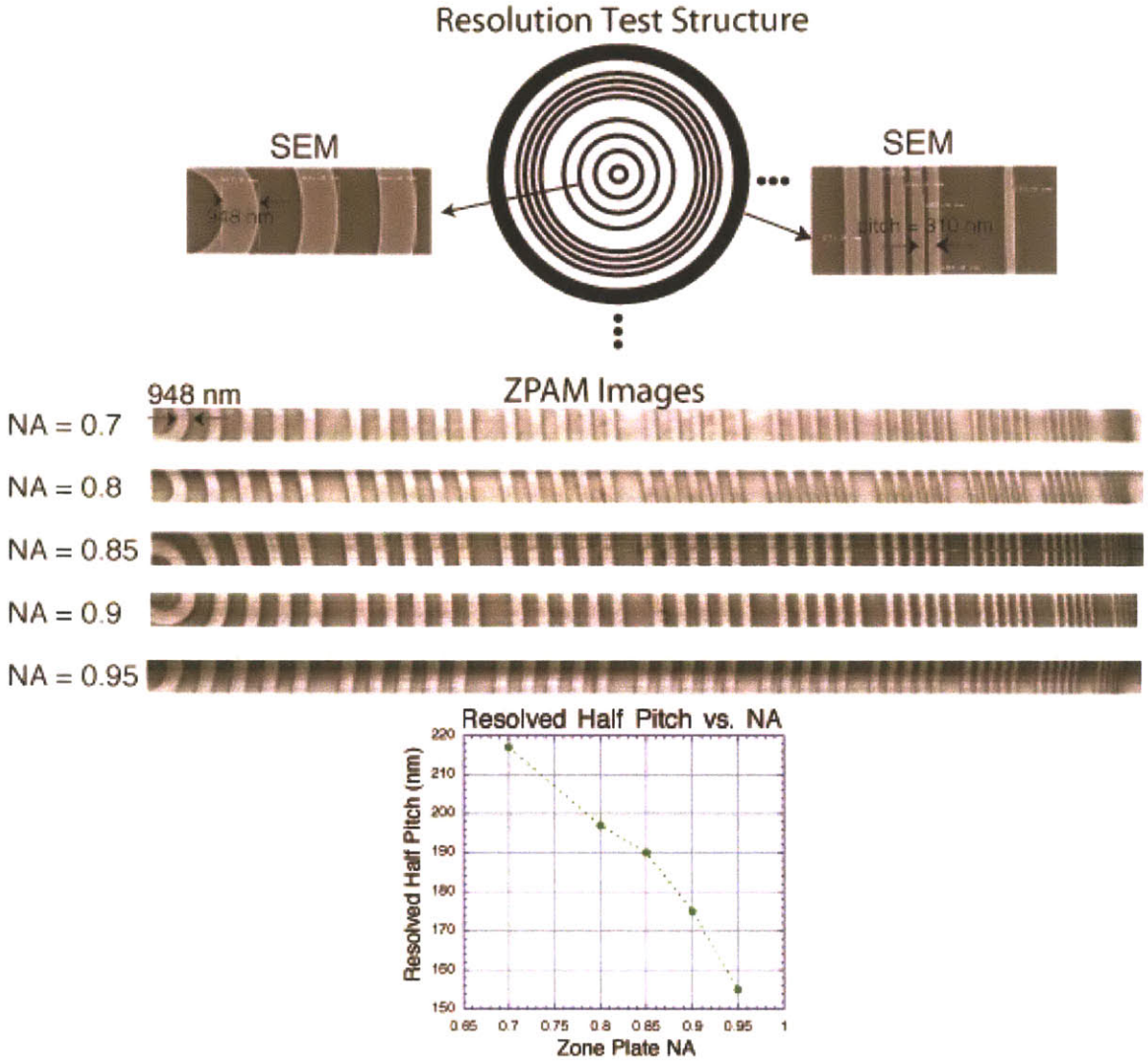

Figure 4 - 13. Characterization of high-numerical aperture zone plates by means of confocal microscopy (ZPAM). Top: Schematic representing the resolution structure utilized for characterization. The structure is a chirped circular grating with linewidths varying from 1 μm to 150 nm (see scanning-electron micrographs at the top-right and top-left of the figure). The figure includes five ZPAM images of the chirped grating taken with high-NA zone plates operating at λ = 442 nm. Bottom: Plot of the resolved half-pitch of the chirped gratings vs. the Numerical Aperture (NA) of the zone plate. As the numerical aperture increases, all the way to 0.95, the zone plate is able to resolve finer and finer features, demonstrating that very high-NA zone plates can be utilized for imaging.

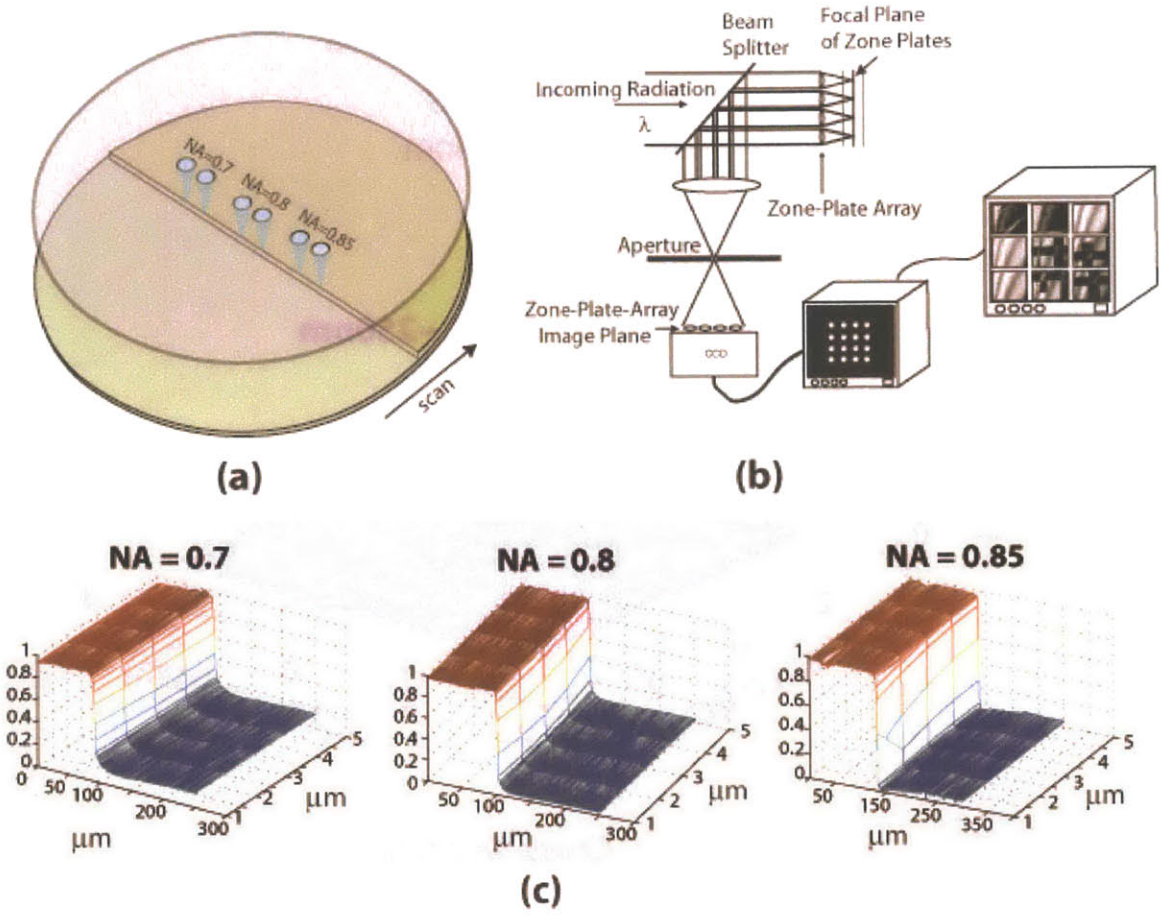

Figure 4 - 14. Knife-edge scans for the PSF characterization of zone plates. (a) The focused spot is scanned across a sharp-edge defined by a cleaved Si wafer bonded to a substrate. (b) The signal reflected from the knife-edge scan is collected by means of the ZPAM setup illustrated in the figure. (c) Three knife-edge scans performed with ZPAM with zone plates having numerical apertures of 0.7, 0.8, 0.85. As the numerical aperture increases, the slope of the edge also increases. As can be seen in Figure 4-15, the PSF can be reconstructed from these knife-edge scans.

beam-diameters for both optical and electron-beam focusing systems. Figure 4-14 shows three knife-edge scans obtained with zone plates having numerical apertures of 0.7, 0.8 and 0.85 respectively. Clearly, as the numerical aperture increases, the slope of the edge-transition also increases, indicating that the focal spot was smaller.

In a more quantitative manner, from the knife-edge scans the point-spread function of the high-numerical-aperture zone plates can be reconstructed. This will provide yet another method (the first one was discussed in section 4.1.1) to quantify the characteristics of the PSF.

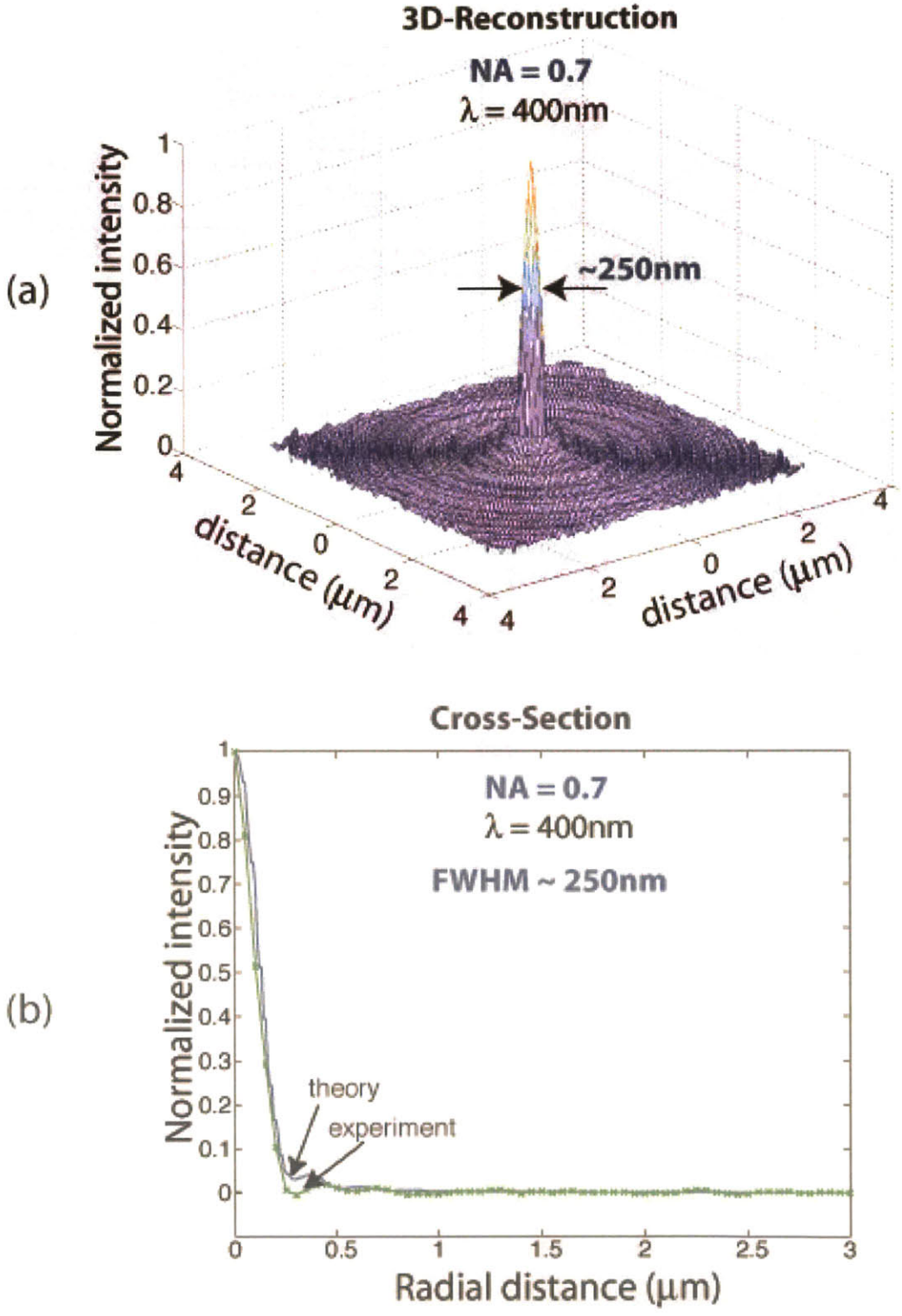

Figure 4 - 15. Reconstructed PSF of a 0.7 NA zone plate operating at λ=400nm. (a) The 3-D reconstruction is obtained from the cross-section and then rotated assuming circular symmetry. (c) Cross-section of the reconstructed PSF. Note that excellent agreement with theory. The spatial resolution of the knife-edge data was 50nm.

We begin by processing the data presented in Figure 4-14. Assuming a perfect confocal microscope, the knife-edge response can be expressed as a convolution of the PSF of the zone plate with the knife-edge [Ref 4-5]. We can then write:

$$U = h^2 \otimes t \qquad \textbf{4 - 9}$$

where h is the point-spread-function of the zone plate, and t is the scanned object (i.e. the knife-edge). The PSF appears as a square term since the signal passes through the zone plate twice (once as it focuses the incident radiation onto the object, and the second time as the reflected light is collected on the way back through the zone plate).

Since knife-edge can be modeled as a step function (this is a good approximation, since the sample was a cleaved silicon wafer), carrying out the convolution in equation 4-9 we get:

$$U = -\int_{-\infty}^{+\infty} dy' \int_{-\infty}^{x'} h^2(x',y')dx' \qquad \textbf{4 - 10}$$

by differentiating the above expression, the line-spread function can be obtained:

$$\frac{dU}{dx'} = -\int_{-\infty}^{+\infty} h^2(x',y')dy' \qquad \textbf{4 - 11}$$

The line-spread function is the tomographic projection of the point-spread function along the scan direction. The PSF can be reconstructed by inverting equation 4-11, via an operation known as the *inverse Radon transform* However, this operation is very sensitive to noise, and hence careful averaging over the area of the scan has to be applied. Figure 4-15 shows the results obtained for a zone plate with a numerical aperture of 0.7 operating at λ=400nm. Once again, we can see that the zone plates performed as expected, with diffraction-limited focusing that is in excellent agreement with theory.

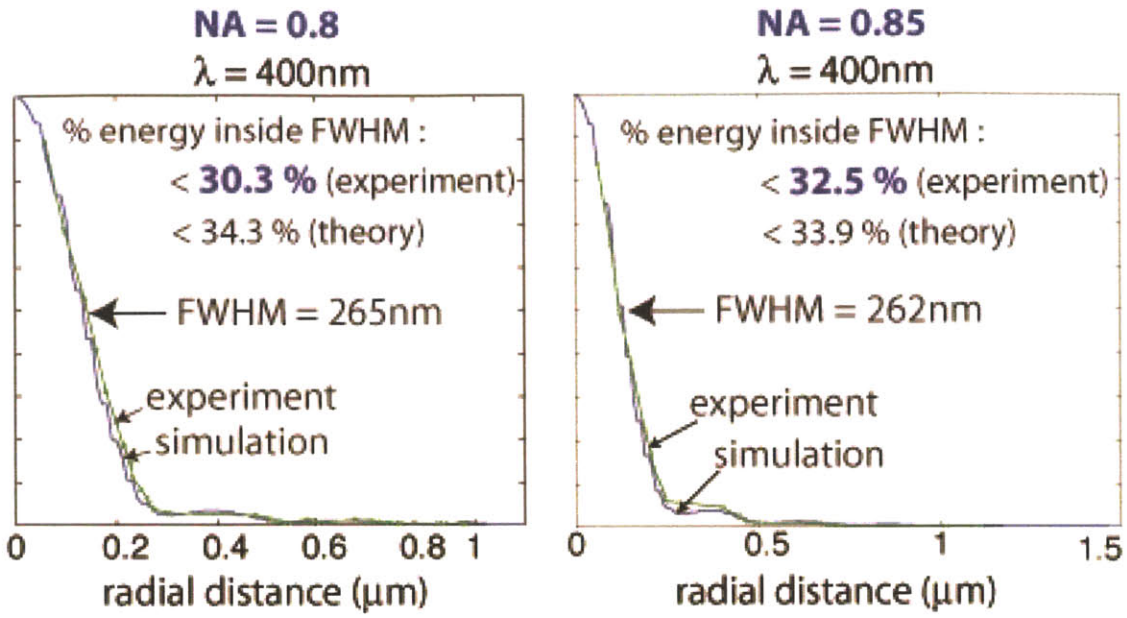

Figure 4 - 16. Experimental versus theoretical comparison of the efficiency into the focused spot for two zone plates with numerical apertures 0.8 and 0.85.

4.2.2. Efficiency Measurements

From the experimentally obtained cross-section of the point-spread-function, it is relatively straightforward to calculate the efficiency that was achieved into the focused spot. The method relies on integrating the energy under the area of the PSF from the center of the spot up to the full-width-at-half-maximum (FWHM), and dividing the obtained number by the total energy that is under the entire PSF. This very simple calculation can provide an upper-bound on the efficiency obtained with the fabricated zone plates. A comparison of the experimentally determined and the calculated PSF, along with the expected and achieved focusing efficiencies is plotted in Figure 4-16. Note that the efficiencies that can be achieved are close to the ideal performance.

Chapter 5

The ZPAL Prototype System

This chapter presents progress towards the implementation of a prototype ZPAL-system operating at an exposure wavelength of 400 nm, and capable of quick-turn-around, maskless lithography. Extensive lithography results are presented, detailing writing strategy, dose control and proximity-effect correction techniques. The development of a high-speed data delivery system is also discussed, as well as a multiplexing scheme that will enable the ZPAL prototype to achieve 210 nm feature sizes at a moderate but useful throughput of ~0.25 cm^2 in 20 minutes. The specifications for a high-throughput ZPAL system with sub-100nm resolution are also presented.

5.1 The ZPAL Architecture

As discussed in Chapter 2, zone-plate-array-lithography uses a narrow bandwidth source, an array of Fresnel zone plates, a multiplexing device capable of controlling the illumination to each zone plate in the array, and a scanning stage, to print arbitrary patterns on a wafer without a mask. The entire array of zone plates is illuminated and

then shuttered by the multiplexing device. The stage is scanned at the same time, enabling the creation of arbitrary patterns. Aside from the necessary beam-shaping optics needed to properly illuminate the pixels of the multiplexing element such that one pixel illuminates one and only one zone plate (ensuring that there is no crosstalk between zone plates as well as a uniform phase front across each of them), the optical train of the ZPAL architecture is inherently simple and inexpensive. As discussed in Chapter 3, for the UV and deep UV, the array of zone plates can be fabricated with a planar process that is simple and robust. The micromechanical elements employed are reliable commercial products of modest cost. The more expensive components are the radiation source and the scanning stage, a cost common to all lithography systems. But, with an architecture that offers a radical departure from a century-old tradition of refractive optics, a high-NA system can be built at a cost no higher than a low NA one.

We now proceed with a description of the components utilized in the ZPAL prototype system.

5.1.1 The GaN Diode Laser

The invention of the blue-light-emitting diode and blue semiconductor laser in 1991 by Shuji Nakamura[1], has resulted in the commercialization of compact, versatile, and highly cost-effective blue, violet, and ultraviolet lasers that can be utilized in ZPAL. These new lasers are ideal replacements for bulky, inefficient gas lasers. In terms of cost, the availability of compact GaN-diode lasers has reduced the price of blue lasers from tens of thousands of dollars to a only few thousand dollars. Furthermore, being diodes, no "warming-up" is required when the laser is turned on (as is required with HeCd-gas lasers), and they can be switched ON/OFF electronically at MHz rates. Two pictures illustrating the very significant size reduction achieved with the GaN lasers are included in Figure 5-1.

[1] At the time of the invention an employee of Nichia Corporation (who still owns the basic patent) and now a Professor at UC Santa Barbara

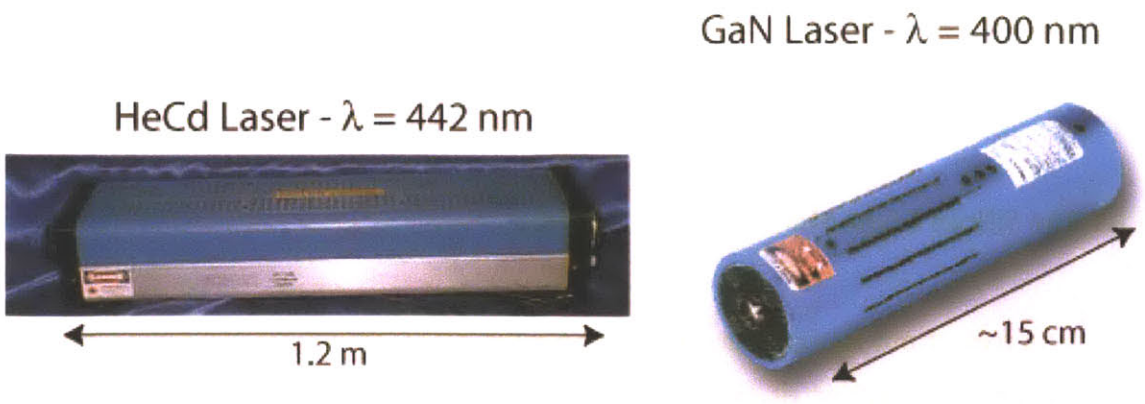

Figure 5 - 1. Two of the blue lasers utilized in ZPAL. The availability of compact GaN-diode lasers has reduced the price of blue lasers from tens of thousands to a few thousand dollars. Furthermore, being diodes, no warm-up is required (as is the case with HeCd-gas lasers), and they can be switched ON/OFF electronically at MHz rates.

For all the lithography results presented in this chapter, a λ = 400nm diode laser manufactured by Power Technology Inc. [Ref 5-1] with a nominal output power of 25mW was utilized. The laser comes with an integrated thermoelectric cooler that maintains the laser diodes operating at 20°C, prolonging the life of the diode and achieving wavelength stability[2], something that is important in ZPAL given the highly chromatic nature of zone plate focusing. In addition, an astigmatic lens placed at the output of the laser module corrects the highly divergent, elliptical, and astigmatic beams typically produced by diode lasers.

For the ZPAL prototype, the output of the laser is fed into an electro-optic feedback loop designed to reduce any noise or amplitude variations that might be present. A low voltage electro-optic light modulator manufactured by ConOptics [Ref 5-2] is then used to achieve dose control and modulation at high speeds. The modulator is connected to the ZPAL control computer via a high-speed input/output board.

In ZPAL, the micromechanical elements are responsible for dose control, bypassing the need for any other dose modulator. However, in order to characterize the lithographic performance of zone plates, as well as to optimize the writing-strategy and proximity-effect correction techniques, it is often preferred to run the system without the

[2] The blue diode has an excellent temperature coefficient of 0.05nm/°C

micromechanical elements. In this configuration, a dose modulator is required, and hence its presence in the prototype optical configuration.

5.1.2 The Silicon Light Machines GLV Module

As part of our design considerations for the ZPAL prototype, we have switched from our original method of multiplexing the light for ZPAL, the Texas Instruments DMD™ micromirror array, to the Silicon Light Machines Grating Light Valve™ (GLV™) linear array [Ref 5-3]. Although the GLV™ has a smaller number of pixels (1,088) compared to the DMD™ micromirror array (~1 million or more), the higher speed of operation of the GLV™ (20ns rise time as opposed to 20 μs for the DMD™), the fact that gray-scaling is built in, and its diffractive mode of operation (making it compatible with shorter wavelengths, possibly even down to 157nm) made it a superior choice for this ZPAL prototype.

5.1.2.1 Principle of Operation

The GLV™ is a micromechanical phase grating consisting of parallel rows of reflective Al ribbons. Alternate rows of ribbons can be pulled down electrostatically in a controlled manner to create diffraction effects on incident light. When no force is applied, all the ribbons lie in the same plane. If illuminated, incident light will be reflected from their surfaces at the same angle at which it is incident. When alternate ribbons are pulled down, a grating structure is created. In this state diffraction will produce light at an angle different from that of the incident light. By alternating between these two states (i.e. from flat ribbons to a grating structure) the GLV™ can switch light ON and OFF. Furthermore, by tuning the applied electrostatic force, the depth to which the ribbons are pulled down can be controlled, impacting the amount of light diffracted into the first order. Grayscaling of the incident light can be achieved in this manner. Each of the 1088 pixels present in the linear array can accept 8-bits of grayscaling (256 levels). Since the motion involved in switching the pixels of the GLV™ is small (one-quarter wavelength),

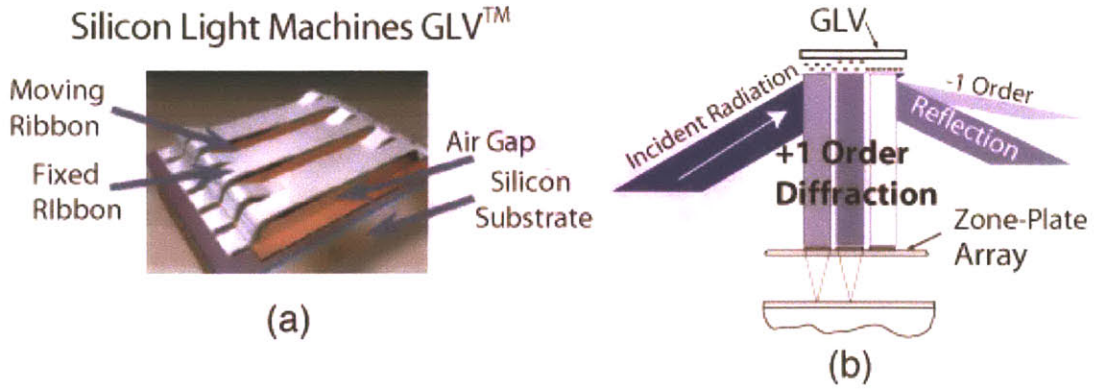

Figure 5 - 2. The Silicon Light Machines Grating Light Valve™ (GLV™) (a) one pixel of the GLV™ (each pixel can be thought of as a "mini-grating"), (b) intended implementation of the GLV™ with our linear array of zone plates indicating gray scaling.

the GLV™ is capable of very high switching speeds, with a rise time from the ON to the OFF position of only 20ns [Ref 5-4]. One pixel of the linear array is depicted schematically in Figure 5-2, along with the intended implementation in ZPAL.

5.1.2.2 Efficiency

The specific electro-optic response for a GLV pixel is shown in Figure 5-3. The first-order diffracted light intensity is essentially zero when no voltage is applied. Two factors lead to this result. First, most of the incident light is simply reflected specularly by the GLV device, which has a relatively large ribbon width-to-ribbon gap ratio (~6:1). Second, any potentially diffracting features, such as the ribbon gaps, are expressly created at twice the spatial frequency of the alternate ribbon ON state. Thus any undesirable diffraction occurs at larger angles, and does not affect contrast in the first-order diffraction beams. As can be seen in Figure 5-3(c), the GLV device performs smoothly and monotonically for well over three decades of intensity. Under idealized conditions, individual device contrast has been measured at over 4,000:1[Ref 5-5].

The efficiency of the GLV device depends on three main factors: the diffraction efficiency, the aperture ratio (or fill factor), and the reflectivity of the aluminum surface. In an ideal square-well diffraction grating, 81% of the diffracted light energy is directed into the +/- 1st orders.

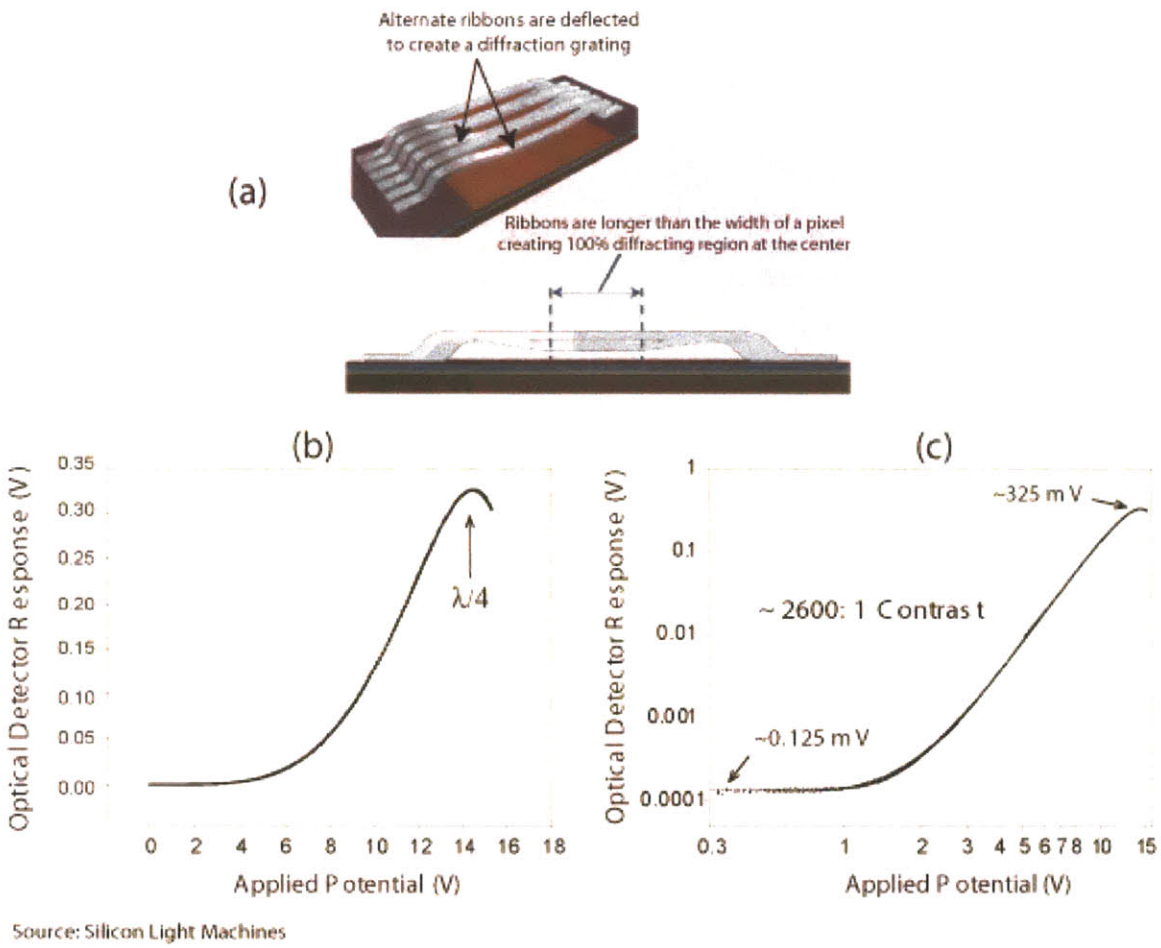

Figure 5 - 3. A GLV pixel with alternate reflecting ribbons electrostatically deflected to produce a diffraction grating. Note that the ribbons are longer that the width of a single pixel (vertical deflection greatly exaggerated). (b) GLV electro-optic response for 1st order diffraction, (c) GLV electro-optic response for 1st order diffraction on a logarithmic scale.

For maximum efficiency the ribbons have to be vertically deflected by a distance d, given by:

$$d = \frac{\lambda}{4} \qquad \textbf{5 - 1}$$

where λ is the wavelength of light.

An important design consideration required to achieve the maximum *overall efficiency* for any ZPAL system utilizing the GLV, has to do with how this MEMS device is illuminated. Ideally we would like to illuminate the GLV with a beam as close to a

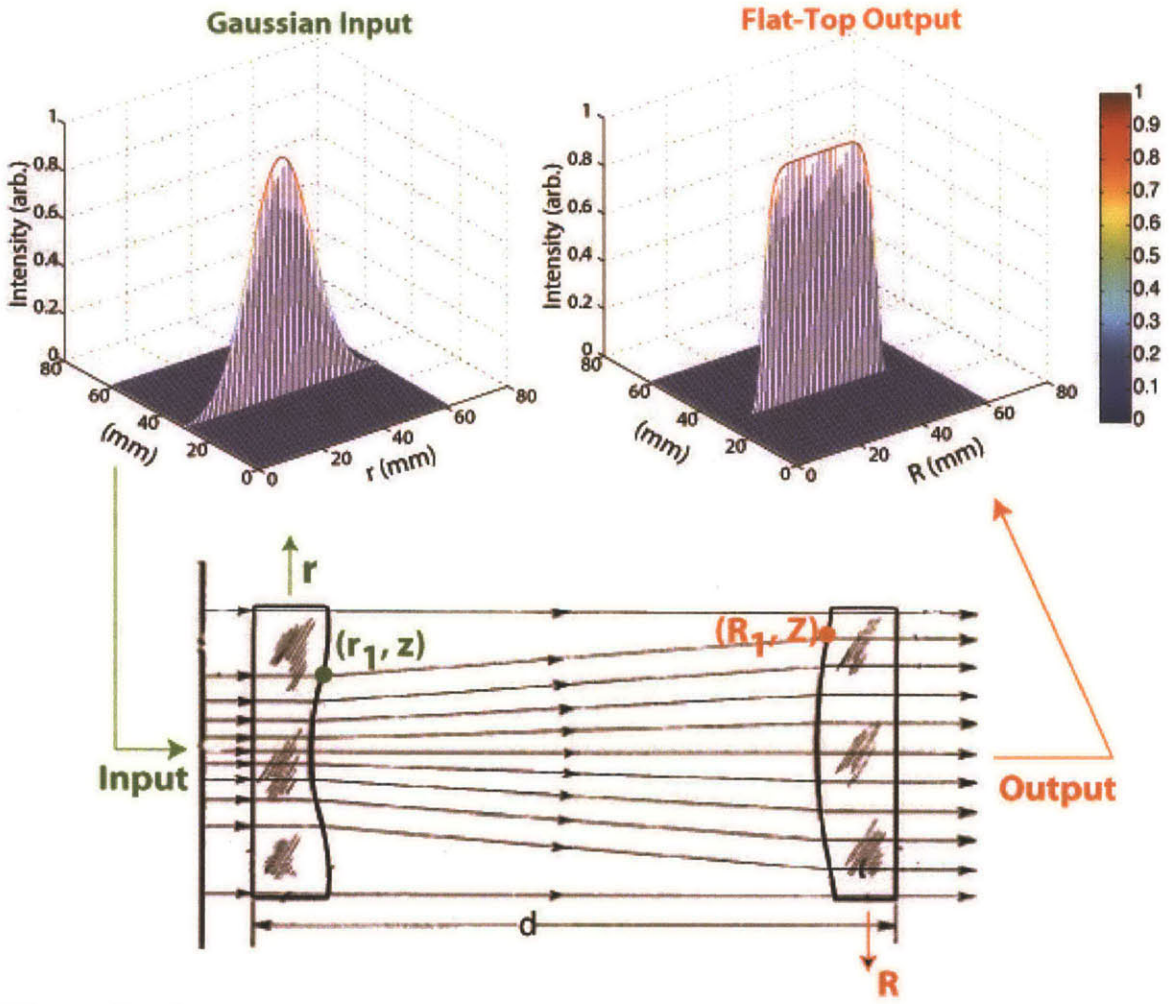

Figure 5 - 4. Two properly designed aspheric lenses can convert a Gaussian input intensity profile into a flat-top intensity profile.

flat-top as possible, in order to avoid the Gaussian distribution (typical of most lasers) of intensities across the 1,088 diffracted beams. Such a distribution would result in different zone plates receiving vastly different intensities, resulting in an unacceptable dose control for lithography applications. Although one could always correct for the Gaussian illumination via grayscaling (i.e. lower the efficiency of the central pixels of the GLV to match their diffracted intensities to the pixels at the edges of the device), this would result in a very significant loss of total power. It would be much preferable to properly illuminate the device with a flat-top beam capable of providing a uniform intensity across all 1,088 pixels. A methodology for designing a pair of aspheric lenses capable of

converting a collimated Gaussian beam to a flat-top beam is presented below [Ref 5-6, Ref 5-7].

Consider the schematic presented in Figure 5-4. It presents a Gaussian input beam impinging on a lens. By appropriately designing the curvature of this first lens, the rays can be redirected in such a way so as to redistribute the "density of the rays" into a uniformly distributed intensity profile. A second aspheric lens can then be used to collimate the beam to obtain the desired top-hat profile, as shown on the top-right of the figure. The problem is to find an expression for the curvature of the two aspheric lenses that will achieve such a transformation.

Let us denote by d the distance between the faces of the two aspheric lenses, as illustrated in Fig.5-4. Lets also define two coordinate systems (r, z) and (R, Z), centered at the intersection of the lens surfaces with the optical axis. We would like to obtain an expression for the curvature of the two lenses through the condition that a ray entering the first lens at (r_1, z) comes out collimated at (R_1, Z). A relation then exists between the rays entering and exiting the optics of the form:

$$R = h(r) \qquad \textbf{5 - 2}$$

Disregarding loses due to absorption and reflections in the lens elements, energy conservation requires that the total power in the input and output beams to be maintained. This condition will allow us to obtain a more explicit relation for equation 5-2. The energy conservation requirement can be expressed as:

$$\int_0^{2\pi}\int_0^{R_o} I_{in}(r) r dr d\theta = \int_0^{2\pi}\int_0^{R_o} I_{out}(r) r dr d\theta \qquad \textbf{5 - 3}$$

The left-side of equation 5-3 is the total energy in an energy beam having a distribution $I_{in}(r)$. In our case, this will be a Gaussian distribution, expressed as:

$$I_{in}(r) = e^{-\left(\frac{r}{a}\right)^2} \quad \text{for} \quad r < R_o \qquad \textbf{5 - 4}$$

where a is a scaling factor, and $R_0$is the outer radius of the first aspheric lens.

The right-hand side of equation 5-3 is an expression for the total energy of the output beam. Given that we would like to have an output beam with circular symmetry and a uniform (i.e. constant) energy distribution, the equation can be rewritten as:

$$\int_0^{2\pi}\int_0^{R_o} e^{-\left(\frac{r}{a}\right)^2} r dr d\theta = I_{out}\pi\ R_o^2 \qquad \textbf{5 - 5}$$

Performing the integration and solving for I_{out}, we get:

$$I_{out} = a^2\left(\frac{1-e^{-\left(\frac{R_o}{a}\right)^2}}{R_o^2}\right) \qquad \textbf{5 - 6}$$

A further constraint can now be imposed. Given the fact that the light rays in the central region in the incident beam are progressively spread out toward the peripheral region of the second aspheric lens, if we divide the incoming Gaussian beam into annular sections of radius r_1 and width dr, these sections must map onto a second annular section at the second aspheric lens of radius R_1 and width dR. We can apply, once again, the conservation of energy principle to each of these pairs of annuli. By also using equations 5-4 and 5-6, we get:

$$e^{-\left(\frac{r_1}{a}\right)^2} r_1 dr_1 = a^2\left(\frac{1-e^{-\left(\frac{R_o}{a}\right)^2}}{R_o^2}\right) R_2 dR_2 \qquad \textbf{5 - 7}$$

integrating equation 5-7, a relationship between r_1 and R_1 can be obtained:

$$R_1 = R_o\sqrt{\left(\frac{1-e^{-\left(\frac{r_1}{a}\right)^2}}{1-e^{-\left(\frac{R_o}{a}\right)^2}}\right)} \qquad \textbf{5 - 8}$$

Equation 5-8 provides a mapping of where each ray entering the first aspheric surface at r_1, should end up at the second aspheric surface. Now, applying Snell's law at

each of the interfaces, an expression for the curvature of each of the surfaces can be obtained. The curvature will naturally depend on the index of the materials used, the separation and size of the lenses, as well as on the scaling parameter a regarding the size of the input Gaussian beam. Bypassing the geometrical derivation and application of Snell's law at each interface, a final expression for the curvature of each lens is obtained:

$$z(r) = \int_0^{R_o} \left\{ \left(n^2 - 1\right) + \left[\frac{(n-1)d}{R_1 - r_1} \right]^2 \right\}^{-1/2} dr_1 \qquad \textbf{5 - 9}$$

by using the expression for R_1 given by equation 5-8, the curvature of the first aspheric surface is defined. For the second surface, Snell's law dictates the following expression:

$$Z(R) = \int_0^{R_o} \left\{ \left(n^2 - 1\right) + \left[\frac{(n-1)d}{R_1 - r_1} \right]^2 \right\}^{-1/2} dR_1 \qquad \textbf{5 - 10}$$

where an expression for r_1 can be obtained via equation 5-8.

By appropriately computing the integrals of equations 5-9 and 5-10, the profiles can be obtained (i.e. for each radial distance, the amount of lens material that has to be removed is calculated). The resulting table of "location in lens" vs. "amount of material to remove" can be used to fabricate the aspheric lenses via a numerically controlled optical finishing machine. The design presented above, once implemented, should enable an efficient illumination of the GLV for the ZPAL prototype.

5.1.2.3 A Data Delivery System for the GLV

Given the fact that the Silicon Light Machines GLV module was purchased without any driving electronics, or software interface, a custom electronic system to deliver the pattern data from the ZPAL control computer to the 1,088 pixels of the GLV™ array at very high speeds had to be built. Very briefly, the implementation is as

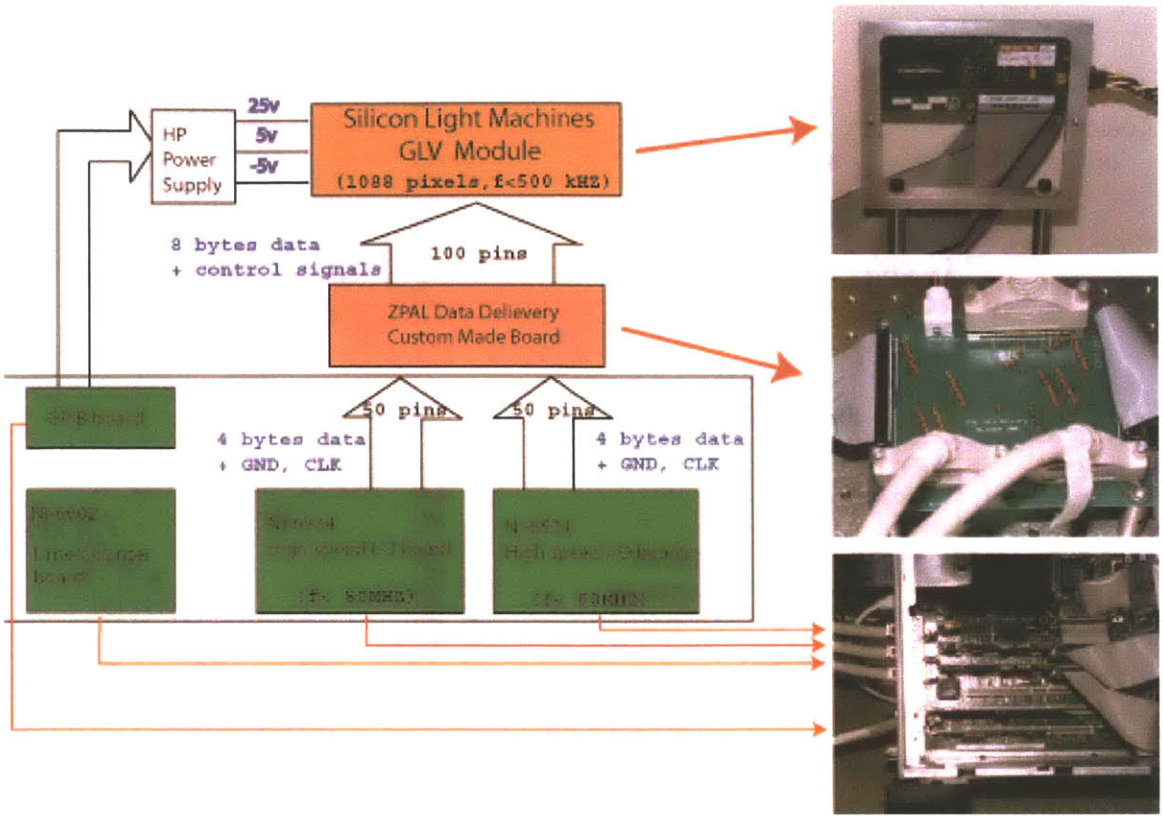

Figure 5 - 5. Data delivery implementation for the GLV module in the ZPAL prototype.

follows[3]. Data is first transferred from the computer through the PCI bus to a National Instruments digital I/O board (Model#: 6601). The data is then sent from the I/O board to the GLV™ through a custom made printed circuit board (PCB), which performs the data routing and interpretation as required by the GLV™ electronics. The I/O board, equipped with an 80Mhz clock to enable clocking the data at very high speeds, has the capability of both reading data from the control computer and sending data to the GLV™ simultaneously. In practice, two I/O boards are used in parallel to achieve high data rates. All the software was written in LabView on a Dell windows workstation. Figure 5-5 provides a schematic representation as well as pictures of the system that was built.

In order to test the data delivery system, an experimental setup was assembled, as shown in Figure 5-6 (a). Light from a Helium-Neon laser is collimated and directed onto the GLV™. A lens is used to focus the 1st order diffracted beam onto a detector. Data is

[3] A much more detailed analysis and description will be the basis of a Master's thesis by Amil Patel, currently a member of the ZPAL team.

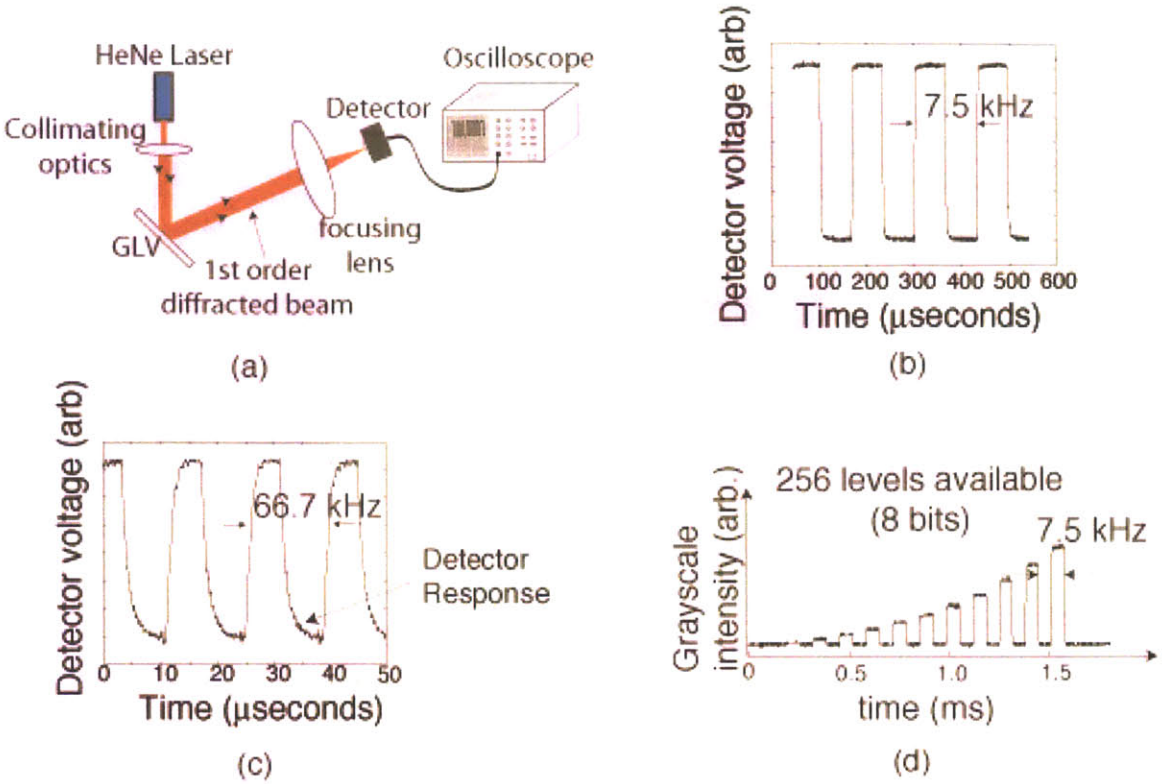

Figure 5 - 6. (a) Schematic of the experimental setup for testing the data delivery system for ZPAL. (b) The GLV operating at 7.5 kHz, the required speed for our prototype system. (c) The GLV operating at 66.67 kHz, corresponding to a 1Gbit/sec data rate. (d) Grayscaling at 7.5 kHz.

sent to the GLV™ and the modulation of the light on the detector is measured. Figure 5-6(b) shows the detector signal as a function of time when the GLV™ was driven with "ON-OFF" data at a frequency of 7.5 kHz (the specification required for our prototype system), corresponding to an average data transfer rate of 130 Mbits/s. The vertical axis is the detector voltage, but it was not calibrated and hence is not labeled in the figure.

Since the GLV™ is capable of operating at much higher frequencies (~500 kHz), the system was tested in order to determine the limits of the data delivery architecture, even though the achieved requirements are sufficient for the current specifications of the ZPAL prototype. Figure 5-6(c) shows the GLV™ operating at a frequency of 66.67 kHz, corresponding to a data transfer rate of about 1Gbit/s. At the time this experiment was performed, the response time of the detector used was the limiting factor, but data from a logic analyzer integrated into the system indicates that rates in excess of 100 kHz can be successfully sent with this implementation.

Since dose control is an important requirement for good lithographic performance, the ability to grayscale is paramount in any multiplexing device to be employed in a ZPAL system. The GLV™ offers 8-bits of grayscaling (256 levels), 3 bits more than what is needed for the ZPAL writing strategy, which requires 5-bits [Ref 5-8]. As shown in Figure 5-6(d), the data-delivery system is capable of achieving all 8-bits of grayscaling without sacrificing switching speed.

5.1.3 The Zone Plate Array

Although no further discussion is needed with regard to the role of the zone plates in ZPAL, a practical question that is worth addressing is how to experimentally place a photosensitive-resist-coated substrate precisely at the focal plane of the zone-plate array. The two surfaces must be parallel to each other while maintaining the plane of focus as the substrate is scanned. These matters are in practice challenging experimentally, especially for high-numerical-aperture zone plates, which can have focal lengths as short at 30 μm, and very shallow depths of focus.

5.1.3.1 Parallelization and Gapping in ZPAL

A Michelson interferometer provides a viable technique for parallelizing the zone-plate array and the substrate. The interferometer, as implemented in the ZPAL prototype, is shown in Figure 5-7. A Helium-Neon (HeNe) laser is first passed through a spatial filter and collimated by a lens. The beam is then divided into two beams by means of a beam-splitter cube. One of the beams proceeds by transmission toward the zone-plate array and the wafer, while the other proceeds by reflection towards the mirror (this is the reference arm). The waves are reflected at 3 surfaces (the mirror, the chrome pad on the back of the zone-plate substrate, and the wafer to be exposed with ZPAL).

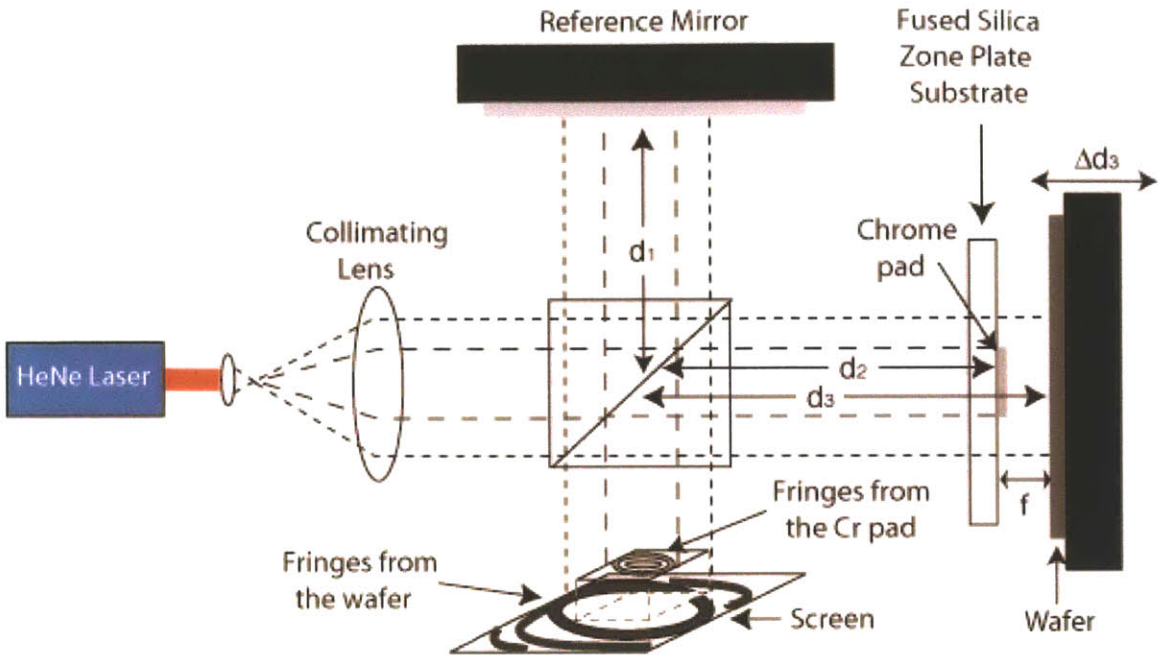

Figure 5 - 7. A Michelson interferometer can be used to set the zone plate substrate and the wafer to be exposed parallel to each other.

Interference fringes are observable on the screen (also depicted in the figure) due to all the reflected waves, so long as the optical-path difference between the arms is less than the coherence length of the light used for the interferometer. The very long coherence length of the HeNe laser ensures that the length of the reference arm, d_1, and those to the zone-plate substrate and wafer need not be matched with any significant precision. By gimbaling the zone plate substrate, observing the change in the fringes, and then adjusting the tilt of the substrate, parallelization can be achieved.

Once parallel, the next step consists on getting the wafer that is to be exposed at the focal plane of the zone plates, with a control that must be better than the depth-of-focus. This can be a considerable challenge for very-high numerical aperture zone plates that can have depth-of-focus of only a few hundred nanometers.

The confocal signal obtained in the Zone-Plate-Array Microscopy (ZPAM) mode of ZPAL, provides an excellent method for positioning the wafer at the focal length of the array. The implementation of a gapping technique with ZPAM is straightforward (see Figure 5-8), with the only constraint that one cannot use for gapping the same radiation that is used for exposing patterns, since in the gapping sequence the resist would be

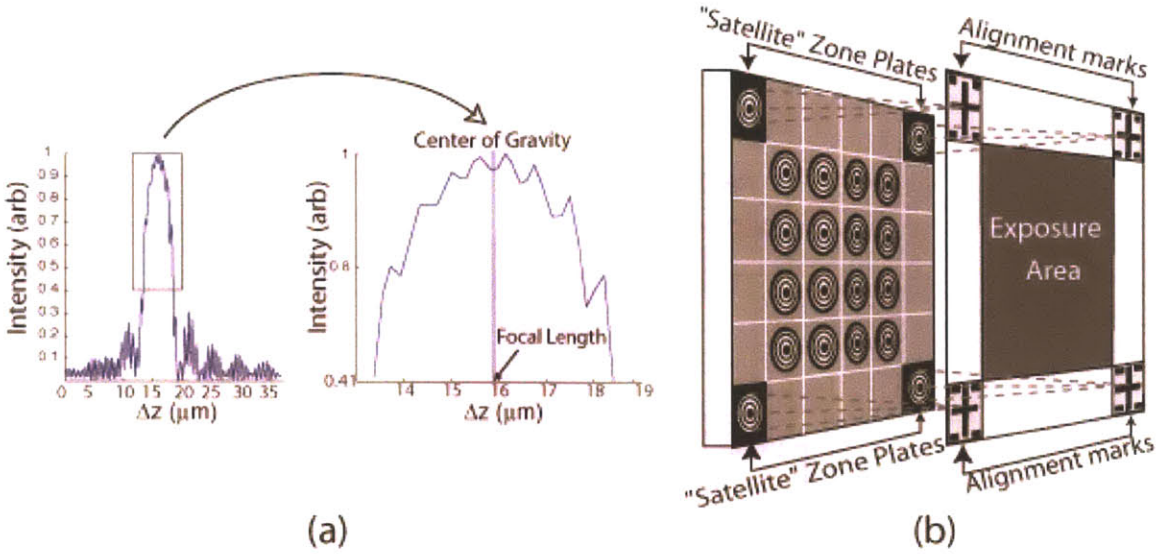

Figure 5 - 8. Gapping with confocal microscopy. (a) An experimental confocal signal. A center-of-gravity algorithm enables gap-setting with sub-100nm precision. (b) Illustration of the concept of "satellite" zone plates. These zone plates are designed to have the same focal length as the zone plates in the array, but operate at a non-exposing wavelength (e.g. λ=633nm). If the substrate to be exposed is scanned, the "satellite" zone plates can obtain images that can serve to align the exposure to a previous layer.

exposed. The solution lies in fabricating a set of "satellite" zone plates at the edges of the zone-plate array, designed so that they have the same focal length as the exposing zone plates, but operate at a non-exposing wavelength (e.g. λ=633nm). The fabrication of these "gapping" zone plates can be readily integrated with that of the exposing zone plates. The scheme allows for sub-100 nm gapping precision, as well as real-time measurements during exposure.

Two other applications can be implemented with the "satellite" zone-plate confocal scheme. The first is achieving parallelization between the zone-plate array and the substrate. This can be done by matching the intensity readings from a set of three "satellite" zone plates spaced sufficiently apart. The readings from each of the three zone plates can be used to feedback to three piezos connected to the zone plate substrate, to then set the array parallel to the substrate.

The second application of ZPAM in ZPAL is level-to-level alignment. If the substrate to be exposed is scanned, the "satellite" zone plates can obtain images that can

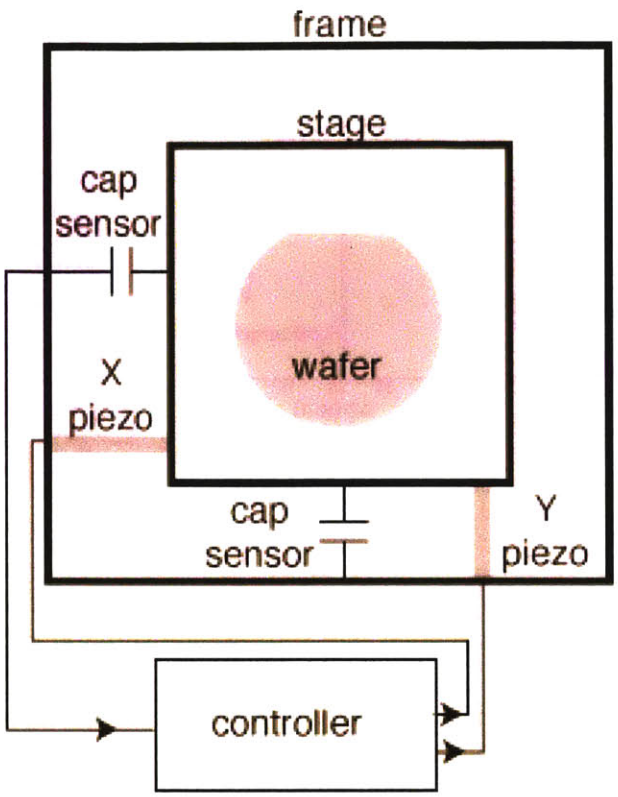

Figure 5 - 9. Schematic of the experimental implementation of the continuous-scanning stage in the ZPAL prototype.

be used to align the exposure to a previous layer. This last concept is illustrated in Figure 5-8(b).

5.1.4 The Scanning Stage

The scanning stage in ZPAL is responsible for the creation of complex patterns by displacing the substrate to be exposed to the appropriate positions in synchrony with the flashing laser exposures. Given that zone plates can create high-quality diffraction-limited spots, it is apparent that the quality of ZPAL lithography with ZPAL will be limited by the scanning accuracy and precision of the stage.

Initially implemented as a step-and-settle scanning system (i.e. the stage moves, the stage settles, spots are exposed, the stage moves again, etc), the stage in the ZPAL prototype now has the ability to scan in continuous mode. The scanning system used is a piezo-actuated stage from Physik Instrumente (model P-770), offering a scan range of

200x200 μm^2, with a positioning accuracy of less than 10nm. Capacitive sensors are used for determining position. Custom built velocity feedback circuits were implemented to enable continuous-velocity scanning. The stage scans the substrate in a raster fashion. During exposure, custom-built lithographic pattern generation software ensures that any unwritten rows and repeated pixels are discarded from the pattern, minimizing writing time. A schematic of the experimental implementation of the continuous-scanning stage in the ZPAL prototype can be seen in Figure 5-9.

5.2 Lithographic Performance

The results presented in the following sections are the highest quality lithographic patterns ever produced with ZPAL, showing good fidelity, low edge roughness, and the ability to pattern very dense features down to the minimum spot size. As will be described, features as small as 150nm were patterned with ZPAL. This is a remarkable performance for a system operating at $\lambda = 400nm$. The capability of ZPAL to pattern features at a resolution well below half the wavelength, enables ZPAL to compete head-to-head with state-of-the-art multimillion-dollar systems.

5.2.1 Writing Strategy

In Zone-Plate-Array Lithography patterns are created through the incoherent addition of spots. The two-dimensional pattern of energy that is deposited in the resist is the result of the convolution of the point-spread function (PSF) of the zone plate with the geometric pattern to be exposed. This concept is illustrated in Figure 5-10.

The convolution has an important consequence: the dose at a given location depends not only on the dose delivered at that location, but also on the dose delivered at nearby locations. Dose from neighboring regions of the pattern can "spill over" and give rise to what are known as proximity effects. A description of the nature of these effects in ZPAL, as well as a methodology for correcting them, is presented in section 5.2.1.2.

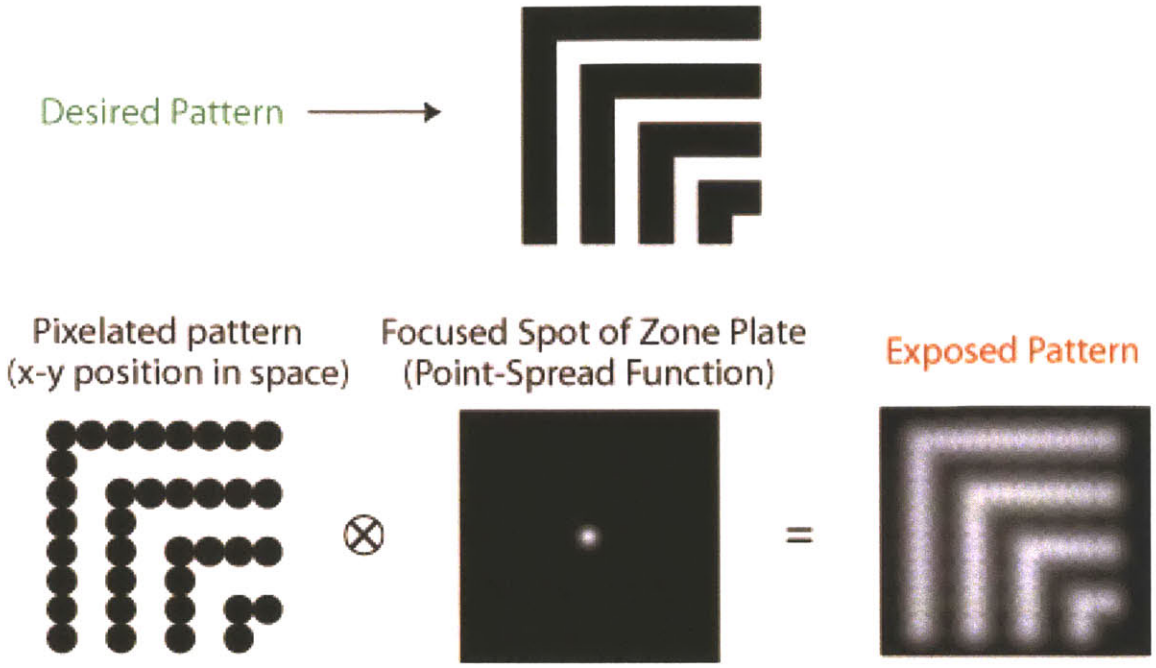

Figure 5 - 10. ZPAL writes pattern through the incoherent addition of spots. This addition is the result of the convolution of the pixilated version of the desired pattern and the Point-Spread Function of the zone plate.

5.2.1.1 Dose Control and Sub-Pixel Stepping

A lithography system should be able to control linewidth and edge placement of all exposed features with a precision much finer than the minimum feature size (i.e. the spot size in the case of ZPAL). For spot-based lithography systems, this can be done by stepping the exposures on a grid with a spatial period finer than the spot size. This is called sub-pixel stepping. By using this stepping technique, one can envision patterning features as small as the spot size, but with size increments only as small as the stepping grid, e.g., for pattern edge-placement one tenth of the minimum feature size, one would need a grid size one-tenth the spot size. This would severely impact throughput. However, by combining subpixel stepping with gray scaling (i.e the dose to each pixel is controlled) linewidth and edge placement can be controlled to much better than the stepping grid, with minimal throughput impact. This method of patterning has been used for scanning-electron-beam lithography [Ref 5-9, 5-10,5-11] and for scanning laser beam

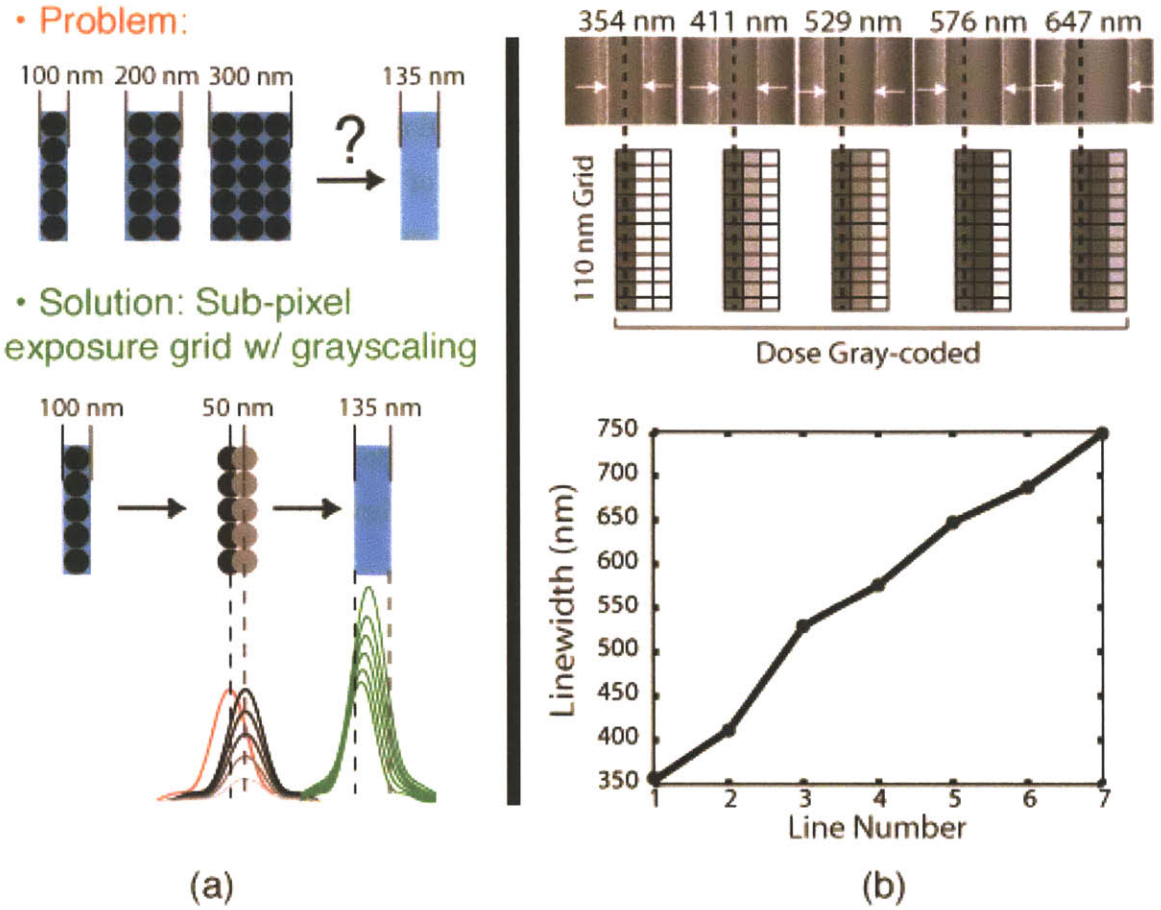

Figure 5 - 11. Writing strategy in ZPAL. (a) Since patterns in ZPAL are written by the addition of many spots, the stepping-grid determines the widths that can be created. By stepping a fraction of the spot-size after each spot exposure, while controlling the dose for each exposure, a width and pattern-placement control can be achieved with a resolution that is much better than the size of the spot. (b) Lines of varying width printed with ZPAL with a combination of sub-pixel stepping and gray scaling. Pixels (~330 nm in size) were exposed on a 110 nm grid. To widen the lines, a second line of pixels was exposed at increasing doses, then a third line was added. Top: SEM micrographs of lines. Middle: Schematic of exposure conditions for each line. Bottom: Plot of linewidth vs. line number.

lithography [Ref 5-12, 5-13]. A schematic illustrating what can be achieved with sub-pixel stepping in combination with gray-scaling is presented in Figure 5-11(a).

Figure 5-11(b) shows a series of ZPAL exposures which use sub-pixel stepping (in this case on a 110 nm grid, equal to one third the pixel size), in combination with pixel gray-scaling, to vary linewidth smoothly from a single pixel to greater than two pixels. The leftmost SEM image shows a single-pixel line exposed with a pixel spacing of 110 nm, as indicated in the schematic below the image. The linewidth for this image is

plotted as the leftmost data point in the plot at the bottom of Figure 5-11(b). The next three images and data points show the effect of exposing a second column of pixels, 110 nm away from, and parallel to, the first, at increasing dose. The rightmost SEM image and fifth data point show the effect of a third column of pixels exposed at a low dose. Subsequent data points, for which SEM images are not shown, show the effect of increasing the dose of this third pixel column. This result clearly shows that sub-pixel spacing can be used in combination with dose gray scaling to change linewidth with a precision not only finer than the spot size, but also finer than the exposure stepping grid. This can be done starting at a minimum feature size equal to the spot size. Extension to wider lines, or edge placement for large features, is straightforward.

5.2.1.2 Proximity Effects and their Correction

All forms of optical lithography exhibit deterioration in pattern quality due to diffraction and the finite aperture of the optics. In scanning spot systems, this effect arises from the spatial spreading of the focused spot (i.e, the PSF has sidelobes that extend in space and contribute to the dose delivered at other points). In image-projection systems, deterioration arises from the finite aperture of the optics. In this section, the origin of proximity effects in ZPAL as well as methods to compensate for these effects are presented.

As previously described, in ZPAL the exposure dose at a given location depends not only on the dose delivered at that location, but also on the dose delivered at nearby locations. Due to the spatial extent of the PSF, dose from neighboring regions of the pattern can "spill over" and give rise to what are known as proximity effects. The effect is illustrated in Figure 5-12. In Fig.5-12(a) we can see that for a nominal resist-clipping level, the contribution of the background results in adding a DC component to the PSF. The resist will then clip the PSF at a different level, resulting in a wider spot. In Fig.5-12 (b) a simulation shows how background effects (i.e. proximity effects) can result in the inability to print dense features if they are sufficiently close-packed. Proximity-effect correction can alleviate this problem by altering the dose delivered to each pixel to the

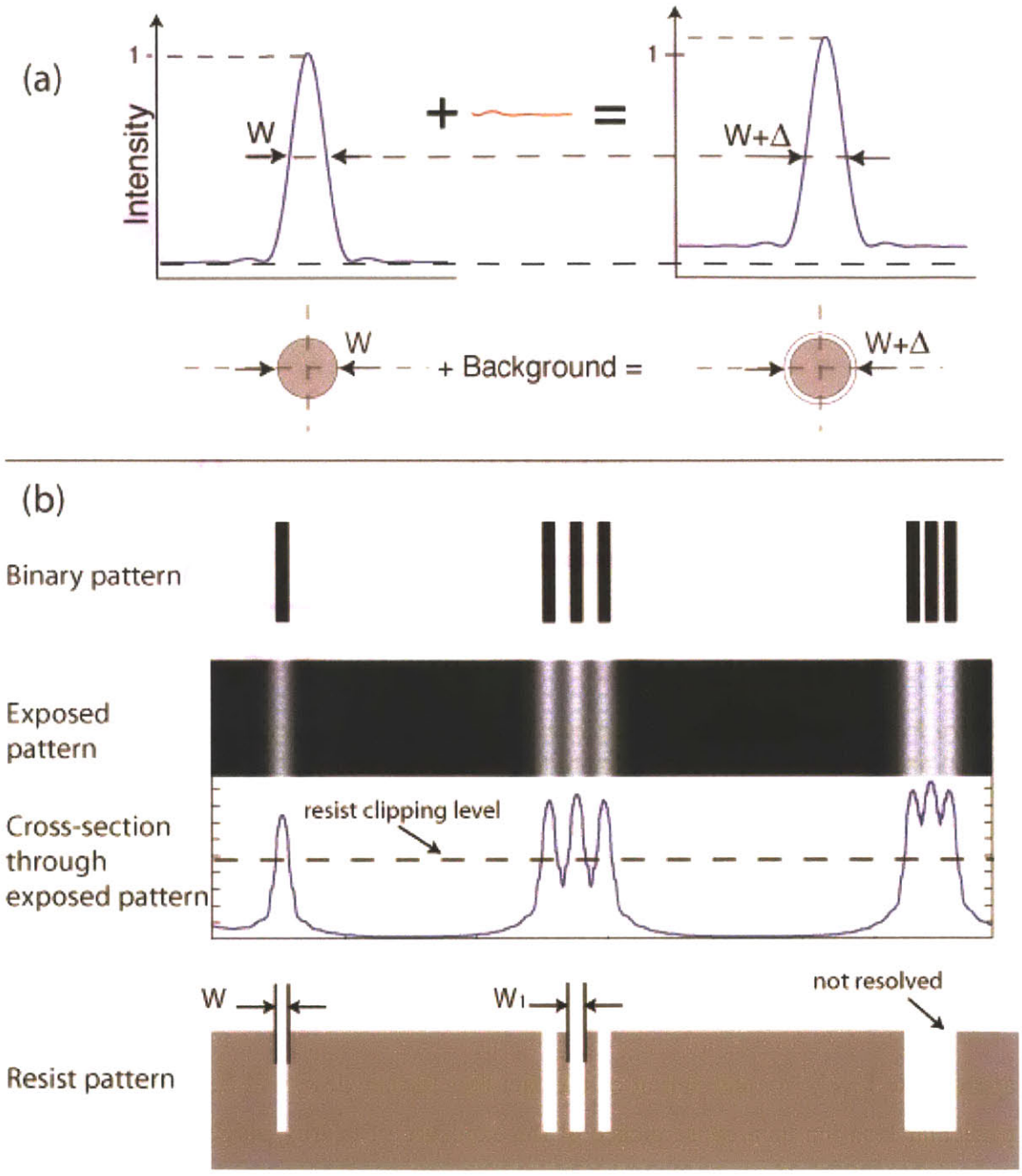

Figure 5 - 12. Proximity effects in ZPAL. The spatial extent of the PSF contributes to the total dose delivered at nearby exposed pixels. (a) For a nominal resist-clipping level, the contribution of the background results in adding a DC component to the PSF. The resist will then clip the PSF at a different level, resulting in a wider spot. (b) Background effects (i.e. proximity effects) can result in the inability to print dense features if they are sufficiently close-packed. Proximity-effect correction can alleviate this problem by altering the dose delivered to each pixel to the appropriate level, *in anticipation* of the fact that further dose will be delivered to that particular location as a consequence of the exposure of nearby pixels.

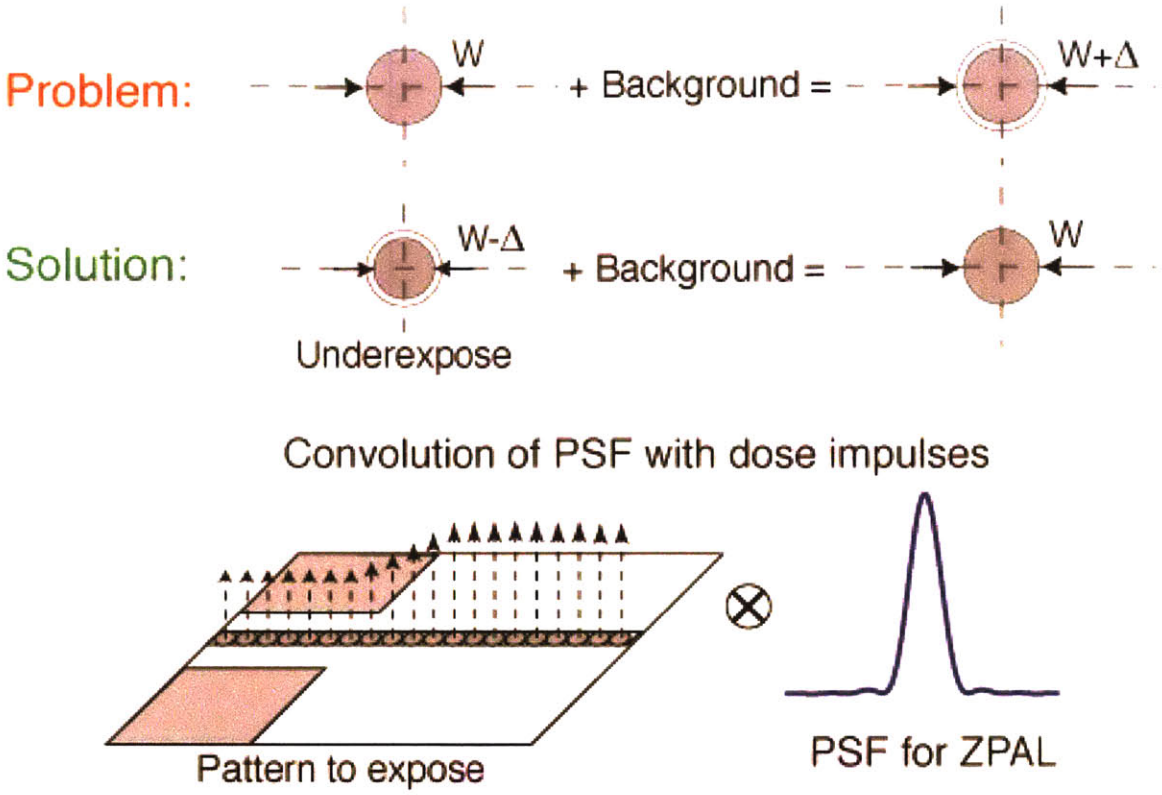

Figure 5 - 13. Proximity effects and how to correct them. Background arising from the spatial extent of the PSF contributes to the total dose delivered at nearby pixels. If the PSF is well-known, and given that writing in ZPAL results from the convolution of the pattern to be exposed with the PSF, the exposure dose to each pixel can be calculated in advance to achieve the desired *final* dose at each exposed location. The bottom-left diagram of the figure shows a sample pattern illustrating how the dose delivered at different pixel locations changes for a narrow line placed, for a part of its total length, between two large exposed pads. As expected, the pixels in the line closer to the pads require a different (i.e. lower) dose than the pixels that are far away.

appropriate level, in anticipation of the fact that further dose will be delivered to that particular location as a consequence of the exposure of nearby pixels. The concept is illustrated in Figure 5-13.

Proximity effects in ZPAL can, in general, be corrected by pre-compensating the patterns before writing. This requires accurate knowledge of the point-spread function (PSF) of the zone plate. If we assume a binary-clipping model for the resist, the normalized dose that is to be delivered for a given binary pattern B(x, y), intended to be exposed is:

$$B(x,y) = \left\{ \begin{matrix} 1 & \text{inside pattern boundary} \\ 0 & \text{otherwise} \end{matrix} \right\} \qquad \textbf{5 - 11}$$

The exposed pattern $E(x, y)$ is then given by:

$$E(x,y) = \sum_{i=1}^{N_{exp}} B(x_i,y_i) \times P(x - x_i, y - y_i) \qquad \textbf{5 - 12}$$

where (x_i, y_i) denote the exposed pixel locations, N_{exp} is the total number of exposed pixels, and $P(x, y)$ is the two-dimensional PSF of the zone plate. Thus, the exposed pattern is the discrete convolution of the binary pattern and the PSF. From this, we see that there are two degrees of freedom we can change in order to pre-compensate the pattern (i.e. to correct for proximity effects). These are: (1) the location of the points of exposure (x_i, y_i), and (2) the exposure dose. In practice, the points of exposure (these are known as pixels) are chosen as a grid of period one-half the spot-size for the reasons explained in section 5.2.1.1, namely to achieve good dimensional control and edge placement. We are then left with dose modulation as the only handle available for proximity-effect correction (PEC).

If we express the dose-modulated pattern as $D(x, y)$, then the exposed pattern is given by

$$E(x,y) = \sum_{i=1}^{N_{exp}} D(x_i,y_i) \times P(x - x_i, y - y_i) \qquad \textbf{5 - 13}$$

The problem of PEC then consists of calculating $D(x_i, y_i)$ for a given binary pattern and PSF. Three methods of solving this problem, as well as an experimental demonstration of the effectiveness of PEC are included below.

PEC Method #1: Direct Solution

Equation 5-13 represents a linear system of equations. If we set the exposed pattern, $E(x, y)$ equal to the binary pattern, $B(x, y)$, we can invert this system of equations to calculate the values for $D(x_i, y_i)$. The main disadvantage with this method is that it is not easy to put constraints on the values of $D(x_i, y_i)$. Care must be taken to consider the negative values of $D(x_i, y_i)$ since they represent a non-physical quantity, namely, a negative dose. One way to deal with negative values is to add a DC dose value to all

pixels so as to "bump up" all the values to 0 or greater. However, this results in a decrease in the process latitude, since the resist has to "clip" features at a higher level to maintain the feature sizes. In practice, this method turns out to be a poor solution, especially for complex and dense patterns.

PEC Method #2: Linear Programming

This method takes advantage of the highly non-linear nature of photoresists. Assuming a simple "clipping" model (e.g. after a threshold dose value is delivered at a given location, the resist will clear, creating a binary step profile), the desired pattern must have the following constraint:

$$E(x,y) \begin{cases} >LT & \text{inside pattern boundary} \\ <UT & \text{otherwise} \end{cases} \qquad \textbf{5 - 14}$$

where LT is the lower threshold dose above which all resist clears, and UT is the upper threshold dose below which no resist clears. Incorporating the constraints in equation 5-14 into the system of equations 5-13, results in a linear programming (LP) problem. In this LP problem, the objective is to minimize the difference between the exposed pattern, $E(x, y,)$ and the binary pattern, $B(x, y)$, by modifying the exposure doses, $D(x_i, y_i)$. The allowed modifications are subject to the constraints imposed by equation 5-14.

Although LP problems are well known and applied in a wide variety of fields, for this application the method was applied with moderate success. The chief problem that arose had to do with computational time; the time required to calculate the optimum doses increased dramatically for larger patterns.

PEC Method #2: Iterative Error-Correction Algorithm

This is a novel technique developed during the course of ZPAL research[4]. It consists of correcting the error contributions of the exposure doses in an iterative manner.

[4] See Rajesh Menon's Ph.D. thesis for a more extensive discussion of this method [Ref 5-15].

The steps are as follows:

1. We begin with the binary pattern (all doses equal to 1). Then we compute the exposed pattern, through the discrete convolution described in Equation 5-12.

2. The difference between the exposed pattern and the original binary pattern is denoted as the "error", *Err(x, y)*.

$$Err(x,y) = E(x,y) - B(x,y) \qquad \textbf{5 - 15}$$

3. For each point *(x, y)*, which has non-zero error, a search is performed to determine its nearest exposed point, (x_i, y_i). Then depending on the sign of the error at *(x, y)*, the dose at (x_i, y_i) is modified by a dose quantum. The dose quantum is the dose-control resolution achievable in the system.

$$D(x,y) = d(x,y) + sign(Err(x,y)) \cdot DQ \qquad \textbf{5 - 16}$$

where *DQ* is the dose quantum.

4. Using the dose-modulated pattern, *D(x, y)*, the exposed pattern is again calculated. Steps 2-4 are repeated until an acceptable level of error is achieved.

This method is straightforward to implement in software. Since, the dose quantum is automatically taken into account in the calculations, spurious dose quantization effects can be avoided. In practice, this method seems to offer very fast convergence as well. An experimental implementation of these technique in ZPAL is shown in Figure 5-14. The figure shows two scanning-electron micrographs with identical patterns exposed with ZPAL, one optimized (right) and one non-optimized (left). Note the dramatic improvements. Key features are color coded in both micrographs. For instance, the large square was designed to have a single unexposed spot at its center. If all exposed pixels are patterned with the same dose, proximity effects cause the spot to "wash-out" and disappear. By proximity-effect correcting the pattern prior to exposure, the spot can be retained.

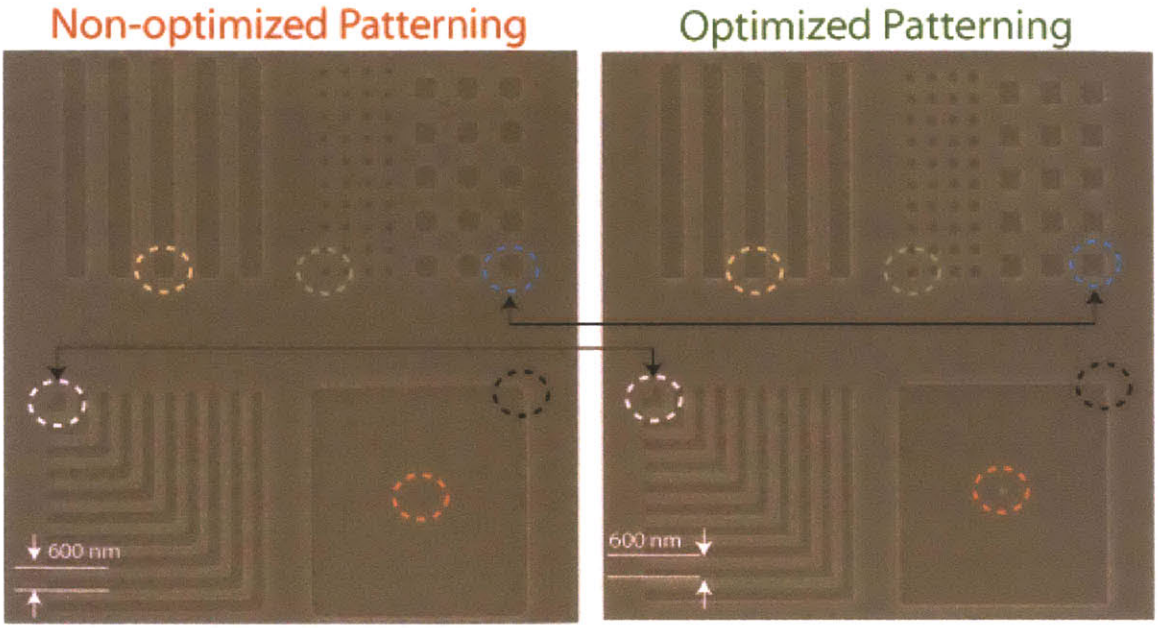

Figure 5 - 14. Patterns can be optimized prior to exposure by means of proximity-effect correction techniques. Such techniques allow greatly enhanced patterning capabilities in ZPAL, providing better edge definition and sharper features. The figure shows two scanning-electron micrographs with identical patterns exposed with ZPAL, one optimized (right) and one non-optimized (left). Note the dramatic improvements. Key features are color coded in both micrographs. For instance, the large square was designed to have a single unexposed spot at its center. If all exposed pixels are patterned with the same dose, proximity effects cause the spot to "wash-out" and disappear. By proximity-effect correcting the pattern prior to exposure, the spot can be retained.

5.2.2 Lithographic Results

The results that are now presented in the following pages are some of the highest quality lithographic patterns ever produced with ZPAL. A very large number of patterns have been exposed with the system, including many lithographic test structures, optical devices (such as waveguides and 2D photonic bandgap structures), devices for MEMS applications (microcomb structures), as well as diffractive optical elements (zone plates).

All exposures employed a 25 mW GaN laser diode operating at $\lambda = 400$ nm. For these experiments no multiplexing device was used, i.e., all zone plates in the array wrote the same pattern simultaneously (parallel patterning with active multiplexing has been demonstrated earlier [Ref 5-14]).For all the patterns presented, it is worth noting that

even though all exposed pixels received the same dose, proximity effects are minimal in the exposures.

The confocal gapping technique described earlier was used to set the substrate at the right gap with respect to the zone-plate array. All exposed substrates, unless otherwise indicated in the caption of the figures, were 75cm-diameter silicon wafers, spin-coated with 200 nm of BarLi ARC (spun at 3,000 rpm and baked on a hot-plate at 175° C for 90 seconds), with 150 nm of thinned Shipley 1813 photoresist on top (spun at 5000 rpm and baked on a hot-plate at 90° C for 60 seconds). The exposed patterns were developed in Shipley 351 developer diluted with water in the ratio 1:5 for 45 seconds.

A word about resolution in ZPAL. ZPAL shares with all other optical lithography systems the property that the minimum feature size that can be printed is determined by the following equation:

$$\text{Resolution} = k_1 \frac{\lambda}{NA} \qquad \textbf{5 - 17}$$

where λ, is the wavelength of light, *NA* is the numerical aperture, and k_1 is a proportionality factor having to do with the process latitude of the entire lithography process (it includes imperfections on the exposure system, resist and development limitations, etc). From equation 5-17 it is clear that for a given exposure wavelength, in order to achieve the maximum resolution one would like a NA as high as possible and a k_1 as low as possible. In Chapter 4 we saw that zone plates with numerical apertures in excess of 0.9 were capable of diffraction-limited performance. It is important then to understand what k_1 means for ZPAL, and how low it can be pushed.

Quantitative studies that go beyond obtaining pretty SEM pictures have been undertaken, and for the first time we are able to quantify the process latitude of our current system as well as the k_1 limits of zone plates. Figure 5-15 shows a set of scanning electron micrographs of dense lines and spaces with varying k's, from 0.56 to 0.32. Systematic characterization of lithographic exposures is allowing us to determine that the process latitude for our current system is in excess of 13% (even when operating at k_1 in the 0.3-0.4 regime).

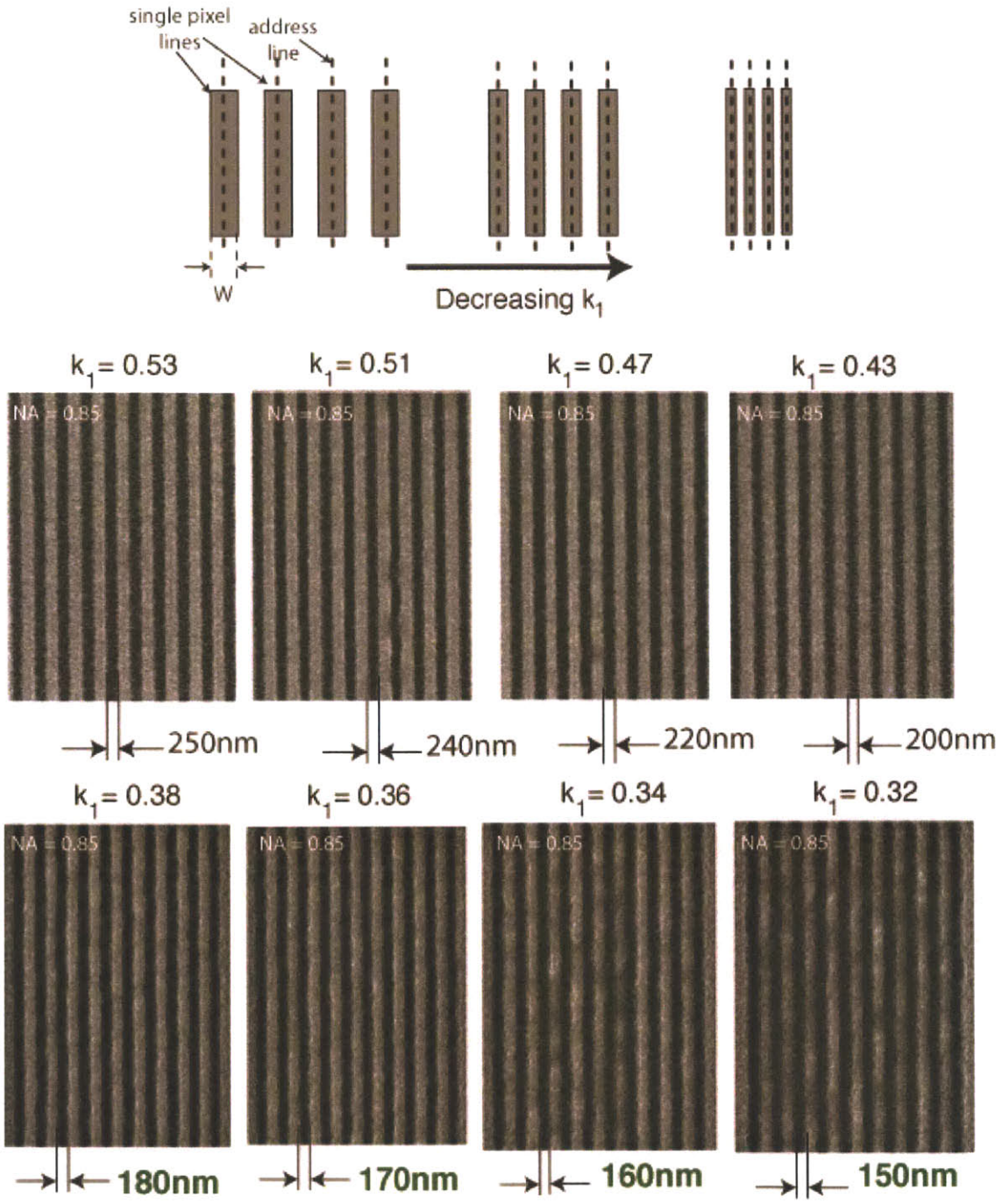

Figure 5 - 15. Meaning of k_1 in ZPAL. Top: Decreasing the $k_1$factor in ZPAL implies squeezing the address lines (depicted in figure) further and further. The goal is to be able to still pattern dense features with 50-50 duty cycles and an acceptable pattern quality. Bottom: Experimental determination of the limits of k_1 for a 0.85 NA zone plate operating at λ=400nm. While it is clear that the quality of the printed lines decreases as k_1 is reduced, 150nm lines and spaces can be patterned with λ=400nm light, a remarkable result.

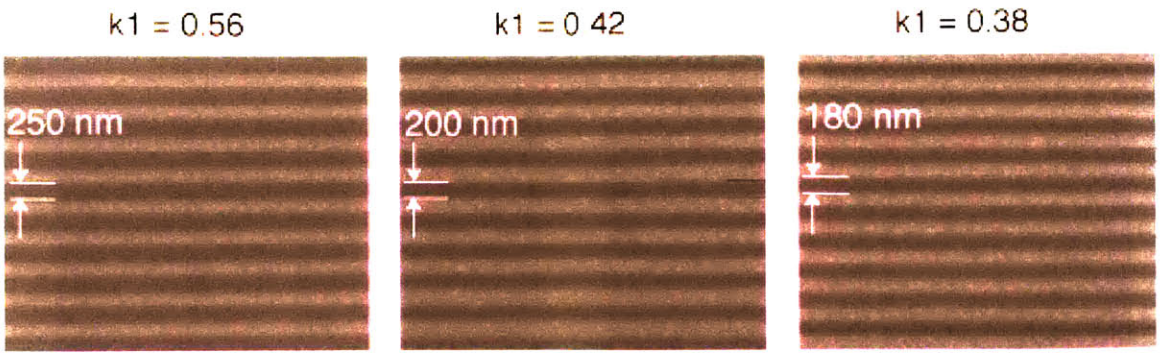

Figure 5 - 16. Exploring the limits of k1 with ZPAL. High numerical aperture zone plates (0.85 and 0.9) can operate at low k_1 factors (even below 0.4). Sub-70 nm patterning should be possible, by operating at the demonstrated k1=0.38, with 0.9NA zone plates and λ = 157nm.

As can be seen in Figures 5-15 and 5-16, the resolution that has been achieved with zone plates operating at λ=400nm is nothing short of remarkable. Optical lithography systems used in the semiconductor industry are able only to operate at k_1 factors in the 0.3-0.4 range through extraordinarily complex procedures that require phase-shift masks, angular illumination, and optical proximity correction (OPC) in the masks. The implementation of these techniques requires teams of scientist and engineers that optimize patterns, one a time, for each individual tool. The process is very sophisticated, and very costly. Being able to achieve with ZPAL, in a laboratory setup, sub-200nm resolution with λ=400nm, provides an exciting indication that with the demonstrated k_1 factor of 0.38, 0.9 NA zone plates, and a λ = 157nm source, sub-70nm dense patterning will be possible. For semi-dense features, the sub-50nm regime will be accessible.

The results included in Figures 5-17 through 5-22 provide a sample of the very-high-quality patterning that can be achieved with ZPAL. The figures include scanning-electron micrographs of lithographic test structures (Figure 5-17), optical devices (Figure 5-18 and Figure 5-19), as well as devices for a number of other applications, ranging from MEMS, to diffractive optics, to magnetic memory (Figure 5-20). Also included are the first field-stitching experiments, which resulted in the creation of large set of 4.5mm-long lines through the combination of 45 zone-plate fields (Figure 5-22).

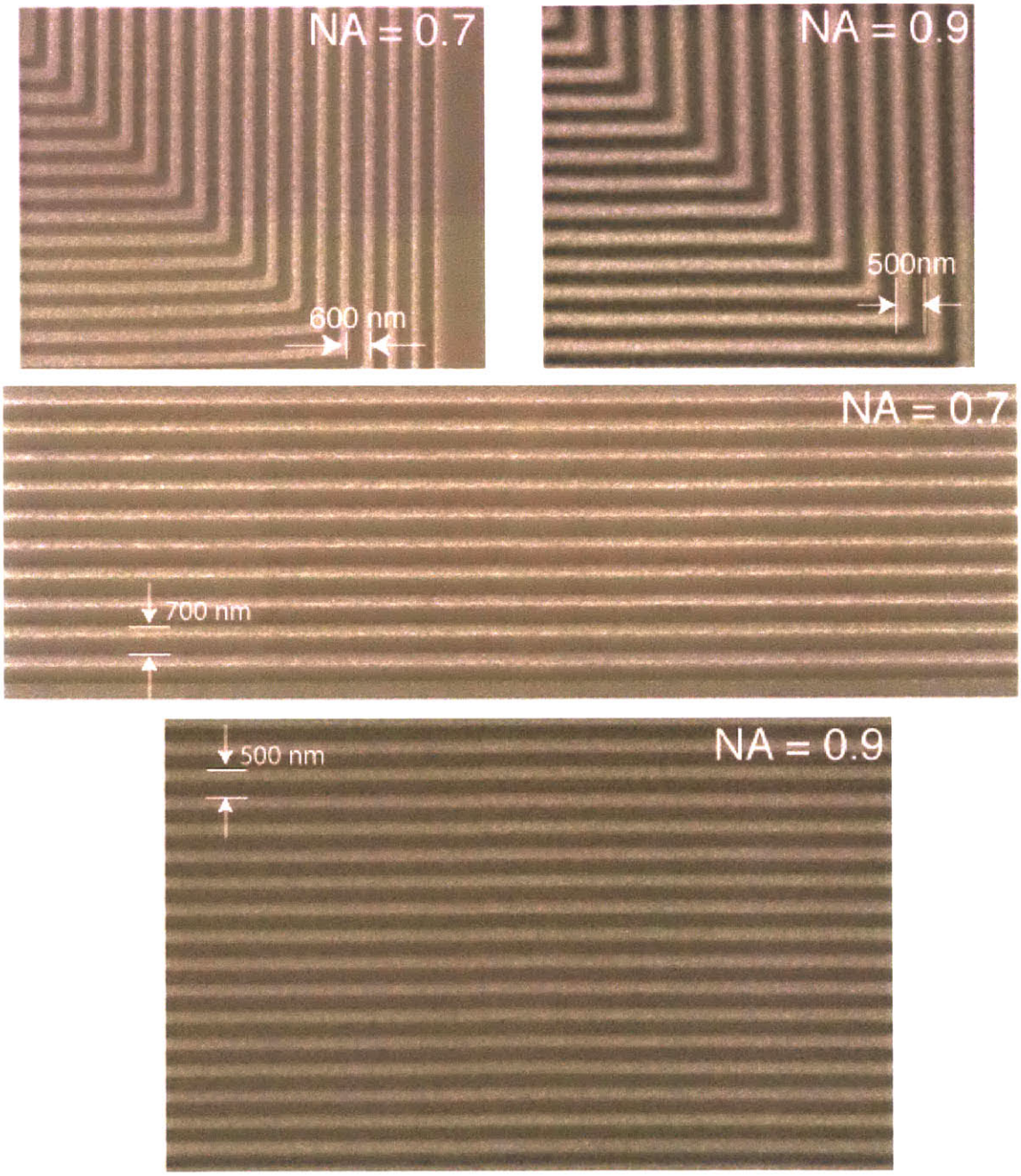

Figure 5 - 17. Scanning-electron micrographs of ZPAL patterned lithographic test structures. Top: Nested L's structures created with 0.7 and 0.9 numerical aperture zone plates. Bottom two: Dense 1:1 gratings pattern written with 0.7 and 0.9 NA zone plates.

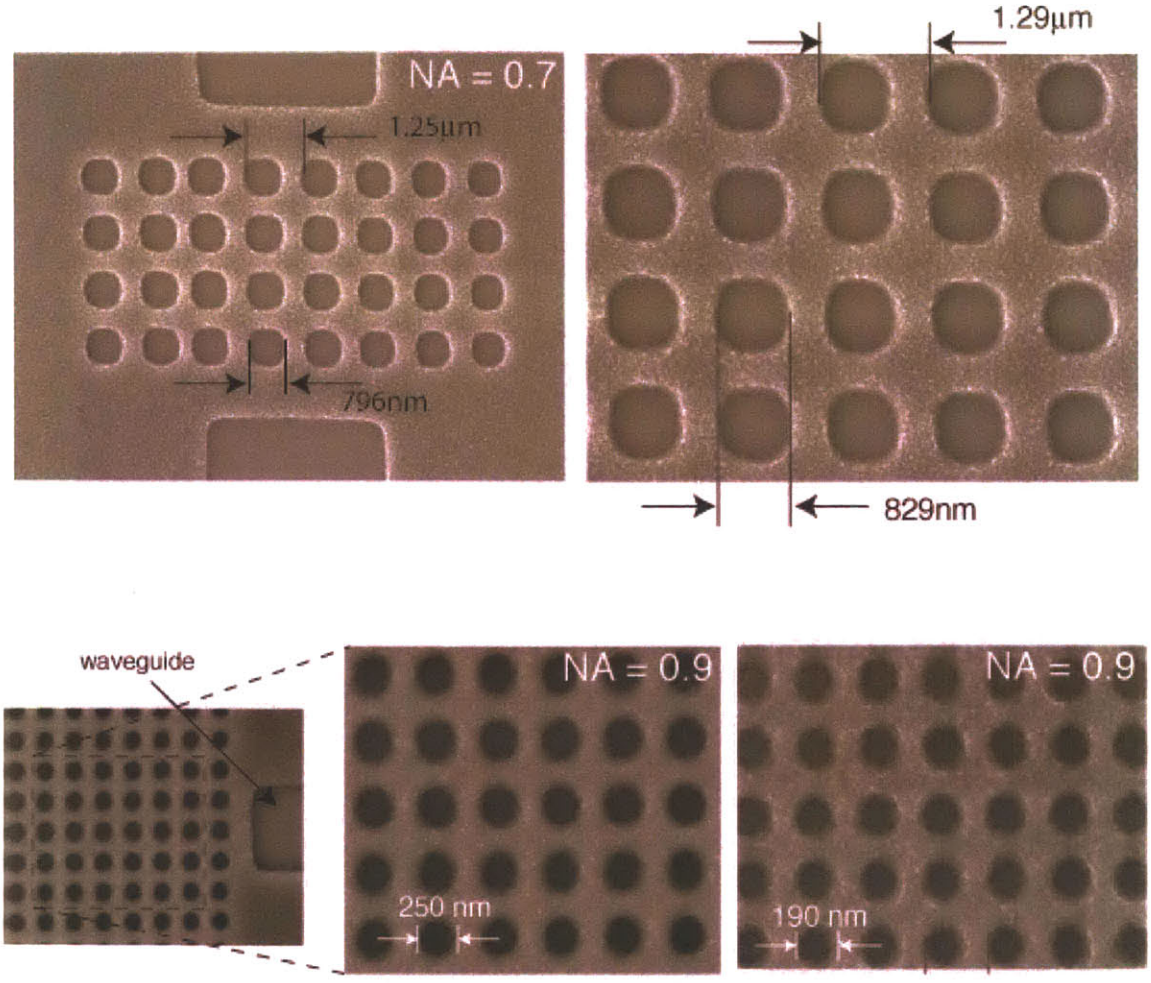

Figure 5 - 18. Scanning-electron micrographs of patterns exposed with the continuous-scan UV-ZPAL system. Top: 2D photonic bandgap structures with 1.29µm period, Bottom: 2D photonic bandgap structures with 500 nm period, and also with 400nm period.

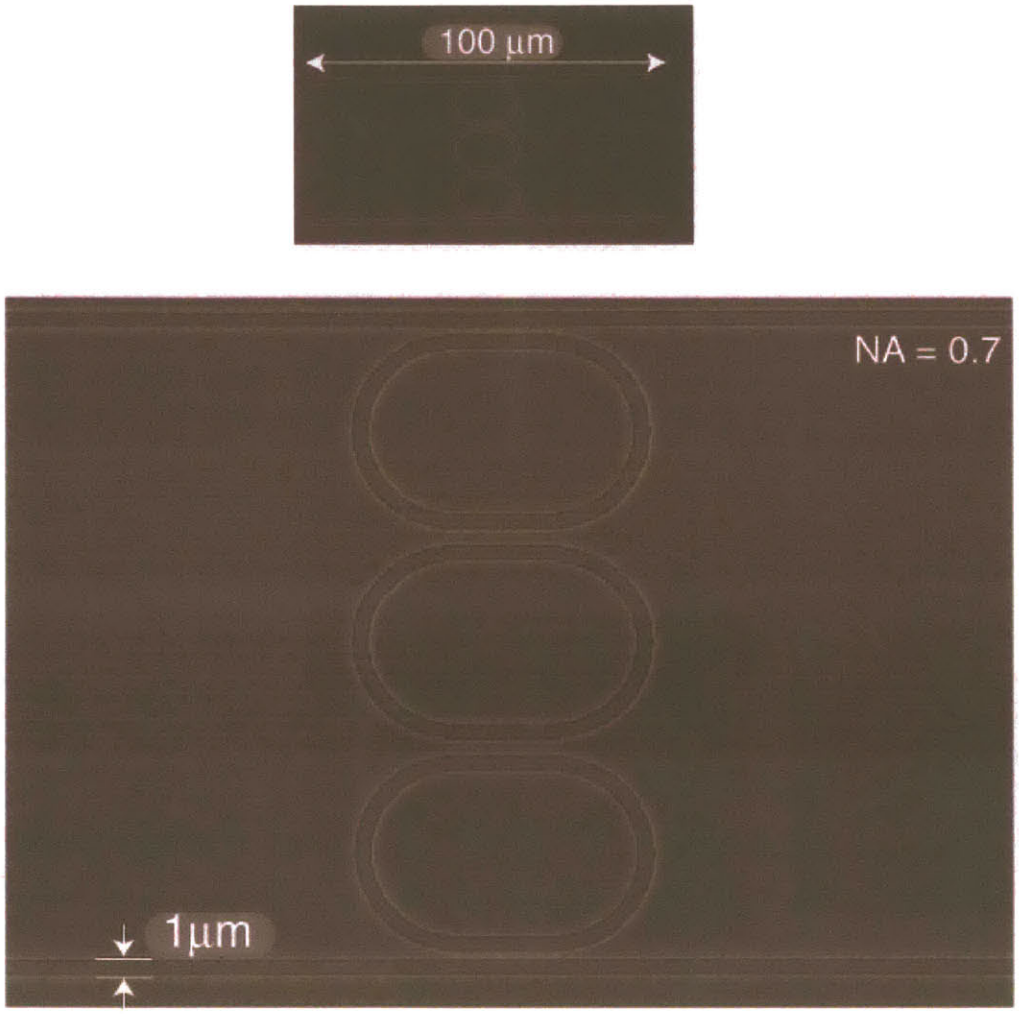

Figure 5 - 19. Scanning electron micrograph of a three-ring optical resonator pattern exposed with the continuous-scan UV-ZPAL system, showcasing ZPAL's ability to expose non-Manhattan geometries.

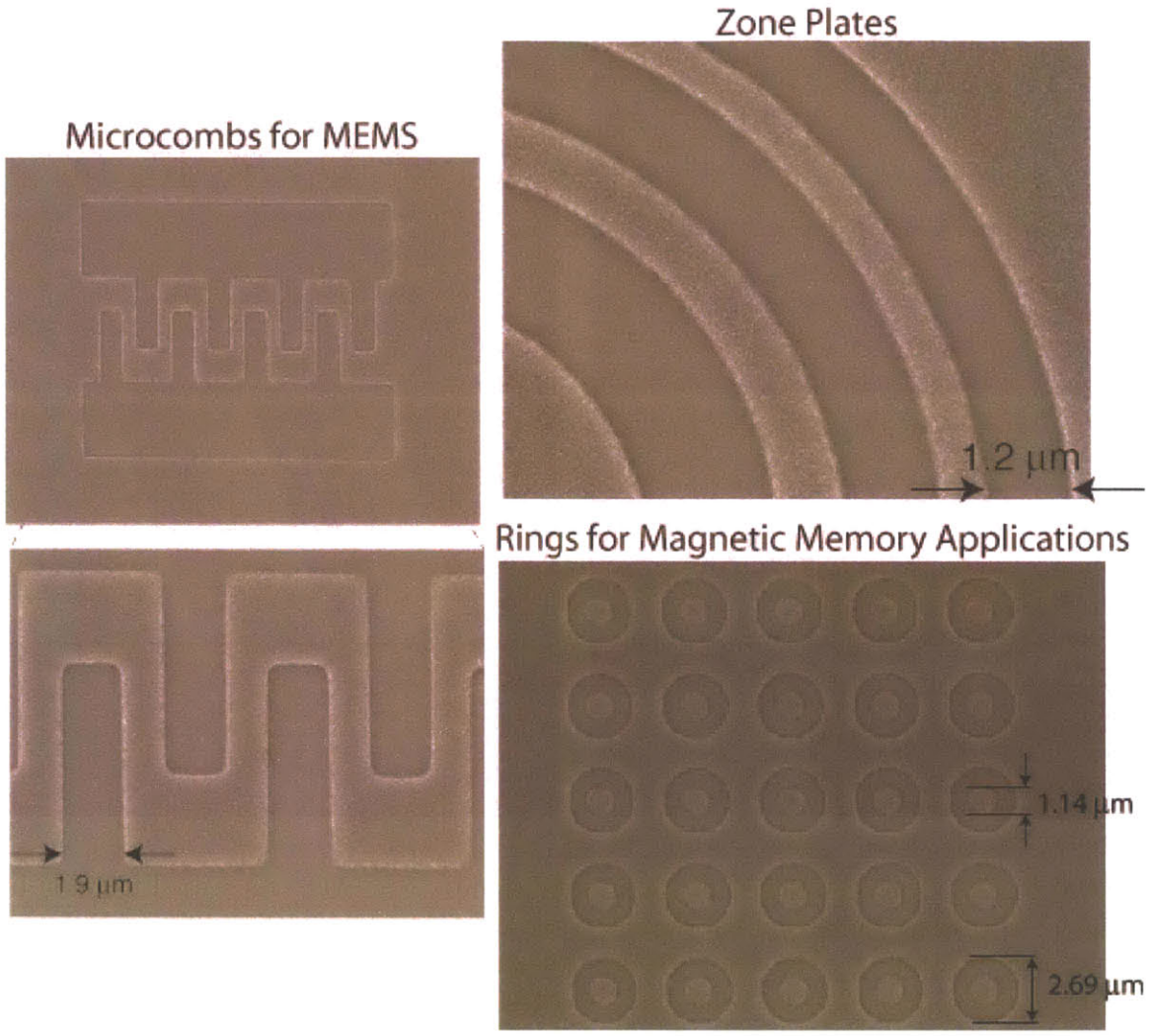

Figure 5 - 20. ZPAL is a versatile technique that can satisfy the lithography needs for a wide variety of applications, from MEMS, to diffractive optics, to magnetic memories. Left: Microcomb structure for MEMS. Top-Right: Portion of a zone plate. Bottom-right: Rings for magnetic memory applications.

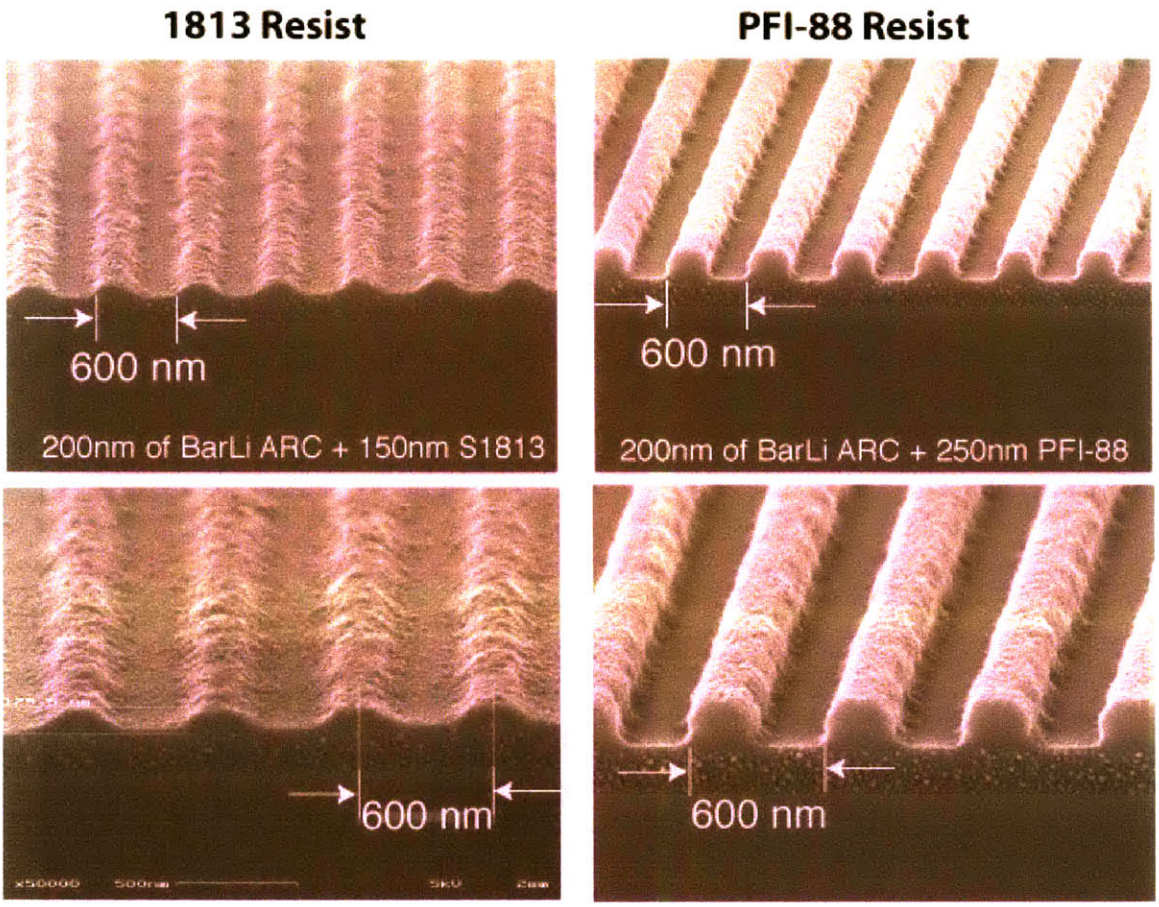

Figure 5 - 21. The importance of resist optimization in ZPAL. As was illustrated in Figure 1-9, advancements in resist chemistry are key for high-resolution lithography, and ZPAL is no exception. The same system exposing the same pattern can lead to vastly different results depending on what resist is utilized. Four scanning-electron micrographs of a 600nm-period grating exposed with NA=0.7 ZPAL (λ=400nm) are shown in the figure. It is clear that PFI-88 resist yields much better results than the low-resolution 1813 series from Shipley.

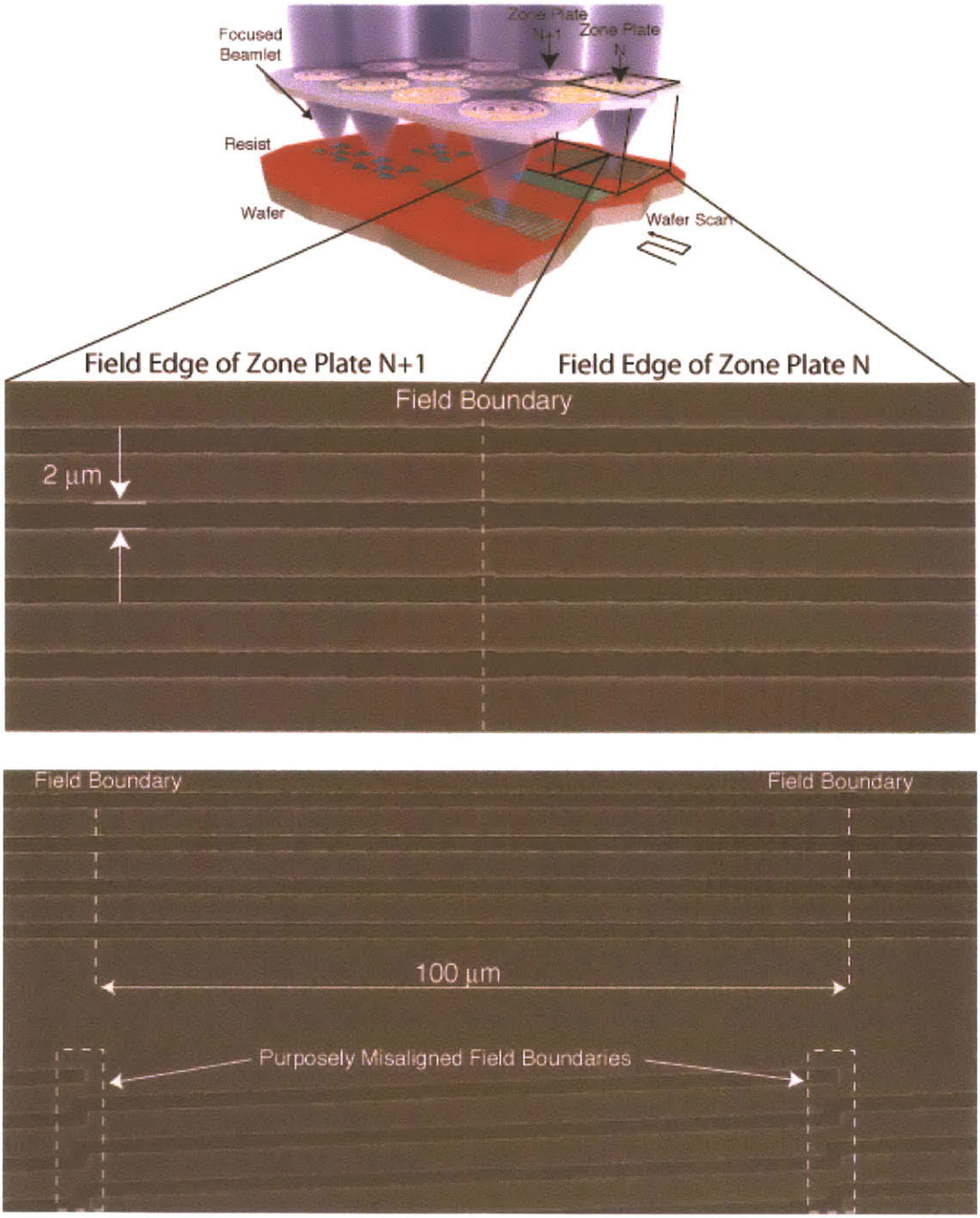

Figure 5 - 22. Stitching field boundaries in ZPAL. Top: Schematic of the ZPAL system without the micromechanics. Large-area patterns are created by stitching adjacent fields, with a field defined as the square area located underneath any given zone plate (a field, depicted with black lines, is shown in the figure). Each zone plate is "responsible" for patterning the field that lies directly underneath it, and stitching at the edges of the fields allows features to be connected with patterns written in adjacent fields. Bottom: Experimental demonstration of field stitching, which resulted in the creation of large set of 4.5mm-long lines through the combination of 45 zone-plate fields (each field was 100μm in size).

5.3 Specifications for a High-Throughput ZPAL System

For a ZPAL system operating with CW radiation, the only input parameters needed to analyze the throughput of the system are:

- λ, the wavelength of the radiation used
- Spot Size: the minimum feature size that the system will be able to resolve.
- f_m, the operating frequency of the micromechanics.
- The number of grayscaling levels.
- V_{stage}, the stage velocity
- #ZPs, the maximum number of zone plates that can be manufactured with nearly identical characteristics.

The time needed for any given zone plate to expose one pixel is set primarily either by the response time of the micromechanics (if using a CW laser with sufficient power), or by the repetition rate of the laser (in case a pulse source is used). To a smaller extent, the stage velocity also determines the time needed to expose a pixel, since it takes some finite amount of time to travel from one pixel to the next. However, since in ZPAL the distance traveled from pixel to pixel can be as short as 50 nanometers, and given that stages today can travel at speeds in excess of hundreds of mm/s, the contribution of the stage response to the time needed to expose a pixel is negligible compared to the micromechanics addressing time. Given this approximation, it is easy to prove that the number of wafers per hour that can be exposed with ZPAL is determined by the following expression:

$$Wafers/Hour = 3600 \cdot \left(\frac{f_{Micromirrors}}{\#GrayScalingLevels} \right) \cdot \frac{(SpotSize^2) \cdot (\#ofZonePlates)}{WaferDiameter^2} \qquad \textbf{5 - 18}$$

By inspecting equation 5-18 it is easy to get a feeling of how the different parameters affect ZPAL's throughput. The frequency of the micromechanics and the number of zone plates both exhibit a linear behavior. Doubling them doubles the throughput, and so on. The number of grayscaling levels is inversely related to throughput. The remaining two parameters, the spot size and the wafer diameter, provide a quadratic response. Decreasing the minimum feature size by a factor of 2 decreases the throughput by a factor of 4.

As described earlier, in order to achieve appropriate linewidth control and edge placement, sub-pixel stepping is often required in addition to grayscaling. A pixel dimension of one half the spot size, in combination with 5-bits of grayscaling ensures dimensional control that is much finer than the pixel dimension. If sub-spot stepping is employed, the throughput will be reduced by a factor of 4 from the numbers that can be obtained from equation 5-18.

Case 1: Continuous Wavelength (CW) Source

If a CW source is employed, provided it has sufficient power, the limiting factor in terms of throughput will be the speed at which the micromechanical elements can be switched ON/OFF (the limitation might lie in the data delivery or in the mechanical response time of the individual MEMS device). In order to get a throughput number for a ZPAL system operating with a CW source, let's assume the following parameters:

- Wafer Size = 300mm
- MEMS array size = 1024 x 1024
- Zone Plate array size = 1024 x 1024
- MEMS have built-in grayscaling
- NA = 0.85
- Focal length of Zone Plates = 25 μm
- Sub-spot stepping = 1/2 minimum resolution of system
- λ = 257nm

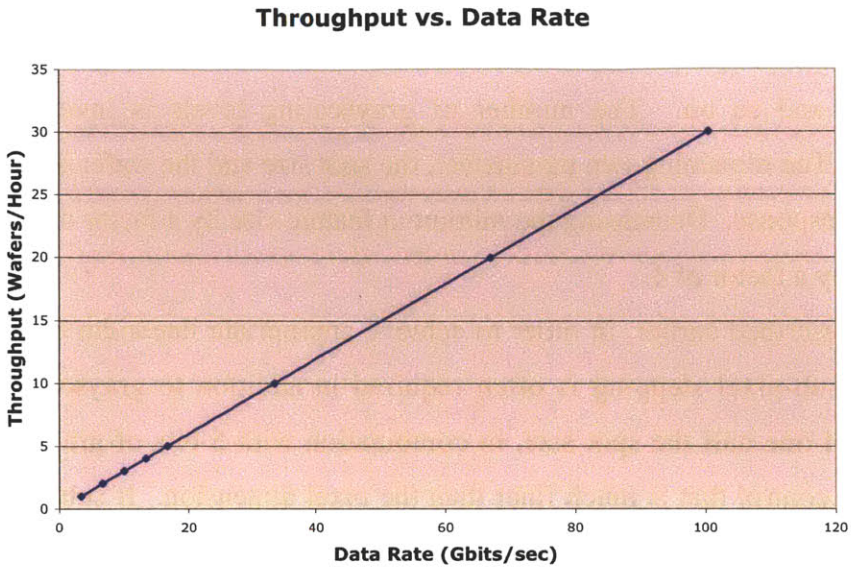

Figure 5 - 23. Throughput for ZPAL operating at λ=257nm (CW) vs. data rate, with sub-150nm resolution

Under these assumptions, Figure 5-23 provides a plot of the number of 300mm wafers that could be exposed per hour as a function of the achievable data rate.

Case 2: Pulsed Source

If a pulsed source is employed (as will be required for λ=193nm and λ=157nm), the ZPAL system will be chiefly limited by the repetition rate of the laser. In order to get a throughput number for a ZPAL system operating with a pulsed source, let's assume the following parameters:

- Wafer Size = 300mm
- MEMS array size = 1024 x 1024
- Zone Plate array size = 1024 x 1024
- MEMS have built-in grayscaling
- NA = 0.85
- Focal length of Zone Plates = 25 μm
- Sub-spot stepping = 1/2 minimum resolution of system
- λ = 157nm

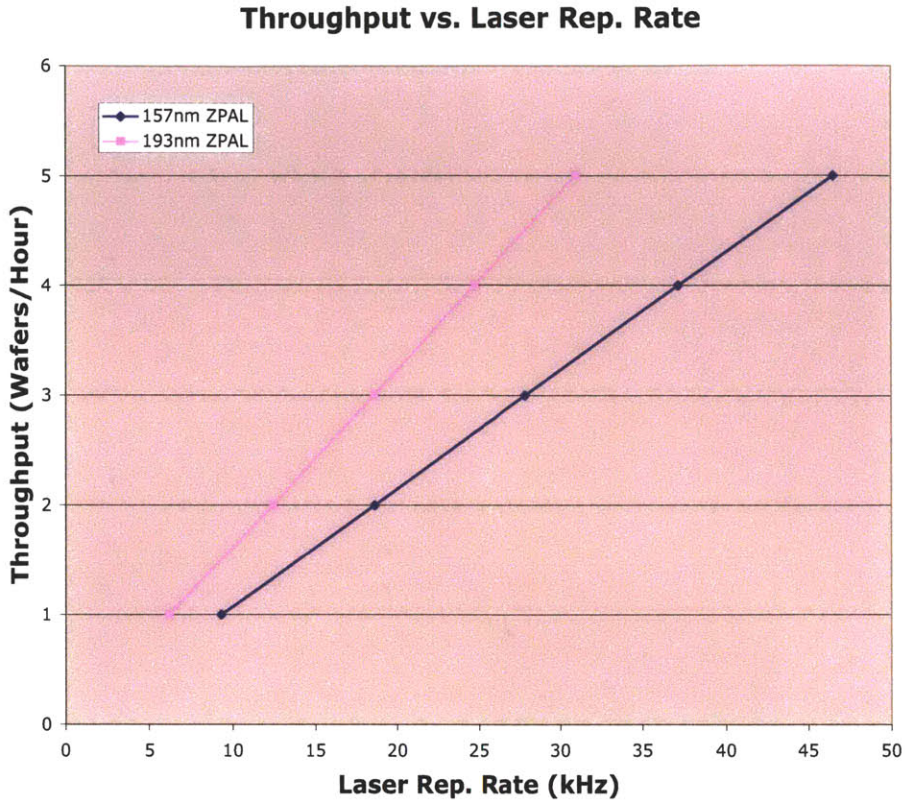

Figure 5 - 24. Throughput for ZPAL operating at λ=193nm and λ=157nm (pulsed) vs. laser repetition rate. At λ = 157nm, the system will be capable of sub-90nm resolution (and as small as 60nm, depending on pattern)

Under these assumptions, Figure 5-24 provides a plot of the number of 300mm wafers that could be exposed per hour as a function of the repetition rate of the laser.

In order to compensate for pulse-to-pulse variations (something common in many pulsed lasers) a double-pass strategy might be required. The consequence of such averaging will be a throughput reduction of one half from that presented in Fig.5-24.

Finally, for the numbers presented in this analysis, the assumption was made that all the exposed features are written at the maximum resolution of the system. Were this not to be the case for certain applications (e.g. writing non-critical layers), the required pixel size could be significantly larger, and the throughput will increase quadratically as a result.

As a conclusion, we can see that with current technology, ZPAL will be limited to throughputs that are, at best, a few 300mm wafers per hour.

Chapter 6

Conclusions and Future Work

Given the current industry interest in maskless lithography, it is crucial that the community investigates all the proposed maskless alternatives with an open mind. The work presented in this thesis has hopefully proven the efficacy and the advantages of diffractive-optical elements in general, and zone plates in particular, for maskless lithography applications. We have proven that (1) high-NA zone plates work, (2) the contrast in ZPAL is adequate for large-area patterning, and (3) large arrays can be manufactured with close to ideal performance. With k_1 factors that can be pushed into the 0.3-0.4 regime and numerical apertures of 0.9 (and possibly even higher), 157nm lasers will potentially allow ZPAL to reach the 50nm node. Beyond that, zone plates will still be able to function if a source is provided, be it 121nm, EUV or x-rays. It should hence be possible for ZPAL to reach the limits of the lithographic process.

6.1 Beyond Zone Plates?

The promise of diffractive optics for maskless lithography applications can, and must, extend beyond the capabilities offered by traditional binary phase zone plates. Optimizing zone plate designs (e.g. apodizing the zones, blazing, etc) can yield diffractive optical elements whose focusing characteristics are particularly suited for certain lithography applications. One could envisage diffractive arrays designed for the lithographic patterning of curved-surfaces (e.g. by having zone plates designed to form spots at different focal lengths such that the curvature of the substrate to be exposed is appropriately matched). Or one could go a step further and envision a totally new form for focusing light.

In an exciting development, a new kind of diffractive-optical focusing element has been indeed proposed recently by Kipp et al.[Ref 6-1]. The new optic has been called a *photon sieve*. In its conception it is related to the familiar amplitude Fresnel zone plate. The photon sieve consists of a large number of pinholes distributed appropriately over the zones of a Fresnel zone pattern (see Figure 6-1). For a given minimum resolution in the fabrication, it achieves a sharper focus than the corresponding amplitude Fresnel zone plate, and, in addition, higher orders of diffraction and secondary maxima are suppressed by several orders-of-magnitude (i.e., they are substantially eliminated) as shown in Figs. 6-1(c-d). In the photon sieve, the distribution of pinholes (and hence the *utilization* of the incident radiation) is adjusted in such a way that the sidelobes or secondary maxima are suppressed (i.e. a form of apodization). Through this apodization, the strength of the *utilization* is varied as a function of radial distance so as to follow approximately the functional form of a Gaussian distribution. As a result, the secondary maxima or sidelobes of the focal spot are reduced or substantially eliminated.

The photon sieve as described by Kipp et al. is less efficient in focusing incident radiation into a first-order focus than an amplitude Fresnel zone plate. However, because of its ability to suppress third and higher-order foci, as well as sidelobes, it is an attractive alternative to conventional Fresnel zone plates for the diffractive focusing elements in those situations where efficiency of focusing is not an important consideration but sidelobe suppression is. Accordingly, given the concern commonly expressed regarding the inevitable presence of multiple diffracted orders in zone plates, one could conceive

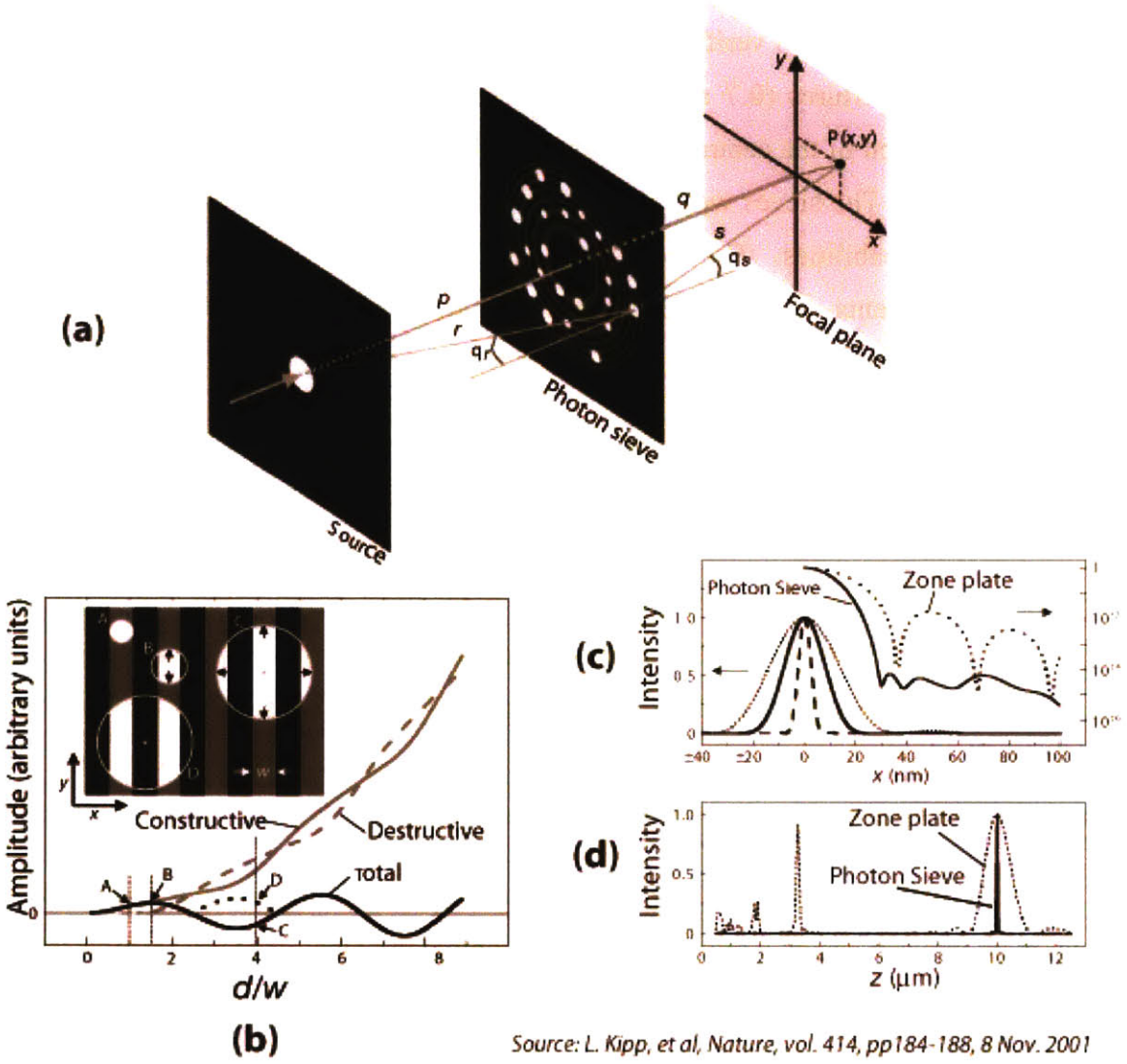

Source: L. Kipp, et al, Nature, vol. 414, pp184-188, 8 Nov. 2001

Figure 6 - 1. The photon sieve. (a) Diagram showing point-to-point imaging through appropriately positioned pinholes. (b) Examples of photon sieve pinholes together with the underlying zone-plate geometry and the contributions of a single pinhole to the focal amplitude. Constructive and destructive interference contributions from `white' and `black' areas inside the pinhole are plotted as solid and dashed grey curves, respectively. The total amplitude at the focus from a single pinhole of diameter d centered on a transmissive zone (A, B, C) of width w is given by the solid black curve; the total contribution to the amplitude at the focus from a pinhole centered on an opaque zone (D) is given by the dotted black curve. (c-d) Comparison of calculated intensity distributions of photon sieves and zone plates. Note that sidelobes are suppressed compared to those present in zone plates, and that a single focus is obtained (i.e. no other orders are present).

utilizing an array of photon sieves in substitution for the array of Fresnel zone plates in a maskless lithography system.

With the purpose of verifying the viability of the idea, a set of photon-sieves with high-numerical apertures (0.7 and 0.8) were designed and fabricated. A scanning-electron micrograph of the central pinholes of the 0.7 numerical-aperture sieve is shown in Figure 6-2(a). The sieves were incorporated into the ZPAL system in order to test their focusing capabilities. The results presented in Figure 6-2(b-d) are the very first focusing experiments ever reported with sieves at the UV[1] (and at high numerical apertures!), as well as the first ever use of sieves for lithography.

The results are very interesting. As expected, a reduction factor was achieved with respect to the minimum-feature-size present on the sieve. Recall that for the case of a zone plate, the size of the focused spot is roughly determined by the minimum feature size of the zone plate (i.e. the width of the outer-most zone). For the sieve, an appropriate design can result in the creation of a focused spot that is 1/2 the size of the minimum pinhole diameter, as illustrated in Figure 6-2(b). This capability relaxes the fabrication requirements of the diffractive elements, something that can be very beneficial as we progress towards the sub-100nm regime.

As a final note regarding these novel optical elements, although not described by Kipp, et al, one can design a photon sieve based on the principal of phase shifting rather than amplitude modulation. This offers the promise of higher efficiencies while maintaining all of the virtues of the photon sieve: (1) low sidelobes, (2) single diffracted order, (3) minimum feature in the photon sieve is a multiple of the focused spot full-width-at-half maximum (FWHM). This would provide an exciting future research direction with high-potential payoffs. The possibility of creating a diffractive optical element that can be fabricated with a planar process, operate with high-efficiency, while achieving a single diffraction-limited focus (with even some demagnification!) is a promise that is certainly worth pursuing.

---

[1] The only reported experimental results with photon sieves (by Kippp et al) were performed at x-ray wavelengths, with microscopy applications in mind.

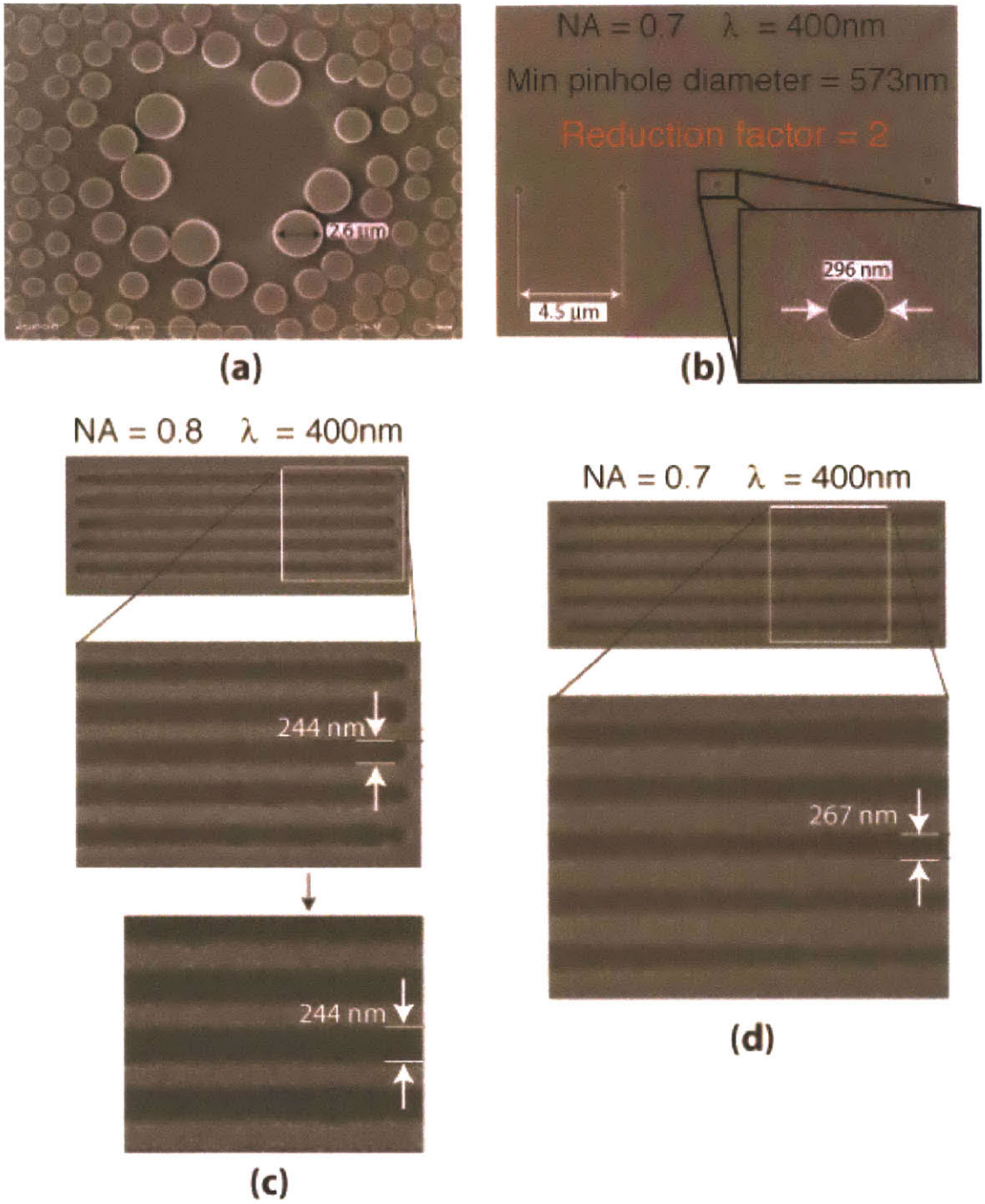

Figure 6 - 2. First ever focusing results with photon-sieves at the UV. (a) Central pinholes of a 0.7 NA sieve with a focal length of 40µm, designed to operate at λ=400nm. (b) A photon sieve can create a focused spot that is a fraction of the minimum feature size of the sieve. For the results presented, a sieve with a minimum pinhole diameter of 573nm was able to create a 296nm spot, a reduction of a factor of 2. (c-d) Scanning electron micrographs of the first lithography results ever produced with photon sieves. Numerical apertures as high as 0.8 were achieved.

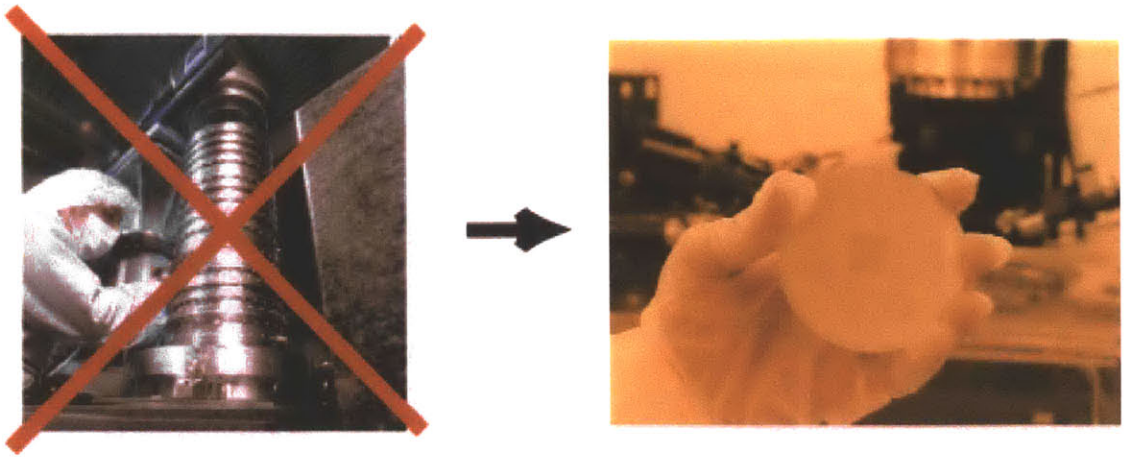

Figure 6 - 3. Vision of the power of employing diffractive optics for lithography. Diffractive optics are manufactured using nanofabrication, with techniques similar to those used in chip production

6.2 The Dream of Total Integration

In this final section I would like to end with the dream of a maskless lithography system that would function without *any* macroscopic optical elements. In Chapter 2, an image (reproduced in Figure 6-3) illustrating the power of diffractive optics was introduced. The symbolism of this image is very powerful. It represents a new path for optical lithography, a path based on reducing the complexity and cost of systems by taking advantage of the blossoming of our nanofabrication capabilities.

I would like to propose going one step further. ZPAL, in its current implementation, although simpler than other maskless lithography architectures, still requires a relatively large number of conventional refractive optical elements. After all, light from the laser has to be collimated, then shaped appropriately to illuminate the multiplexing device, and then mapped (by more optics) onto the array of diffractive elements. When all is said and done, the ZPAL setup in our laboratory ends up looking as is shown in Figure 6-4. It is still too complicated.

A further step towards total integration, where no macroscopic optical components would be required for the entire optical train, can be envisioned with the recent appearance of diode lasers, and VCSELs (Vertical Cavity Surface Emitting Lasers) capable of operation at UV wavelengths. It is satisfying to see that the existing and mature semiconductor laser technology for the near-infrared and red is finally extending to encompass the blue and near-ultraviolet regions.

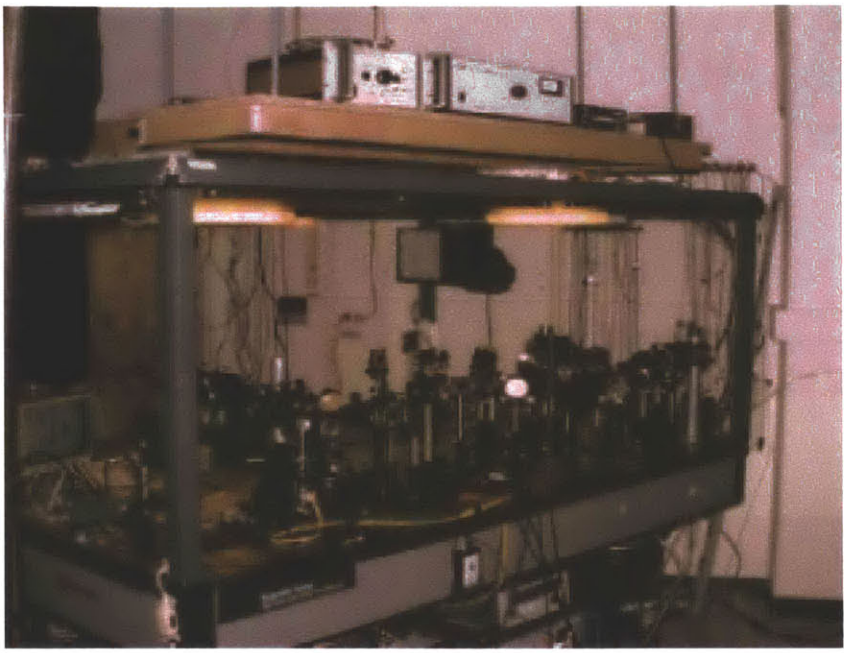

Figure 6 - 4. Experimental implementation of ZPAL at M.I.T.'s NanoStructures Laboratory.

These new lasing elements, given their planar fabricated process, can be created into arrays [Ref 6-3], and are capable of dose modulation, high-power, and extremely fast switching rates. In combination with an array of diffractive elements, a multi-optical-column writing technique would result in a high-resolution, high-throughput maskless patterning system. The vision is illustrated in Figure 6-5. The author is hopeful that this vision will become a reality in the not too distant future.

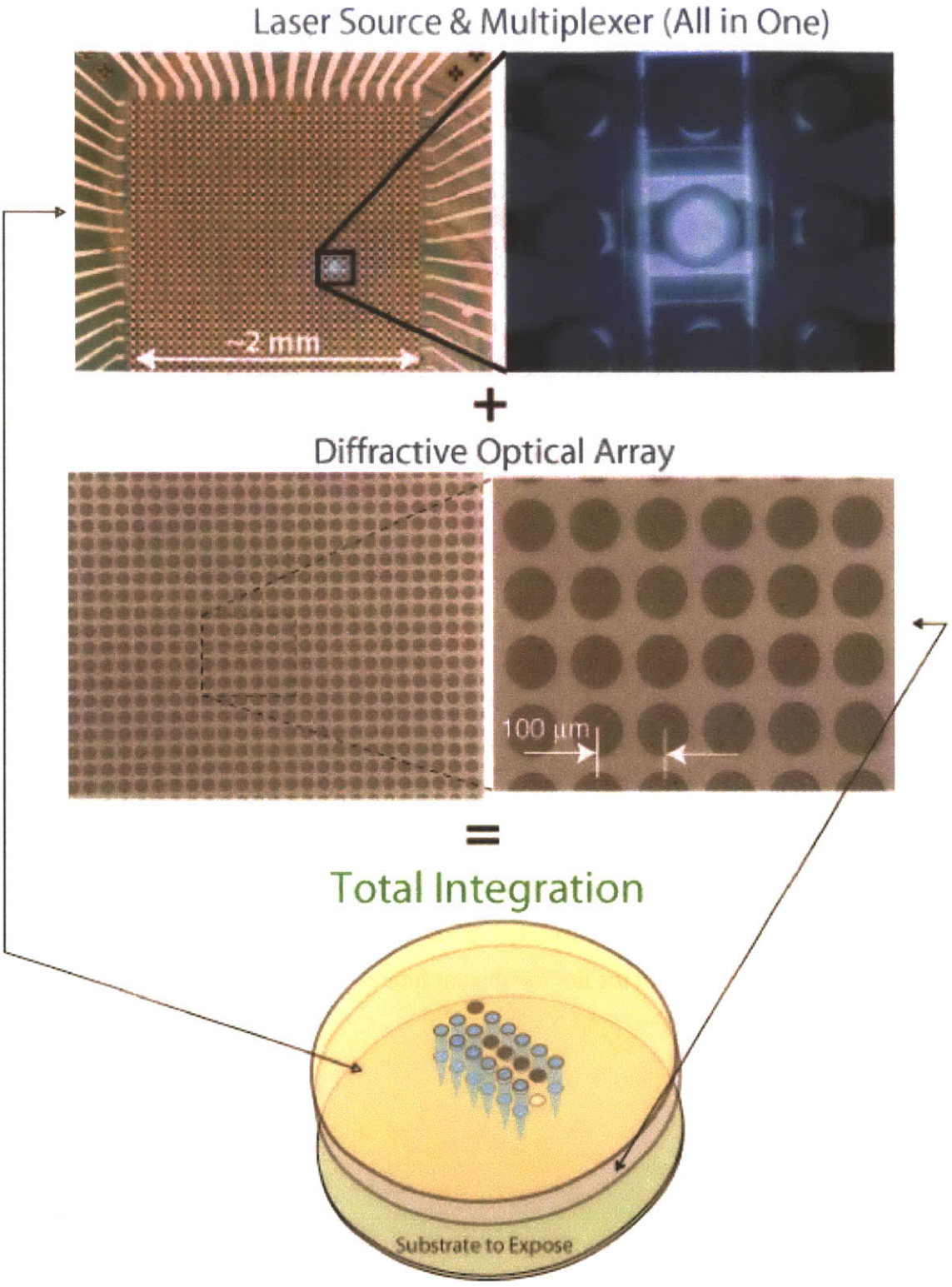

Figure 6 - 5. The vision of total optical integration for maskless lithography by combining arrays of laser diodes with diffractive optical arrays. Top-Left : Optical micrograph of at blue emitting 32x32 LED array. Top-right: Close-up view of a single LED element. Source: Ozden et al [Ref 6-3].

Appendix A

Zone Plate Processing

This appendix describes the processing necessary to fabricate zone plates by means of scanning-electron-beam lithography and x-ray lithography.

A.1 Fabrication by means of Scanning-Electron-Beam Lithography

Chronological sequence of steps required:

1- **Design zone plates** as described in Chapter 3. Obtain values for:
   a. λ, the wavelength at which the zone plates are intended to operate.
   b. The focal length (in microns)
   c. The Numerical Aperture of the zone plates (or alternatively, the radius in microns)

2- **Generate pattern files** that can be read by the electron-beam-lithography system. A custom-software program[1] was written in MATLAB to generate the zone plate files required for patterning with the RAITH-150 and the VS-26 scanning-electron-beam-lithography systems available at MIT's NanoStructures Laboratory. Screen captures of the interface of the RAITH-150 version of the program, as well as the VS-26 version, are respectively included in Figure A-1 and Figure A-2.

3- **Prepare zone plate substrate**. The substrate obviously has to be transmissive for the operating wavelength of the zone plates. All the zone plates of this thesis were fabricated on double-side-polished fused-silica substrates.

   a. Spin resist. For the Self-Aligned HSQ process, knowing the index of refraction of HSQ (at the intended wavelength of operation of the zone plates) determines the thickness of this layer (for a π-phase shift, the thickness required, t, is determined by $t = \frac{\lambda}{2} \cdot \frac{1}{n_r - 1}$, where n_r is the real part of the index of refraction, and λ is the wavelength of light). A plot of the index of refraction versus wavelength is included in Figure 3-31 (pg 101).

   b. Bake the resist. Two bakes are required for HSQ:

      i. Bake 1: 150^0C for 2min (on a hot-plate)

      ii. Bake 2: 220^0C for 2min (on a hot-plate)

   c. Evaporate 5nm of Aluminum. This step is required to prevent charging effects during the electron-beam lithography exposure, since the substrate (fused silica) is non-conductive.

4- **E-beam exposure.** Load substrate. Create exposure layout by importing the generated pattern files from Step-2 into either the RAITH or the VS-26. The RAITH Code version of the software generates files with the extension **.asc** ,

[1] The program can be found on the nano server, under the following directory: **/nano/nsl/dgil/ZonePlateSoftware/**. The directory contains two folders, called **VS-26 Code** and **RAITH Code**. Within each of these directories the main programs running all other sub-programs are called **ZPmainGUI_VS26.m** and **ZPmainGUI_RAITH.m** respectively.

which can be readily imported via the RAITH-layout software. The VS-26 version of the software generates files with the extension **.pat**

a. If using the RAITH-150

i. **Create an exposure layout** and transfer it into the position list.

ii. **Select acceleration voltage** (30keV will work best for thick HSQ layers)

iii. **Select the exposure dose**. Note that the zone-plate files are composed of a large number of single-pixel lines (see section 3.2.2.1). Therefore, it is important to select the exposure dose for single-pixel lines (i.e. line dose) as oppose to area dose. For 475nm-thick HSQ layers (the thickness required for a π-phase shift at λ=400nm), the optimum line dose should be ~ 225 pC/cm.

iv. **Calibrate desired field size**. This requires setting values for the magnification and the field size. It is **very important** that the chosen magnification results in a ***magnification range* of 2** (this can be checked in the LEO-SEM software under *View/SEM Status*. A *magnification range* of 1 operates the deflection amplifiers under a very noisy gain setting (there are three settings available), with the consequence that the patterns will be extremely rough[2]. The *magnification range* is a function of the acceleration voltage and the working distance. For relatively large field sizes (e.g. 150μm and above) this dependence might require operating at larger working distances in order to obtain the desired *magnification range* of 2. As an example, for 185μm field sizes, at 30keV, the working distance had to be increased to 10.2mm to get the desired *magnification range.*

v. **Expose the zone plates**. Writing times vary depending on zone plate design. As an example, a NA=0.7, f=40μm, λ=400

[2] The author learned this problem the hard way, resulting in months of wasted time.

zone plate, writing with a 225 pC/cm dose, takes ~2m15sec/zone plate. For long-writes, use the automatic-beam-current measurement to achieve good dose stability throughout the exposure.

vi. **Develop patterns**.

1. **For HSQ exposures**. Develop in any TMAH-based developer. The author always used Microposit MF CD-26. Development time is a very insensitive parameter for HSQ (and very slow!). The author obtained great results with a development time of 1h for thick layers of HSQ. It is **important** to always develop HSQ in a **single development step**.
2. **For PMMA** exposures. Mix the developer (1:2 MIBK:IPA) in a beaker big enough to fit the wafer. The temperature should drop to 16°C upon mixing. The developing temperature is 21°C. To get to this temperature warm beaker with hands while monitoring the temperature. Have the beaker covered to prevent the evaporation of MIBK. Develop for 90 sec. Rinse for 60 sec with IPA + 60 sec H_2O. If the substrate has been coated with a thin metal film to prevent charging, it must be removed with the appropriate metal etchant prior to development.

b. **If using VS-26**

i. **Convert and transfer files into VS-26**. Login to the nano server via **trajan.mit.edu** and access the following directory: ~/dgil/ZonePlateSoftware. The directory contains a C program called pat2vsx.c, written to convert **.pat** files into **.vsx** files (this is a format that the VS-26 can read). Copy this program into your directory in the nano server and compile the program (by typing **cc -o pat2vsx pat2vsx.c**). Place the previously

generated zone-plate files into the directory containing the **pat2vsx** program, and convert to **.vsx** via the following command:

>./pat2vsx *filename*.pat **filename.vsx**

The files can then be transferred to the VS-26. Make sure that if you use ftp to transfer the files, the transfer is done in binary format.

ii. **Load files.** It is very important that **Ihsan's** version of the code is used, since this is the only version that can handle circles.

iii. **Layout the files to be exposed.**

iv. **Expose patterns.** A good dose for PMMA is ~330μC/cm^2.

v. **Develop patterns.**

1. **For HSQ exposures**. Develop in any TMAH-based developer. The author always used Microposit MF CD-26. Development time is a very insensitive parameter for HSQ (and very slow!). The author obtained great results with a development time of 1h for thick layers of HSQ. It is **important** to always develop HSQ in a **single development step**.
2. **For PMMA** exposures. Mix the developer (1:2 MIBK:IPA) in a beaker big enough to fit the wafer. The temperature should drop to 16°C upon mixing. The developing temperature is 21°C. To get to this temperature warm beaker with hands while monitoring the temperature. Have the beaker covered to prevent the evaporation of MIBK. Develop for 90 sec. Rinse for 60 sec with IPA + 60 sec H_2O. If the substrate has been coated with a thin metal film to prevent charging, it must be removed with the appropriate metal etchant prior to development.

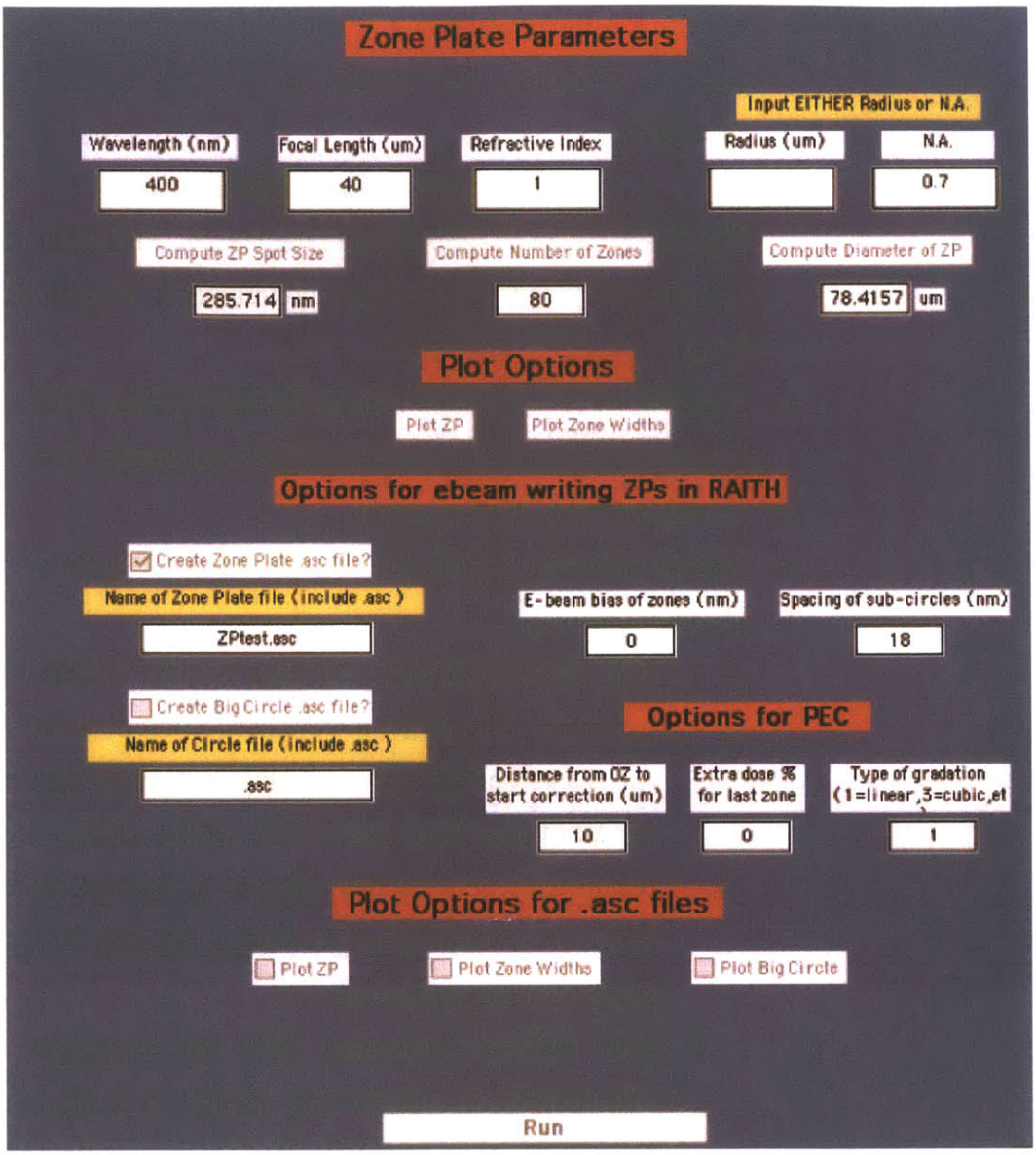

Figure A - 1. Screenshot capture of the interface of the software program capable of generating zone plates for the RAITH-150 scanning-electron-beam lithography system. Once all parameters have been chosen, the program is executed by clicking the Run button. This will generate the desired **.asc** file (in the example shown in the figure, a file called ZPtest.asc will be created). Comments: (1) the spacing of the sub-circles refers to the spacing of the single-pixel line polygons explained in section 3.2.2.1. The default of 18nm provides excellent results. (2) make sure the *Create Zone Plate .asc file?* box is checked for the file to be created. (3) E-beam bias of the zones accepts positive and negative values, (4) *Options for PEC* refers to proximity effect correction techniques for zone plates (see section 3.2.2.1). (5) If the box of *Create Big Circle .asc file?* is checked and a filename is input, a circle the size of the zone plate will be created. This pattern is necessary for both the *Silicon Process* and the *Chromium Process* (described in Chapter 3).

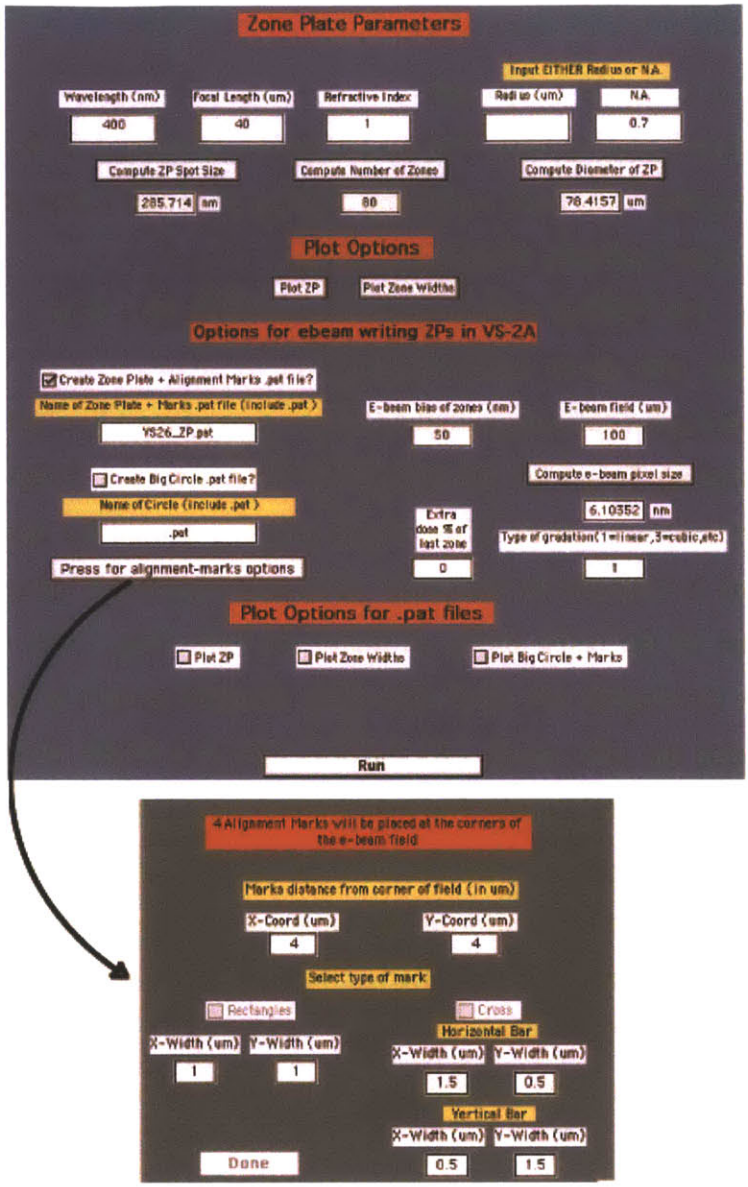

Figure A - 2. Screenshot capture of the interface of the software program capable of generating zone plates for the VS-26 scanning-electron-beam lithography system. Once all parameters have been chosen, the program is executed by clicking the Run button. This will generate the desired **.pat** file (in the example shown in the figure, a file called VS26_ZP.pat will be created). Comments: (1) Choose an e-beam filed size bigger than the zone plate diameter, (2) make sure the *Create Zone Plate… .pat file?* box is checked for the file to be created. The alignment marks (located at the four edges of the field) will only be created if the *Press for Alignment Marks Options* button is pressed and one of the two alignment-mark options (rectangles or crosses) is selected, (3) E-beam bias of the zones accepts positive and negative values, (4) *Extra dose % last zone* provides a form of proximity effect correction (see section 3.2.2.1). (4) If the box of *Create Big Circle .pat file?* is checked and a filename is input, a circle the size of the zone plate will be created. This pattern is necessary for both the *Silicon Process* and the *Chromium Process* (described in Chapter 3).

A.2 Fabrication by means X-Ray Lithography

1. Start with a clean x-ray mask
2. Evaporate plating base. For all the masks fabricated in this thesis a "thin-plating base" was used, consisting of 10nm of Ti and 1.8nm of Au.
3. Spin resist, typically PMMA (~250nm).
    a. For PMMA, bake mask in oven at 180°C for 1 hour
4. E-beam write mask, as described in A.1.
5. Flood-expose optically with the OAI the rims of mask (i.e. all areas except the membrane). In our lab this is typically referred to as a "lollipop" exposure, in reference to the shape of the fixture that can is used for this step (the metal fixture is typically by the OAI). A 30 min exposure is more than enough to expose all the resist sitting on top of the Pyrex ring. This optical exposure (once developed) will allow for a clean electrode contact in the plating step.
6. Develop the x-ray mask. Mix the developer (1:2 MIBK:IPA) in a beaker big enough to fit the mask. The temperature should drop to 16°C upon mixing. The developing temperature is 21°C. To get to this temperature warm beaker with hands while monitoring the temperature. Have the beaker covered to prevent the evaporation of MIBK. Develop for 90 sec. Rinse for 60 sec with IPA + 60 sec H_2O.
7. UV-Ozone for 30sec. Rinse in H_2O and blow dry. The mask is ready for plating.
8. Electroplate the x-ray mask. To give an idea of plating rates and parameters utilized, the plating sequence of an x-ray mask containing arrays of zone plates is included in Figure A-3. The plating is monitored by means of an atomic-force microscope (AFM).
9. Remove the resist once the desired plating height has been achieved (~200nm of Au is a good goal). For PMMA, an acetone bath for 10min will do it. Ashing is another alternative.
10. Evaporate studs (typically ~3μm tall) onto the mask.
11. The x-ray mask can now be used in an x-ray lithography system to create and/or replicate zone plate arrays.

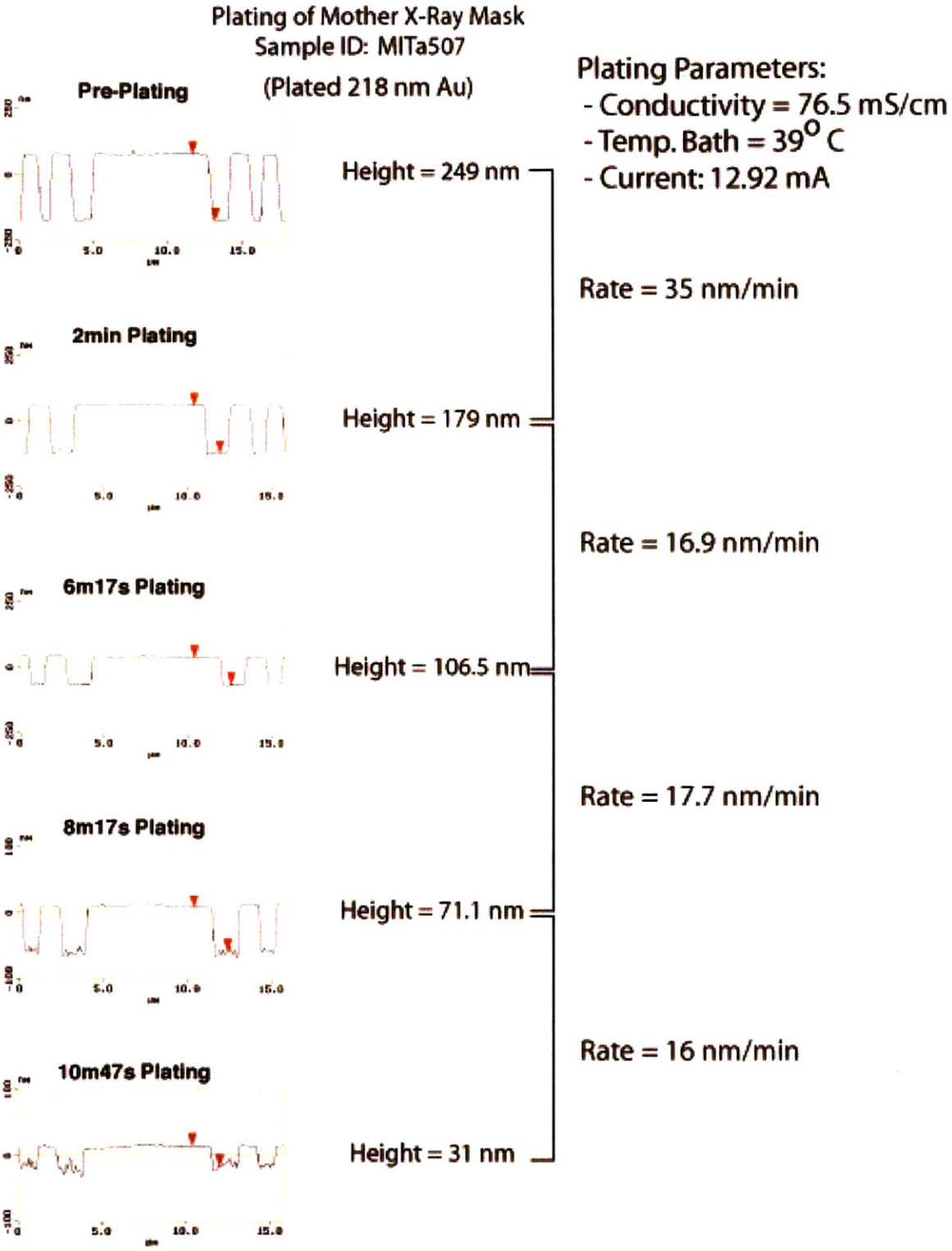

Figure A - 3. Sample gold electroplating of x-ray mask containing arrays of zone plates. The plating is monitored by means of an atomic-force microscope (AFM) throughout the process.

References

Chapter 1

[Ref 1-1] Michael Lewis, *The New New Thing,* W.W. Norton & Company; 1999.

[Ref 1-2] Clayton M. Christensen. *The Innovator's Dilemma*, Harper Business, 200

[Ref 1-3] H. C. Manoharan, C. P. Lutz, D. M. Eigler, Quantum mirages formed by coherent projection of electronic structure, Nature 403, 512 - 515 (2000)

[Ref 1-4] Bass et al, "The Future of the Microprocessor Business, *IEEE Spectrum*, April 2002].

[Ref 1-5] Alfred Kwok-Kit Wong, *Resolution Enhancement Techniques in Optical Lithography*, SPIE Press 2001

[Ref 1-6] Anton, P.S., Silberglitt, R, Schenider, J, *The Global Technology Revolution,* National Defense Research Insitute, RAND Corporation (www.rand.org)

[Ref 1-7] G.E.Moore, "Cramming More Components onto Integrated Circuits", Electr.Mag., 114 (19 April 1965)

[Ref 1-8] "DuPont to cut mask costs by dividing offering", EE Times, July 24, 2002

[Ref 1-9] Freye, Jorge, *The Impact of the Photomask on Design* -- Electronic News, 6/3/2002

[Ref 1-10] Willson, C. Grant, Dammel, Ralph A, and Reiser, Arnost, *Photoresist Materials: A Historical Perspective*, SPIE Vol.3049, pg.28-41, 1997.

[Ref 1-11] http://www.micronic.se

[Ref 1-12] http://www.amat.com

[Ref 1-13] Allen, Paul, DUV Laser Scanning for Mask Pattern Generation at the 130 and 100nm Nodes, White Papers, www.amat.com

[Ref 1-14] E.Spiller, Soft X-Ray Optics, pg. 5, SPIE, Bellingham, WA, 1994.

[Ref 1-15] J.Bjorkholm, "EUV Lithography-The Successor to Optical Lithography?", Intel Technology Journal Q3, 1998.]

[Ref 1-16] E.Spiller, Soft X-Ray Optics, pg. 5, SPIE, Bellingham, WA, 1994.

[Ref 1-17] N.Choksi et al., "Maskless extreme ultraviolet lithography", J.Vac.Sci.Technol. B 17(6), Nov/Dec 1999

[Ref 1-18] D.A.Buck and K.R.Shoulders, Proceedings of the Eastern Joint Computer Conference, 1958],

[Ref 1-19] A.N.Broers and M.Hatzakis, Scientific American 227, 34 (1972)).

[Ref 1-20] M. McCord, "Electron beam lithography for 0.13μm manufacturing", J.Vac Sci. Technol. B 15(6), Nov/Dec 97

[Ref 1-21] T.R.Groves and R.A.Kendall, J.Vac Sci. Technol. B 16(6), Nov/Dec 98.

[Ref 1-22] H.Yasuda, S.Arai,J. Kai, Y. Ooae, T. Abe, S. Maruyama, and T.Kiuchi, J.Vac. Sci. Technol. B 14, 3813 (1996)

[Ref 1-23] T.H.P. Chang, M.G.R. Thomson, E. Kratschmer, H.S. Kim, M.L. Yu, K.Y. Lee, S.A. Rishton, and B.W. Hussey,"Electron-beam microcolumns for lithography and related applications", J.Vac. Sci. Technol. B 14, 3774 (1996)

[Ref 1-24] T.R.Groves and R.A.Kendall, J.Vac.Sci.Technol. B 16(6), Nov/Dec 1998

[Ref 1-25] T.H.P.Chang et al. J.Vac.Sci.Technol. B 14, 3774 (1996)

[Ref 1-26] S.T.Coyle et al, J.Vac.Sci.Technol. B 20(6), 2657 (2002)

[Ref 1-27] P.Kruit, J.Vac.Sci.Technol. B 16(6), 3177 (1998)

[Ref 1-28] http://www.mapperlithography.com

[Ref 1-29] J. T. Hastings, Michael H. Lim, J. G. Goodberlet, and Henry I. Smith, "Optical Waveguides with Apodized Sidewall Gratings via Spatial-Phase-Locked E-Beam Lithography.". J.Vac.Sci.Technol B 20(6), Nov./Dec.2002, 2753-2757.

Chapter 2

[Ref 2-1] Doak RB et. al, Physical Review Letters, 83 (21): 4229-4232, 1999

[Ref 2-2] Henry I. Smith. *A proposal for maskless, zone-plate-array lithography.* J.Vac.Sci.Technol. *B*, 14(6):4318-4322, Nov/Dec 1996.

[Ref 2-3]Ihsan J. Djomehri,*Zone-Plate-Array Lithography in the Deep UV*, Master's Thesis, Massachusetts Institute of Technology,1998

[Ref 2-4]Ihsan J. Djomehri,T.A.Savas, and Henry I. Smith, *Zone-plate-array lithography in the deep ultraviolet*, J.Vac.Sci.Technol. B, 16(6):3426-3429,Nov/Dec 1998.

[Ref 2-5] D. J. D. Carter, Dario Gil, Rajesh Menon, Mark K. Mondol, H. I. Smith and E. H. Anderson, *Maskless parallel patterning with zone-plate-array lithography*, J.Vac.Sci.Technol. B 17 (6), Nov/ Dec, 1999

[Ref 2-6] Digital Light Processing World Wide Web site: http://www.dlp.com/

[Ref 2-7]White papers on Silicon Light Machines GLV technology: http://www.siliconlight.com/htmlpgs/glvtechframes/glvmainframeset.html

[Ref 2-8] Feldman, M, OSA Proceedings on Soft X-Ray Projection Lithography, 1993, Vol.18

[Ref 2-9] Dario Gil, Rajesh Menon, D. J. D. Carter and H. I. Smith, *Lithographic Patterning and Confocal Imaging with Zone Plates,* J.Vac.Sci.Technol B 18 (6), 2881-2885, Nov/ Dec, 2000

Chapter 3

[Ref 3-1] *Euvres Completes d'Augustin Fresnel*, Vol. 1, Note 1, pp. 365-372 (1886).

[Ref 3-2] E.Hecht, Optics, Addison-Wesley Publishing (1987).

[Ref 3-3] Max Born and Emil Wolf, Principles of optics, Pergamon Press, 1984.

[Ref 3-4] Rajesh Menon, Diffractive Optics for Mask less Lithography and Imaging, PhD Thesis, M.I.T., June 2003

[Ref 3-5] Myers Jr, Ora E., American Journal of Physics, Vol. 19(6), pp. 359-365 (1951).

[Ref 3-6] Baez, Albert V., Journal of the Optical Society of America, Vol. 51(4), pp. 405-412, April 1961

[Ref 3-7]Baez, Albert V., Journal of the Optical Society of America, Vol. 51(4), pp. 405-412, April 1961

[Ref 3-8] Spiller, E, Soft X-Ray Optics, pp 90-91,SPIE Press, 1994

[Ref 3-9] F.Vasey et al, J.Vac.Sci.Technol.] B 12(6) Nov/Dec 1994

[Ref 3-10] Todd Hastings, Nanometer-Precision Pattern Placement and Applications in Integrated Optics, Ph.D. Thesis, M.I.T., June 2003

[Ref 3-11] Henry I. Smith, Submicron and Nanometer –Structures Technology,2nd edition, NanoStructures Press, Sudbury (1994)

[Ref 3-12] D.L. Spears and H.I. Smith, "High-Resolution Pattern Replication using Soft X-rays", Electronics Lett. 8, 102-104 (1972)

[Ref 3-13] D.L. Spears and H.I. Smith, "X-ray Lithography: A New High Resolution Replication Process", Solid State Technol. 15, No. 7, 21-26 (1972).

[Ref 3-14] D.Attwood, *Soft X-rays and Extreme Ultraviolet Radiation*, pg. 408, Cambridge University Press, 1999.

[Ref 3-15] H.I. Smith, M.L. Schattenburg, S.D. Hector, J. Ferrera, E.E. Moon, I.Y. Yang, and M. Burkhardt, "X-ray Nanolithography: Extension to the Limits of the Lithographic Process", Microelectronic Engineering 32, 143-158 (1996).

[Ref 3-16] L.E.Ocola and F.Cerrina, J.Vac. Sci. Technol. B 12, 3986 (1994) & H.I.Smith, J.Vac. Sci. Technol. B 13, 2323 (1995)

[Ref 3-17] D.Attwood, *Soft X-rays and Extreme Ultraviolet Radiation*, pg. 410, Cambridge University Press, 1999

[Ref 3-18] Ken-ichi Murooka, Michael H. Lim, and Henry I. Smith, J. Vac. Sci. Technol. B 18, 2966 (2000); Ken-ichi Murooka et al, J. Vac. Sci. Technol. B 19, 1229 (2001)

[Ref 3-19] G. Schneider, T. Schliebe, and H. Aschoff, J. Vac. Sci. Technol. B **13**, (1995)

[Ref 3-20] E.Anderson et al, "*Nanofabrication and diffractive optics for high-resolution x-ray applications* ", J. Vac. Sci. Technol. B **18**(6), pp. 2970-2975, 2000.

[Ref 3-21] T. Tanaka, M. Morigami, and N. Atoda, Jpn. J. Appl. Phys. **32**, 6059 (1993)

[Ref 3-22] Azalia A. Krasnoperova, et al J. Vac. Sci. Technol. B 13(6), Nov/Dec 1995

[Ref 3-33] Fulton et al, Appl.Phys.Lett., Vol 42, No.8, 15 April 1983.

[Ref 3-34] Dolan et al, IEEE Electron Device Letters, Vol. EDL-4, No.6, June 1983

[Ref 3-35] http://www.etec.com

[Ref 3-36] Aboud, F. et al, *"Raster Scan Patterning Solution for 100nm and 70nm OPC masks"*, White Paper, http://www.appliedmaterials.com/products/mask_technical_papers.html

[Ref 3-37] Stephen Y. Chou, Peter R. Krauss, Wei Zhang, Lingjie Guo, and Lei Zhuang , "*Sub-10 nm imprint lithography and applications*," J. Vac. Sci. Technol. B 15, 2897 (1997)

Chapter 4

[Ref 4-1] Kwok-Kit Wong A., Resolution Enhancement Techniques in Optical Lithography, SPIE Press, Bellingham, Washington, 2001

[Ref 4-2] M.Born and E.Wolf, *Prinicples of Optics,* Cambridge Univ. Press, New York 1999, 7th Ed, pp.441

[Ref 4-3] M.Minsky, US patent 3,013,467, 19 Dec 1961, filed 7 Nov. 1957.

[Ref 4-4] H.J.Tiziani, R.Achi, R.N.Kramer and L.Wiegers, "Theoretical analysis of confocal microscopy with microlenses." Appl. Opt. 35(1). 120-125 (1996).

[Ref 4-5] Rajesh Menon, Optimum volume-holographic confocal microscope: Area Exam Report. Technical Report, 2002. MIT.

Chapter 5

[Ref 5-1] http://www.powertechnology.com

[Ref 5-2] http://www.conoptics.com

[Ref 5-3]White papers on Silicon Light Machines GLV technology:
http://www.siliconlight.com/htmlpgs/glvtechframes/glvmainframeset.html

[Ref 5-4]White papers on Silicon Light Machines GLV technology:
http://www.siliconlight.com/htmlpgs/glvtechframes/glvmainframeset.html

[Ref 5-5]D.T.Amm and R.W.Corrigan, "Optical performance of the grating light valve technology", Projection Displays, V.M.H.Wu ed., Proc.SPIE 3634, 71-78 (1999).

[Ref 5-6] J.A.Hoffnagle and C.M.Jefferson, Applied Optics, Vol.39, No.30, 2000.

[Ref 5-7] J.L.Kreuzer, U.S. Patent 3,476,463, 4 November 1969

[Ref 5-8] Dario Gil, Rajesh Menon, D.J.D. Carter, and Henry I. Smith, "Lithographic Patterning and Confocal Imaging with Zone Plates." *Journal of Vacuum Science and Technology B* **18**(6), 2881-2885, Nov/Dec 2000

[Ref 5-9] A. Murray, F. Abboud, F. Raymond, and C. N. Berglund, J. Vac. Sci.Technol. B 11, 2390 (1993)

[Ref 5-10] F. Abboud et al., Photomask and X-ray Mask Technology IV, Proc. SPIEVol. 3096 (SPIE Bellingham, WA, 1997), pp. 116–124.

[Ref 5-11] R. Dean, D. Alexander, J. Chabala, T. Coleman, C. Hartglass, M. Lu, C.Sauer, and S. Weaver, 15th European Conference on Mask Technology for Integrated Circuits and Microcomponents '98, Proc. SPIE Vol. 3665 (SPIE, Bellingham, WA, 1999), pp. 166–178.

[Ref 5-12] M. L. Rieger, J. A. Schoeffel, and P. A. Warkentin, Laser Microlithography,Proc. SPIE Vol. 922 (SPIE, Bellingham, WA, 1988), pp. 55–64.

[Ref 5-13] B. J. Grenon, D. C. Defibaugh, D. M. Sprout, H. C. Hamaker, and P. D.Buck, 14th Annual BACUS Symposium on Photomask Technology and Management, Proc. SPIE Vol. 2322 (SPIE, Bellingham, WA, 1994), pp.50–55.

[Ref 5-14] D.J.D. Carter, Dario Gil, Rajesh Menon, Mark K. Mondol, Henry I. Smith, and Erik H. Anderson, "Maskless, Parallel Patterning with Zone-Plate Array Lithography." *J. Vac. Sci. Technol. B* **17(6)**, 3449-3452, Nov/Dec 1999.

[Ref 5-15].Rajesh Menon, Diffractive Optics for Mask less Lithography and Imaging, PhD Thesis, M.I.T., June 2003

Chapter 6

[Ref 6-1] L. Kipp, et al, Nature, vol. 414, pp184-188, 8 November, 2001

[Ref 6-2] J. W. Goodman, Introduction to Fourier Optics" , McGraw Hill, pp 151-154, (1996).

[Ref 6-3] Ozden I, Diagne M, Nurmikko AV, Han J, Takeuchi T, Physica Status Solidi A-Applied Research, 188 (1): 139-142 Nov (2001)